Porphyrin arrays for FET devices

A thesis submitted to the board of the faculty of Physical Sciences in partial requirement for the degree of:

Doctor of Philosophy of the University of Oxford

Matthew Wicks

Merton College, Oxford

Christmas 2004

Abstract

Porphyrin Arrays for FET devices

A thesis submitted to the board of the faculty of Physical Sciences in partial requirement for the degree of Doctor of Philosophy by:
Matthew Wicks, Merton College, December 2004.

Field effect transistors (FETs) are a key component of modern electronic devices. They require a semiconducting material that is traditionally made from doped silicon. Recently however it has been shown that porphyrin systems can be used in the same capacity.

This thesis therefore describes the investigation of new methods of porphyrin functionalization to synthesise 1,4,5,8-tetraazaanthracene-bridged porphyrin arrays, and their application to the synthesis of extended arrays for use in FETs. The 1,4,5,8-tetraazaanthracene bridge is synthesised through the condensation of a porphyrin *alpha*-dione with 1,2,4,5-tetraaminobenzene. Accordingly, the synthesis of an extended array requires a porphyrin tetra-one monomer unit.

Two methods for the synthesis of porphyrin tetra-ones have been investigated. The first approach attempts to adapt Knudsen's hydroxylation of an aryl halide by sodium benzaldoximate to a porphyrin system. Initial regiospecific halogenation of a porphyrin has been successfully achieved. However when hydroxylation was attempted, partial dehalogenation of the substrate was observed; and when applied to the synthesis of the porphyrin tetra-one the methodology failed.

The second approach involves the allylic oxidation of a chlorin (a reduced porphyrin) on silica. The transformation's mechanism has been thoroughly investigated and it has been successfully applied to the synthesis of a porphyrin tetra-one.

This methodology has then been applied to the synthesis of extended porphyrin arrays. A sample incorporating 12 porphyrin units has been successfully constructed. It has been characterised by NMR, MALDI, GPC and UV-VIS spectroscopy. By comparison with previous results it has been concluded that the aromatic system- which spans 181 Ångstroms

from end to end- can be described as a series of weakly interacting chromophores, in agreement with theoretical predictions made by Hush.

In addition a medium-scale synthesis of an array incorporating four porphyrins has been achieved so that it may now be tested as the semiconducting material in a FET.

Acknowledgements

First of all I would like to acknowledge you, the reader, for picking up this thesis. I hope that you find it interesting, or at the very least, not boring. This might also be the appropriate point to apologise for including two appendices, but having these two sections nicely self-contained satisfies my autistic tendencies.

Anyway, onto the people who have made this thesis possible. Firstly, without Neil I would certainly have never made it to the end of three years- I am indebted for all his support. Other people in the group who have made life good include (in chronological order) Mike, Laurence, Will, Sanjay, Bimlesh, Kevin and Pete. Thanks to the littl'uns for making for a lively last few months- Fumiaki, Sarah, little Laurence and Mel- G5 will always be the better lab. Thanks you also to Laurence for organising such a great laboratory, to Neil Oldham for knowing so much about MALDI, to Barbara for knowing so much about NMR, to Harry for discussions about exciton coupling, to Neil, Samia and Pete for their help with GPC, to Jong-Jin for his help with the DSC and thin-film UVs, and to Chris, Kevin and Neil for reading this thesis over. Also thanks to Graham Richards for building a new laboratory.

I am indebted to both Tim and Veronique for all their academic guidance and inspiration- I am sorry not to have lived up to expectations. Bob is also a great man for showing me how science should be done. Thanks must go to Paul for giving me such an interesting DPhil project three years ago, for his support as a supervisor, for giving me the opportunity to teach and for his help in putting this thesis together. And Steve, the man from MERCK, is a great person for giving me so much money and not expecting very much in return. That goes for my parents as well, who have been very supportive in all senses for my seven years here, especially in terms of food.

Finally I should acknowledge people outside the lab who have had to endure an awful lot of grumpiness. I am indebted to big Ben for his friendship, and to Eva for her kindness. I am thankful to Debbie and little Ben for being there. I am thankful to Melina and Vikram for inviting me to their wedding, and to Jane and Angus for South Africa (Microsoft spellchecker suggests I replace Vikram with 'Vicar'- I am in no way thankful to Bill Gates).

And finally, I am completely indebted to Claire. Without you nothing would be possible. If everything goes to plan, you'll be seeing much more of me very soon.

Contents

Glossary of Abbreviations

Ac	acyl
AIBN	2,2'-Azobis(2-metnylpropionitrile)
Bu	butyl
cm	centimetre
conc.	concentrated
c.f.	cross reference
COSY	homonuclear Correlation Spectroscopy
DDQ	Dichlorodicyano-Quinone
DMSO	Dimethyl Sulphoxide
DMF	Dimethyl Formamide
$E_{1/2}$	half-wave potential
eqv.	equivalents
EL	Electroluminescence
EPR	Electron Paramagnetic Resonance
Et	ethyl
EtOH	Ethanol
FET	Field Effect Transistor
GPC	Gel Permeation Chromatography
^1H	proton
HMBC	Hetronuclear Multiple Bond Connectivity
HMQC	Hetronuclear Multiple Quantum Coherence
HMTA	Hexamethylene Tetraaamine
HOMO	Highest Occupied Molecular Orbital
IBX	Iodoxybenzoic Acid
LDI	Laser Desorption Ionization
LUMO	Lowest Unoccupied Molecular Orbital
LUMO+1	Next to Lowest Unoccupied Molecular Orbital
MALDI	Matrix Assisted Laser Desorption Ionization
mCPBA	*m*-Chloroperoxybenzoic Acid
Me	methyl
MeOH	methanol
NMR	Nuclear Magnetic Resonance
NOE	Nuclear Overhauser Effect
PDT	Photodynamic Therapy
Ph	Phenyl
porphyrin	damned porphyrin
ppm	parts per million
RFID	Radio Frequency Identification
SET	Single Electron Transfer
t and *tert*	tertiary
THF	Tetrahydrofuran
TLC	Thin Layer Chromatography
TOF	Time of Flight
UV-VIS	Ultra-Violet/ Visible
vs.	versus
w.r.t.s.m.	with respect to the starting material

Abbreviations of units are given in accordance with normal scientific convention.

Chapter One
Introduction

Chapter One
Introduction

Sir Walter Raleigh was an Elizabethan man of leisure, reputed for bringing the potato and tobacco to England. In the later part of his life however he fell out with the establishment and was imprisoned in the Tower of London, where he put his time to good use and started writing his version of the 'History of the World.' In its preface he states[1]:

> "Man cannot give a true reason for the grass under his feet
> why it should be green rather than red or any other colour."

These words of Raleigh put into context the work of the great chemists Hans Fisher[2] and RB Woodward[3], who three hundred years later completed the total syntheses of haemin and chlorophyll respectively. Together they proved how one biological motif, the porphyrin macrocycle, is responsible for the green colour of grass, and that but for two hydrogens it would be red; and conversely why with two extra hydrogens even an Englishman as red-blooded as Raleigh would have blue blood running through his veins.

This biological motif, the porphyrin macrocycle, has been repeatedly used in nature[4]. Some of these uses are illustrated in Figure **1.1**. Porphyrins play a crucial role in the major energy-generating systems of this planet as chlorophyll acts as the main light-absorbing element in the photosynthetic pathway. They play an equally significant role in coenzyme F_{430} in the energy production systems of methane-producing bacteria. Conversely porphyrins allow the most prevalent user of natural energy to thrive on this planet, as the macrocycle is key to the function of haemin in the oxygen-transport system in humans. Porphyrins have also found their role in a more subtle variety of biochemical functions. Vitamin B_{12}, whose structure was elucidated by Oxford's own Nobel prize-winning Dorothy Hodgkin[5], has important biological functions as a coenzyme and contains a porphyrin-type macrocycle at its reaction centre. Similarly, cytochrome P_{450} (not shown) is a chemically fascinating oxidative enzyme that has the ability to hydroxylate various chemical substrates.

Within this diversity of function in nature, three distinct characteristics of the porphyrin macrocycle are exploited. Firstly, the porphyrin macrocycle is rigid and planar and can therefore act as a structural element. This structural role is exploited in oxygen-transport in haemoglobin where iron is incorporated into the protein structure by coordination to a

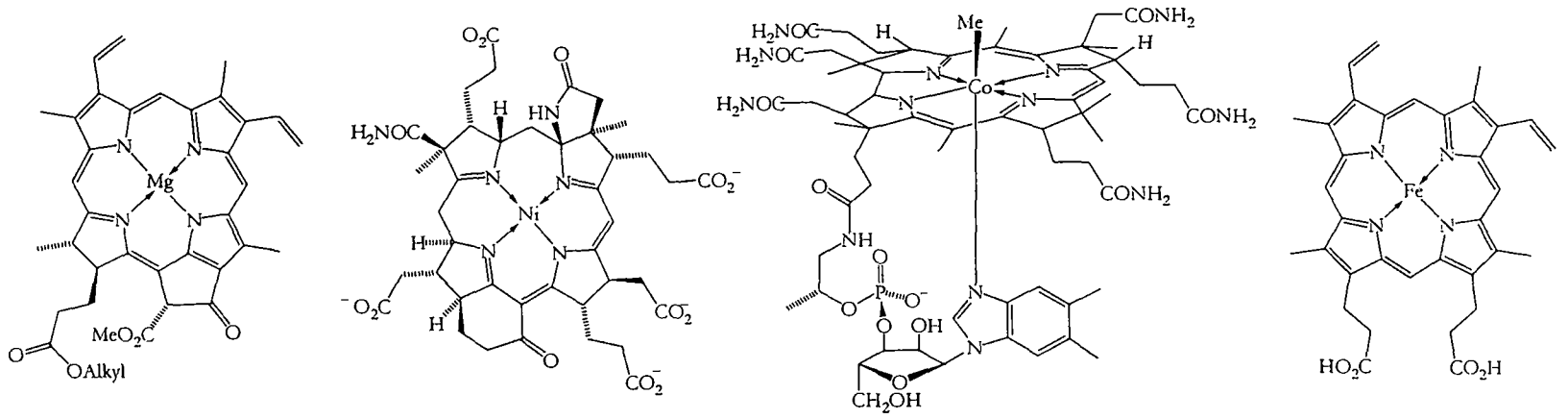

Figure **1.1**- important natural porphyrins. From left to right: chlorophyll *a*, coenzyme F_{430}, coenzyme B_{12} and heme.

porphyrin. Subtle changes of the iron's binding to the porphyrin when itself coordinated to oxygen, leads to an allosteric effect in its binding of oxygen. Then porphyrins are brightly coloured and are used for this asset as the main absorbing species in the photosynthetic pathway. Finally the electrons in the porphyrin's π-system are delocalized, leading to the porphyrin exhibiting a rich redox chemistry. This is exploited in oxidative enzymes and coenzymes, such as cytochrome P_{450} and vitamin B_{12}.

Taking this lead from nature, a huge amount of synthetic chemistry has been developed so that these three properties of the porphyrin can be understood and then exploited. This development has coincided with the establishment of the field of supramolecular chemistry where porphyrins have found their own niche. For example, by attaching a suitable functionality to a porphyrin it can act as a chemical sensor, so that many different types of molecule can be chemically detected through monitoring changes in the porphyrin's absorption spectrum. The potential application of porphyrins to supramolecular chemistry has been further extended by advances in porphyrin synthesis; so now a whole range of unsymmetrical and substituted, expanded and contracted porphyrin structures, even some where a pyrrole has been replaced by a furan or thiophene, can be readily synthesized. The ultimate supramolecular goal of the porphyrin chemist must be to emulate the careful supramolecular order that is observed at the photosynthetic centre and to achieve long-lived charge separated states on a nanomolecular level.

Of late porphyrins have started to be applied to a new area of chemistry, namely the use of organic substrates as the active layer in electronic devices. Because of their electronic and photochemical properties porphyrins have been used both in photovoltaic applications and in light emitting diodes. Organic substrates have also started to be examined as semiconducting materials for field effect transistors (FETs), and because of a porphyrin's

advantageous structural and electronic properties, porphyrins might be considered as ideal substrates in this role.

1.1 An introduction to porphyrins

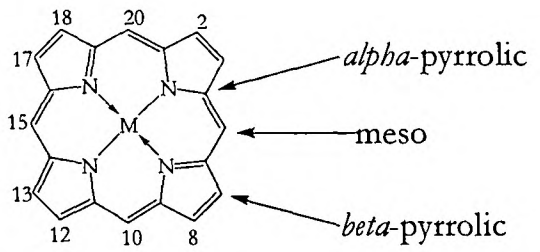

Figure **1.2**- the different positions on the porphyrin periphery. The numbering system for the porphyrin is also illustrated.

Porphyrins are tetra-pyrrole molecules. The bare porphyrin macrocycle possesses D_{4h} symmetry, and therefore there are three different types of positions on the porphyrin periphery (see Figure **1.2**). The macrocycle is planar or slightly ruffled due to its delocalized electronic structure. This delocalized structure causes large electronic ring currents, so that the β-pyrrolic and meso protons appear significantly deshielded in their ^{1}H NMR spectra. The delocalization also results in a porphyrin's characteristic colour and UV-VIS absorption spectrum; after all, the name 'porphyrin' originates from the Greek 'porphyrios' meaning purple. The rigid structure also results in a well-defined central cavity in the middle of the macrocycle that can accommodate almost any metal.

Natural porphyrins are generally of very complicated structure, as exemplified by those in Figure **1.1**. However it can be seen from these examples that natural porphyrins are usually substituted in their β-pyrrolic positions, leaving their meso positions free. Synthetic porphyrins on the other hand tend to be of a much more symmetric structure, and can be

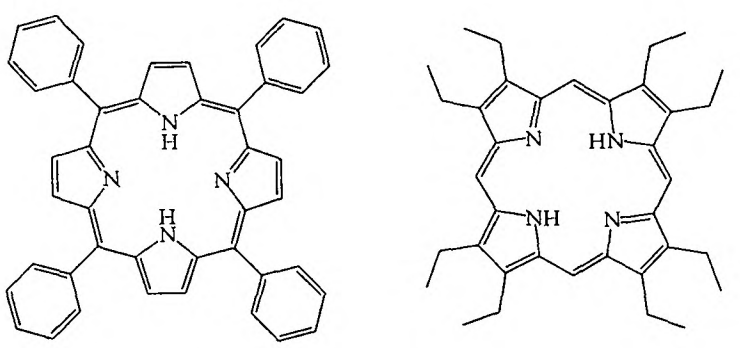

Figure **1.3**- tetraphenyl- and octaethyl-porphyrins.

meso- or β-pyrrolic substituted, or even both. The two simplest synthetic porphyrins are tetraphenyl-porphyrin and octaethylporphyrin, and these are illustrated in Figure **1.3**.

The simplest synthetic porphyrins can be synthesized by the direct condensation of an aldehyde with a suitable pyrrole. This route was originally reported for the synthesis of tetraphenyl-porphyrin by Rothemund[6]. Adler and Longo modified this methodology by replacing Rothemund's high-temperature sealed-tube condensation with refluxing propionic acid. This synthesis was finally optimized by Lindsey, who used a high dilution technique in conjunction with a Lewis acid catalyst[6]. Octaethyl-porphyrin can be synthesized by a similar monopyrrole tetramerization. Less symmetrical porphyrins can be synthesized through a variety of powerful techniques[6].

1.2 Porphyrin arrays

Whilst one porphyrin by itself has very admirable electronic and structural properties, much work has gone into the design and synthesis of molecules containing more than one porphyrin unit. This is partially a response by the chemist to the supramolecular challenge posed by nature, which uses several very carefully arranged arrays of chlorophyll molecules at the heart of the photosynthetic systems[7]. Literally hundreds of porphyrin arrays have been constructed that attempt to mimic these special arrangements and to try to understand the nature of porphyrin-porphyrin interactions, or to exploit the properties of these porphyrin arrays[8]. Different methods of connecting individual porphyrins have been attempted[9], whether it is by non-covalent or covalent means; and if joined covalently, whether it is by connecting through either the meso or β-pyrrolic positions. And in order to be able to compare the different types of arrays, firstly the effects of bringing two porphyrins in close proximity to one another need to be appraised.

1.2.1 The effect of porphyrin-porphyrin interactions on photophysical properties

When comparing the properties of a porphyrin oligomer to its respective monomer, there are two principle effects that manifest themselves in the photophysical spectra (see Appendix One for a basic examination of the UV-VIS spectra of porphyrins):

1. **Delocalization**- in a covalently-linked porphyrin oligomer the ground electronic states of adjacent porphyrin units may interact with one another. This is generally

characterised in the UV-VIS spectrum by a shift of the lowest energy absorption (the Q band) to a longer, lower-energy wavelength.

The effects of delocalization are qualitatively relatively easy to understand. A greater degree of delocalization leads to a smaller HOMO- LUMO gap and therefore a red-shifted absorption spectrum.

2. **Exciton coupling**- an exciton is a description of the hydrogenic state that is the combination of the hole and the electron created by photochemical excitation. Exciton coupling *does not* involve any ground state interaction of the individual chromophores and therefore does not require a covalent link between two porphyrin units. Rather it is the stabilization or destabilization of an electronic transition of a chromophore through electrostatic interactions with a second chromophore. This manifests itself as a shift, a broadening or a splitting of the various bands in the UV-VIS spectrum. It can also result in changes in the fluorescence spectrum, both in a shift in the wavelength and a change in the intensity of fluorescence.

The effects of exciton coupling are subtle and can be complex. For example in a molecular dimer the B band of the absorption spectrum is blue-shifted if the chromophores possess a face-to-face conformation; but a component of it is red-shifted if the chromophores possess a side-by-side conformation. The extent to which the wavelength of absorption is perturbed by exciton coupling is measured by the **exciton coupling energy, ΔE_0.** In addition when the number of chromophores in an array increases the magnitude of the exciton coupling increases as well. Finally, it is generally noted that exciton coupling is only observed between B band transitions. More details as to the theory of exciton coupling are given in Appendix Two.

1.2.2 Non-covalently linked arrays

Porphyrins are large conjugated systems and therefore tend to aggregate both in solution and in the solid state. This can be seen from the electro-luminescence (EL) spectra of the simple 2,3-dihydro-tetraphenyl-porphyrin **1**[10]. The photo-luminescence spectrum in solution is characterized by one emission band, but the solid-state EL spectrum in addition exhibits two red-shifted bands. This can be interpreted in terms of exciton coupling occurring within 'J-aggregates,' where the individual porphyrin cores are orientated slightly offset from one another. Hydrogen and dative bonding provide a stronger interaction between neighbouring porphyrins. For example Lehn's system **2** favours the illustrated dimeric structure at low concentration[11], and because this causes a change of the porphyrins'

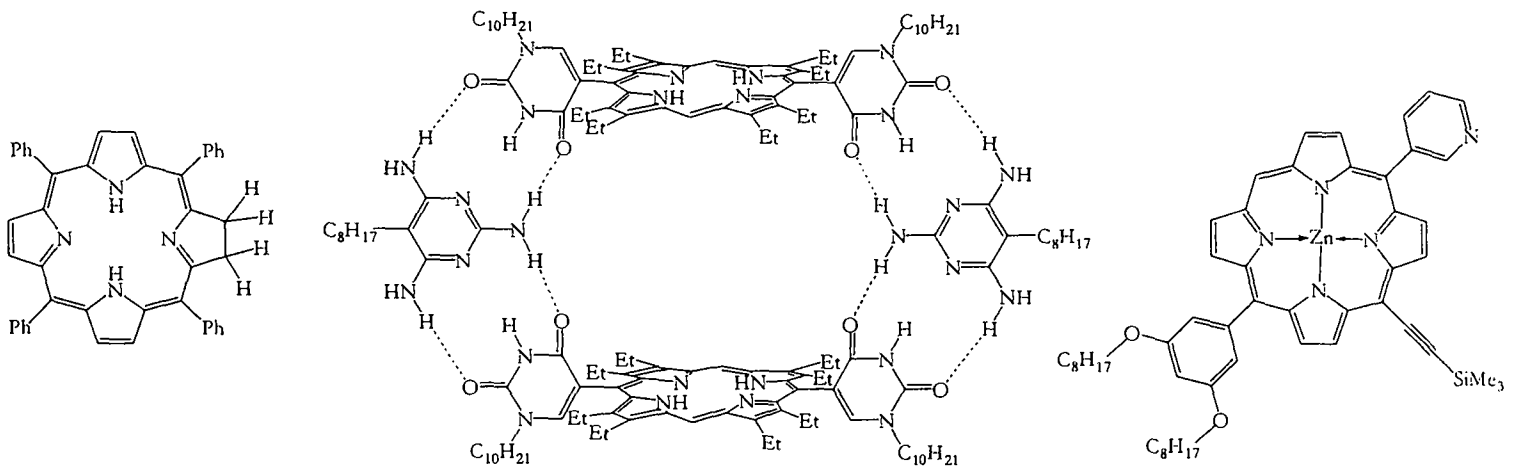

(1) (2) (3)

Figure **1.4**- non-covalently bonded porphyrin arrays.

fluorescence compared to the monomer the system can act as a molecular sensor. Non-covalent interactions can also be temperature-dependant, as demonstrated by the behaviour of **3** in solution which has been used as a 'supramolecular thermometer' because it changes colour with varying temperature[12]. In this case self-assembly is caused by a dative interaction between the 3-pyridyl and the zinc.

1.2.3 Meso-meso covalently-linked arrays

Whilst linking porphyrins by non-covalent methods is appealing because it means that extended systems can be self-assembled from the monomer units, the extent of self-assembly is difficult to control and varies with subtle factors such as concentration and temperature. Therefore many porphyrin dimers and oligomers have been constructed using covalent linkages because of their more reliable properties. And because methodology for the functionalization of the meso position is more prevalent and successful than for the functionalization of the β-pyrrolic position, the majority of covalently-linked porphyrin arrays have neighbouring units linked through their meso positions.

One way to connect two porphyrins is to substitute a pyridine onto one of the meso positions and then to coordinate the pyridyl nitrogen to a metal atom. This is illustrated by the 'cup and ball' bisporphyrin **4** (in Figure **1.5**) that can be used to accommodate C_{60} through non-covalent interactions[13]. The methodology can be further extended to the synthesis of Drain and Lehn's tetrameric system **5**[14], and even further to the synthesis of a cyclic nonamer[15]. The porphyrins in these arrays show a red-shifted broad B-band absorption with a small exciton coupling energy E_0 of around 450 cm^{-1}, indicating a greater interaction than in a non-covalent dimer.

A second much-favoured method of meso-functionalization is through an amide linkage on a meso-aromatic substituent. This was the initial approach of Imahori with the aim of designing systems for long-lived charge separation. By joining C_{60} and ferrocene on the ends of a bisporphyrin joined by an amide linkage in **6**, a charge separated state with a lifetime of 1.6 seconds at 163 K and a total quantum yield of formation of 34% could be achieved[16,17]. This quantum yield can be increased by incorporating Osuka's directly-linked porphyrins (as in **8**) instead of the amide-linked bisporphyrin[18]. This is a remarkable result as it is comparable to the electron transfer properties of the bacteriochlorophyll dimer radical cation/ secondary quinine radical anion pair in the bacteria photosynthetic reaction centre.

More rigid linkers can be used to connect two neighbouring porphyrins. These have the advantage that they can also allow a greater extent of inter-porphyrin communication. Thus the phenylene bridged dimer **7** has been synthesised by Osuka and an oligomer incorporating nine porphyrins has been constructed in a similar fashion[19,20]. This shows some interaction between neighbouring porphyrin units with the B band being split by exciton coupling with a respectable exciton coupling energy E_0 of 1600 cm^{-1}; but the wavelength of the lowest energy absorption does not change significantly with oligomer length, indicating that there is little electronic delocalization along the array. Osuka has also synthesised a series of directly linked porphyrin arrays[21-23]. This direct linkage is shown in the dimer **8**, and these arrays have been extended to an impressive length of 1024 porphyrins[24]. These show a much greater extent of exciton coupling with a large exciton coupling energy E_0 of 4300 cm^{-1}. The wavelength of the lowest absorption band does red-shift with an increasing number of porphyrin units; but instead of being interpreted in terms of electronic delocalization, this has been explained by exciton coupling *within the Q band absorptions* with an exciton coupling energy E_0 of 1150 cm^{-1} [25]. The lack of electronic delocalization has been attributed to the fact that two neighbouring porphyrins adopt a perpendicular orientation, thereby allowing no ground-state electronic interaction. Further interpretation of Osuka's results is given in Appendix Two.

So far therefore meso-meso linkages have shown some interaction between neighbouring porphyrin units but little electronic ground-state communication. In this way the butadiyne spacer investigated by Anderson is special[19,26]. A series of arrays have been investigated, from the dimer **9** to the hexamer. As the oligomer length increases the B band shifts to longer wavelengths and significantly broadens, both signs of exciton coupling between neighbouring porphyrins. In addition the position of the lowest energy Q band is moved to

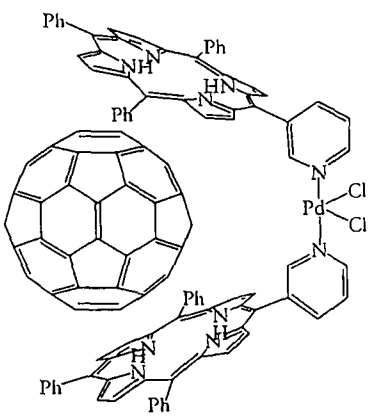

(4)

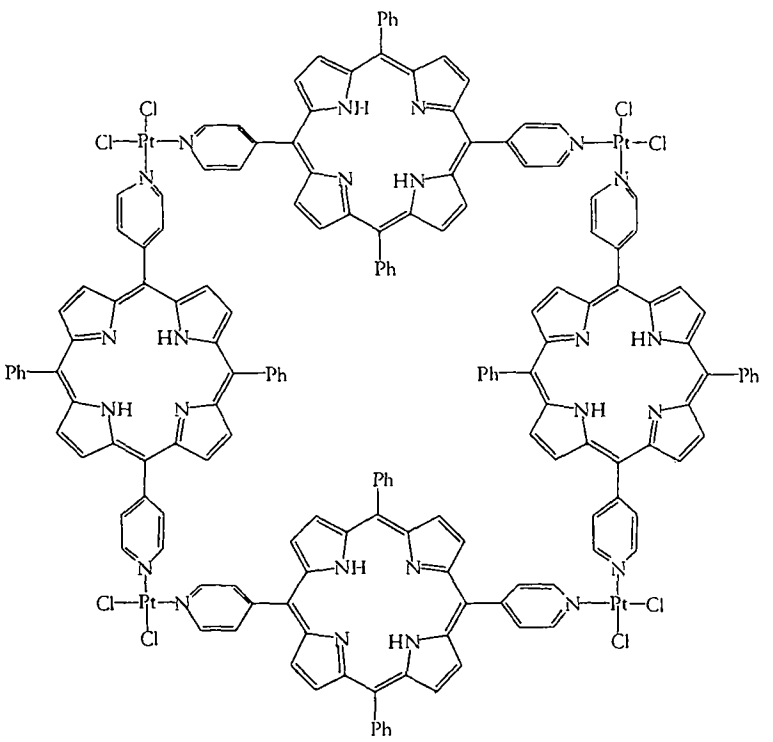

(5)

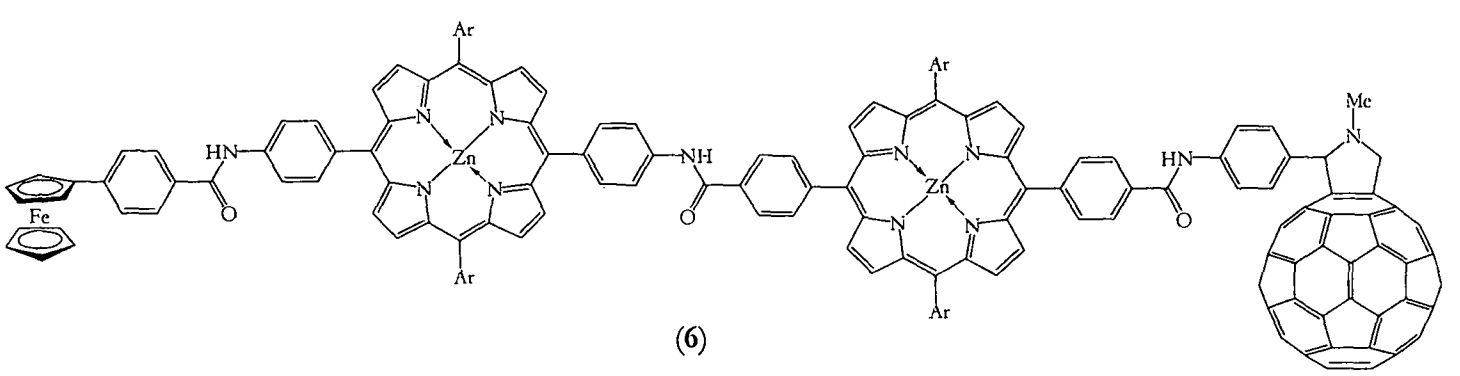

(6)

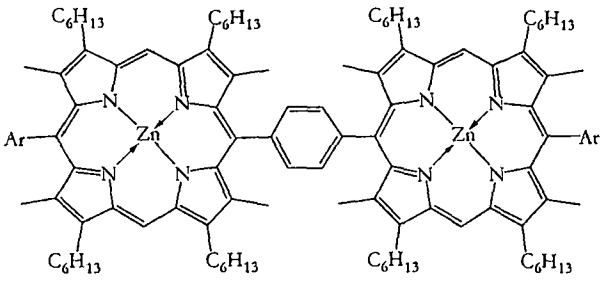

(7)

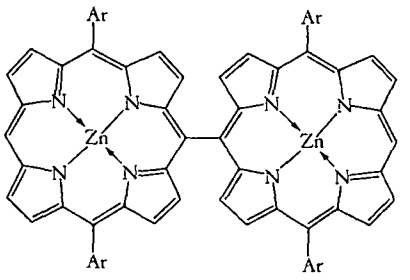

(8)

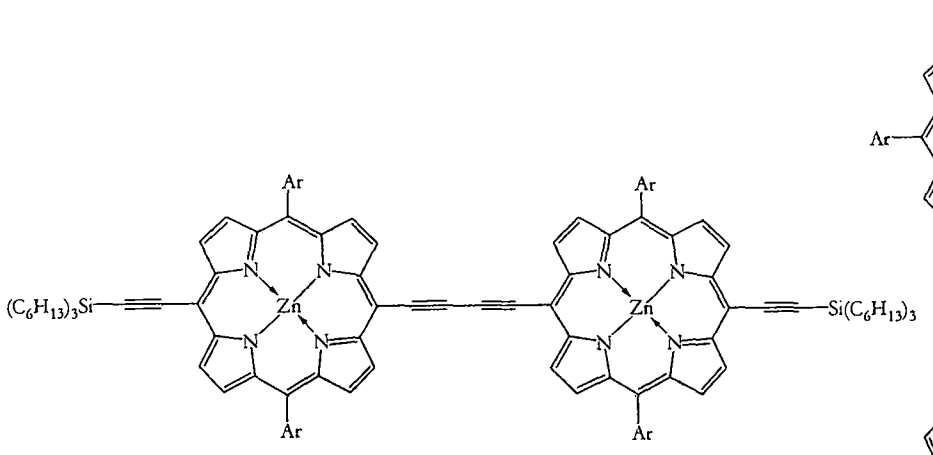

(9)

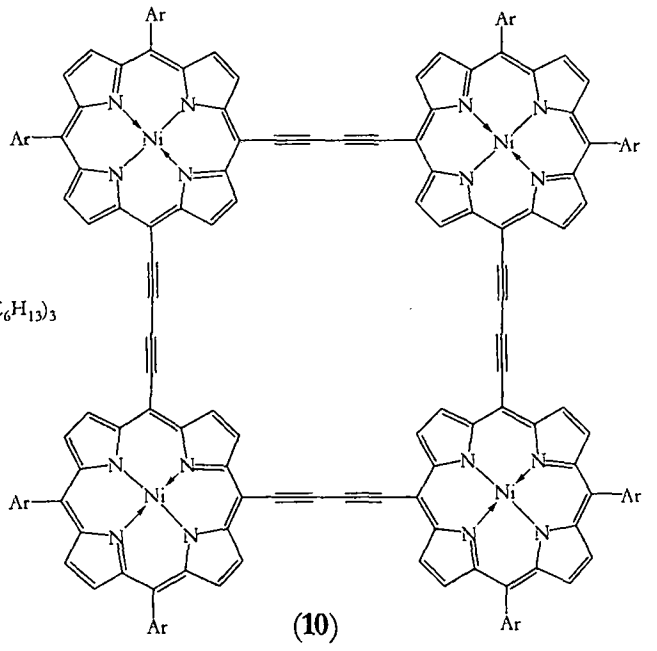

(10)

Figure **1.5**- meso-meso covalently-linked porphyrin arrays. Ar= 3,5-di-*tert*-butylphenyl.

a longer wavelength as the oligomer length is increased. This is a result of significant ground state electronic interactions causing a reduction in the HOMO- LUMO gap as the oligomer length is increased. This delocalization is advantageous in non-linear optical applications as it gives rise to a high polarizability and two-photon absorption cross-section[27].

This methodology has been taken one step further with the synthesis of the square tetramer **10** by Sugiura[28]. Recently this has been spectacularly extended to the synthesis of a square nonamer in a total yield of 0.007% over 22 steps[29]. The nonamer possesses a 2 nm diameter cavity in its centre that is hoped to give rise to new nano-host-guest chemistry.

1.2.4 *β*-pyrrolic covalently-linked arrays

Only a handful of *β*-pyrrolic covalently-linked porphyrin arrays have been investigated, primarily because they are more difficult to synthesise. Kevin Smith[30] has made two arrays, specifically the crucifix pentamer **11**[31] and the directly linked porphyrin trimer **12**[32] (Figure **1.6**). These both show very altered absorption spectra compared to their monomer units, but a systematic study varying the length of the arrays was not possible due to the method of synthesis. This is not a problem shared by the arrays of Ono who has recently synthesised a series of conjugated arrays based on an unconjugated precursor[33,34]; the conjugated dimer **13** shows a significant red-shifted spectrum compared to its unconjugated precursor, indicating electronic delocalization across the bridges connecting two neighbouring porphyrin units.

Max Crossley- at this point it should be noted that Paul Burn carried out the work under Crossley's supervision, so when Max Crossley's name is mentioned it implicitly also refers to the work of Paul Burn- has also investigated the synthesis of *β*-pyrrolic covalently-linked porphyrin arrays. His approach has been to use a 1,4,5,8-tetraazaanthracene bridge to fuse the *β*-pyrrolic positions of two tetraaryl-porphyrins together as in the dimer **14**[35]. This methodology was extended to the synthesis of a linear tetramer[36]; later Promarak showed how the incorporation of a dendritic solubilizing unit onto the end positions of the array could extend the system to a length of seven porphyrin units[37]. The electronic properties of these arrays has been investigated by Burn, who on the evidence of electrochemical measurements suggests that the 1,4,5,8-tetraazaanthracene linker allowed electronic interaction of two neighbouring porphyrins mainly through their LUMO. Narang has independently extended this methodology to the synthesis of linear polymers, and claims that this can lead to the incorporation of 20 to 2400 porphyrin units in one polymer chain as measured by gel permeation chromatography[38,39].

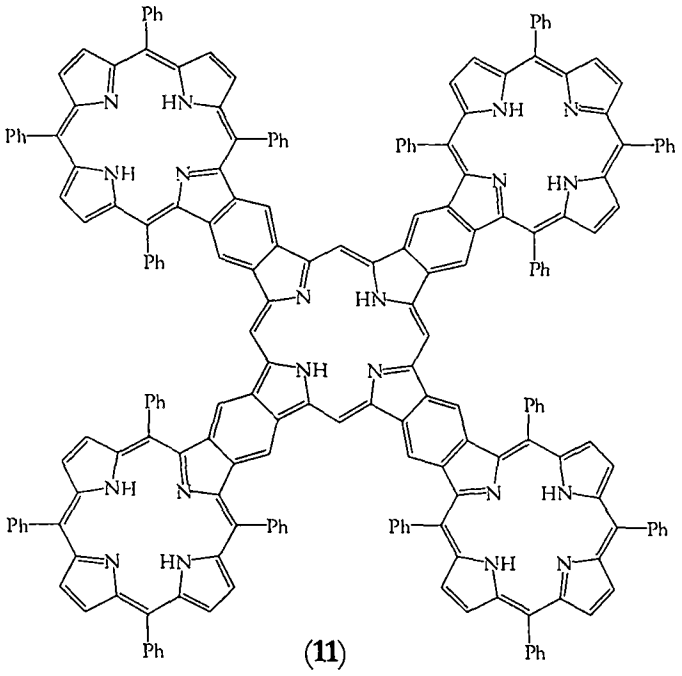

(**11**)

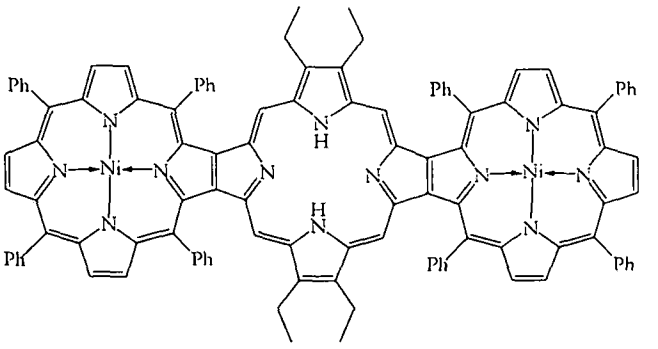

(**12**)

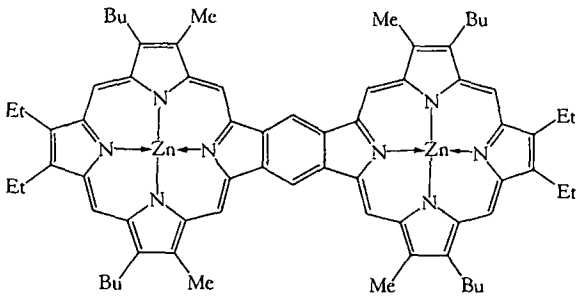

(**13**)

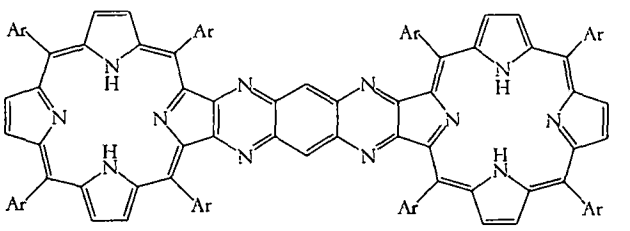

(**14**)

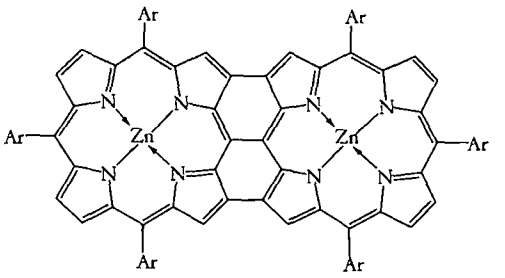

(**15**)

Figure **1.6**- β-pyrrolic covalently-linked porphyrin arrays. Ar= 3,5-di-*tert*-butylphenyl

Finally Osuka has synthesised a series of meso-meso, β-β, β-β triply-linked arrays through a mild oxidation of his singly-linked arrays[40,41]. This is illustrated by the dimer **15** in Figure **1.6**. He has extended this rigid array to twelve porphyrin units' length, and these arrays show remarkable electronic properties. There are two bands whose progression can be interpreted in terms of strong exciton coupling between the B bands of 'neighbouring' porphyrins, with massive exciton coupling energy E_0 of around 6300 cm^{-1} [42]. The most remarkable feature however is the Q band that is shifted to increasingly longer wavelengths with increasing number of porphyrin units- from around 550 nm for a single porphyrin to 1500 nm for the dimer, and up to 2500 nm for the 12mer. This has been interpreted in terms of a particle-in-a-box model where the length of 'the box' corresponds to the length of array's backbone[42].

1.2.5 Dendritic arrays and polymers

One class of molecule that does not fit easily into the classifications of covalently-linked meso or β-pyrrolic covalently-linked porphyrin arrays is that of the polymeric porphyrins.

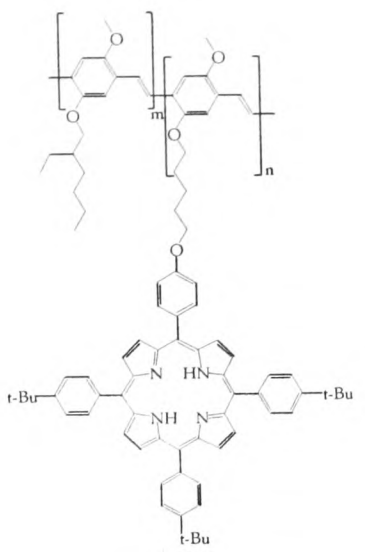

(16)

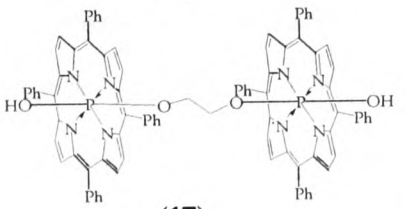

(17)

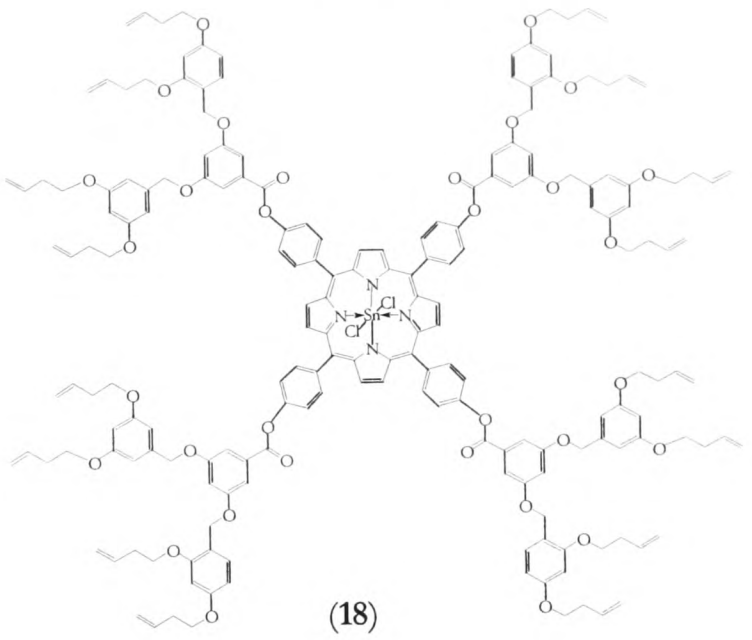

(18)

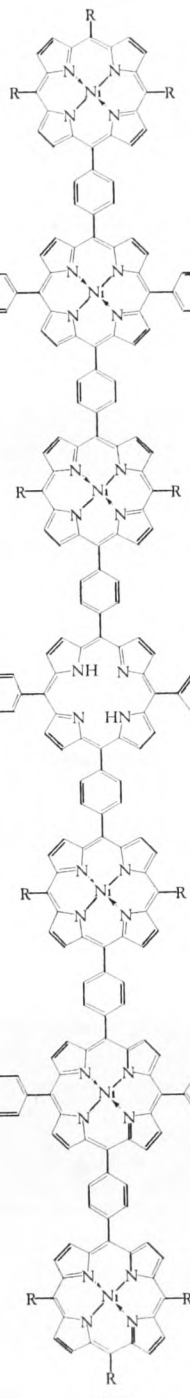

(19)

Figure **1.7**- polymeric and dendritic porphyrin arrays.

One such example incorporates a porphyrin chromophore into a polymeric organic light-emitting diode in the polymer **16**[43]. It was found that red luminescence from the porphyrin was hampered by aggregation of the chromophores in the polymer film, leading to exciton interactions reducing the photo-luminescent efficiency of the polymer.

Porphyrin polymers have also been applied to the construction of new molecular architectures. Phosphorus dichloride porphyrins can be polymerised to create a face-to-face stack[44] as shown by **17**; once again a splitting in the B band by exciton interactions is observed, with a small exciton coupling energy of 650 cm^{-1}. This idea has been extended to the tin porphyrin **18**, where the polymerisation of a dendritic tin porphyrin in a similar fashion followed by the ring-closing metathesis of the alkene surface groups and the removal of the porphyrin core leads to the construction of a 'nanorod' [45].

Finally, Sugiura has constructed a porphyrin dendrimer incorporating an impressive 21 porphyrin units (**19**)[46]. As seen with his square meso-meso linked arrays[29] Sugiura shows that he is not afraid of low yields, the final product being obtained in 0.15% over 17 steps. The UV-VIS spectrum of the dendrimer shows only a 4 nm red-shifted B band and a small reduction in the intensity of fluorescence compared to a monomer unit.

1.3 Field Effect Transistors (FETs)[47-50]

It is evident that the porphyrin is nature's molecule of choice in a plethora of situations, and that the chemist has tried hard to mimic nature's diligence. The challenge now is to exploit the porphyrin in new ways and in new fields. The knowledge of the porphyrin's rich electronic properties therefore begs the question whether the porphyrin can be applied as a charge-carrying substrate in an electronic device, for example in a transistor.

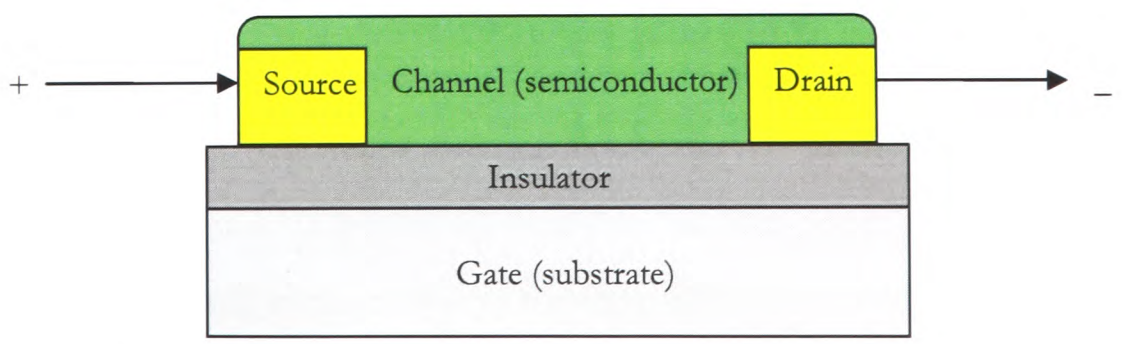

Figure **1.8**- a schematic illustration of a 'thin film' transistor.

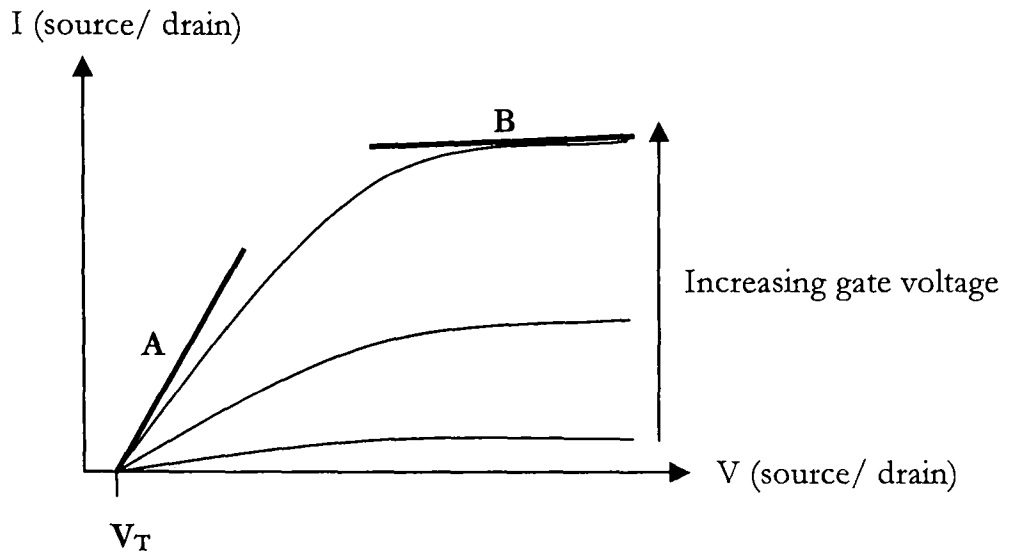

Figure **1.9**- typical output characteristics of a transistor.

The structure of a transistor is shown in Figure **1.8**. Simply a transistor is an electronic switch. The flow of current in one direction (through the channel, from the source to the drain) can be switched on by the application of a potential perpendicular to the direction of the current flow. This is shown graphically in Figure **1.9** where at a constant source/ drain potential the source/drain current increases with increasing gate potential.

The important characteristics of an idealised transistor are also illustrated by Figure **1.9**. Firstly, there is no source/ drain current (I_{SD}) when the source/drain potential (V_{SD}) is less than the **threshold voltage**, V_T. Then when V_{SD} becomes greater than V_T, I_{SD} increases at first almost linearly with increasing potential. This regime is called the **linear regime** and is illustrated in Figure **1.9** by line 'A'. As V_{SD} increases further I_D tends to level off, and this regime is called the **saturation regime**. It is illustrated by line 'B'.

Two important performance characteristics are also illustrated by Figure **1.9**. The **mobility** (□) of the transistor is a measure of how much current passes through it for every unit of potential applied across it, with units of $cm^2V^{-1}s^{-1}$. The source/ drain current at a given source/drain potential is given by Equation **1.1**:

$$I_{SD} = \frac{W}{2L} C_{ii} \mu (V_G - V_T)^2 \qquad (1.1)$$

W is the width of the channel; L is its length; and C_i is the capacitance per unit area of the insulating layer. It is evident from Equation **1.1** that in order to maximize the current passing through a transistor, μ has to be maximized. The second important performance characteristic is the **on/ off ratio** of the transistor. This is defined as the ratio of V_{SD} when V_G (the gate potential) = 0 (the 'off state) and when $V_G >> 0$ (the 'on' state). Both the mobility and the on/ off ratios often vary with both V_{SD} and V_G so it is important to ensure

that mobilities of different transistors are compared at similar source/ drain and gate potentials.

One final important characteristic of a transistor is whether it carries either holes or electrons. This is reflected by whether the transistor operates at either a positive or negative source/ drain potential. The former is called a **p-type** transistor; the latter is called an **n-type** transistor. If a transistor displays both qualities is termed **ambipolar**.

The transistor plays an important part in many modern technologies. The highest performance transistors are required in computer chips, where methods for the miniaturization of circuitry also play a critical role. Transistors to operate flat-screen liquid crystal displays also require relatively high performance transistors, with mobilities in the region of 0.1 to 1 $cm^2V^{-1}s^{-1}$, on/off ratios of at least 10^6, and low operating voltages. Lower performance transistors can be incorporated into less demanding technologies such as RFID (radio frequency identification) tags. In an RFID tag, in its most basic form, a current induced by an outside electric field passes through a series of transistors. This generates a simple signal such as a binary number that is then transmitted and picked up by a receiver. In this way it is hoped that RFID tags can take the place of barcodes in supermarkets, and can be used to monitor the logistical operations of businesses.

1.4 Organic materials for FETs

Transistors for many years have been synthesised from inorganic substrates. It is important therefore to emphasise where organic substrates might have an advantage over their inorganic counterparts; and it is also important to explore what types of substrate are suitable for exploitation in a transistor.

1.4.1 Inorganic vs. organic materials for FETs [47-50]

The channel material of modern FETs is typically made from hydrogenated silicon (*alpha-Si*). Silicon processing is reliable and silicon-based FETs can be mass-produced. However the silicon used has to be of a very specific composition and this has high processing costs associated with it. Equally the process used to imprint circuitry onto the substrate (lithography) is expensive and requires large-scale production for cost-efficiency. In addition the high processing temperatures required for the deposition of *alpha-Si* (typically 360°C)

means that it is not possible to deposit silicon-based transistors onto a plastic substrate. This unfortunately causes devices incorporating silicon-based FETs to be inflexible.

In theory organic semiconductors overcome all of these problems. Firstly organic materials can be easily purified. Then circuitry can be laid onto the substrate using 'contact printing' rather than by lithography. The organic material can then be applied through an ink-jet printing process. This means that an application can be designed and produced over a short time scale; it means that short-production runs are economically feasible; and most importantly it leads down the road down to low cost electronic devices. Finally organic materials generally do not require a high deposition temperature and therefore can be used in flexible devices, allowing the manufacture of flexible displays. In practice however organic materials are at a substantial disadvantage for use as the channel material because they naturally exhibit lower mobilities than their inorganic counterparts. So the organic material needs to be molecularly engineered to display the desired characteristics. In this way silicon will probably always take pride of place in applications that require high performance transistors; but organic materials have the potential for exploitation in a very wide range of low-cost electronic devices that do not require the same high performance.

The physics of organic and inorganic devices are actually very different. The charge-carrying mechanism in an inorganic semiconductor can be viewed as operating through *delocalized* states and is limited by the scattering of carriers by vibrations in the lattice structure of the substrate. However charge transport in amorphous organic semiconductors can be described by a *localized* model where charge hops from one molecule to the next. This dichotomy in charge-transport mechanisms has important implications. For example it means that in inorganic semiconductors the charge mobility decreases with increasing temperature, whereas in amorphous organic systems it increases with increasing temperature. It is only in highly crystalline organic systems that display mobilities comparable to *alpha-Si* that the distinction between the two mechanisms becomes blurred. A second implication of the localized model is that charge-transport in an organic channel is limited to a layer extending to approximately 5 nm from the semiconductor/ insulator interface rather than charge being carried through the bulk structure[51]. This means that the molecular structure at this interface plays a critical role in the conduction process.

1.4.2 Classes of organic semiconductors [47-50]

Semiconductors can be n-type and/ or p-type. It turns out that most organic semiconductors display solely p-type behaviour under normal conditions. This has been attributed to the trapping of electrons by hydroxyl groups at the (usual) silicon dioxide dielectric/ semiconductor interface so that under normal conditions n-type conduction is not observed (see Friend in *Nature* **434**, 194-199 (10 March 2005));. Therefore all of the mobilities given in the following discussions correspond to p-type conduction.

There are then two ways of depositing an organic semiconductor onto the insulating layer. In the case of **vacuum deposition** the organic material is evaporated and then condensed onto the insulator. Whereas with **solution processing** the organic material is dissolved in solvent and then deposited onto the insulator before the solvent is allowed to evaporate. Vacuum deposition has the advantage over solution processing that it can produce very ordered films with an associated high mobility; however vacuum deposition can be applied only with difficulty to high surface area substrates, and has higher processing costs associated with it. Therefore solution processing would be the preferred method of deposition for commercial applications.

1.4.3 Organic channel materials part i- pentacene

Pentacene is the Rolls-Royce of all organic channel substrates. Vacuum-deposited pentacene films have been shown to be capable of mobilities comparable to those of an inorganic substrate, typically in the order of 1 $cm^2V^{-1}s^{-1}$ [52]. However pentacene itself is not suitable for solution-processing because of its low solubility. One method to attempt to circumvent this problem has been to use a **soluble precursor**. The principle behind this is that the precursor molecule is soluble in common organic solvents and therefore can be deposited from solution onto the insulating layer. Then by heating the system the elimination of a small, volatile molecule converts the precursor molecule into the insoluble substrate. In an example by Klaus Müllen, tetrachlorobenzene can be eliminated to give pentacene[53] (Figure **1.10**). Films of this type have shown mobilities of up to 0.2 $cm^2V^{-1}s^{-1}$ and are now being developed for commercial applications by Philips[54].

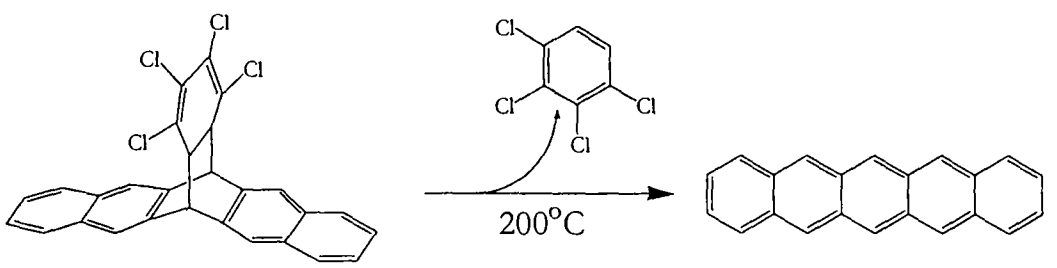

Figure **1.10**- Müllen's precursor route to pentacene.

1.4.4 Organic channel materials part ii- oligo- and poly-thiophenes

Whilst pentacene is the best performing organic molecule in an FET device, the thiophenes are a class of molecule that show great promise. In particular, studying the effect of changing the thiophene's structure emphasises that **molecular morphology** is one of the key factors in determining the mobility of a substrate.

Thiophene polymers are versatile channel materials that can be solubilized by adding alkyl groups to the 3 position of the thiophene ring. Devices incorporating regiorandom poly(3-hexylthiophene) show mobilities in the order of 10^{-4} $cm^2V^{-1}s^{-1}$ [55]. When the hexyl side-chain is replaced by longer alkyl chains this mobility is observed to decrease[56]. In contrast when the regiorandom polymer is replaced by its regioregular counterpart, the mobility is observed to increase up to 0.1 $cm^2V^{-1}s^{-1}$ [57]. This observation can be attributed to the difference in the structure of the films of the regioregular and regiorandom polymers. The regiorandom polymer forms an amorphous film whereas the regioregular polymer can form a well-ordered lamellar structure with an edge-on orientation of the thiophene rings relative to the insulator. This structure is similar to that shown by thin films of pentacene, and it shows the importance of the degree of order in the film's morphology in determining the mobility, especially at the semiconductor/ insulator interface.

Oligothiophenes have also been incorporated into transistors. They are typically substituted at either end of the oligomer by an alkyl chain. These exhibit low solubilities in organic solvents, and whilst they can be solution processed giving mobilities in the order of 10^{-1} $cm^2V^{-1}s^{-1}$ [58], vacuum deposition leads to films with higher mobilities, up to 1 $cm^2V^{-1}s^{-1}$ [59]. It has been shown that increasing the length of the thiophene backbone in these oligothiophene films has little effect on its charge mobility, and that increasing the length of

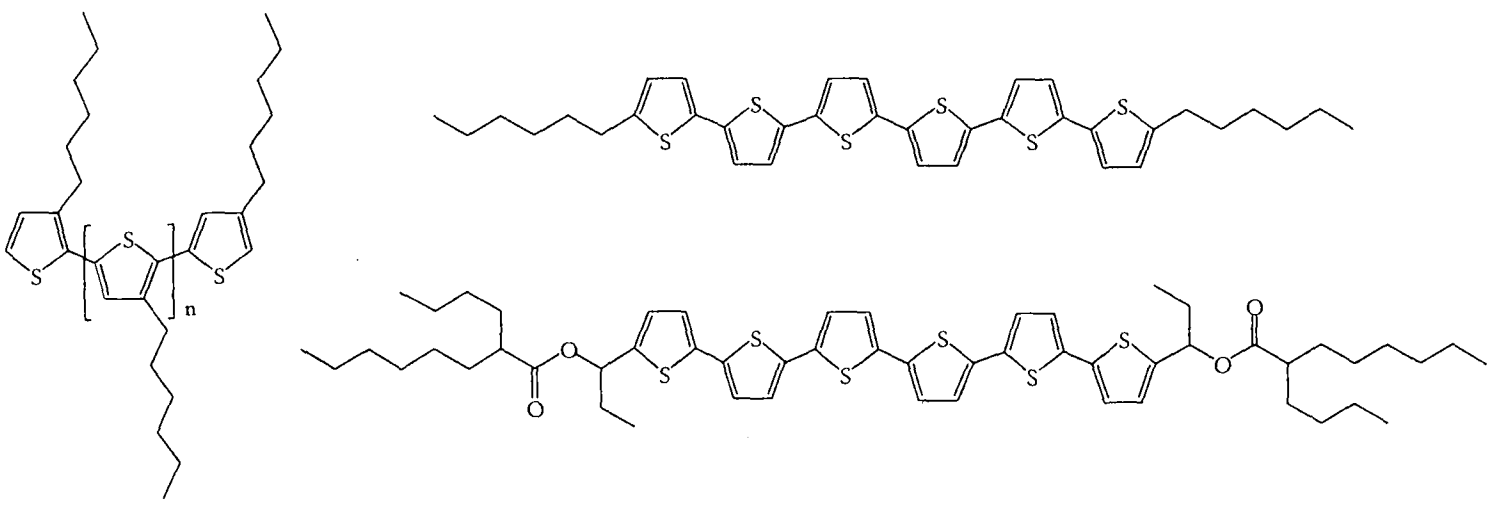

Figure **1.11**- thiophenes used as channel materials. Clockwise from top right- dihexyl-sexithiophene, Fréchet's soluble precursor sexithiophene, and a regioregular polythiophene.

the alkyl substituents also has a limited effect[59]. This again demonstrates that the overriding feature in determining charge mobility is the global molecular organisation rather than the structure of the molecules themselves.

A soluble precursor route to an oligothiophene has also been developed. In this case, retro-ene elimination leads to the desired sexithiophene with a charge mobility of 0.03 $cm^2V^{-1}s^{-1}$ [60].

1.4.5 Organic channel materials part iii- other organic substrates

Tetrapyrrole substrates have also been developed into possible channel materials. Phthalocyanines have demonstrated moderate mobilities[61], but their sensitivity to oxygen makes them difficult to exploit. Porphyrin substrates have also demonstrated moderate to good mobilities[62-64]. The most promising of these approaches is that of Ono[65] who uses a soluble precursor route to thin films of tetrabenzo-porphyrin with a mobility of 10^{-2} $cm^2V^{-1}s^{-1}$. Ono revealed recently[66] that a modification of this procedure (probably with the use of tetranapthyl-porphyrin) can lead to very promising mobilities of over 10^{-1} $cm^2V^{-1}s^{-1}$.

Because mobility depends so much on morphology, it is not surprising that good mobilities can be derived from a liquid-crystalline polymer substrate. When deposited from solution and aligned in its nematic liquid crystal phase, the liquid crystalline polymer illustrated in Figure **1.12** has illustrated promising mobilities of 10^{-2} $cm^2V^{-1}s^{-1}$ parallel to its alignment direct, and 7 to 8 times lower perpendicular to its alignment direction[67].

1.4.6 Problems still to be resolved with organic FETs [47-50]

Whilst the chemist has concentrated on strategies focused on increasing the mobilities displayed by organic channel materials, there are also several operational details that need to

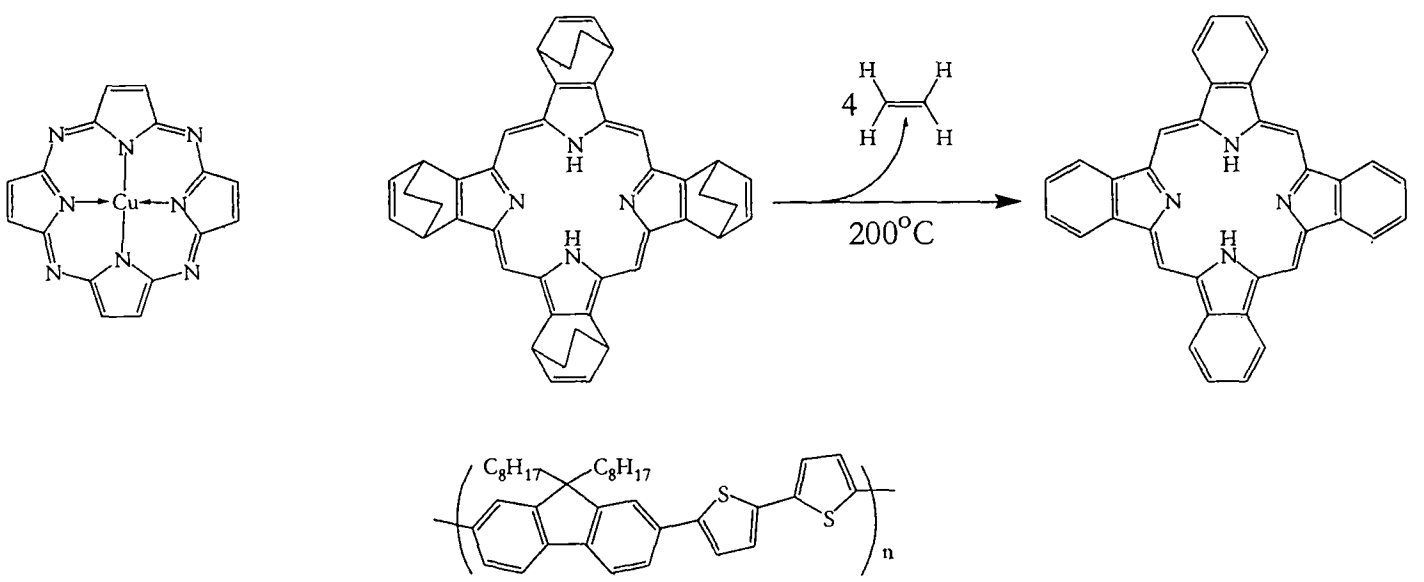

Figure **1.12**- molecules for organic channel materials. Clockwise from top left- copper phthalocyanine; Ono's precursor route to benzo-porphyrins; and a soluble liquid-crystalline polymer.

be overcome before organic channel materials can be seriously commercially exploited. The main one is concerned with the effects of oxygen doping. The reduction potential of molecular oxygen and the oxidation potential of many of these polyaromatic substrates are sufficiently close that doping with oxygen is inevitable. This can lead to an increase in the 'off' current of the device, reducing the on/ off ratio. It can lead to the **drift** of the threshold voltage causing inconsistent device performance. It can also lead to decreased charge mobility by creation of '**traps**' within the substrate that trap charge as it travels across the channel. All these effects serve to reduce the **lifetime** of the device.

An ancillary problem with organic channel materials is the selection of a suitable insulating layer. Equation **1.1** shows that the source/ drain current is directly proportional not only to charge mobility but also to the dielectric of the insulating layer. By using an insulator with a relatively low dielectric such as silicon dioxide, very high operating voltages are required for the desired device performance. Hence different dielectrics have been developed to improve device performance. These have included self-assembled monolayers of hydrocarbons on silicon[68,69] and thin films of metal oxides such as barium zirconate titanate[70].

A final problem with the use of organic channel materials is that in order to gain maximum performance they need to be of very high purity. Small impurities create traps within the device, and therefore methods for the synthesis of ultra-high pure substrates also need to be considered.

1.5 'Single molecule' devices

There has been some surprise that such a simple molecule as pentacene has consistently given rise to the highest charge mobilities of all organic substrates. To improve on pentacene, it has been suggested[47] that systems need to be molecularly engineered to build in the desired characteristics. One conceivable method of achieving this would be through the self-assembly of a molecular architecture incorporating strong intermolecular interactions. A rigid crystalline structure could increase the magnitude of intermolecular interactions and therefore decrease the barrier to intermolecular charge transfer. A second conceivable method would remove the requirement of unpredictable intermolecular charge transfer by spanning the source and drain by a single array of charge carriers. In this way intermolecular transport is replaced by intramolecular transport.

This second idea has received a significant amount of attention and the term 'single molecule device' is used to describe this concept. This can be achieved either by spanning the electrodes with a very large, structurally defined molecule or by making the electrodes so close to one another that they can be spanned by a single molecule. In this way a carbon nanotube[71,72], C_{60}[73], a di-vanadium[74] and a cobalt[75] complex, a series of oligothiophenes[76] and a phenylenevinylene oligomer[77] have all been used to span two electrodes. Electrical conduction through Osuka's two types of porphyrin arrays has also been demonstrated[78]. His directly singly-linked porphyrin array shows semiconductor characteristics; whereas his triply-linked porphyrin array shows electrical conductance. It would therefore be conceptually interesting to consider whether the use of porphyrin arrays in 'single molecule devices' can be further extended to understand more deeply the factors affecting semiconductor behaviour.

1.6 Porphyrin arrays for FET devices- β-pyrrolic vs. meso-coupling

Single porphyrins have shown themselves to be very apt substrates for exploitation in FETs. However porphyrin arrays in theory should be even better substrates for two principle reasons:

- High charge mobility in an FET requires a high degree of intermolecular order. By joining individual porphyrin units together in a porphyrin array, this order is already imposed upon the system. Hence any hole or electron passing between source and drain will spend an increased amount of time travelling in an intramolecular manner as compared to single porphyrin units.
- Any electronic delocalization along an array will also facilitate the intramolecular passage of electrons and holes.

However a couple of disadvantages can also be considered for the incorporation of a porphyrin array into an FET:

- The extension of a delocalised system will lower its HOMO-LUMO gap. This can have adverse consequences because it can encourage doping of the system by molecular oxygen.
- And a porphyrin array with high polydispersity could also lead to impaired device performance.

Therefore the correct type of porphyrin array has to be selected in order to exploit the advantages of using a porphyrin array in a FET, whilst minimizing the impact of the disadvantages.

Non-covalently bonded arrays would be considered unsuitable for exploitation in an FET device because the non-covalent character of the linkages might not predictably provide the desired degree of high intermolecular order. Equally polymeric structures, although interesting, would not provide the desired electronic properties. Instead covalently-linked porphyrin arrays will provide the desired degree of intramolecular order.

Covalently-linked porphyrin arrays can be joined either through their β-pyrrolic or meso positions. These two points of attachment lead to different electronic properties of the resulting arrays, principally because of the different delocalization properties of the linkages. This has been examined by Therein[79,80] in a series of ethylene- and butadiyne-linked porphyrin dimers, and he concluded that the order of electronic communication between the porphyrins depended on the position to which the bridging unit was attached as follows:

$$\beta\text{-}\beta < \beta\text{-meso} < \text{meso-meso}$$

This can be explained in terms of Gouterman's four orbital HOMO-LUMO model (see Appendix One) where the majority of the electron density is placed on the porphyrin's meso position. In exploitation in an FET, some delocalization within the array is desirable but too much will lead to oxidative doping of the device. In this way a β-β linked array would serve as a good starting point for the examination of porphyrin arrays in transistors.

Finally, arrays linked through more than one position will be superior to singly linked arrays. The rigidity that this should provide to the array's structure will result in a higher degree of intramolecular order than an array with adjacent porphyrins linked through a single position.

Crossley's tetraazaanthracene-bridged porphyrin arrays (see Section **1.2.4**) fulfil all the desired characteristics described above. They are expected to be structurally rigid, whilst the double β-pyrrolic linkages have been said to provide some delocalization between neighbouring porphyrin units. However they do not appear to provide the extent of delocalization exhibited in Osuka's triply-linked arrays, which would almost certainly lead to a significant amount of oxidative doping. Equally they can be constructed in an iterative manner leading to a low polydispersity in the oligomers.

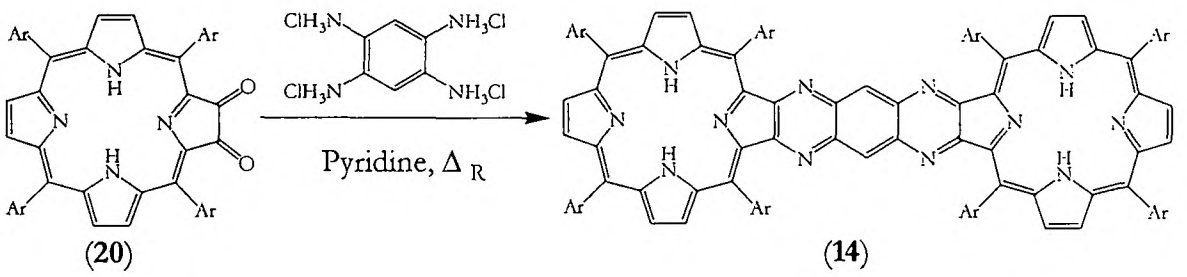

Figure **1.13**- synthesis of the 1,4,5,8-tetraazaanthracene bridge. Ar= 3,5-di-*tert*-butylphenyl.

Crossley's tetraazaanthracene-bridged porphyrin systems also fulfil the requirements for a single molecule device. Structural rigidity in an extended porphyrin array would mean that these molecules might usefully span the electrodes of a practical device.

1.7 Tetraazaanthracene-bridged porphyrin systems

Crossley's tetraazaanthracene-bridged porphyrin systems would certainly be conceptually interesting to study in a field-effect transistor. However these systems are difficult to synthesise as there are a limited number of routes to the monomer units.

1.7.1 Formation of the 1,4,5,8-tetraazaanthracene bridge

Crossley's tetraazaanthracene-bridged system is constructed by the condensation of two porphyrin *alpha*-diones with benzene-1,2,4,5-tetraamine[35] (Figure **1.13**). This reaction is in fact a two step reaction. The first step is fast and involves the condensation of the first porphyrin *alpha*-dione with 1,2,4,5-tetraaminobenzene. The solvent (pyridine) serves not

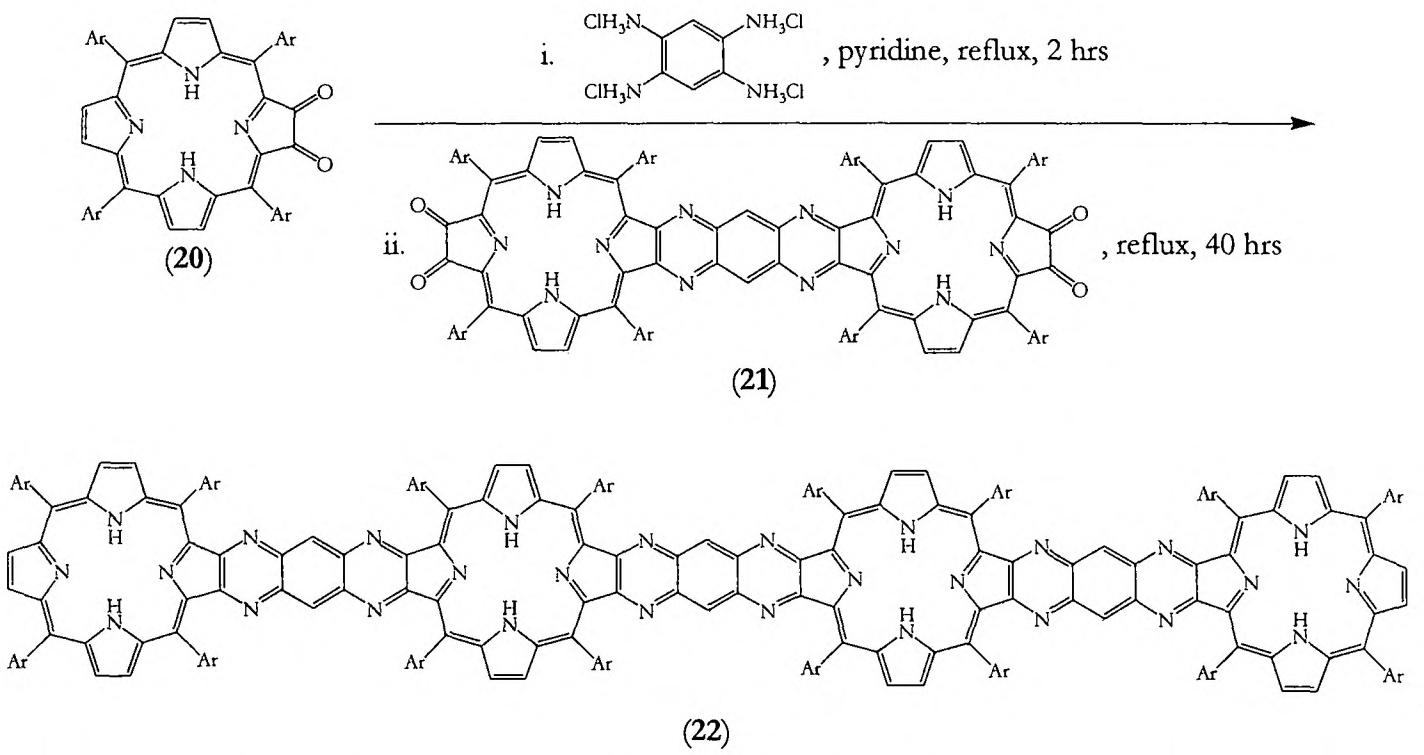

Figure **1.14**- Crossley's porphyrin array. Ar = 3,5-di-*tert*-butylphenyl.

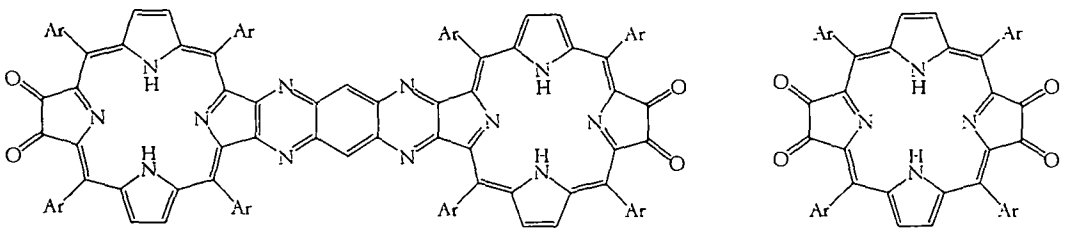

(21) (23)

Figure **1.15**- monomer units required for the synthesis of an extended porphyrin array. Ar= 3,5-di-*tert*-butylphenyl.

only to solvate the porphyrin but also to deprotect the tetraamine *in situ*. The second step is slow and involves the condensation of the intermediate porphyrin diamine to a second porphyrin *alpha*-dione[81]. This two step reaction can be turned into a two step procedure in which the intermediate porphyrin diamine can be isolated in the middle of the reaction; this can then be condensed in a different solvent (toluene) with a second equivalent of porphyrin *alpha*-dione[82]. This modification to a two step procedure is important as it allows the selective formation of bridging units between non-equivalent porphyrins.

Crossley and Burn extended this methodology to the formation of a tetrakis porphyrin array. For this a porphyrin tetra-one unit was required to build up the array from both ends at once[36] (Figure **1.14**). For the construction of an extended porphyrin array based on this methodology it follows that a porphyrin tetra-one unit is required (Figure **1.15**).

1.7.2 Routes to porphyrin *alpha*-diones

The synthesis of a porphyrin *alpha*-dione is a relatively simple, high-yielding procedure. Three viable routes have been explored and are examined in Figure **1.16**. The first and most recent route involves the dihydroxylation of tetraphenyl-porphyrin with osmium tetroxide[83-85]. This obtains the porphyrin *alpha*-dione in 50% yield over two easy steps and is therefore a favoured route of porphyrin functionalization. However the toxicity of osmium tetroxide and the fact that it is used in a stoichiometric quantity means that this method is not practical for a large scale preparation of the porphyrin *alpha*-dione.

The second and third routes to porphyrin *alpha*-diones both start off with the nitration of a metallated porphyrin. The second route then adapts Knudsen's hydroxylation of a nitro-arene by the benzaldoxime anion[86] to this nitro-porphyrin to produce the hydroxy-porphyrin. This is then oxidized in its free-base form to the porphyrin *alpha*-dione either by the Dess-Martin periodinane[87] or in its copper form by photochemical means[88]. The third route reduces the free-base nitro-porphyrin to the amino-porphyrin; this is then oxidized in a

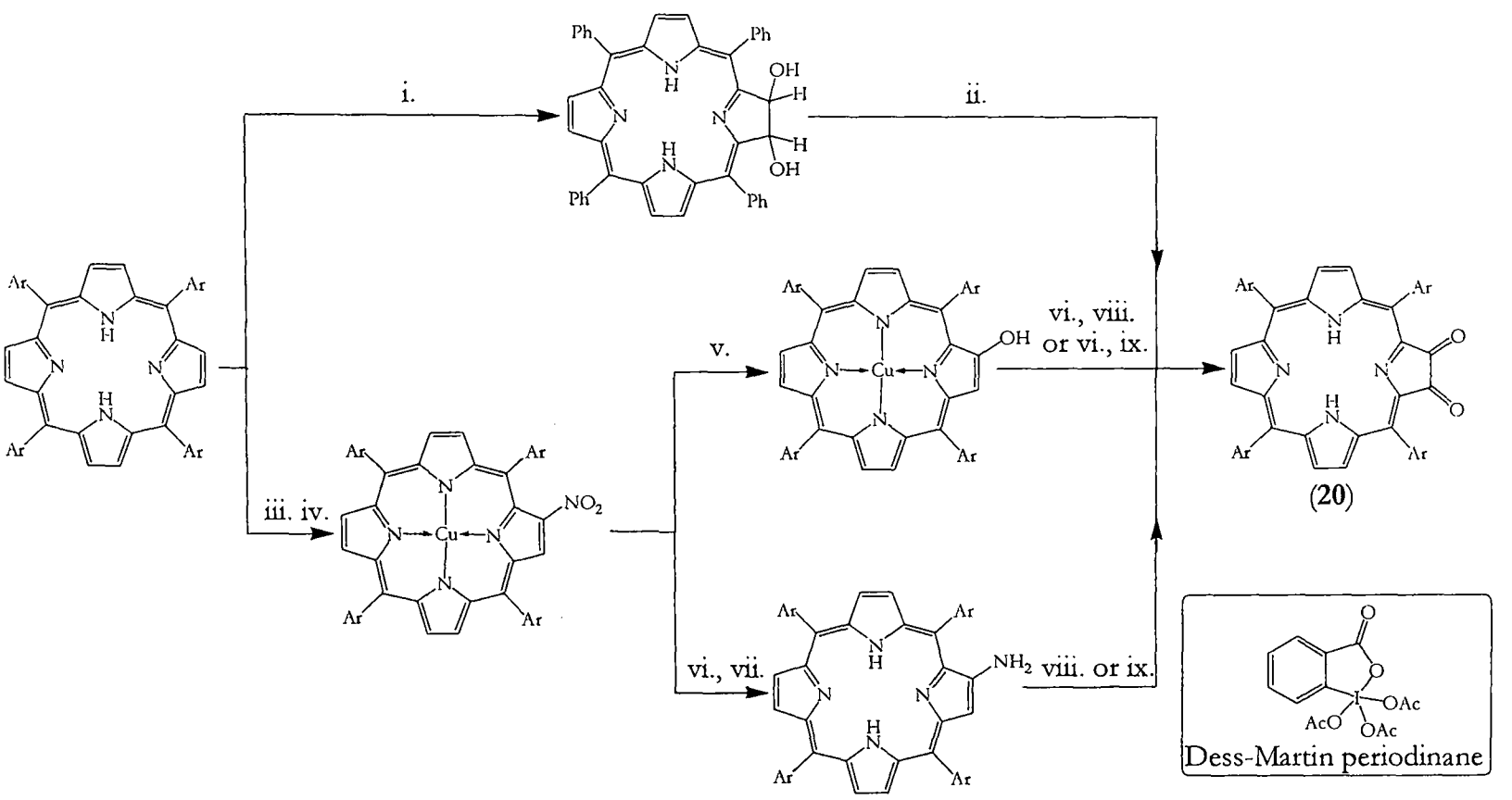

Figure **1.16**- routes to porphyrin *alpha*-diones. i. 1 eqv. OsO_4, pyridine, $CHCl_3$, then H_2S; ii. DDQ, C_6H_6, Δ_R; iii. $Cu(OAc)_2$, CH_2Cl_2/ CH_3OH, Δ_R; iv. NO_2 in light petroleum, CH_2Cl_2; v. 11 eqv. benzaldehyde oxime, 10 eqv. NaH, $(CH_3)_2SO$/ tetrahydrofuran, Δ_R; vi. conc. H_2SO_4, CH_2Cl_2; vii. $SnCl_2{\cdot}2H_2O$, conc. HCl, CH_2Cl_2; viii. 1 eqv. Dess-Martin periodinane, CH_2Cl_2; ix. O_2, Rose Bengal, CH_2Cl_2. The structure of the Dess-Martin periodinane is also illustrated. Ar = 3,5-di-*tert*-butylphenyl.

similar manner to the hydroxy-porphyrin[89,90]. Both of these routes obtain the porphyrin *alpha*-dione in around 50% yield; and both routes should be applicable for a large scale preparation of the *alpha*-dione.

1.7.3 Routes to porphyrin and bis-porphyrin tetra-ones

So the routes to porphyrin *alpha*-diones are relatively well-established, successful and high-yielding; however current routes for the synthesis of a porphyrin tetra-one are not. This can be attributed to one reason. **Most functionalizations at the β-pyrrolic positions require the use of a metallated porphyrin, as this allows preferential reaction of the β-pyrrolic positions over the meso positions.** Hence in order to successfully nitrate a porphyrin at its β-pyrrolic positions a metal has to be coordinated at its centre. **However in order to obtain the regiospecific antipodal di-functionalization of the porphyrin, i.e. the functionalization of the pyrroles across from one another in the porphyrin macrocycle, a free-base porphyrin is required.**

This dichotomy is exemplified by two routes to porphyrin tetra-ones, outlined in the top half of Figure **1.17** and in Figure **1.18**. The first adapts a route already established for the

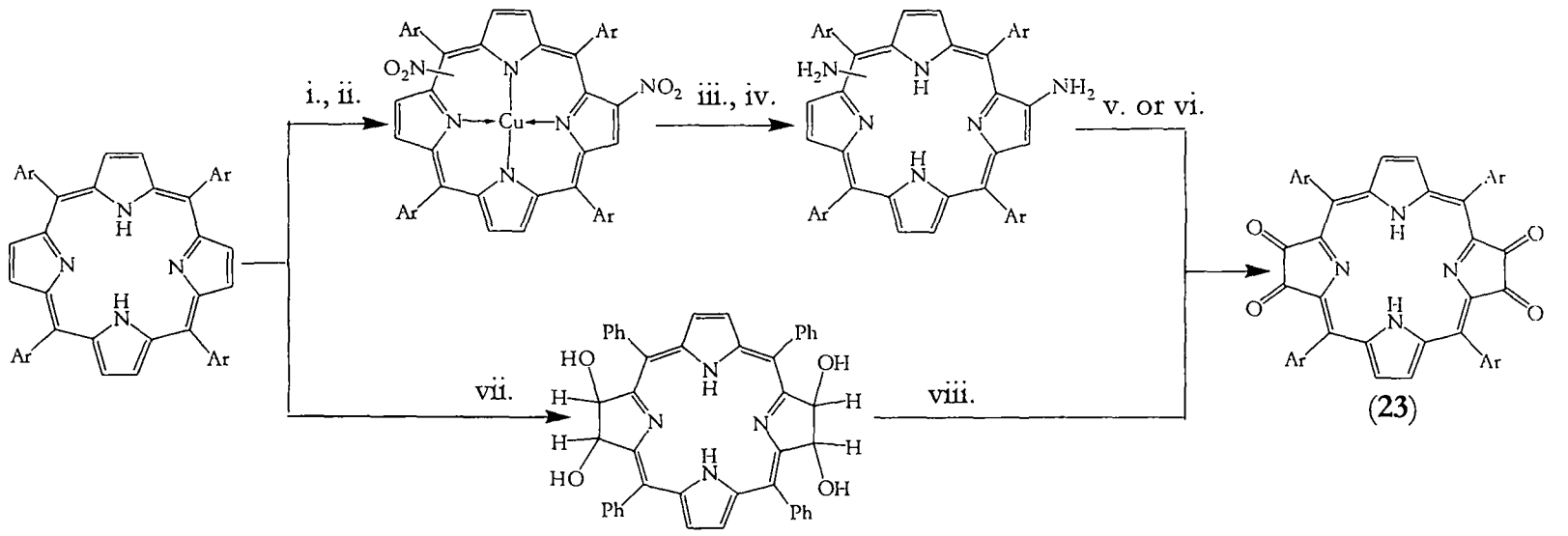

Figure **1.17**- routes to the single porphyrin tetra-one and its conversion into the porphyrin tetra-one. i. $Cu(OAc)_2$, CH_2Cl_2/ CH_3OH, Δ_R; ii. 2 eqv. NO_2 in light petroleum, CH_2Cl_2; iii. conc. H_2SO_4, CH_2Cl_2; iv. $SnCl_2{\cdot}2H_2O$, conc. HCl, CH_2Cl_2; v. 2 eqv. Dess-Martin periodinane, CH_2Cl_2; vi. O_2, Rose Bengal, CH_2Cl_2; vii. 2 eqv. OsO_4, pyridine, $CHCl_3$, then H_2S; viii. IBX, $(CH_3)_2SO$, 50°C. Ar = 3,5-di-*tert*-butylphenyl.

synthesis of porphyrin *alpha*-diones. Di-nitration followed by reduction and oxidation can lead to the desired porphyrin tetra-one[82,89]. This is a short route, involving only five steps. However in the second step the addition of the second nitro group occurs essentially with

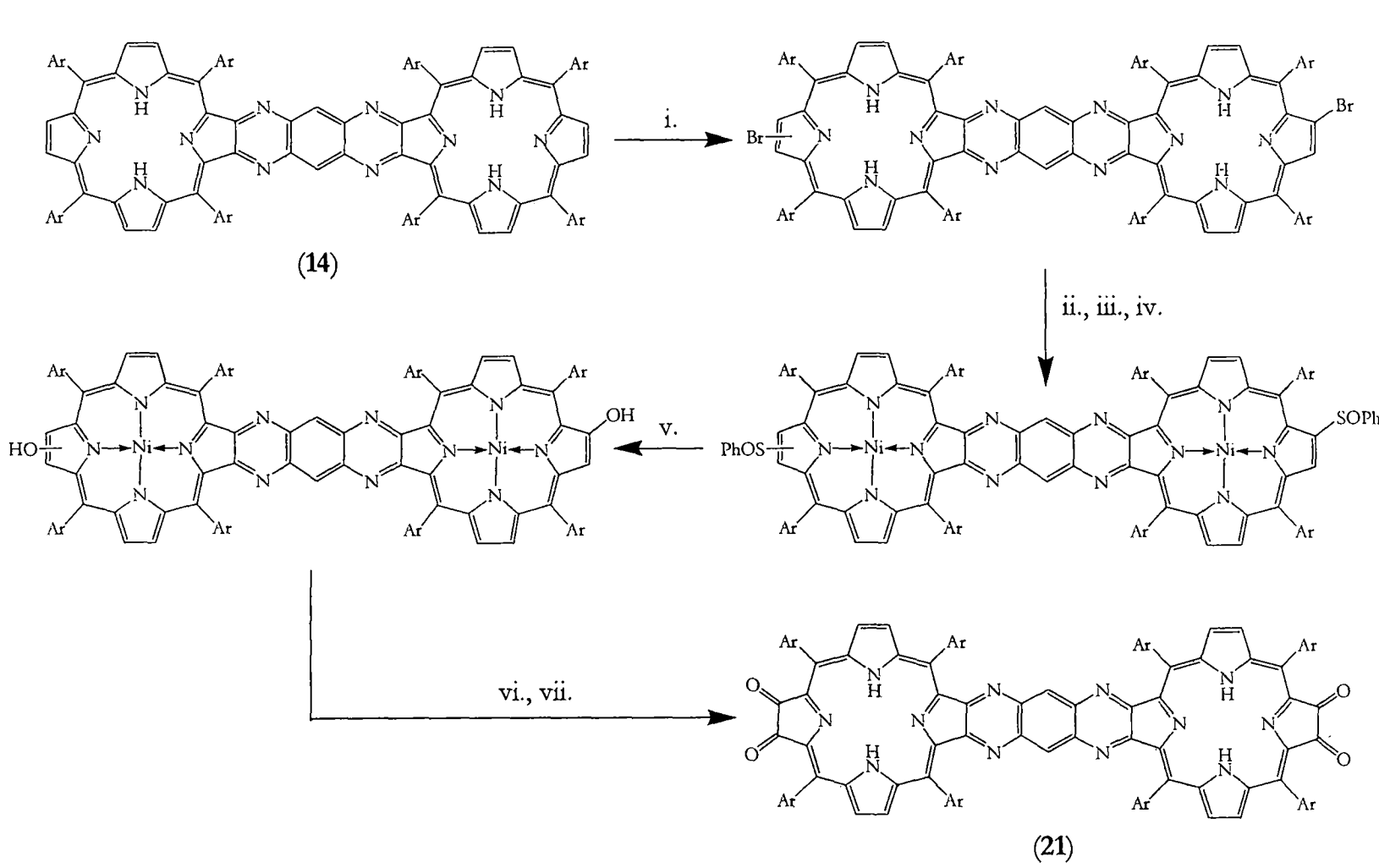

Figure **1.18**- the functionalization of a bis-porphyrin. i. 2.2 eqv. *N*-bromosuccinimide, $CHCl_3$, Δ_R; ii. $Ni(OAc)_2$, *N*,*N*-dimethylformamide, Δ_R; iii. PhSH-LiOH, *N*,*N*-dimethylformamide, 117°C; iv. CH_3CO_3H, toluene; v. benzaldehyde oxime, NaH, $(CH_3)_2SO$, 135°C; vi. H_2SO_4, CH_2Cl_2; vii. SeO_2, dioxane, Δ_R. Ar = 3,5-di-*tert*-butylphenyl.

no regiospecificity with respect to the first; and this leads to a low overall yield of the porphyrin tetra-one, a reported 15 to 20% yield from the unfunctionalized porphyrin.

The second route is shown in Figure **1.18** and takes the opposite approach[36]. Regiospecific functionalization is achieved by bromination of the free-base bis-porphyrin. However much functional group manipulation is required before the desired tetra-one functionality is achieved; so much so that a total of 7 steps is required and the overall yield for the transformation is only 7%. Therefore the advantage of the regiospecific functionalization is negated by the length of the synthesis.

A third route is shown in the second half of Figure **1.17**[91]. This consists of a simple two step procedure with an acceptable overall yield of transformation (12%). Therefore this would be the preferred route of synthesis of the porphyrin tetra-one if it was not for the fact that it involves the stoichiometric use of OsO_4; and again osmium's toxicity therefore it makes it impractical for a large-scale synthesis.

1.7.4 Requirements for a successful new route to porphyrin tetra-ones

So each of the current routes to porphyrin tetra-ones have their drawbacks. For a successful new route, an initial regiospecific functionalization is required. This implies that the initial functionalization has to be on the free-base porphyrin. In addition this regiospecific functionalization needs to introduce a functionality that can be transformed into a porphyrin *alpha*-dione over a small number of steps in order to maximize yields.

1.8 Aims

It is therefore the aim of this thesis to:

- to explore new methodology for the efficient synthesis of the monomer units of 1,4,5,8-tetraazaanthrancene-bridged porphyrin arrays;
- to extend this array as far as the available methodology will allow;
- and to evaluate the viability of exploiting these arrays in FET devices.

Chapter Two

Regiospecific halogenation of a porphyrin

Chapter Two
Regiospecific halogenation of a porphyrin

Any new useful route to porphyrin *alpha*-diones must involve an initial regiospecific functionalization of the porphyrin and a minimal number of steps to obtain the desired *alpha*-dione. A proposed new route that has the potential to fulfil these criteria is shown in Figure **2.1**.

The functionalization involves the regiospecific halogenation of a porphyrin, followed by the nucleophilic displacement of the halogen by the benzaldoximate anion and oxidation to the required *alpha*-dione. This is a modification of a method described by Crossley[88] who has already shown that the benzaldoximate anion can be used to displace a bromine substituent on the porphyrin periphery. However this displacement was not successful on functionalized porphyrins because of their apparent poor solubility in dimethyl sulphoxide (DMSO). This was the explanation of why, in order to successfully synthesize the bis-porphyrin tetra-one **21**, the initial antipodal functionalization of the bis-porphyrin with bromine was followed by a series of functional group manipulations in order to obtain a system that is soluble in DMSO (see Figure **1.18**). Recently however it was shown by Burn[87] that the solubility of the substrate could be increased by using a 1:1 solvent mixture of DMSO and tetrahydrofuran (THF).

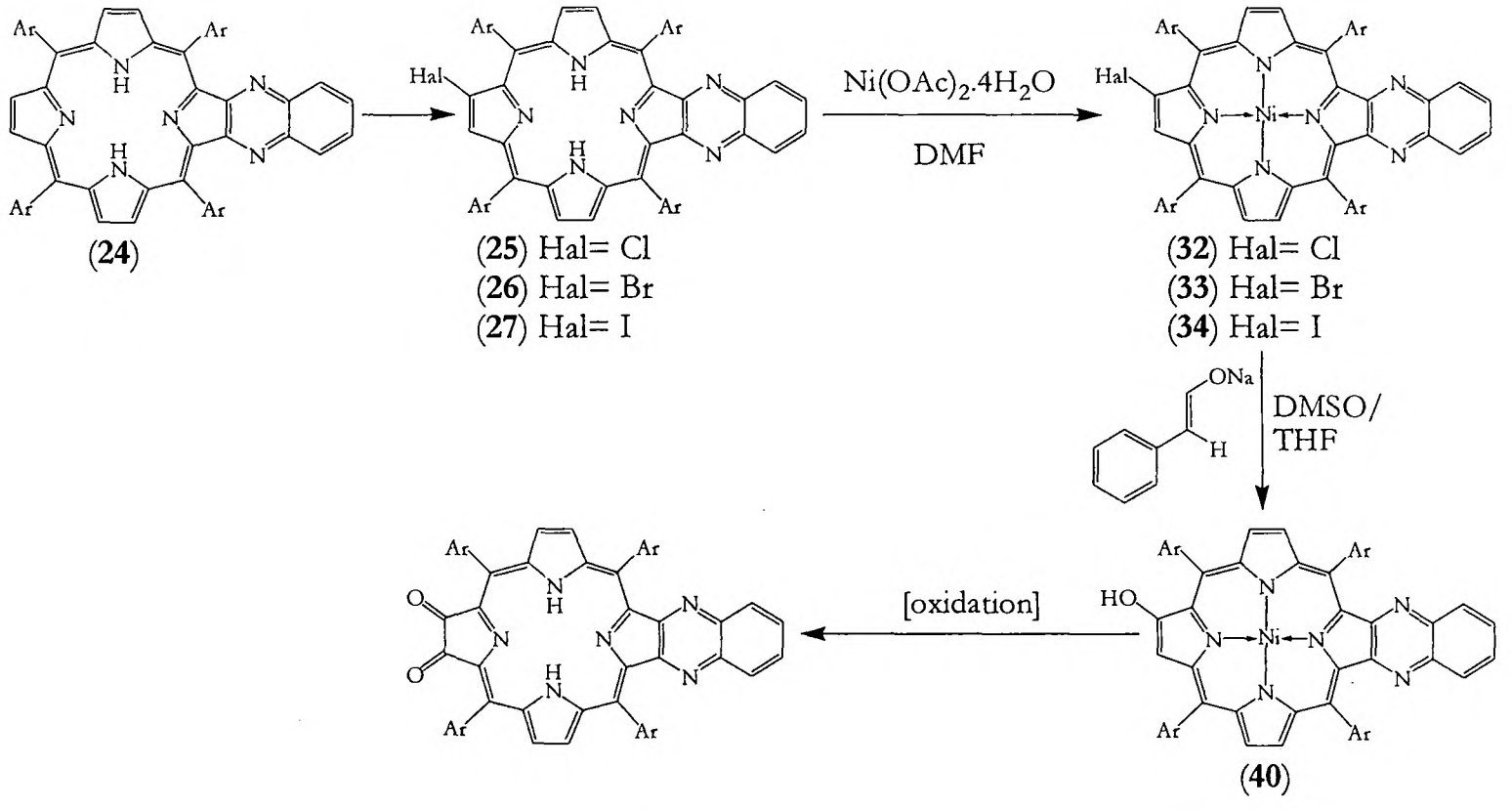

Figure **2.1**- proposed new regiospecific functionalization of a porphyrin. Ar = 3,5-di-*tert*-butylphenyl.

The porphyrin unit chosen for initial investigation of this functionalization is the [2,3-b]-quinoxalino-porphyrin **24**, quinoxaline for short. This is because in the past it has served as a model system for the bis-porphyrin **14**[88], so that any methodology developed for the synthesis of the quinoxaline *alpha*-dione might then be applied to the bis-porphyrin **14**.

This chapter will concentrate on the initial regiospecific functionalization of both the quinoxaline **24** and the bis-porphyrin **14**; Chapter Three will describe the attempted nucleophilic displacement of the halogen by the benzaldoximate anion.

2.1 Regiospecific functionalization of a porphyrin

There are very few methods currently available for the regiospecific functionalization of the porphyrin periphery[92]. This is because the vast majority of porphyrin functionalizations are carried out on metallated systems[92]. For example it would be desirable to attempt the di-nitration of a free-base porphyrin system and see whether antipodal functionalization could be achieved. However successful nitration on a free-base porphyrin has only been reported twice under very specific conditions[93,94]. A simple attempt to replicate one of these nitration procedures[94] on the quinoxaline **24** using I_2/ $AgNO_2$ in dichloromethane/ acetonitrile failed with only recovery of starting material (36%).

Apart from the reductive processes leading to chlorins discussed in Section **4.1**, the only standard route to regiospecifically functionalized porphyrins is through their halogenation. Callot[95], Crossley[96] and other workers[97-99] have demonstrated the regiospecific bromination of the simple porphyrin at its antipodal positions (Figure **2.2**). Meanwhile, the regiospecific chlorination of the free-base porphyrin with *N*-chlorosuccinimide required much harsher conditions with the use of the high boiling-point 1,2-dichloroethane as the solvent[100]. Chlorination at antipodal meso positions has also been observed with octaethylporphyrin[101]. Regiospecific iodination has not been previously demonstrated.

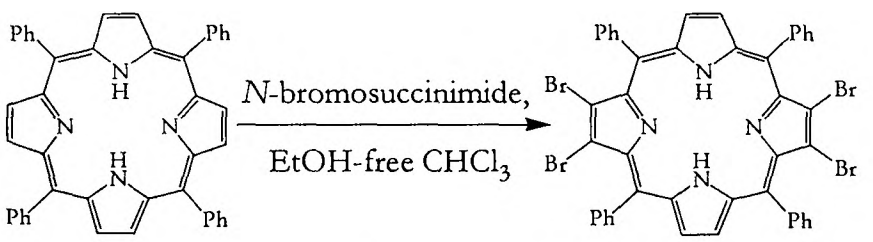

Figure **2.2**- Crossley's regiospecific bromination of a porphyrin at antipodal positions.

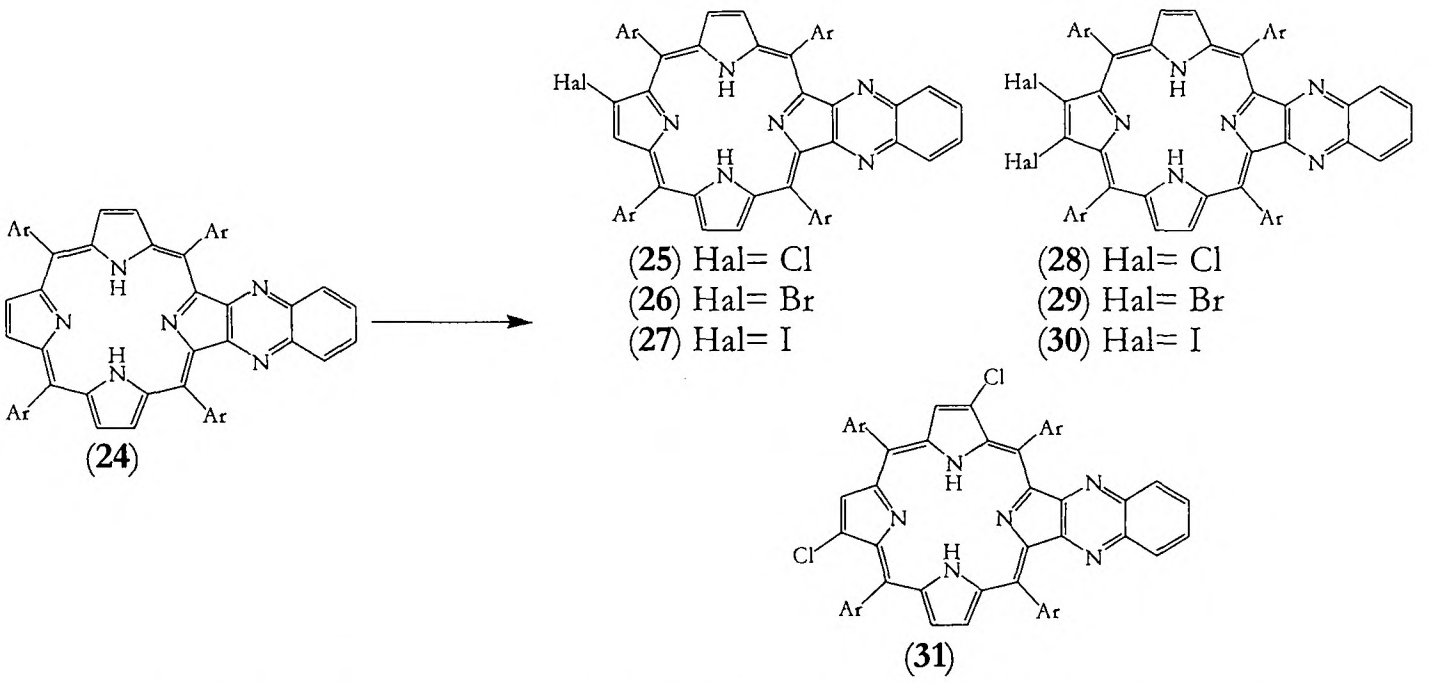

Figure **2.3**- the halogenation of the quinoxaline **24**. Ar = 3,5-di-*tert*-butylphenyl.

2.2 Halogenation of a porphyrin

2.2.1 Bromination

Regiospecific bromination of the porphyrin was repeated for the present system. A critical factor in the repetition of these results was to ensure that the chloroform solvent was ethanol-free, otherwise very little reaction was evident. Results are summarized in Table **2.1**.

2.2.2 Iodination

Since *N*-bromosuccinimide proved successful in the bromination of **24**, iodination was initially attempted using *N*-iodosuccinimide in chloroform (entry 1 in Table **2.2**). However reaction in chloroform proceeded only with a 9% recovery of *chlorinated* product **25**, presumably originating from direct reaction with the solvent. Changing the solvent to dimethyl formamide (DMF) did lead to isolation of iodinated product, but only in 8% yield (entry 2 in Table **2.2**). Therefore another reagent was sought.

	Isolated yields (%)		
Equivalents of *N*-bromosuccinimide	Unsubstituted quinoxaline **24**	12-bromo-quinoxaline **26**	12,13-dibromo-quinoxaline **29**
1.1	10	78	10
2.5	-	-	99

Table **2.1**- product distribution for the bromination of the free-base quinoxaline **24**. Reactions were carried out at a concentration of *N*-bromosuccinimide of below 15 mmoldm^{-3} and at reflux in chloroform for 2 hours.

Reagent (equivalents)	**Concentration of reagent** (mmoldm^{-3})	**Solvent**	**Isolated yields (%)** Unsubstituted quinoxaline **24**	12-iodo-quinoxaline **27**	12,13-diiodo-quinoxaline **30**
N-iodosuccinimide (5.3)	17	chloroform	58	*	-
N-iodosuccinimide (7.8)	30	DMF	55	8	-
iodine (5.7)	24	chloroform	82	11	-
iodine (4.7)	17	DMF	75	20	-
iodine (25.8)	340	DMF	36	47	15

Table **2.2**- attempted iodination of the free-base quinoxaline **24**. *- 9% 12-chloro-quinoxaline **25** was isolated. Reactions with *N*-iodosuccinimide were carried out at reflux for over 12-46 hours; reactions with iodine were carried out at reflux for 5-7 hours.

One method useful for iodination at the meso positions of meso-unsubstituted free-base porphyrins is to use iodine[102]. When the meso-tetraaryl-substituted quinoxaline **24** was heated with iodine in chloroform only 11% of regiospecifically iodinated product **27** was isolated (entry 3 in Table **2.2**). The yield of the iodinated product **27** could be slightly improved by using the higher-boiling point DMF as the solvent (entry 4 in Table **2.2**). More usefully a large improvement in product yields could be obtained by using less solvent and more reagent, so that 47% of 12-iodo-quinoxaline could be isolated (entry 5 in Table **2.2**). In addition a further 15% of product (**30**) resulting from di-iodination of a single pyrrole was isolated, the first time that this kind of product has been reported from the direct iodination of a porphyrin. This kind of highly-iodinated product might be useful for exploitation in optical-limiting applications[103] where the substitution of heavy atoms onto the porphyrin is beneficial as heavy atoms increase the population of the porphyrin's triplet excited state on photoexcitation, and consequently the associated lifetime of the excited state.

The regiospecifity of iodination was assigned by analogy with the brominated products. In addition for both the mono-iodo- and di-iodo-quinoxalines **27** and **30** the regiochemistry could be directly elucidated in the ^{1}H NMR by the NH coupling pattern with the β-pyrrolic protons, in a similar manner to that described in Appendix One. A C_{2v} symmetry is also required to explain the β-pyrrolic region of the di-iodo-quinoxaline **30**.

2.2.3 Chlorination

As regiospecific chlorination of tetraphenyl-porphyrin has already been demonstrated[100] with *N*-chlorosuccinimide, this reagent was applied to the present quinoxaline system. Results are shown in Table **2.3**. Very little reaction was observed in chloroform (entry 1 in Table **2.3**) so

Reagent (equivalents)	**Concentration of reagent** (mmoldm^{-3})	**Solvent**	**Isolated yields (%)** Unsubstituted quinoxaline **24**	12-chloro-quinoxaline **25**	12,13-dichloro-quinoxaline **28**
N-chlorosuccinimide (4.6)	20	chloroform	71	8	-
N-chlorosuccinimide (4.5)	20	DMF	37	25	10
N-chlorosuccinimide(7.9)	29	DMF	4	6	-
N-chlorosuccinimide (4.6)	24	chloroform+ 5% pyridine	18	30	9 (*)
ICl (2.4)	6	chloroform	-	93	-

Table **2.3**- product distributions from the attempted chlorination of the quinoxaline **24**. The first two entries were heated to reflux for 20 hours; the third entry for 3 hours; and the fourth entry for 4 hours. *- a non-regiospecific dichlorinated product was also isolated.

the solvent was replaced by the higher boiling-point DMF. This did succeed in giving a greater yield of chlorinated products (entry 2 in Table **2.3**), but increasing the concentration of the reagent in order to try to encourage even further reaction resulted in very little isolation of any product on purification (entry 3 in Table **2.3**). This has previously been observed for reactions with *N*-bromosuccinimide and has been attributed to the bromination of the inner nitrogens and reaction with a second reagent molecule[102]. Hence a different solvent system was sought. It was found that chlorination proceeded to a reasonable extent in a chloroform/ pyridine mixture (entry 4 in Table **2.3**). Unfortunately the unregiospecific 7,13-chloro-quinoxaline **31** product was also isolated in a 5% yield.

Because of this unpredictability in using *N*-chlorosuccinimide, an alternative chlorination reagent was sought. A variety of reagents have been used in the chlorination of porphyrins[92], but many of them are incompatible with the free-base porphyrin. For example a metallated porphyrin can be chlorinated by molecular chlorine in conjunction with a Lewis acid catalyst ($FeCl_3$)[104,105], but if this was to be attempted on the free-base system metallation of the porphyrin by $FeCl_3$ would result. One functionalization that is compatible with a free-base porphyrin has been described by Dolphin[106]. He suggests that iodine monochloride (ICl) can be used to chlorinate the meso positions of porphyrins, so this methodology was now applied to the chlorination of the β-pyrrolic positions. Indeed, it was found that ICl regiospecifically introduces a chlorine substituent onto the quinoxaline with an exceptionally high yield of 93%.

^{1}H NMR was used to confirm the regiospecifity of all the chlorinated products, in a similar manner to that already described for the iodinated products. In addition an NOE difference

experiment confirms the regiochemistry of the 7,13-dichloro-quinoxaline **31**. An NOE was observed between the β-pyrrolic protons and the C(2)H and C(6)H protons of the closest meso-aryl ring. Two singlets are observed in the β-pyrrolic region of the ^{1}H NMR of **31**, and these share an NOE with a single C(2)H and C(6)H resonance. The only structure consistent with this observation is the 7,13-dichloro derivative.

2.2.4 Application to a bis-porphyrin

In order to demonstrate the utility of the new methodologies to the possible synthesis of the bis-porphyrin tetra-one **21**, the chlorination of the bis-porphyrin with ICl was attempted. It was found that a good yield of dichlorinated bis-porphyrin could be easily obtained from the bis-porphyrin **14** (64%) by refluxing in chloroform with 5 equivalents of ICl. The regiospecifity of the product could not be definitively established because of the complicated nature of its ^{1}H NMR. However the singlet at 8.65 ppm can be reasonably assigned to the C(3) and the C(22) or C(23) protons. It does not show any coupling with the NH protons so it is thought that the regiospecifity shown in Figure **2.4** is correct. The complicated nature of the ^{1}H NMR is not unexpected as it exists as an equimolar mixture of two isomers. In addition the bromination of the bis-porphyrin system with *N*-bromosuccinimide in chloroform, as reported by Crossley[96], was repeated successfully.

2.2.5 Metallation of the halo-porphyrins

It was found that all the halo-quinoxalines could be metallated in good yield by heating with an excess of nickel diacetate in DMF under similar conditions as described for the metallation of the bromo-quinoxaline **26**[81,96].

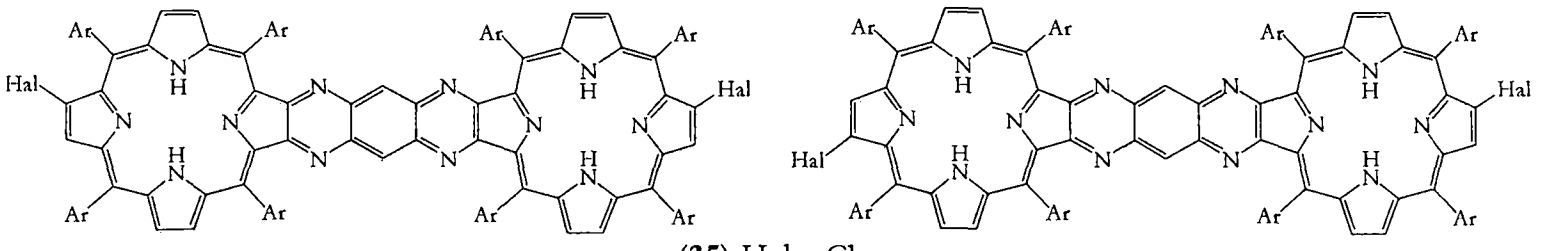

(**35**) Hal= Cl
(**36**) Hal= Br

Figure **2.4**- structures of the two antipodal-functionalized dihalo-bis-porphyrin isomers. Ar= 3,5-di-*tert*-butylphenyl.

2.3 Conclusions and discussion of factors favouring halogenation

It is clear that the regiospecific functionalization of the quinoxaline **24** can now be achieved relatively easily and reliably. Chlorination is achieved with ICl, bromination with *N*-bromosuccinimide and iodination with iodine. In addition these results reflect something about the wider chemical behaviour of porphyrins.

2.3.1 Regiospecifity of functionalization

The assumption that free-base porphyrins will react regiospecifically has been shown not to be valid in all cases. Thus whilst no unregiospecific product is isolated from the reaction of the quinoxaline **24** with either *N*-bromosuccinimide or iodine, reaction with *N*-chlorosuccinimide is shown to be unregiospecific with respect to the substitution of a second chlorine atom onto the porphyrin. The observed regiospecifity of halogenation has previously been explained by a 'delocalization pathway' argument[92,107]. Although simplistic and somewhat naive, properly interpreted this can provide an intuitive understanding of the origin of the regiospecifity. The 18 electron system illustrated on the left of Figure **2.5** is considered to impart the majority of the aromaticity to the free-base porphyrin, and therefore the formation of an intermediate that interrupts this system will be energetically disfavoured over an intermediate that does not interrupt this system. In this way, reaction at the non-protonated pyrroles is favoured. In a metallated porphyrin however, the system that imparts the aromatic stabilization energy to the macrocycle is considered to be closer to that shown on the right of Figure **2.5**, and therefore reaction at all the pyrroles involves roughly an equal energetic cost.

Ideally, further understanding of the factors affecting halogenation would be derived from a full frontier molecular orbital treatment of the porphyrin system. Current mechanistic understanding interprets the reaction of the halosuccinimides as proceeding through an electrophilic aromatic substitution pathway[92] whilst reaction with both iodine and ICl might proceed through the porphyrin π-radical cation (see Section **2.3.2**). Both of these pathways

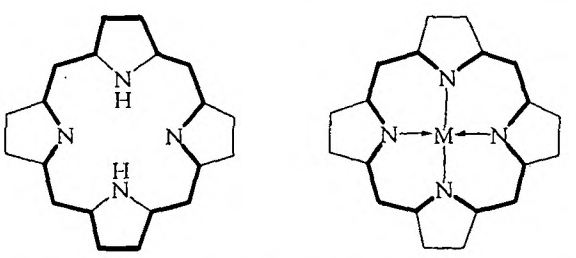

Figure **2.5**- pathways that impart aromaticity to a free-base porphyrin (left) and a metallated porphyrin (right)

would be dictated by reaction through the HOMO. But current molecular orbital interpretations of the pertinently substituted porphyrin systems show only the LUMO+1 orbitals with a significantly greater proportion of their electron density at the reactive β-pyrrolic positions[108-110], and therefore the origin of this regiospecifity remains elusive.

2.3.2 Chlorination with iodine monochloride

The reaction of the quinoxaline **24** with ICl produces the unexpected chlorinated product. This is the unexpected product as ICl is more normally associated with the iodination of aromatic compounds that is explained by the preferred orientation of the polarized $^{\delta+}$I-Cl$^{\delta-}$ on its approach to an electron-rich aromatic system. However the opposite course of the reaction with a porphyrin can be explained by two studies of the halogenation of polyaromatic compounds by ICl[111,112]. In these studies it is suggested that the reaction of an aromatic compound proceeds through a charge-transfer interaction to form the aromatic π-radical cation (see Figure **2.6**); the ICl is then said to spontaneously decompose into I$^{\cdot}$ and Cl$^{\cdot}$. Chlorination is achieved through ion-pair collapse and iodination through radical-radical combination. The observed chemoselectivity of either iodination or chlorination is then explained by a combination of steric factors and unpredictable and unexplained electronic factors. Steric factors are relevant as the iodine atom is much larger than the chloride ion and therefore has a greater steric demand in its addition to the π-radical cation.

These observations easily explain why the porphyrin system is chlorinated instead of iodinated. Chlorination is favoured over iodination primarily because the porphyrin

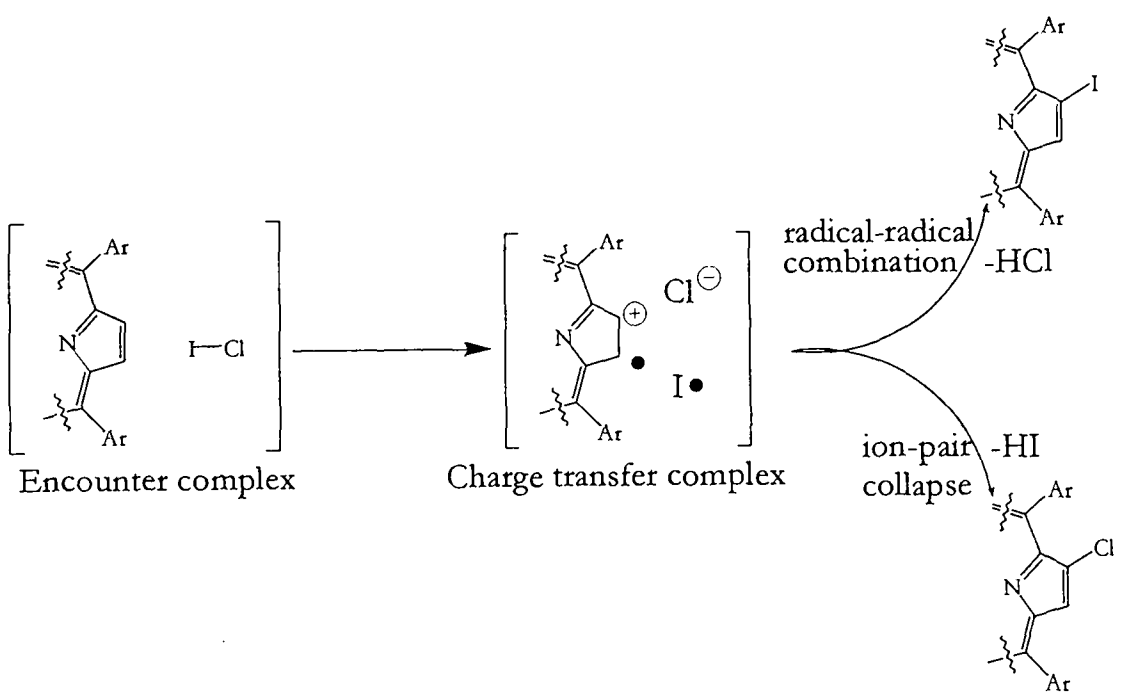

Figure **2.6**- possible reaction mechanism for the formation of the chlorinated product from the reaction of the quinoxaline **24** with ICl. Ar = 3,5-di-*tert*-butylphenyl.

macrocycle is sterically encumbered by bulky meso-3,5-di-*tert*-butylphenyl substituents. The proposed mechanism should also be put into the context of the wider role of electron transfer complexes in electrophilic aromatic substitution reactions, and this is done in Section **3.5**. In addition, similarities between this mechanism and those described for the nucleophilic substitution of a halo-porphyrin in Chapter Three, for the allylic oxidation of a chlorin in Chapter Five and the nitration of the dendritic porphyrin in Chapter Six suggest that the formation of charge-transfer complexes can be considered a fingerprint of porphyrin chemistry.

Chapter Three

Nucleophilic attack on a halo-porphyrin

Chapter Three
Nucleophilic attack on a halo-porphyrin

The nucleophilic displacement of a halogen or nitro group from an aromatic system by the anion of benzaldehyde oxime in DMSO was originally described by Knudsen[86], and then adapted to a porphyrin system by Crossley[36,113] and later Burn[87]. In unpredictable porphyrin systems it has been shown to be a high-yielding transformation, and the modification of using a THF co-solvent[87] not only makes this a more reproducible process, but also widens the scope of the transformation to less soluble substrates. This chapter therefore describes the attempted application of Knudsen's hydroxylation to the nucleophilic displacement of halo-substituted porphyrins, and the search for a mechanism to explain the results.

3.1 Nucleophilic attack on different halogens

An initial investigation into the feasibility of the proposed route to porphyrin *alpha*-diones was made by attempting the hydroxylation of the three regiospecifically halogenated quinoxalines whose syntheses were described in Chapter Two. Nucleophilic substitution was attempted on the nickel(II) quinoxalines as nickel serves as an electron-withdrawing substituent, thereby facilitating the substitution process[113]. Copper has been used for the same purpose, but it is paramagnetic so its products cannot be analyzed by ^{1}H NMR.

Results of the substitution reactions on the halogenated quinoxalines are shown in Figure **3.1** and Table **3.1**. The reactions of the three halogenated quinoxalines were carried out under similar conditions. Typically a fifteen-fold excess of sodium hydride was dissolved in DMSO; a ten-fold excess of benzaldehyde oxime was then added and the mixture was transferred under nitrogen to the relevant quinoxaline dissolved in THF. The reactions were then heated at reflux for 17 hrs.

From Table **3.1** it is evident that there are two main products, namely the desired hydroxylated quinoxaline **40** and the unsubstituted quinoxaline **39**. The issue is slightly complicated by the observation that the hydroxy-quinoxaline **40** could be oxidized on purification over silica to the dioxo-quinxoaline **41**. It is also evident that there is a clear

Halogen	Isolated yields of products (%)				
	Starting material	Unsubstitued quinoxaline **39**	Hydroxy-quinoxaline **40**	Dioxo-quinoxaline **41**	Lactone-quinoxaline **43**
Chlorine	20	-	72	-	-
Bromine	-	43	19	14	6
Iodine	-	56	-	-	11

Table **3.1**- yields of products for the attempted nucleophilic substitution of the halo-quinoxalines **32, 33** and **34** by sodium benzaldoximate in a 1:1 mixture of THF and DMSO. The first two entries were carried out at a concentration of the quinoxaline of around 0.0023 $mmolml^{-1}$, whereas reaction of the iodo-quinoxaline was carried out at a concentration of 0.011 $mmolml^{-1}$.

trend in the yields of the two types of products as the halogen substituent is varied. Thus the yield of the unsubstituted quinoxaline **39** varies according to the series:

$$Cl < Br < I$$

Whereas the yield of the hydroxylated quinoxaline **40** varies with the halogen in an opposite manner:

$$Cl > Br > I$$

In addition two other products were also isolated. The 'lactone-quinoxaline' **43** was sometimes isolated in moderate yield. This is thought to be a product from the undesired oxidation of the intermediates, as has been observed previously[90]. The methylthio-quinoxaline **42** was also sometimes isolated from the reaction mixtures. This type of product has previously been misidentified as a porphyrin substituted by $-CH_2SCH_3$[114,115]. However the mass of the parent ion peak in the LDI spectrum and the appearance of only

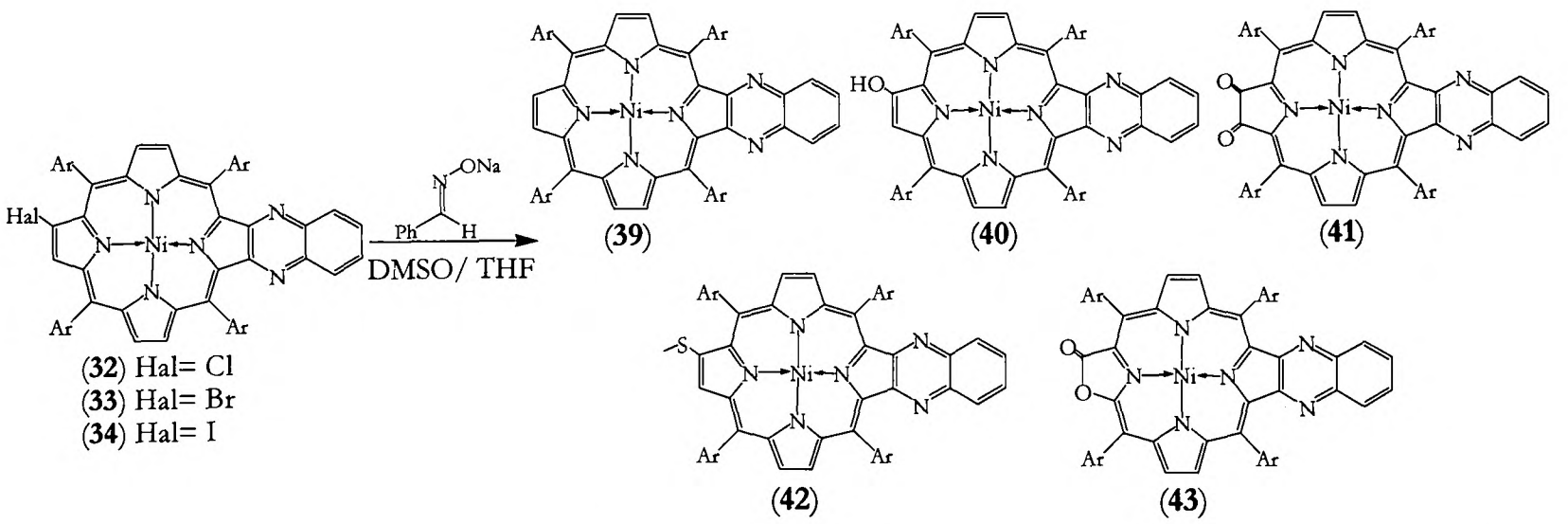

Figure **3.1**- products from the nucleophilic displacement of the halo-quinoxalines by sodium benzaldoximate in a 1:1 mixture of THF and DMSO. Ar= 3,5-di-*tert*-butylphenyl.

one singlet integrating to 3H at 2.52 ppm in the ^{1}H NMR spectrum confirm the correct structural assignment. The origin of this product is discussed further in Section **3.3.1**.

3.2 Initial mechanistic interpretation: S_NAr versus $S_{RN}1$ pathways

An initial mechanistic evaluation of the reaction comes from trying to understand what is behind the apparent competition between hydroxylation and dehalogenation. The simplest explanation would be to evoke a competition between two distinct mechanistic pathways as illustrated in Figure **3.2**. The first pathway that leads to the desired hydroxylated products proceeds by a normal S_NAr reaction. The mechanism of the second pathway leading to the unsubstituted quinoxaline **39** can be assigned by analogy with the reaction of certain aryl halides with nucleophiles. For these systems reductive dehalogenation is usually interpreted in terms of the $S_{RN}1$ mechanism[116]. It was noted early in the development of the $S_{RN}1$ mechanism that the rate of reductive dehalogenation depends very much on the identity of the halogen[117]. This is because the lifetime of the radical anion produced by single electron transfer to the substrate will be partially dependent on the strength of the carbon-halogen bond. So the lifetime of the radical anion of an aryl iodide will be less than that of an aryl bromide or an aryl chloride and hence the concurrent rate of dehalogenation will be faster. This is reflected in an example of a thermal $S_{RN}1$ reaction which involves the facile reductive dehalogenation of 3-iodopyridine when treated with sodium methoxide[118]. However the substituted methoxy product predominates for the 3-chloro and 3-bromo derivatives[119]. This is very similar to the present porphyrin system. Therefore it can be concluded that reductive dehalogenation results from an $S_{RN}1$ pathway, with the increase in the yield of the

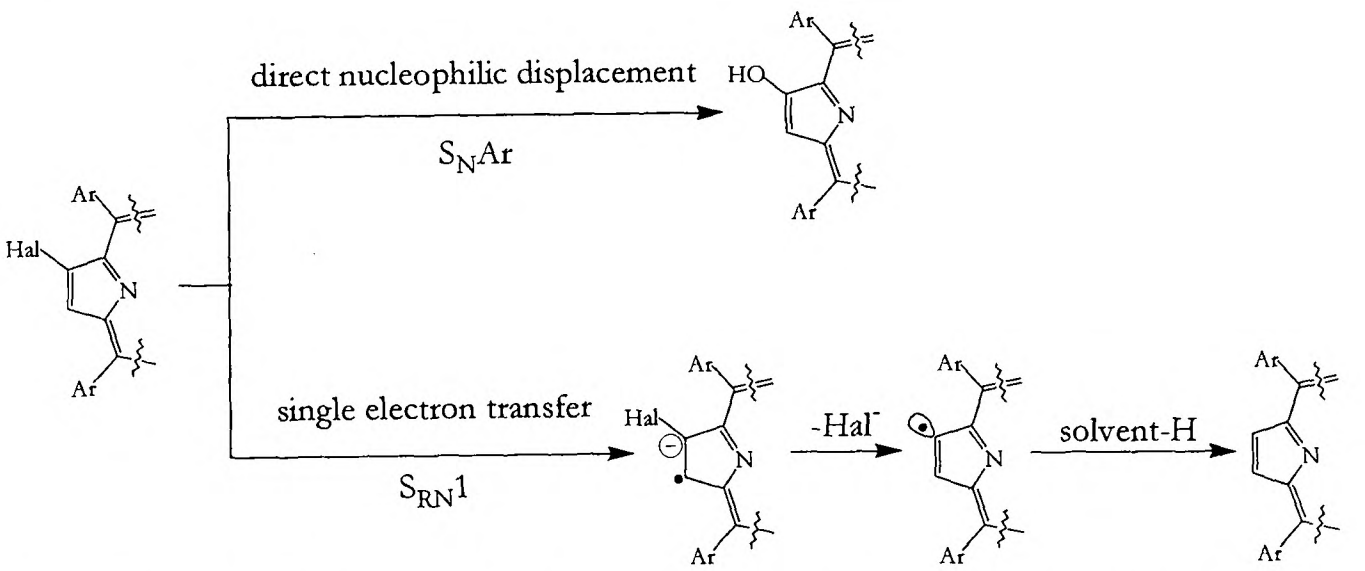

Figure **3.2**- an initial interpretation of reactivity- competing S_NAr and $S_{RN}1$ pathways. Ar= 3,5-di-*tert*-butylphenyl.

dehalogenated product as chlorine is replaced by bromine and then iodine being attributed to the decrease in lifetime of the radical anion.

This type of mechanism in a porphyrin system is not as unusual as it might seem at first as single electron transfer (SET) mechanisms leading to de-functionalized products in porphyrin systems are quite common. Reductive denitration has been observed in the treatment of a β-nitro-porphyrin with 2-aminobenzenethiol[120]. Equally reductive denitration is observed when a β-nitro-porphyrin is treated with *tert*-butyl magnesium bromide[121] or sodium methoxide[122]. Reductive dehalogenation can be observed when certain β-bromo-porphyrins are heated in the presence of copper(I) bromide[123] or copper(I) cyanide[124]. Indeed a SET mechanism in porphyrin reductive dehalogenation reactions is consistent with electrochemical observations[125] that show that on the first porphyrin-centred reduction of a cobalt(II) β-bromo-porphyrin, elimination of Br^- occurs. Therefore it is not surprising to once again observe chemically-induced reductive dehalogenation.

3.3 Variables in the nucleophilic attack

The mechanistic evaluation of Section **3.2** is very simple, and therefore it is desirable to use this interpretation to maximize the yields of the desired hydroxylation reaction. Whilst it has already been shown that the yield of **40** resulting from nucleophilic displacement of the chloro-quinoxaline **32** is very impressive at 90% with respect to recovery of the starting material, attempts to maximize the yields of this transformation for other halogen substituents could help widen the application of this procedure. Furthermore this will also lead to a greater understanding of the mechanism's intricacies.

3.3.1 Inhibiting the formation of the methylthio-quinoxaline 42

Initially it was thought that the main factor that would prevent the synthetic utility of this transformation was the isolation of the methylthio-quinoxaline **42**. The process leading to this product was therefore investigated further. In preliminary experiments (not shown in Table **3.1**) its yield was observed to increase in parallel with the yield of the hydroxylated product in the series:

$$Cl > Br > I$$

In this way it was thought that any conditions that would favour the formation of the desired

Molar ratio of reactants- substrate: oxime : NaH	**Isolated yields of products (%)** Unsubstituted quinoxaline **39**	Hydroxy-quinoxaline **40**	Dioxo-quinoxaline **41**	Lactone-quinoxaline **43**	Methylthio-quinoxaline **42**
1: 12: 15	43	19	14	6	2
1: 26: 15	49	7	24	15	4
1: 0: 17	31	-	-	-	-

Table **3.2**- changing the proportion of benzaldehyde oxime in the reaction of the bromo-quinoxaline **33** with benzaldehyde oxime/ sodium hydride in a 1:1 mixture of DMSO and THF. Apart from the proportion of the oxime, reaction conditions were left unchanged. No starting material was recovered on any occasion.

hydroxylated quinoxaline would also favour the formation of the undesired methylthio-quinoxaline.

Quinoxaline **42** can therefore be assumed to originate from the nucleophilic displacement of the halogen substituent with a nucleophile derived from DMSO. It was considered that this nucleophile might itself originate from the dimsyl anion. Hence the proportion of benzaldehyde oxime in the reaction mixture was increased so as to disfavour the presence of the dimsyl anion. As shown in Table **3.2** this had no appreciable effect on the product distribution. And indeed when the bromo-quinoxaline was reacted with the dimsyl anion itself without the presence of the oxime the only product isolated was the dehalogenated product **39**, without any methylthio-quinoxaline **42**.

However, it was fortuitously discovered that the manner by which the THF co-solvent was purified before reaction had a direct effect on the formation of methylthio-quinoxaline **42**. When the THF was purified by distillation over sodium wire then **42** appeared in the product mixture; but when the THF was purified by passing through a column of alumina, **42** was never isolated. Whilst this is a strange observation it does mean that the hydroxylation can be carried out without the worry of the isolation of products originating from reaction with the solvent.

On further investigation of the literature it was found that similar unexpected methylthio-products have been previously isolated under different circumstances for reactions on non-porphyrin substrates in DMSO. They have been isolated as a by-product from Ullmann-type couplings[126,127], from attempted nucleophilic attack on an aromatic system by the fluoride ion[128-130], from the electrochemical reduction of aryl halides[131,132] and in one case

from the reaction of a ketoxime[133]. The electrochemical studies seem to suggest that this product originates form the formation of the $MeS^{-}=O$ anion. In the present system if such an ion was to be formed, it could undergo nucleophilic substitution with the substrate; equally the difference between the two methods of solvent purification might be explained by the presence of residual water in the THF purified by passing through alumina that could then protonate this reactive intermediate. However, the reason why excess benzaldehyde oxime would not protonate this reactive intermediate in turn is not clear.

3.3.2 Attempts to favour hydroxylation over dehalogenation

Attempts to favour hydroxylation over dehalogenation were made for the nucleophilic displacement of the bromo-quinoxaline **33**. After all Crossley had already observed the successful hydroxylation of a bromo-porphyrin with sodium benzaldoximate in DMSO[88], the main differences between the current procedure and the reported one being the presence of a bulkier aryl substituent, the lower oxidation and reduction potentials of the substrate, and the use of a co-solvent.

Most previous examples of $S_{RN}1$ reactions have been shown to be radical chain processes[116]. The usual method for proving the existence of a radical chain process is to add a radical inhibitor to the reaction. The radical inhibitor serves to trap electrons and in this way prevents the propagation of the radical chain mechanism. Therefore in order to investigate the radical-chain character of the present system and in the aspiration of preventing chain propagation, various radical inhibitors were added to the reaction mixture for the hydroxylation of the bromo-quinoxaline **33**. Results are summarized in Table **3.3**.

	Isolated yields of products (%)				
Additive (equivalents)	Starting material **33**	Unsubstituted quinoxaline **39**	Hydroxy-quinoxaline **40**	Dioxo-quinoxaline **41**	Lactone quinoxaline **43**
None	-	49	7	24	15
1,2-Diphenylethylene (6 eqv.)	-	44	21	31	-
Benzophenone (6 eqv.)	-	36	49	-	-
Nitrobenzene (25 eqv.)	-	35	49	15	-
p-Dinitrobenzene (4 eqv.)	26	33	23	18	-
Azoxybenzene (4 eqv.)	-	65	-	-	-

Table **3.3**- effect of additives on the attempted nucleophilic substitution of the bromo-quinoxaline **33**. All entries were carried out at the same substrate concentration using roughly a 25-fold excess of benzaldehyde oxime and a 13-fold excess of sodium hydride.

It is observed that the three radical inhibitors 1,2-diphenylethylene, benzophenone and nitrobenzene slightly reduce the yield of the dehalogenated product **39** isolated from the reaction, whilst the combined yields of the products **40** and **41** (and possibly **43**) resulting from hydroxylation seems to increase very slightly. *p*-Dinitrobenzene prevents the reaction from going to completion, whilst azoxybenzene actually favours the formation of the dehalogenated product over the substituted product. These results are on the face of it somewhat disappointing, since a whole range of radical inhibitors have been shown not to significantly retard the formation of the dehalogenated product contrary to what was originally wanted. However these results do say something significant about the reaction mechanism. Since radical inhibitors do not significantly affect the course of the reaction, this strongly suggests that in this particular case the pathway leading to the dehalogenated *does not* proceed through a chain propagation mechanism.

3.3.3 Varying the nucleophile

One possible consequence of the lack of a chain propagation pathway is that in fact what is being observed is the direct competition between electron-transfer and bond-formation between the nucleophile and the quinoxaline. This is an unusual idea[134,135] and it has been demonstrated only on one previous occasion[136]. Its implication for the present system is that by varying the nucleophile, or more specifically by varying the oxidation potential of the nucleophile, one mechanism should start to predominate over the other. Hence as the nucleophile is made more difficult to oxidize the rate of electron-transfer from the nucleophile to the quinoxaline should be reduced and the hydroxylated product should be favoured. Therefore the nucleophilic displacement of the bromo-quinoxaline **33** was

Substituted benzaldehyde oxime	**Oxidation potential of the oxime anion** (V)		**Isolated yields of products (%)**		
		Starting material **33**	Unsubstituted quinoxaline **39**	Hydroxy-quinoxaline **40**	Dioxo-quinoxaline **41**
Unsubstituted	-0.559	-	49	7	24
3-bromo	unknown	-	39	31	14
3-nitro	-0.390	52	7	23	-
4-nitro	-0.371	80	-	-	-

Table **3.4**- effect of varying the nucleophile in the displacement of the bromo-quinoxaline **33**. All entries were carried out at the same substrate concentration using roughly a 26-fold excess of benzaldehyde oxime and a 15-fold excess of sodium hydride., Oxidation potentials for the anions of the benzaldehyde oximes are taken from Bordwell[137] who recorded them in DMSO relative to the ferrocenium/ ferrocene couple.

attempted using a series of benzaldehyde oximes with various electron-withdrawing groups substituted onto the benzene ring.

The results in Table **3.4** show that varying the nucleophile can have a significant effect on the overall course of the reaction. However the extremes of reactivity are not particularly reflected by extremes in the preferred product. Thus the 3-bromo-benzaldehyde oxime shows a similar extent of reaction as the unsubstituted oxime, and it also comparatively marginally favours the hydroxylated product over the dehalogenated product. On moving to the 3-nitro-benzaldehyde oxime a great reduction in the extent of reaction is observed combined with a reasonable preference for the hydroxylated product. And the 4-nitro-quinoxaline shows no reactivity at all, with only starting material being recovered.

Therefore whilst it is encouraging that varying the nucleophile does slightly alter the balance between the hydroxylated and dehalogenated products, the effect is not as dramatic as hoped and is outweighed by more dramatic variations in the extent of reaction.

3.4 Approaches to the bis-porphyrin tetra-one

Finally in order to apply this methodology to the synthesis of a bis-porphyrin tetra-one, the attempted nucleophilic displacement of the di-chloro bis-porphyrin **37** (Figure **3.3**) was attempted.

The nucleophilic displacement was attempted in exactly the same manner that had been so successful for the chloro-quinoxaline **32**. Hence 30 equivalents of sodium hydride were dissolved in DMSO and then 51 equivalents of benzaldehyde oxime added; this solution was then transferred under nitrogen to **37** dissolved in THF and heated to reflux for 17 hours. However on purification an 80% yield of starting material was recovered with a further small proportion of possibly partially dehalogenated product also isolated.

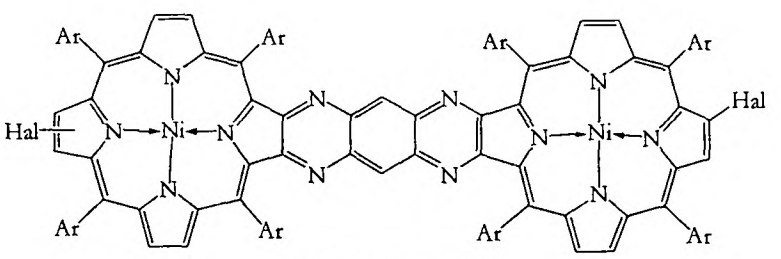

(**37**) Hal= Cl
(**38**) Hal= Br

Figure **3.3**- the di-halo bis-porphyrins. Ar= 3,5-di-*tert*-butylphenyl.

It is known that the bis-porphyrin system has a less negative reduction potential than the quinoxaline[81], so it was thought that perhaps the reason for the lack of the reaction of **37** was the favouritism of a dead-end electron-transfer pathway over a bond-forming pathway. If this was to be the case then the parallel reaction of the di-bromo bis-porphyrin **38** would be expected to result in facile dehalogenation. However when **38** was subject to the same conditions, once again mostly starting material was recovered (71%) with the isolation of only a small proportion of partially dehalogenated product **44** (26%).

In a final attempt to increase the extent of reaction the nucleophile was also varied. But reaction of the di-chloro bis-porphyrin **37** with 3-bromo-benzaldehyde oxime and 3-nitro-benzaldehyde oxime only resulted only in recovery of starting materials in 73% and 83% yields respectively.

3.5 Final mechanistic interpretation and conclusions

The intricacies of this reaction are certainly a challenge to interpret. Initial inspection concluded that the reaction proceeds though the competition between a S_NAr and a $S_{RN}1$ pathway. However the lack of evidence for a radical chain process led to the conclusion of a *direct* competition between bond-formation and electron-transfer between the oxime and the quinoxaline. Attempts to manipulate this competition by varying the oxidation potential of the benzaldehyde oxime anion didn't really produce the desired results. Meanwhile attempted transfer of this methodology from the model quinoxaline system to the bis-porphyrin system resulted in neither significant hydroxylation nor significant dehalogenation.

These are a frustrating set of observations because just as a reasonable understanding is arrived at, another piece of evidence seems to point to something else happening. Whilst it is clear that a complete mechanistic interpretation with full experimental justification cannot at this point be achieved, the real factors that have led to the eventual failure of this methodology can be speculated upon. In this spirit, a speculative mechanism is shown in Figure **3.4** that attempts to emulate the mechanism of Figure **3.2**.

The mechanism depends on both products originating from the formation of a charge-transfer complex between the nucleophile and the substrate. Radical combination from this intermediate leads to the hydroxylated product whilst the fragmentation of the radical anion leads to the dehalogenated product. Thus this competition between radical combination and

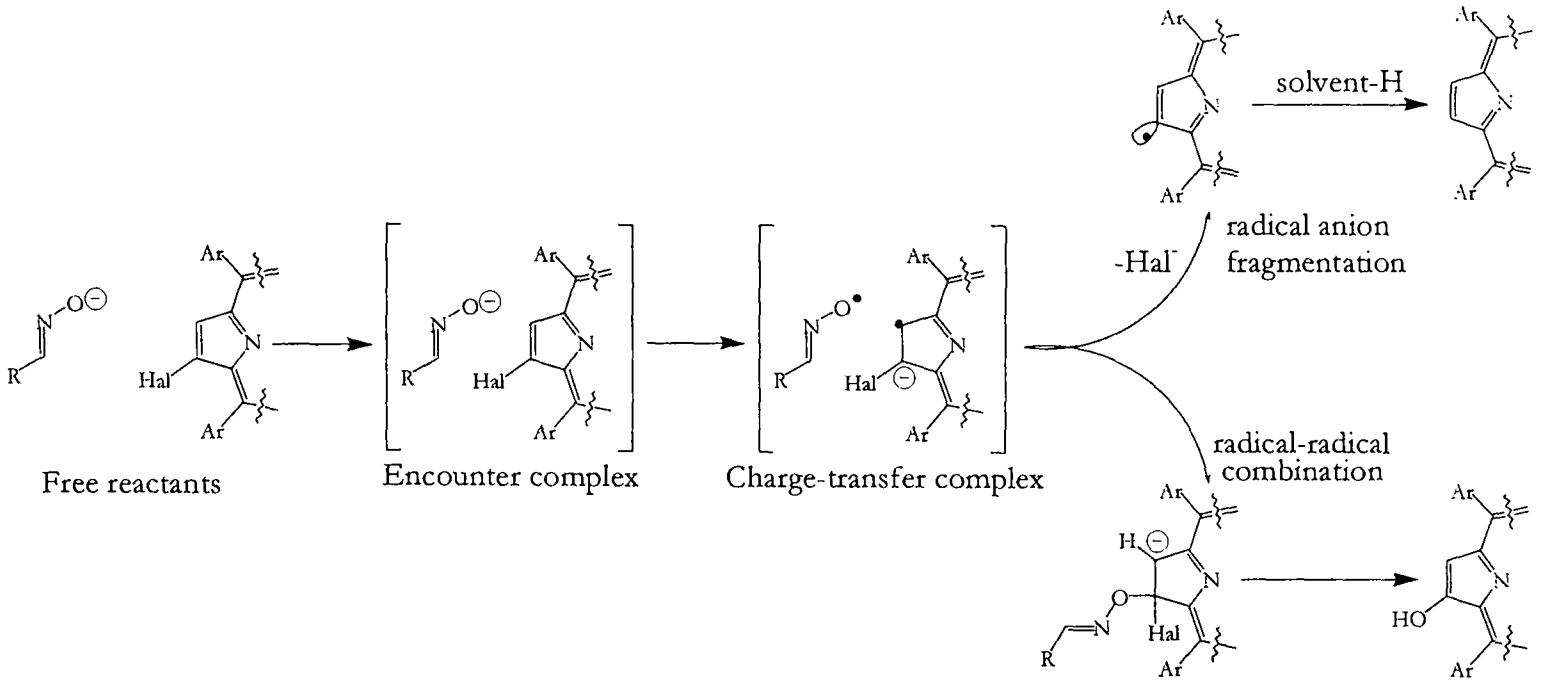

Figure 3.4- further speculation on the mechanism of nucleophilic substitution. Ar= 3,5-di-*tert*-butylphenyl, R= the relevantly substituted benzene.

hydroxylation replaces the idea stemming from Figure **3.2** that the two products originate from the direct competition between electron-transfer and bond-formation between nucleophile and substrate.

The formation of a precursor charge-transfer state is an appealing concept because it puts a lot of observations into context. Firstly the proportion of dehalogenated product is solely dependent on the ability of the halogen to act as a leaving group, and therefore the greatest proportion of dehalogenated product is observed from the reaction of the iodine-substituted substrate. And this means that such a mechanism does not require a radical chain component for the propagation of the formation of the dehalogenated product.

More subtly this concept helps to explain the implicit relationship between the formation of the dehalogenated product and the hydroxylated product. As the nucleophile is made more difficult to oxidize the formation of this charge-transfer complex is made less favourable and therefore the main effect that is observed is a 'switching off' of reactivity. Electron-withdrawing groups substituted on the nucleophile would also serve to unpredictably affect the rate of radical-radical combination which is why the ratio of hydroxylated to dehalogenated products additionally varies with the nucleophile.

In a similar vein the mechanism helps to put into context the reasons why the attempted transfer of the methodology from the quinoxaline to the bis-porphyrin proved unsuccessful. Whilst the bis-porphyrin is easier to reduce than the quinoxaline there are other factors that affect the formation of the critical charge-transfer complex. One such factor is the solvation

of the charge-transfer complex. The charge-transfer process is stabilized by solvent interactions, and therefore any factor reducing this solvent stabilization will lead to an increased activation barrier to charge-transfer. And the bis-porphyrin is a larger more lipophilic species than the quinoxaline so the development of charge involved in the formation of a charge-transfer complex will be more poorly stabilized by the solvent. Hence a bis-porphyrin system with an even lower reduction potential is required before significant reaction occurs. In this way the nucleophilic displacement of the di(phenyl sulphoxide) bis-porphyrin by sodium benzaldoximate is successful[36].

The role of charge-transfer complexes in the reactions of normal aromatic compounds is starting to be fully appreciated. The most studied reaction is the nitration of aromatic compounds by NO_2^+ and although this proceeds through a S_EAr mechanism rather than a S_NAr mechanism it does provide a useful insight into the present discussion. The mixing of the two reactants results in the formation of aromatic π-cations that can be detected spectroscopically, indicating the possibility of the involvement of a charge-transfer complex in the nitration mechanism. It has been widely debated whether the formation of such complexes is just a side-reaction or whether it actually sits on the main reaction coordinate[138.139]. Whilst the trend in the rate of nitration with variously substituted aromatic systems is inconsistent with an outer-sphere electron-transfer mechanism because of the large reorganisation energy required for the one electron reduction of NO_2^+, an inner-sphere-type electron-transfer mechanism of a tightly-bound encounter complex is conceptually feasible[138-141]. And the collapse of this tightly-bound charge-transfer state would lead to observed trends in the formation of nitrated products. Therefore current opinion is in favour of the involvement of a charge-transfer complex in the nitration mechanism[142,143]. Similar conclusions have been drawn for the halogenation of aromatic compounds[142.143].

The existence of such charge-transfer interactions in aromatic nucleophilic substitutions have been less widely studied, although the isolation of charge-transfer complexes from certain attempted nucleophilic substitutions[144] suggest that such a mechanism is feasible. Equally the formation of charge-transfer intermediates has been used to explain the reactivity in an electron-deficient substituted benzene[145]. And because of a porphyrin's extended conjugated system it also has a relatively low reduction potential. Therefore if aromatic nucleophilic substitution can proceed through the formation of a charge-transfer complex then it is likely that the porphyrin system will exhibit such reactivity.

In conclusion, this methodology is mechanistically complicated and unfortunately cannot be applied to the synthesis of a bis-porphyrin tetra-one. In addition once again it is speculated that the formation of charge-transfer complexes can be considered a fingerprint of porphyrin chemistry.

Chapter Four

Introduction to chlorins

Chapter Four
Introduction to chlorins

The previous two chapters have described one particular approach to porphyrin *alpha*-diones. Unfortunately when applied to the synthesis of a bis-porphyrin tetra-one the methodology failed. Therefore alternative new routes to porphyrin *alpha*-diones have been sought. The discovery of the oxidation of a *4H*-chlorin by silica or alumina and its further oxidation by the Dess-Martin periodinane reagent provides the possibility of such a new route for the synthesis of porphyrin *alpha*-diones (Figure **4.1**). This methodology is new and its yields show great promise and therefore it has been investigated thoroughly. This investigation has been further applied to the elucidation of the mechanism of this transformation to gain a greater understanding of the factors affecting it. For simplicity's sake the syntheses of the various chlorins of interest are presented in this chapter; attempts at their allylic oxidation on silica and alumina are described in Chapter Five.

4.1 An introduction to chlorins

Chlorins are porphyrins that have been reduced at one β-pyrrolic position. A porphyrin that has undergone reduction at two β-pyrrolic positions is called a bacteriochlorin or isobacteriochlorin depending on which positions have been reduced.

General interest in chlorins is derived from their photophysical properties. The effect of reducing a porphyrin at its periphery on these properties is shown in Figure **4.3**. The first reduction is characterized by a substantial increase in the intensity of the Q band (the lowest energy absorption band). The second reduction at the antipodal position again increases the

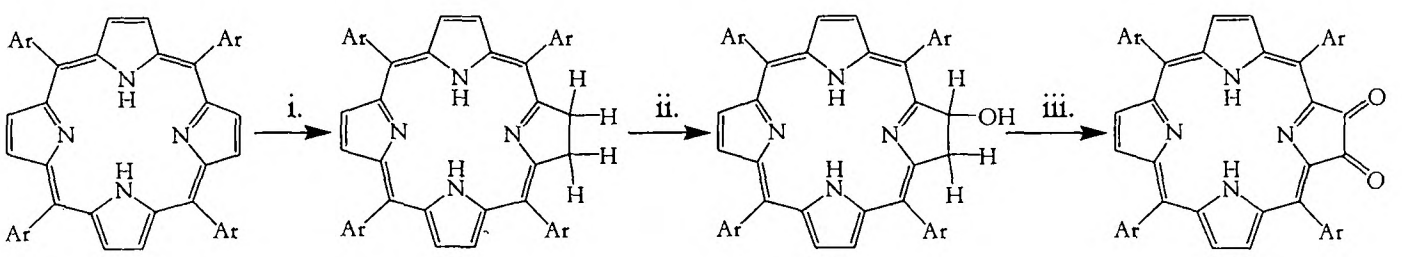

Figure **4.1**- a new route to porphyrin *alpha*-diones. i. BH_3 or N_2H_2; ii. silica or alumina; iii. Dess-Martin periodinane. Ar= 3,5-di-*tert*-butylphenyl.

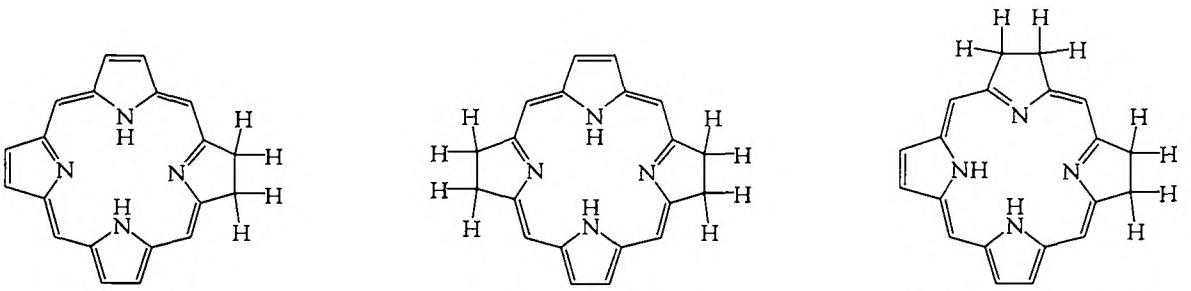

Figure **4.2**- chlorin, bacteriochlorin and isobacteriochlorin structures.

intensity of the Q band, and the lowering of the symmetry is reflected in a significant splitting of the B band into its x and y components.

This increase in the absorption intensity of the low-energy Q band of a chlorin compared to a porphyrin is taken advantage of by the chlorophylls. Chlorophyll is one of the major pigments responsible for light absorption in the photosynthetic pathway, and it is reduced at one β-pyrrolic position making it formally a chlorin. Likewise bacteriochlorophyll is a pigment found in photosynthetic bacteria, and is reduced at two β-pyrrolic positions, making it formally a bacteriochlorin. These photophysical properties lead to the major applications of chlorins. They have been used as substrates for photodynamic therapy (PDT)[146,147] which involves the injection of pigment into a cancerous tumor, and then the selective

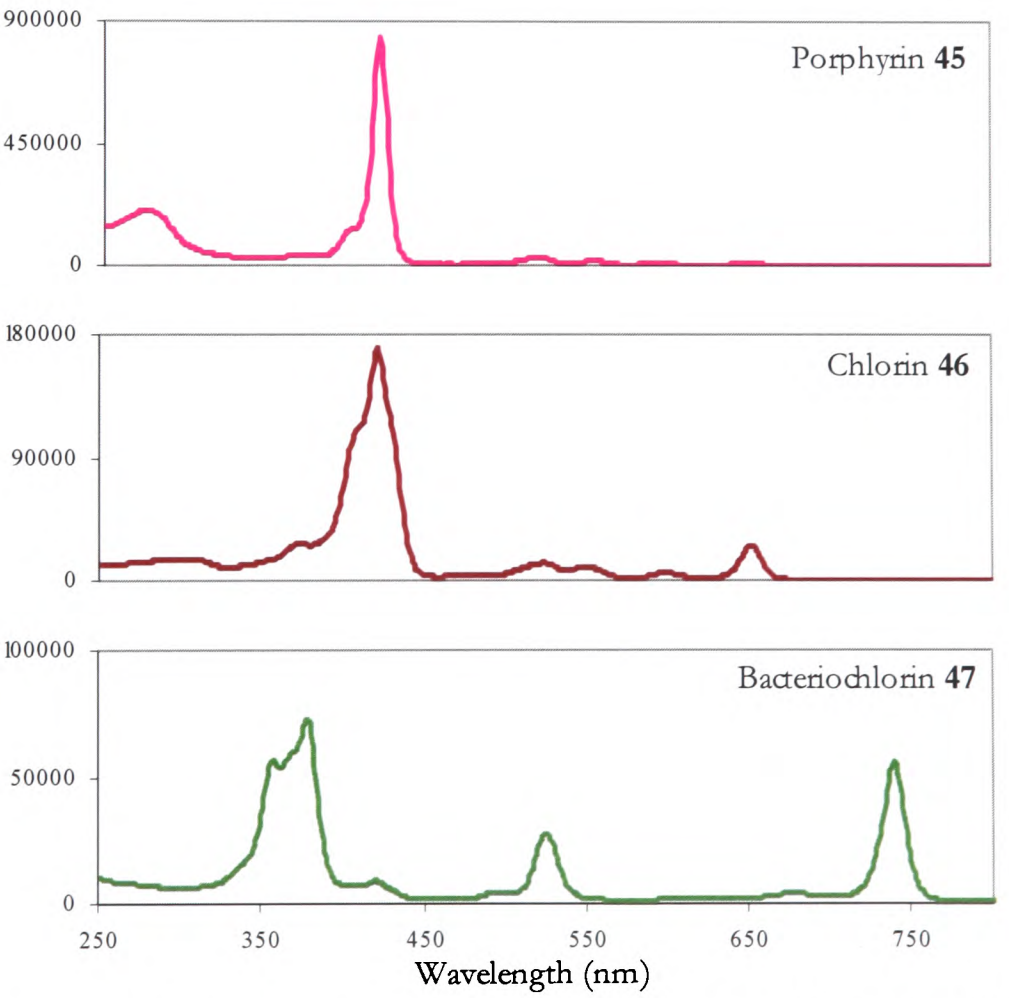

Figure **4.3**- UV-VIS absorption spectra of 3',5'-di-*tert*-butylphenyl-porphyrin (**45**), chlorin (**46**) and bacteriochlorin (**47**). The vertical axis is the absorbance in units of $dm^3mol^{-1}cm^{-1}$.

administration of light to the tumor. The cells photosensitized with the pigment are killed by the administration of light whereas the non-photosensitized cells are left unaffected. The strong absorbance of a chlorin in the red end of the spectrum is required as shorter wavelengths of therapeutic light are absorbed by the skin before reaching the tumor. In this way tetra(*m*-hydroxyphenyl)chlorin has proven itself to be one of the most active photosensitizers requiring very low drug and light doses for efficacy[146].

4.2 Synthesis of the free-base chlorin and bacteriochlorin

4.2.1 Whitlock's diimide reduction

The synthesis of chlorins and bacteriochlorins from their parent porphyrins is well established, with three different chemical functionalizations currently available. The first is Whitlock's reduction[148], which uses diimide produced *in situ* from *p*-toluenesulfonylhydrazine and anhydrous potassium carbonate in pyridine. With this methodology an intentional second reduction of the porphyrin macrocycle occurs regiospecifically with respect to the first. Starting from the free-base tetraphenyl-porphyrin the bacteriochlorin structure predominates, whereas from both the metallated tetraphenyl-porphyrin and the free-base octaethyl-porphyrin the isobacteriochlorin structure predominates.

This diimide reduction was therefore applied to 5,10,15,20-tetrakis(3',5'-di-*tert*-butylphenyl)porphyrin **45**. The reduction was carried out by dissolving the porphyrin in pyridine and heating the reaction to 110°C; small aliquots of *p*-toluenesulfonylhydrazine and anhydrous potassium carbonate were then added at 1¼ and 2½ hour intervals respectively. The progress of the reaction was monitored closely by thin layer chromatography, and when it was judged that all starting material had been consumed heat was removed and the reaction was worked up. The mixture was crudely purified by passing it through a plug of silica and analysis by ^{1}H NMR showed that the product contained both the chlorin **46** and the bacteriochlorin **47**. Integration of the various environments gave an 82% overall yield of the chlorin **46** and a 12% overall yield of the bacteriochlorin **47**. The intentional double reduction to give the bacteriochlorin **47** was successful, and proceeded in good yield to the pure product (65%).

4.2.2 Kevin Smith's diborane reduction

A second method of porphyrin reduction has been recently investigated by Kevin Smith[149]. It involves the reaction of diborane (B_2H_6) with the free-base porphyrin. However since full experimental details have not been published, further investigation of this reduction was required. It was found that reduction of 5,10,15,20-tetrakis(3',5'-di-*tert*-butylphenyl)porphyrin **45** to the chlorin **46** could be achieved in good yield (typically 75 to 90%) by stirring with a ten-fold excess of diborane in THF at room temperature for 3 hours followed by a simple work-up with water. This reduction did not result in significant over-reduction to the bacteriochlorin resulting in typically >95% purity of chlorin **46**, the impurity being the starting porphyrin **45** (see Section **4.2.4**). Because of the relative purity of the product synthesized by this route and because of its sheer simplicity, this reduction was favored for the preparation of **46**.

It was also hoped that the diborane reduction could directly access a hydroxy-chlorin product. Therefore a variety of work-up conditions of the boron-porphyrin adduct were investigated. Alkaline hydrogen peroxide at room temperature and at -78°C, mCPBA and trimethylamine *N*-oxide were all attempted but only *4H*-chlorin **46** was isolated. Stirring the boron-porphyrin adduct overnight under an oxygen atmosphere did result in a small quantity of the desired hydroxy-chlorin product **62** (17%) along with the *4H*-chlorin **46** (20%). It was suspected that the boron-porphyrin adduct was unstable to aqueous conditions and this was confirmed by working-up the reaction with D_2O. One deuterium atom was incorporated into the chlorin product, as confirmed by the integration of the saturated β-pyrrolic region of the ^{1}H NMR where only 3 protons were observed. Furthermore a personal communication from Kevin Smith revealed that in his hands the hydroxy-chlorin product had only been isolated from reduction of the zinc porphyrin, accompanied by an equal recovery of the corresponding *4H*-chlorin. Therefore it was concluded that the diborane reduction could not be successfully applied to access a hydroxy-chlorin product in high yield.

4.2.3 Photoreduction with a secondary amine

The third chlorin synthesis involves the photoreduction of the parent porphyrin in the presence of a secondary amine[150]. However this reduction was not attempted on the present system.

4.2.4 Purity of chlorin substrates

By whatever method the chlorin **46** was prepared it proved very difficult to obtain it in pure form. Typically the parent porphyrin **45** remained as up to a 5% impurity. This is because the chlorin **46** is only very slightly less polar than the parent porphyrin **45** and was therefore very difficult to separate from the porphyrin by column chromatography. In contrast, bacteriochlorin **47** is significantly less polar than either chlorin **46** or porphyrin **45** and therefore could be separated and isolated in pure form.

4.3 Synthesis of the metallated unfunctionalized chlorins

The nickel(II), copper(II) and zinc(II) chlorins **49**, **50** and **51**, were synthesised by refluxing the free-base chlorin **46** with the appropriate metal salt. Both the nickel(II) and zinc(II) chlorins showed a slightly higher level of porphyrin impurity as compared with the free-base starting material in their ^{1}H NMRs; copper is paramagnetic and therefore the purity of the copper(II) chlorin **50** could not be confirmed by ^{1}H NMR. In addition, when trying to isolate the zinc(II) chlorin **51** a significant amount of zinc(II) biliverdin **52** impurity was separated by recrystallization from dichloromethane/ methanol. This could be isolated from both the crude reaction mixture and the purified zinc(II) chlorin product, depending on how long either had been allowed to stand under ambient laboratory light in solution. The product was identified as having one of the structures shown in Figure **4.4**. It was very apparent that the biliverdin definitely resulted from the photo-oxidation of the parent chlorin **51** as discoloration of the chlorin in solution left on the open bench occurred rapidly.

The conclusion from an analysis of the carbon-13 and HMBC NMRs of the biliverdin (**52**), similar to those described for the nickel hydroxy-biliverdin in Section **5.3.1**, is that ring cleavage has occurred adjacent to the reduced pyrrole. However because the two resonances in the ^{13}C NMR above 180 ppm appear within 1 ppm of one another the two environments

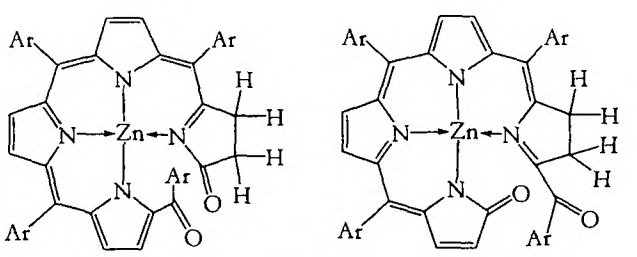

(**52**)

Figure **4.4**- the possible structures of the photo-oxidation product **52**. Ar= 3,5-di-*tert*-butylphenyl.

could not be satisfactorily distinguished from one another in the HMBC spectrum, and therefore no further assignment of regiochemistry could be made.

Diimide reduction of the metallated porphyrins was also attempted in a similar manner to that described for the diimide reduction of the free-base porphyrin **45**, but this resulted in an appreciable amount of impurity, probably isobacteriochlorin in structure, visible by ^{1}H NMR and not separable by column chromatography.

4.4 Synthesis of free-base functionalized chlorins

A series of functionalized chlorins were also synthesized (Figure **4.5**). These were chosen as each of their allylic oxidation would result in a new potential route to a porphyrin tetra-one. Two methods were used to prepare these chlorins, namely the reduction of the parent porphyrin and in one instance the direct functionalization of the chlorin **46**. For the first route Whitlock's diimide reduction[148] was preferred as it was considered that it would be compatible with a wider range of functional groups than Kevin Smith's diborane reduction. The regiospecifity of functionalization was established by ^{1}H NMR, as described in Section **4.4.1**.

In general, Whitlock's diimide reduction was applied to these functionalized systems in a similar manner to that used for the synthesis of the unfunctionalized chlorin **46**. Thus aliquots of *p*-toluenesulfonylhydrazine and anhydrous potassium carbonate were added to the substrate dissolved in pyridine, heated to 110°C. The progress of the reaction was monitored closely by thin layer chromatography, and when it was judged that all the starting

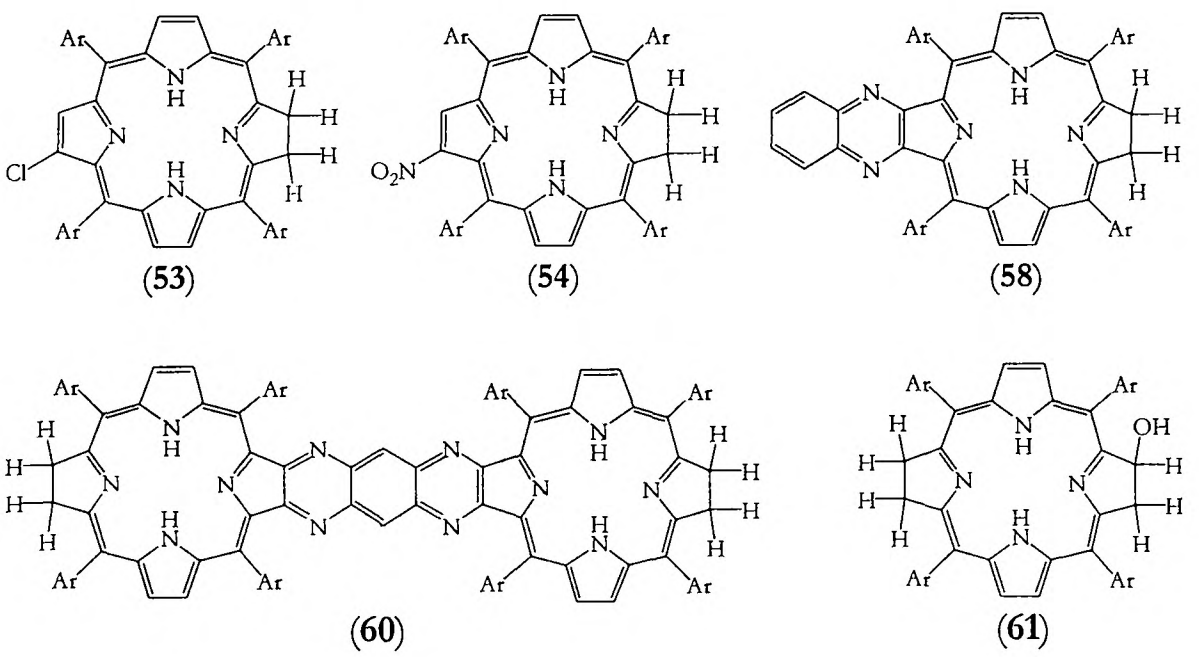

Figure **4.5**- functionalized chlorins. Ar= 3,5-di-*tert*-butylphenyl.

material had been consumed then heat was removed and the reaction was worked-up and purified. In order to obtain pure products, more reagents were added until it was certain that no starting materials remained, and therefore all the functionalized chlorins were obtained without any inseparable impurities of the parent porphyrins.

Firstly the 12-chloro- and 12-nitro-chlorins, **53** and **54**, were synthesized as both these substituents might undergo nucleophilic displacement by the benzaldoximate anion. 12-chloro-chlorin (**53**) was prepared through the chlorination of the unfunctionalized chlorin (**46**) with *N*-chlorosuccinimide in chloroform/ 4% pyridine (10% isolated yield). The major product (83%) of this reaction was the unfunctionalized porphyrin (**45**). Oxidation to this product could occur through the chlorination of one of the inner-nitrogens of the macrocycle as suggested possible in Section **2.2.3**, followed by deprotonation of the saturated β-pyrrolic position and elimination of chloride from the nitrogen.

12-nitro-chlorin (**54**) was prepared by applying Whitlock's reduction to the free base nitro-porphyrin (39% isolated yield). Over-reduction of the porphyrin was observed with the isolation of the unfunctionalized chlorin (**46**) (7%) and bacteriochlorin (**47**) (12%). Three slightly more polar bands were also isolated (each in 2% yield) that exhibited no signals below 0 ppm in the ^{1}H NMR and signals integrating to eight protons in the unsaturated β-pyrrolic region (around 4 ppm), indicating a bacteriochlorin or isobacteriochlorin structure. MALDI-TOF also shows these bands to be two Daltons heavier than the 12-nitro-chlorin (**54**), so these bands have been assigned to products corresponding to unregiospecific reduction of the nitro-porphyrin to produce 7-nitro-bacteriochlorin (**55**), 12-nitro-isobacteriochlorin (**56**) and 13-nitro-isobacteriochlorin (**57**) (Figure **4.6**). The regiochemistry of the 13-nitro-isobacteriochlorin was established by a NOE difference experiment.

The quinoxaline **24** served in Chapters Two and Three as a model system for the bis-porphyrin **14**, so Whitlock's diimide reduction was attempted on **24**. It was successful with the isolation of the 12,13-dihydro-quinoxaline **58** in 71% yield, and with only a 3% isolated

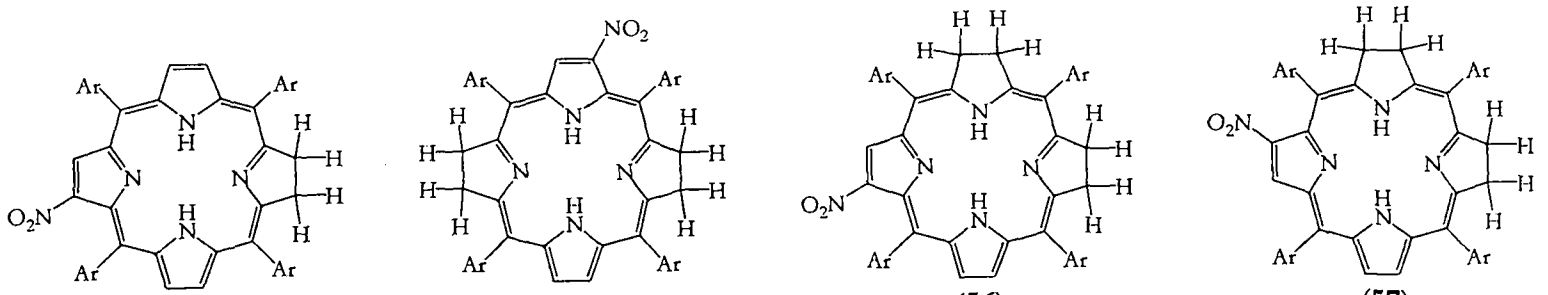

Figure **4.6**- various products from the diimide reduction of 2-nitro-porphyrin. Ar= 3,5-di-*tert*-butylphenyl.

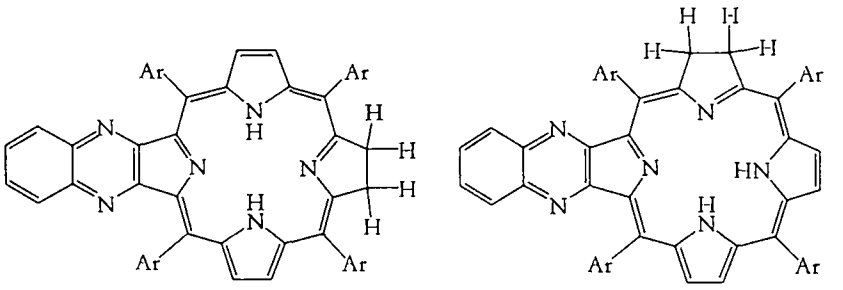

(58) (59)

Figure **4.7**- chlorin and *iso*-chlorin quinoxalines. Ar= 3,5-di-*tert*-butylphenyl

yield of the undesired *iso*-chlorin structure **59**. This *iso*-chlorin structure was isolated by column chromatography as a significantly more polar band than the chlorin; it was also remarkable by its distinctive black colour on silica.

Because of the success of the diimide reduction of the quinoxaline, it was also applied to the bis-porphyrin **14**. It was found that the bis-porphyrin was sensitive to over-reduction, but careful control of the conditions did result in an isolated yield of 50% of the desired bis-porphyrin bis-chlorin **60**. It was also found that by oxidizing the remaining mixture of products with dichloro-dicyano-quinone (DDQ), a further 28% of the bis-porphyrin could be recovered.

Finally 2-hydroxy-bacteriochlorin **61** was synthesised by the diimide reduction of the 2-hydroxy-chlorin **62** (57% isolated yield).

4.4.1 Regiospecifity of functionalization

The regiospecifity of all the functionalized chlorins was established by ^{1}H NMR. This is illustrated for the nitro-chlorin **54**. In the ^{1}H NMR and COSY spectra of **54**, coupling is only observed between the NH protons and four β-pyrrolic doublets as illustrated in Figure **4.8**. In contrast the singlet at 8.76 is not split by coupling to the NH protons. As described

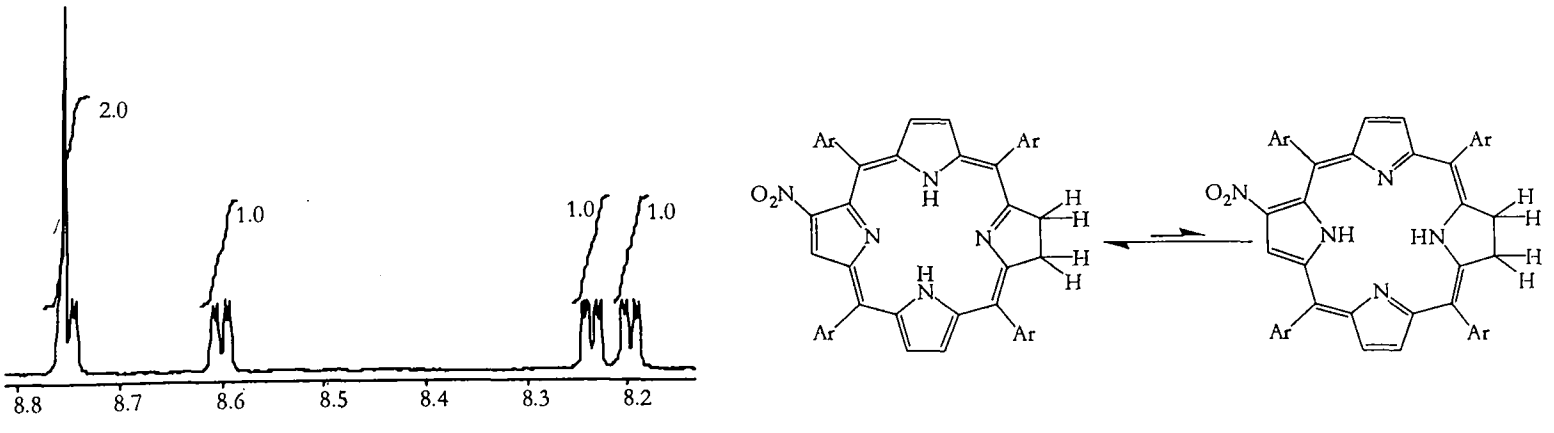

Figure **4.8**- expanded segment of the ^{1}H NMR of the nitro-chlorin **54** showing the unsaturated β-pyrrolic region and the equilibrium between the two NH tautomers of **54**. Ar = 3,5-di-*tert*-butylphenyl.

in Appendix One the only structure that is consistent with this observation is one in which the nitro group is antipodal to the saturated β-pyrrolic positions, and with the equilibrium in Figure **4.8** lying far to the left.

Chapter Five

The allylic oxidation of chlorins

Chapter Five
The allylic oxidation of chlorins

The observation that a chlorin could be oxidized by silica under ambient laboratory conditions was a fortuitous one. On investigation a small number of similar reactions had been observed previously, although no similar synthetic transformation had ever been usefully carried out on silica itself. And because the methods of chlorin synthesis outlined in Chapter Four are relatively well-established, this fortuitous observation represented an excellent opportunity to thoroughly investigate the factors affecting this transformation and its mechanism. The approach of this chapter is to initially concentrate on the investigation of these factors and an elucidation of the mechanism; the utility of the functionalization is then illustrated by its application to the synthesis of various porphyrin *alpha*-diones in Section **5.9**.

5.1 Oxidation of the simple free-base chlorin

5.1.1 Oxidation on silica

This investigation was initiated by the observation that when a sample of the simple chlorin **46** was analysed by thin layer chromatography (TLC) and the plate allowed to dry, then when the TLC plate was re-immersed into solvent the one product **46** had reacted to become two. Hence the oxidation of chlorin **46** was initially investigated on a silica substrate. Results are summarised in Figure **5.1** and Table **5.1**.

Initially the oxidation was attempted on a column of silica, prepared as if carrying out column chromatography. The solvent used to prepare the column and to load the chlorin onto the silica was a 1:8 volume mixture of dichloromethane: light petroleum. After 2½ hours at room temperature a band of similar polarity to the chlorin starting material was eluted, followed by a

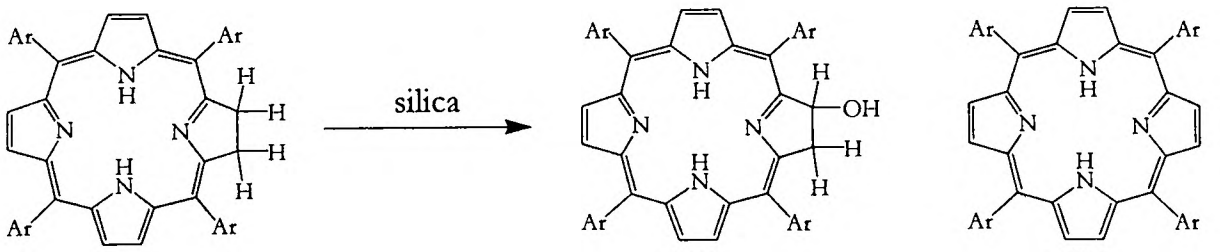

Figure **5.1**- the allylic oxidation of a simple chlorin. Ar= 3,5-di-*tert*-butylphenyl.

Experiment	Solvent*	Special column conditions**	Yields (%) Chlorin (46)	Porphyrin (45)	Hydroxy-chlorin (62)
A	1:8	Solvent is not removed from column	51	9	26
B	1:8		25	5	48
C	1:4		92	-	-
D	dichloromethane		99	-	-
E	toluene		100	-	-
F	1:8	Degassed solvent	93	2	1
G	1:8	2.0 ml water in 100 ml silica	71	2	25
H	1:8	10 ml water in 100 ml silica	86	-	11
I	1:8	Completely in the dark	27	5	52
J	1:8	40°C	23	7	43
K	1:8	40°C for 18 hours	13	12	58
L	1:8 + 0.015 equivalents triethylamine	40°C	38	-	42
M	1:8	Solvent is not removed from column for 17 hours	6	22	58
N	1:8 +0.015 equivalents triethylamine	Solvent is not removed from column for 16 hours	97	-	-
O	1:8	0.8 ml water in 100 ml silica, for 17 hours	4	14	67

Table **5.1**- oxidation of chlorin (**46**) on silica. *- "1:X" refers to volume fractions of dichloromethane to light petroleum. Other solvent fractions are given in terms of volume. **- unless otherwise stated reactions are carried out at room temperature with 'solvent removed' from the column, and with the substrate left exposed to silica for 2½ to 3 hours.

much more polar product. The less polar product was identified by ^{1}H NMR as a mixture of the chlorin **46** and the porphyrin **45**. The respective yields of these two products were then calculated through the integration of the appropriate signals in the ^{1}H NMR and then the subtraction of the small proportion of porphyrin impurity that was present in the starting material, itself quantified by integration of the ^{1}H NMR of the starting material. The more polar product was identified as the pure hydroxy-chlorin **62**. It was isolated in a low yield of 26% (experiment A in Table **5.1**).

In order to better mimic the conditions under which a reaction had occurred on the TLC plate, another column was prepared and this time it was pumped dry by hand. Typically pumping the column dry by hand removed one third of the total solvent retained by the silica on a 'wet' column. This time a reasonable extent of reaction was observed with a 48% yield of hydroxy-chlorin **62** and a further 25% yield of the starting material **46** (experiment B). A smaller amount of porphyrin by-product **45** was also observed (5%), its yield calculated by integration of the ^{1}H NMR of the inseparable chlorin/ porphyrin mixture in the same way as that described for experiment A.

From this starting point factors that might favour or disfavour the formation of both the hydroxy-chlorin **62** and the porphyrin **45** were examined. These investigations were carried out with 'solvent removed' from the column as this was observed to be less sensitive to minor changes in reaction conditions such as temperature than without the solvent removed; in addition in experiment B, where the solvent was pumped off the column, more hydroxylated product and less porphyrin product were isolated than in experiment A, where solvent was not pumped off the column.

It was found that three factors had a significant effect on the extent of the oxidation:

- The polarity of the solvent from which the column was prepared.

The reaction proceeded well when the column was prepared from 1:8 dichloromethane: light petroleum (experiment B), but changing to a slightly more polar solvent mixture of 1:4 dichloromethane: light petroleum effectively caused the reaction to stop (experiment C). Furthermore when the polarity of the solvent was increased further by using either neat dichloromethane or neat toluene to prepare the column, only starting material was recovered at the end of the reaction (experiments D and E).

- Whether the solvent was deoxygenated.

A column was prepared as normal and then pumped through with approximately four volumes' worth of deoxygenated solvent. The substrate was placed onto the silica under argon, and solvent removed from the column with a flow of argon. This resulted in a greatly reduced extent of reaction (experiment F).

- Whether the silica was 'deactivated'.

Silica can be deactivated by mixing it with water. It was found that reducing the activity of the silica had a great effect on the extent of reaction (experiments G and H), with silica corresponding to roughly Brockman grade II showing only a small amount of reaction with the substrate (experiment H).

In contrast the oxidation was surprisingly insensitive to three factors:

- Photochemical activation.

When light was excluded from the reaction by completely covering the column in foil (experiment I) a similar product distribution was obtained as when such precautions were not taken.

- Temperature.

When the temperature was increased from room temperature to 40°C essentially the same product distribution was observed (experiment J).

- Reaction time.

When the reaction was left at 40°C for 18 hours instead of the standard 2½ to 3 hours a slightly increased yield of hydroxy-chlorin was isolated, but 13% of the starting material was still recovered (experiment K).

The origin of the porphyrin product **45** was also investigated. Initially it was thought that it could originate from the dehydration of the hydroxy-chlorin **62** catalyzed by the mildly acidic silica, as well as from direct oxidation of the chlorin **46**. When 0.015 volume equivalents of triethylamine were added to the reaction solvent, the porphyrin product disappeared at little expense to the overall extent of reaction (experiment L versus experiment J). Therefore it seemed that the dehydration might play a prominent role in the origin of **45**. However, it was also considered that triethylamine is not only a Brønsted base but also a Lewis base and therefore could affect the reaction in other ways besides preventing protonation. In order to definitively assign the origin of the porphyrin **45**, the hydroxy-chlorin **62** was loaded onto a column and solvent removed. No porphyrin product was isolated. Therefore contrary to initial expectations, this result strongly suggests that the origin of the porphyrin **45** is from direct oxidation of chlorin **46**.

Attempts to maximize the yield of the hydroxy-chlorin **62** were also made. It was considered that by removing solvent from the column some starting material might be driven onto unreactive sites on the surface of the silica; therefore by leaving solvent on the column and extending the reaction time from the 2½ hours of experiment A, a greater extent of reaction might be achieved. Hence a column without solvent removed was left for 17 hours at room temperature. A good yield of hydroxy-chlorin **62** was isolated (58%) (experiment M), with very little starting material recovered. In an attempt to reduce the yield of the porphyrin product **45** triethylamine was added to the reaction solvent, but now no reaction was apparent at all (experiment N). Instead deactivating the silica with a small amount of water reduced the

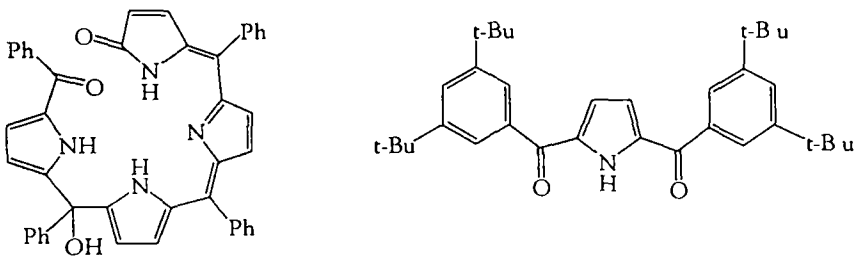

Figure **5.2**- left- the violinic product identified by Jackson *et al.*[151]; a similar product might have been isolated in the oxidation of the free-base chlorin **46** by silica. Right- the possible impurity in the possible violinic product.

proportion of porphyrin product, and an impressive 67% yield of hydroxy-chlorin was isolated (experiment O).

Finally, in all the experiments reported Table **5.1** more polar products were also eluted at the end of the reaction. One of these was a purple product, and this bore several similarities to the purple violinic product described by Jackson *et al.*[151] (Figure **5.2**), specifically in its distinctive purple colour, in the appearance of three NH protons in its ^{1}H NMR at 9.9, 11.1 and 12.6 ppm and in its mass measured by MALDI from a dithranol matrix corresponding to the loss of H_2O from the parent ion. However the product was found to be impure by ^{1}H NMR. Recrystallization from dichloromethane/ acetonitrile resulted in a reduced amount of impurity in the precipitate, but it was not able to remove it completely. By monitoring the relative intensities of the peaks in the ^{1}H NMR before and after recrystallization, the structure of the impurity was found to be consistent with the substituted pyrrole structure shown in Figure **5.2** (6.9 (2H,d), 7.7 (2H, dd), 7.8 (4H, d), 10.4 (1H, s)).

5.1.2 Oxidation on alumina

Since this allylic oxidation has been found to proceed on silica, it was also considered that it might also occur on other inorganic substrates. On investigation of the literature (c.f. Section **5.8**) it was found that two porphyrin substrates had previously shown similar behaviour on alumina[152,153]. Therefore alumina was investigated as an alternative substrate for the present system. Results of the investigation of the oxidation of the simple chlorin **46** on different types of alumina are given in Table **5.2**.

The first thing to note is that the alumina substrate shows similar reactivity to a silica substrate in so much that it oxidizes the chlorin **46** to the hydroxy-chlorin **62**. For neutral alumina, as for silica, there was limited reaction on a 'wet' column, but there was a greater consumption of starting material on the 'dry' column (experiments A and B in table **5.2**). Both raising the temperature to 40°C and leaving the reaction for a longer period of time resulted in a greater

Experiment	Type of alumina	Column conditions*	Yields (%) Chlorin (46)	Porphyrin (45)	Hydroxy-chlorin (62)
A	Neutral	Solvent is not removed from the column	41	27	15
B	Neutral		19	54	21
C	Neutral	40°C	14	62	6
D	Neutral	left for 17.5 hours	-	58	-
E	Neutral	40°C, 2 ml water in 100 ml alumina	-	46	53
F	Acidic		69	12	20
G	Acidic	40°C	-	77	-
H	Basic		87	-	13
I	Basic	40°C	85	3	9

Table **5.2**- oxidation of chlorin **46** on alumina. *- unless otherwise stated reactions are carried out at room temperature with the column prepared from a solvent mixture of 1:8 dichloromethane: light petroleum where the ratio is given in terms of volume fractions; the solvent was pumped off the column; and products were eluted off the column after 2½ to 3 hours.

yield of the porphyrin by-product (**45**) (experiments C and D). However in contrast to silica it was concluded that a major pathway to this porphyrin product was through the elimination of H_2O from the hydroxy-chlorin **62**, as when a sample of the hydroxy-chlorin **62** was loaded back onto a column and left for 2 hours 43% of the sample had been converted to the porphyrin (**45**).

An attempt was therefore made to minimise this unwanted reaction and to concurrently maximise the yield of the desired product **62** through deactivation of the alumina with the addition of water. This indeed resulted in a greater yield of the hydroxy-chlorin **62** (experiment E), but still a significant amount of porphyrin **45** was isolated.

The effect of varying the type of alumina was also examined. Both acidic and basic aluminas were much less effective substrates than neutral alumina under similar conditions (experiments F and H compared to experiment B). The chlorin **46** placed on acidic alumina produced a stark green colour, indicating possible protonation of the inner nitrogens of the free-base chlorin; this would produce a deactivated species and would explain the low extent of reaction on acidic alumina at room temperature. Raising the temperature to 40°C on acidic alumina

resulted in solely isolation of the porphyrin (**45**) (experiment G), but on basic alumina no increase in the low extent of reaction was observed at the higher temperature (experiment I).

5.2 A preliminary model of reactivity- surface active sites

The observations of the reactivity of the chlorin **46** on silica can be used to build up a model of what is occurring at a molecular level. The surface of silica evidently consists of polar active sites. It is on these active sites that the oxidation occurs. It can also be concluded that the activity of the active sites is dependent on the presence of molecular oxygen and does not require photochemical activation. This simple model can be used to explain the observations:

- The reaction initially occurs faster when solvent is pumped off the column.

The effect of removing solvent from the system is to drive the chlorin substrate onto the actual surface of the silica.

- Over a longer period of time the reaction is observed to get closer to completion with solvent remaining on the column.

With the solvent removed from the column the chlorin becomes immobile on the surface of the silica. This is fine if it is absorbed on an active site, but the proportion of molecules not on an active site have no mechanism by which to reach an active site. In contrast when solvent is left on the column, molecules can freely absorb and desorb from active sites on the surface.

- The reaction occurs only when a column is prepared from a non-polar solvent.

The polar substrate **46** will be preferably absorbed onto polar sites on the surface from a non-polar solvent. Hence this is essentially a matter of solvation.

- The reaction will not proceed in deoxygenated solvent.

Molecular oxygen evidently plays an important role in the mechanism of reaction.

- The active site does not require photochemical activation.

Removing all photochemical activation led to no overall diminution in the extent of reaction.

Information about the make-up of these active sites is only hinted at by the present observations. The formation of biliverdin-type products might suggest a single-electron transfer mechanism[154]; but equally the involvement of molecular oxygen might suggest a radical mechanism. In order to gain more information about the active sites and the mechanism of reaction, a greater variety of substrates need to be examined. Through these investigations, presented in the remainder of this chapter, the optimum route to functionalized

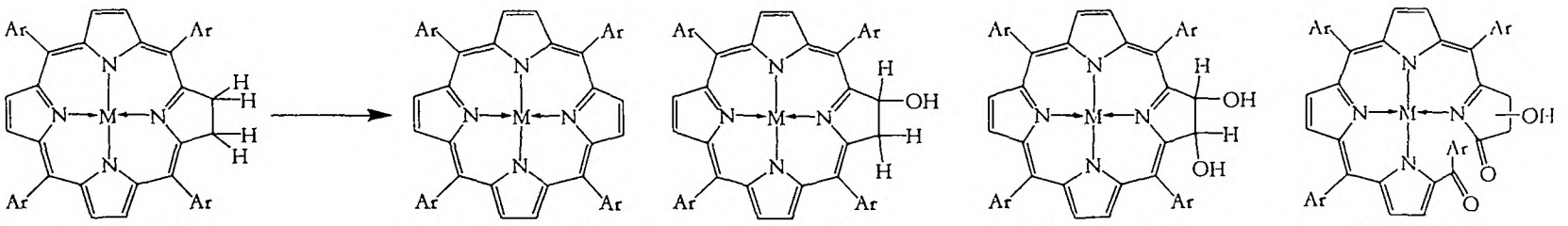

Figure **5.3**- products from the allylic oxidation of the metallated chlorins. Ar= 3,5-di-*tert*-butylphenyl.

hydroxy-chlorins that might lead to the desired regiospecifically functionalized porphyrin *alpha*-diones is also deduced.

5.3 Oxidation of metallated chlorins

To start the investigation into this allylic oxidation of functionalized substrates on silica, the behaviour of the nickel(II) (**49**), copper(II) (**50**) and zinc (II) (**51**) chlorins was examined. Reactions were carried out on columns prepared with silica deactivated by mixing with 2 ml water per 100 ml silica. The columns were prepared with a 1:8 dichloromethane: light petroleum solvent mixture. Once the substrate dissolved in the same solvent had been loaded onto the column, solvent was pumped off the column and the reactions were left at room temperature for 2½ to 3 hours. Results are shown in Figure **5.3** and Table **5.3**.

The change in reactivity of the metallated chlorins compared with the free-base chlorin under similar conditions is stark. The reaction proceeds to a much greater extent, with nearly no starting material recovered and di-hydroxylation observed with the nickel(II) and copper(II) chlorins. In addition a biliverdin product can also be definitively identified from the oxidation

	Yields (%)				
Metal	**Chlorin**	**Porphyrin**	**Mono-hydroxy chlorin**	**Di-hydroxy chlorin**	**Hydroxy-chlorin biliverdin**
None	(**46**) 71	(**45**) 2	(**62**) 25	-	-
Nickel	(**49**) -	(**63**) 38	(**66**) 23	(**69**) 18	(**71**) 5
Copper	(**50**) -	(**64**) 41	(**67**) 26	(**70**) 28	(**72**) 2
Zinc	(**51**) 6	(**65**) 38	(**68**) 42	-	-

Table **5.3**- oxidations of the metallated chlorins **49**, **50** and **51** as shown in Figure **5.3**. **51** and **65** were eluted in the same band, so their yields are calculated by integration of the relevant signals in the ^{1}H NMR.

of the nickel (II) chlorin. But the greatest difference between the metallated chlorins and the free-base chlorin has to be the great increase in the yield of the porphyrin product isolated.

In order to try to deduce the origin of this porphyrin product, the nickel(II) hydroxy-chlorin **66** was loaded onto a column of silica and placed under the same conditions as those under which the reaction had originally proceeded. After 2½ hours, 63% of the starting material was recovered with a further 23% of the di-hydroxylated product and no evidence of any porphyrin product. This strongly suggests that the porphyrin product again originates from the direct oxidation of the chlorin **49** rather from the dehydration of the hydroxy-chlorin **66**.

Finally, the oxidation of the zinc chlorin **51** was temperamental and was found to only be successful when carried out in complete darkness as ambient laboratory light lead to the photo-oxidation of either the starting material or the products.

5.3.1 Characterization of the metallated chlorins

In addition to these major differences in reactivity, there were several differences in the details of the characterization of the metallated chlorins compared with the free-base chlorins. Firstly, in the room temperature ^{1}H NMR spectrum of the hydroxylated nickel chlorins **66** and **69** the *ortho* aryl protons were absent. This indicates hindered rotation of the aryl ring about the meso carbons, and the point of coalescence of the two *ortho* environments on the NMR timescale being close to room temperature. The low temperature ^{1}H NMR revealed the individual *ortho* signals, two of which are at relatively low chemical shift values in each ^{1}H NMR. This shows that the porphyrin framework has been ruffled, and that these low chemical-shift *ortho* protons lie beneath the porphyrin ring and are therefore shielded by ring currents.

Secondly, the relative configuration of the two hydroxyl groups in the nickel(II) di-hydroxy chlorin was unknown. Previously Dolphin showed that it was possible to form the propylidene acetal (Figure **5.4**) from the *cis* di-hydroxy chlorin[84], and therefore the same procedure was attempted for the present system. Thus **69** was dissolved in dry acetone, $ZnCl_2$ was added and the system was brought to reflux. No acetal product was evident in the crude product of the reaction mixture with further purification resulting in an isolated yield of 51% of the nickel hydroxy-porphyrin **73**, a result of the dehydration of **69**, and 47% recovery of the starting material **69**. Hence a tentative assignment of a *trans* stereochemistry to **69** can be made.

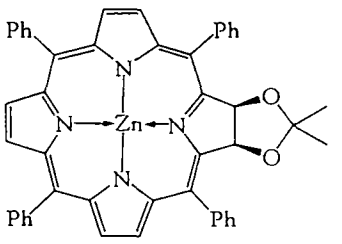

Figure **5.4**- propylidene acetal that can be formed from a *cis*-dihydroxy-chlorin.

The nickel(II) hydroxy-biliverdin product **71** also proved a challenge in the justification of its structure. Carbon-13 and HMBC NMRs of the biliverdin (**71**) demonstrate the regiospecifity of the ring cleavage of the nickel chlorin (**49**). These are shown in Figure **5.5**. The ^{13}C NMR shows two signals corresponding to the two carbonyl groups in **71**, at 183 and 186 ppm. The signal at 183 ppm shows two resonances in the HMBC spectrum with the signals corresponding to two of the unsaturated β-pyrrolic protons belonging to the CH_2 group, at 2.16 and 2.73 ppm in the ^1H NMR. Therefore the break in the chlorin framework has to be adjacent to the reduced pyrrole unit. In addition, the room temperature ^1H NMR shows only one visible doublet in the aryl region at 7.89 ppm corresponding to the two *ortho* protons on one of the aryl groups. As for the nickel(II) hydroxy-chlorins **66** and **69** it is apparent that the other three aryl groups are hindered in their rotation at room temperature so that the signals

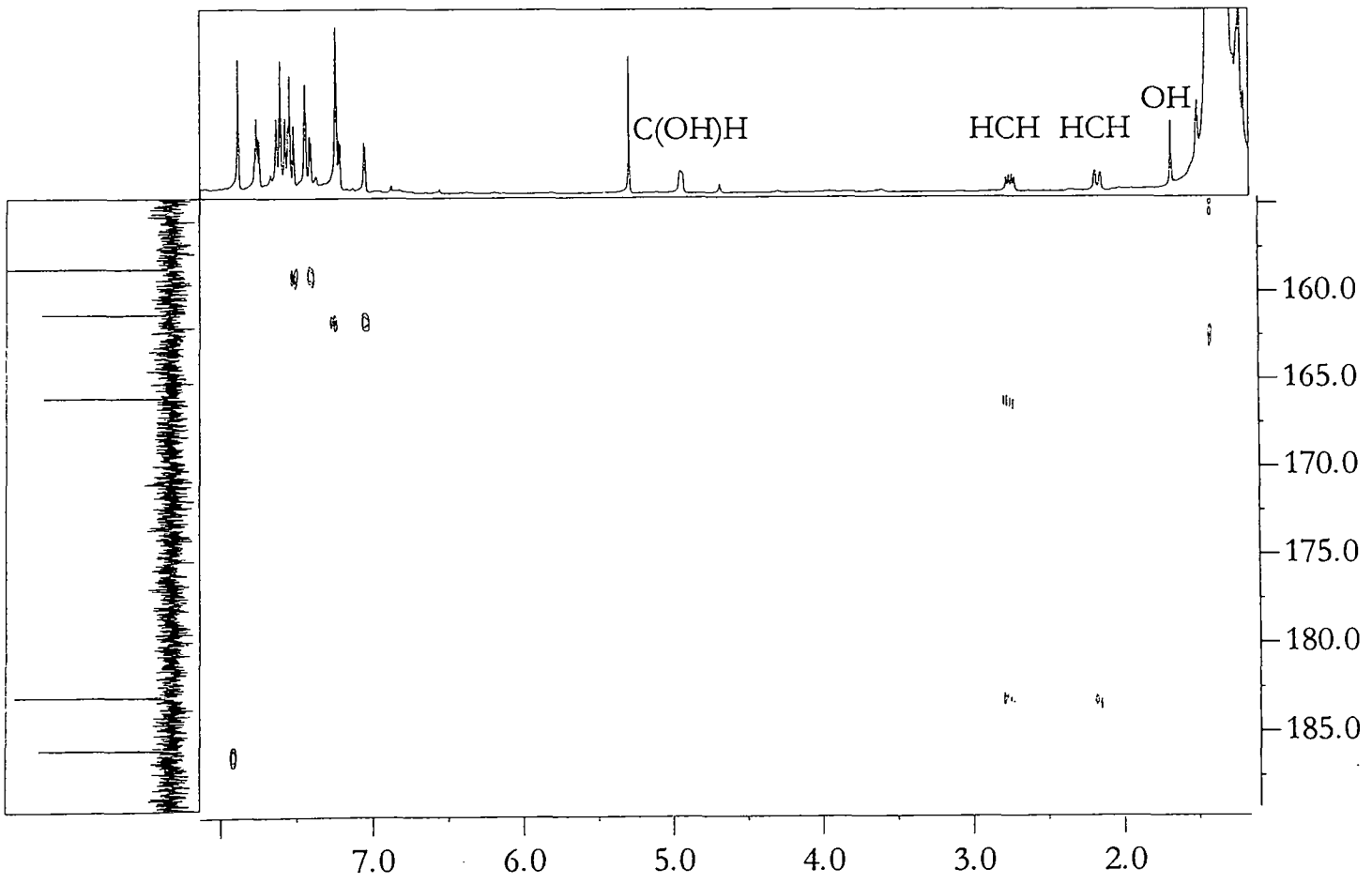

Figure **5.5**- a segment of the HMBC spectrum of the nickel hydroxy-biliverdin **71**. The horizontal and vertical axes are given in ppm. The ^1H NMR is recorded at 233K (the other spectra are recorded at room temperature).

corresponding to their *ortho* protons appear very broad. The visible doublet shows a resonance in the HMBC spectrum with the ^{13}C signal at 186 ppm and there are no other resonances with this carbon. Hence the signal at 183 ppm must correspond to a carbonyl directly fused onto the reduced pyrrole unit, as the carbonyl at 186 ppm is adjacent to an aryl group. Beyond this though, these techniques were not able to identify the regiochemistry of the hydroxy group at the unsaturated position.

A copper biliverdin product **72** was also isolated. However since copper is paramagnetic ^{1}H NMR could not be used to identify any regiospecifity in the product.

5.4 Oxidation of functionalized chlorins

The oxidations of the various functionalized chlorins synthesised in Chapter Four were now attempted on silica. In order that a fair comparison could be made between all results, conditions for each oxidation were kept roughly constant, namely the oxidations were carried out on silica deactivated with 2 ml water per 100 ml silica; solvent was pumped off the column by hand; a constant temperature of around 30°C was maintained; and the products were eluted after 2½ to 3 hours. Deactivated silica was used as some of the products such as the hydroxy-bacteriochlorin **61** were observed to undergo dehydration on purification over normal silica; and since it was desirable to separate the effects of dehydration from the effects of direct oxidation of the chlorin to the porphyrin, using slightly deactivated silica was considered the best way of achieving this.

5.4.1 Oxidation of bacteriochlorins

The oxidations of the unsubstituted bacteriochlorin **47** and hydroxy-bacteriochlorin **61** were initially attempted. Results are shown in Table **5.4**. It was observed that very little or no starting material is recovered in either case, but also a relatively small amount of dihydroxy-

	Yields of products (%)				
Bacteriochlorin starting material	Bacteriochlorin **47**	Hydroxy-bacteriochlorin **61**	Dihydroxy-bacteriochlorins **74** and **75**	Chlorin **46**	Hydroxy-chlorin **62**
Unsubstituted **47**	12	2	15	45	13
Hydroxy-bacteriochlorin **61**	n/a	-	24	11	41

Table **5.4**- the products from the oxidation of the bacteriochlorins **47** and **61** on silica

bacteriochlorins **74** and **75** were recovered. Instead the significant proportion of isolated products resulted from a loss of functionality at one side of the macrocycle. Thus for the unsubstituted bacteriochlorin **47** the major product is the unfunctionalized chlorin **46**; whereas for the hydroxy-bacteriochlorin **61** the major product is the hydroxy-chlorin **62**.

The difference in the major product isolated from each of these oxidations is significant as it implies that the major pathway through which the antipodal functionality is lost is through direct oxidation of a *4H*-chlorin to a *2H*-porphyrin rather than through dehydration of hydroxy-chlorin products. This is the conclusion from examining the converse situation, or in other words what would be the result of the dominant process being dehydration. This is illustrated in Figure **5.6**. In this case all products from the oxidation of the bacteriochlorin **47** would be derived from the first intermediate in the reaction sequence, namely the hydroxy-chlorin **62**. Therefore a similar product distribution would be expected from the oxidation of the bacteriochlorin **47** and the hydroxy-bacteriochlorin **61**. As this is not the case, dehydration must be the minor process.

5.4.2 Characterization of dihydroxy-bacteriochlorins

There are four possible regioisomers of the dihydroxy-bacteriochlorins, as illustrated in Figure **5.7**. These were isolated in two different bands from the column. One band was of very similar polarity to the monohydroxy-chlorin **62** and therefore was not isolated as a completely

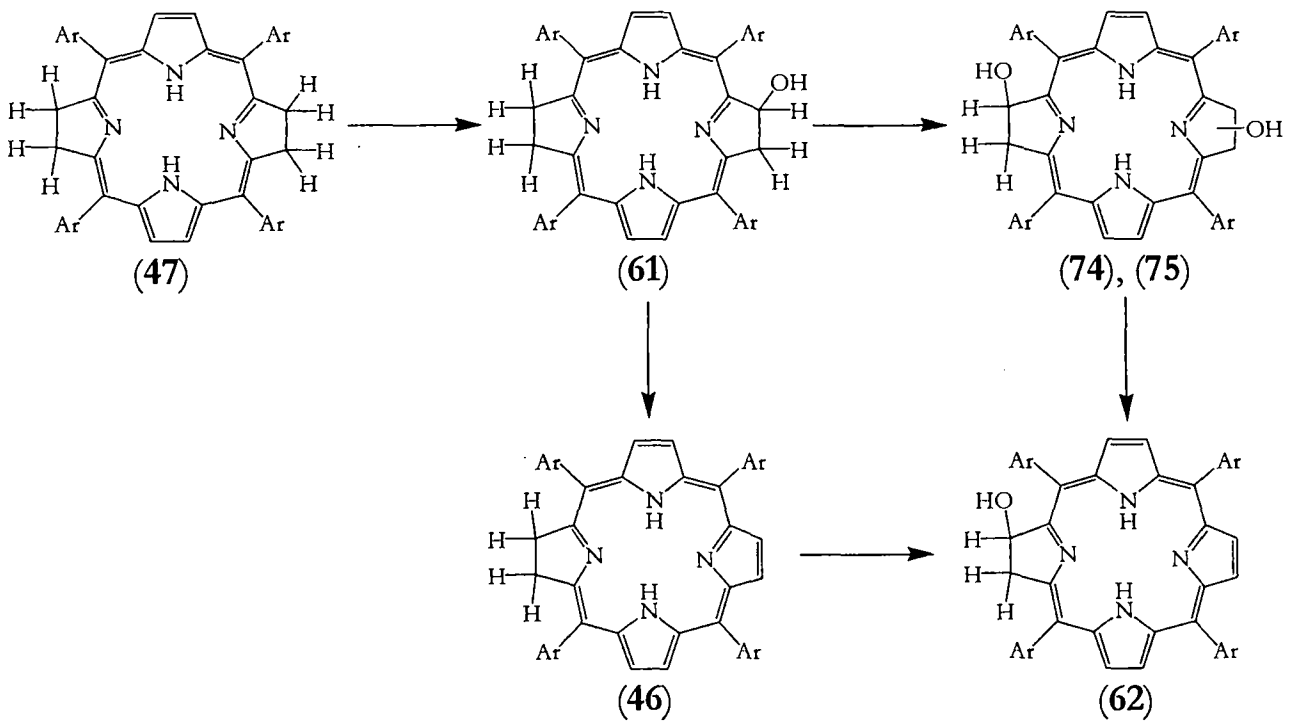

Figure **5.6**- predicted intermediates in the oxidation of bacteriochlorin **47** if the major pathway by which the antipodal functionality is lost is through dehydration of the hydroxy-chlorin products rather than through the direct oxidation of a *4H*-chlorin to a *2H*-porphyrin. Ar= 3,5-di-*tert*-butylphenyl.

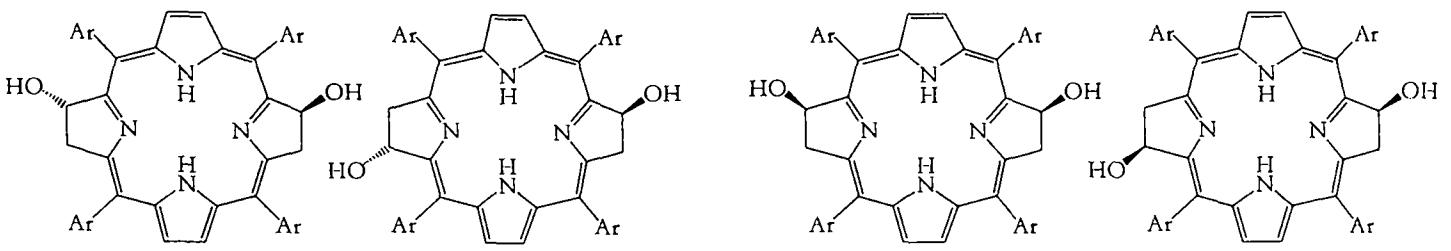

Figure **5.7**- regioisomers of the di-hydroxy bacteriochlorin. Ar = 3,5-di-*tert*-butylphenyl.

pure compound. The second band however was considerably more polar and was isolated and completely characterized without the presence of impurities. The bacteriochlorin nature of these products is confirmed by their UV-VIS spectra. In addition the ^{1}H NMR spectra of both bands are characterised by two different β-pyrrolic environments, as illustrated in Figure **5.8**. Environment 'a' is symmetrical so that the unsaturated β-pyrrolic protons appear as two singlets (then split by coupling to the NH protons), whilst environment 'b' is unsymmetrical, so that the unsaturated β-pyrrolic protons appear as two doublet (split further by coupling to the NH protons). Equally there are two different NH environments- one symmetrical so that a single NH signal is apparent, and one unsymmetrical so that two NH peaks are visible. These two different environments integrate to roughly equal intensities, but the COSY spectra show that the unsymmetrical NH environment is coupled to the symmetrical β-pyrrolic signals (environment 'a' in Figure **5.8**) and that the symmetrical NH signal is coupled to the unsymmetrical β-pyrrolic signals (environment 'b'). This can be interpreted by each band containing a roughly equal mixture of the 2,12-dihydroxy-bacteriochlorin (environment 'b' with symmetrical NH and unsymmetrical unsaturated β-pyrrolic environments) and the 2,13-dihydroxy-bacteriochlorin (environment 'a' with unsymmetrical NH and symmetrical

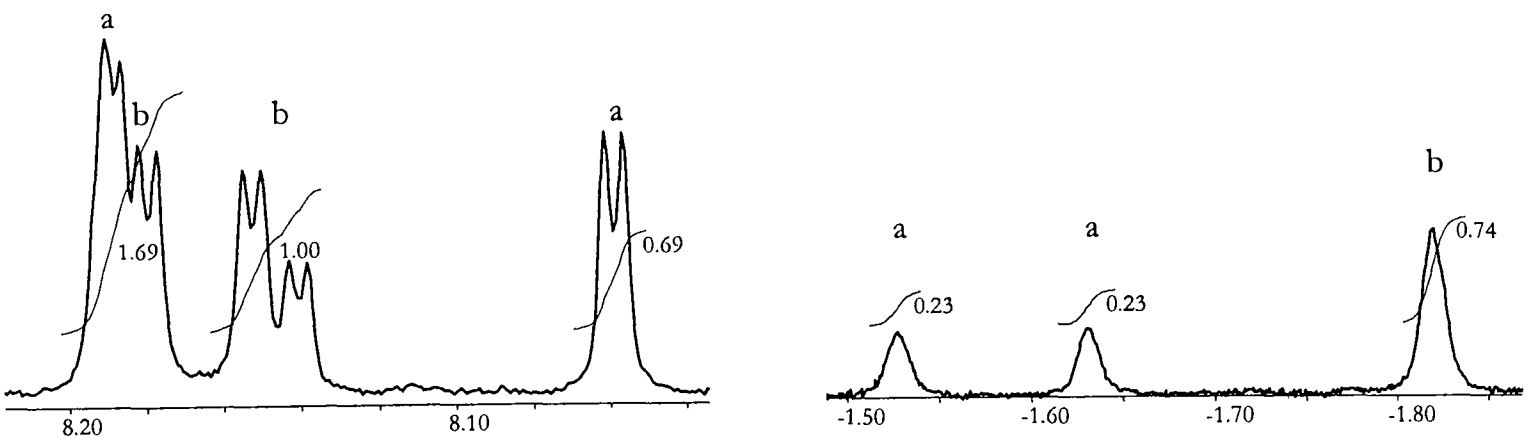

Figure **5.8**- segments of the ^{1}H NMR spectrum of **75a** and **75b**. The left-hand segment shows the unsaturated β-pyrrolic region; the right-hand segment shows the NH region. The quartet centred around 8.19 in the unsaturated β-pyrrolic region consists of a doublet (integrated to an intensity of 0.69) overlapping with one half of an ABX system (integrating to an intensity of 1.00).

unsaturated β-pyrrolic environments). Furthermore the less polar mixture of compounds can reasonably be assigned to the *trans* form **74a** and **74b** and the more polar band to the *cis* form **75a** and **75b** (Figure **5.7**), in a similar manner to the assignment of the structures of the tetrahydroxy-chlorins by Dolphin[83].

5.4.3 Oxidation of other chlorin substrates

The results of the oxidation of the chloro-chlorin **53**, nitro-chlorin **54** and quinoxalino-chlorin **58** under the standard conditions are shown in Table **5.5**. The products of these oxidation were relatively easy to characterize, the only point of note is that there are two regioisomers to the chloro hydroxy-chlorin; as for the dihydroxy-bacteriochlorin isomers these were isolated as one product, and two distinct environments are apparent in the ^{1}H NMR corresponding to the two different regioisomers.

5.5 Initial evaluation of the nature of the surface active sites

The most puzzling aspect of the results from the oxidation of the various chlorins on silica is the isolation of biliverdin by-products. These are unusual but interesting as their presence can be used as a guide in an initial evaluation of the possible mechanisms at work at the 'active sites' on the surface of the silica described as in section **5.2**. And whilst it is possible that the biliverdin products might originate from a completely different mechanistic pathway from the other products, it is still an informative procedure to concentrate on these products for the moment.

It has been postulated that biliverdins can be formed by several different mechanisms. Firstly, these biliverdin products are accessible by the photooxygenation of electron-rich porphyrins[155-157]. It is thought that this photo-oxidation might occur via singlet oxygen

Chlorin Starting material	**Yields of products (%)** Chlorin recovered	Porphyrin Products	Hydroxy-chlorin
Nitro-chlorin **54**	100	-	-
Chloro-chlorin **53**	74	-	(**76**) 6
Quinoxalino-chlorin **58**	20	(**24**) 9	(**77**) 47

Table **5.5**- products from the oxidation of the nitro-, chloro- and quinoxalino-chlorins.

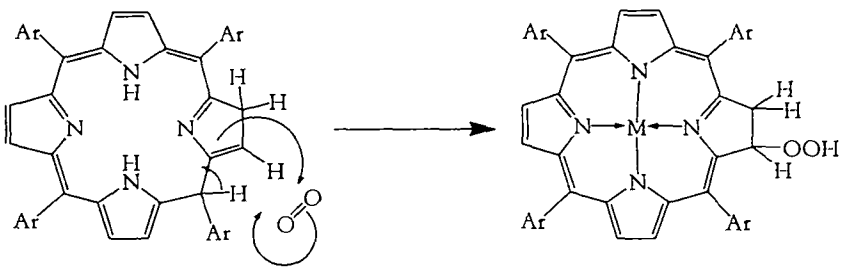

Figure **5.9**- possible singlet oxygen 'ene' addition to a phlorin intermediate.

addition to the porphyrin[157]. Indeed, it has been shown that photo-oxidation of a chlorin in an oxygen atmosphere might lead to hydroxy-chlorin products[158].

A singlet oxygen mechanism could also account for the observed allylic oxidation of a chlorin. This oxidation would presumably occur via ene addition to a phlorin-type intermediate (as shown in Figure **5.9**), and would be similar to the photo-oxidation of 7,8-chlorin-β-phlorins[159]. Whitlock has also demonstrated that there is an equilibrium between the chlorin and phlorin in solution[160]. Furthermore it has been shown by delayed fluorescence measurements that singlet oxygen is readily produced by porphyrins and other substrates absorbed onto silica[161,162]. However photochemical conditions are required for the production of singlet oxygen by porphyrins, and it has been shown that the allylic oxidation of chlorins by silica does not require photochemical activation. Hence it is considered unlikely that singlet oxygen is responsible for this transformation.

A second type of mechanism responsible for the synthesis of biliverdins is exemplified by the metabolism of heme, which proceeds with the breakdown of heme into a biliverdin product. This occurs regiospecifically, as observed for the present oxidation on silica. The reaction pathway proceeds via an intramolecular hydroxyl transfer from an Fe(III)-OOH intermediate[163,164]. This intramolecular hydroxyl transfer is clearly not possible in this case, but a radical mechanism initiated by the abstraction of a hydrogen by triplet oxygen absorbed onto the active sites of the surface of silica, followed by recombination with a oxygen-derived radical is certainly feasible. And a radical substitution reaction might also explain the hydroxy-chlorin products. Therefore a radical mechanism needs to be considered in the present situation.

It has been postulated that a third type of mechanism can lead to biliverdin products. Kevin Smith showed that chlorins treated with thallium (III) trifluoroacetate are cleaved regiospecifically adjacent to the C_2H_4 chlorin group[165]. Smith postulates that the reaction sequence might proceed by a series of single electron transfer (SET) reactions. In the case of

silica, a notional Lewis acidic active site could accept an electron from the chlorin substrate. And it could easily result in hydroxy-chlorin products. Thus a SET pathway could also explain the observed reactivity.

To distinguish between a radical and a single electron transfer mechanism, the variation of the reactivity of the various substrates needs to be accounted for. It is apparent from Sections **5.3** and **5.4** a spectrum of reactivity is observed for chlorin substrates on silica. This ranges from the nitro-chlorin **54** and hydroxy-chlorin **62** that do not react; to the free-base chlorin and quinoxalino-chlorin **58** that show mainly hydroxy-chlorin products; to the bacteriochlorin **47** and hydroxy-bacteriochlorin **61** that show products mainly derived from the direct oxidation of a *4H*-chlorin to a *2H*-porphyrin. This wide spectrum of reactivity has to be explained by the reaction mechanism. It is not totally clear how a radical mechanism could explain this spectrum of reactivity, or how it could explain the formation of products resulting from the direct oxidation of the *4H*-chlorin to the *2H*-porphyrin. However a SET mechanism could explain this spectrum of reactivity, as a chlorin's propensity to undergo reaction will be directly dependent on its oxidation potential. Therefore in order to evaluate the feasibility of a SET mechanism, it was decided to measure the oxidation potentials of the various chlorins. It should also be noted that a similar investigation into the oxidation potentials of meso-substituted tetra-aryl chlorins has not been published to-date.

5.6 Electrochemistry

Oxidation potentials were examined in dichloromethane at room temperature. Cyclic voltammograms are shown in the experimental section and the relevant oxidation potentials in Table **5.6**. All potentials are quoted with reference to the ferrocene/ ferrocenium couple.

The measured $E_{1/2}$'s are typical of porphyrin and chlorin electrochemical oxidations. Increasing the saturation of the porphyrin periphery (in going from the chlorin **46** to bacteriochlorin **47**) shifts the first oxidation potential negatively by roughly 400 mV. Metallation also shifts the first oxidation negatively; the greatest effect is observed for the electron-rich zinc chlorin. Extension of the delocalized system (in going from the chlorin **46** to the quinoxalino-chlorin **58**) again shifts the first oxidation potential negatively as expected; conversely the introduction of an electron-withdrawing influence (in going from the chlorin **46** to the chloro-chlorin **53** and the nitro-chlorin **54**) onto an unsaturated β-pyrrolic position

Compound	$E_{1/2}(o1)$	$E_{1/2}(o2)$
Nitro-chlorin **54**	235	355
Chloro-chlorin **53**	180	355
Di-hydroxy copper chlorin **70**	170	420
Di-hydroxy nickel chlorin **69**	165	420
Free-base hydroxy-chlorin **62**	165	340
Copper hydroxy-chlorin **67**	115	390
Nickel hydroxy-chlorin **66**	110	380
Free-base chlorin **46**	70	375
Quinoxalino-chlorin **58**	0	235
Bis-chlorin **60**	-40	85
Nickel chlorin **49**	-65	315
Copper chlorin **50**	-95	280
Zinc hydroxy-chlorin **68**	-100	170
Hydroxy-bacteriochlorin **61**	-165	-
Zinc chlorin **51**	-200	70
Bacteriochlorin **47**	-345	185

Table **5.6**- First and second oxidation potentials for various chlorins. Values are given in millivolts.

makes the first oxidation potential more positive. Finally, introduction a hydroxyl group onto a saturated β-pyrrolic position also increases the first oxidation potential (on going from **46** to **62** (the free-base system), from **49** to **66** (the nickel system), from **50** to **67** (the copper system), and from **51** to **68** (the zinc system)), typically by between 100 and 200 mV. The introduction of a second hydroxyl group has slightly less effect (going from **66** to **69** (the nickel system) and from **67** to **70** (the copper system)) as the oxidation potential increases by only 50 to 60 mV.

5.7 The Lewis acidic active site model and single electron transfer

5.7.1 A single electron transfer processes

On initial inspection of the oxidation potentials in Table **5.6** it is evident that there is a correlation between oxidation potential and reactivity. Those chlorins with too positive an oxidation potential such as the nitro-chlorin **54** and the free-base chlorin **46** show only a small extent of reaction if any at all, whereas those with a lower oxidation potential show a much greater extent of reaction with the formation of both hydroxylated and porphyrinic products.

Importantly it has already been shown that the porphyrinic products do not originate from the elimination of water from the hydroxy-chlorin on silica, but rather from the direct oxidation of the *4H*-chlorin to the *2H*-porphyrin. The extent of the correlation of reactivity with oxidation

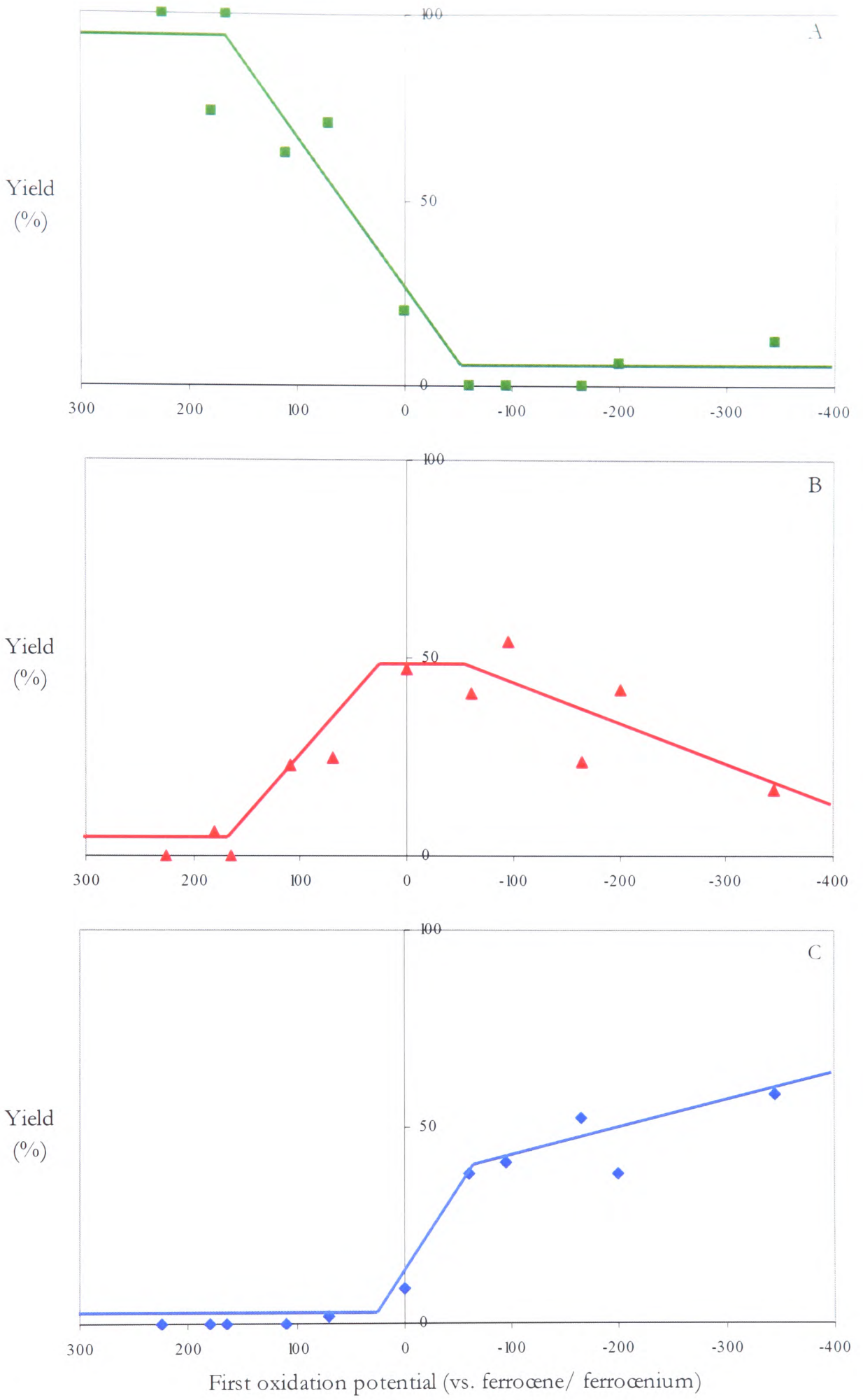

Figure **5.10**- correlation between oxidation potential and reaction product from the oxidation of the various chlorins on silica. **A** = starting material; **B** = hydroxylated product; **C** = product from the direct oxidation of the *4H*-chlorin to the *2H*-porphyrin.

potential is only realized when the yields of the various types of products- whether it be starting material, the hydroxylated product, or the product resulting from direct oxidation of

the *4H*-chlorin to the *2H*-porphyrin (the 'porphyrin product')- are compared directly with the oxidation potential of the parent chlorin. This is shown in Figure **5.10**.

The first thing that is apparent is the clear correlations between oxidation potential and reactivity. This is strong evidence of a single electron transfer mechanism, and therefore of the Lewis acidic nature of silica. Whilst the lines drawn on the graphs are somewhat arbitrary, they do illustrate this correlation. It is also apparent that the correlations between both the yield of the starting material and the yield of the porphyrin product with oxidation potential are strong; the correlation between the yield of the hydroxylated product and the oxidation potential is still evident but a little less strong at more negative oxidation potentials.

These correlations not only make the broad suggestion that this oxidation involves a single electron transfer process, but they in fact suggest the existence of two single electron transfer processes. This is the conclusion from the observation that the yields of the hydroxylated product and the porphyrin product *both* correlate with the oxidation potential of the chlorin, but in a different manner to one another. Thus at intermediate oxidation potentials the hydroxylated product is the dominant product; whereas at more negative oxidation potential the porphyrin product is the dominant product.

5.7.2 Two single electron transfer oxidations

A mechanism that is consistent with the observation of two SET pathways is shown in Figure **5.11**. The mechanism starts with the formation of the chlorin π-radical cation (step 1) followed by deprotonation (step 2). An attractive alternative mechanism is to reverse these two steps. This is attractive as the oxidation potential of the anion would be considerably less positive than the oxidation potential of the neutral system, as the anion is formally placed in a non-bonding orbital. In addition deprotonation followed by single electron oxidation has been suggested for another porphyrin hydroxylation process in the 'allomerization of chlorophyll' [166] (see Figure **5.14**). And a chlorin system is reasonably acidic as it can be deprotonated by sodium methoxide[160]. However deprotonation of the neutral chlorin is considered unlikely in this particular case as the pK_a of the silanol groups on the silica surface are a maximum of 9 [167]; in addition it has been shown that this oxidation occurs on acidic alumina, where an initial deprotonation step is unfeasible.

A surface hydroxyl radical, whose origin is discussed in Section **5.7.3**, then combines with the chlorin radical intermediate either at the β-pyrrolic or at the meso position to give the hydroxylated product (step 3) or the biliverdin product (step 6) after a further oxidation. It

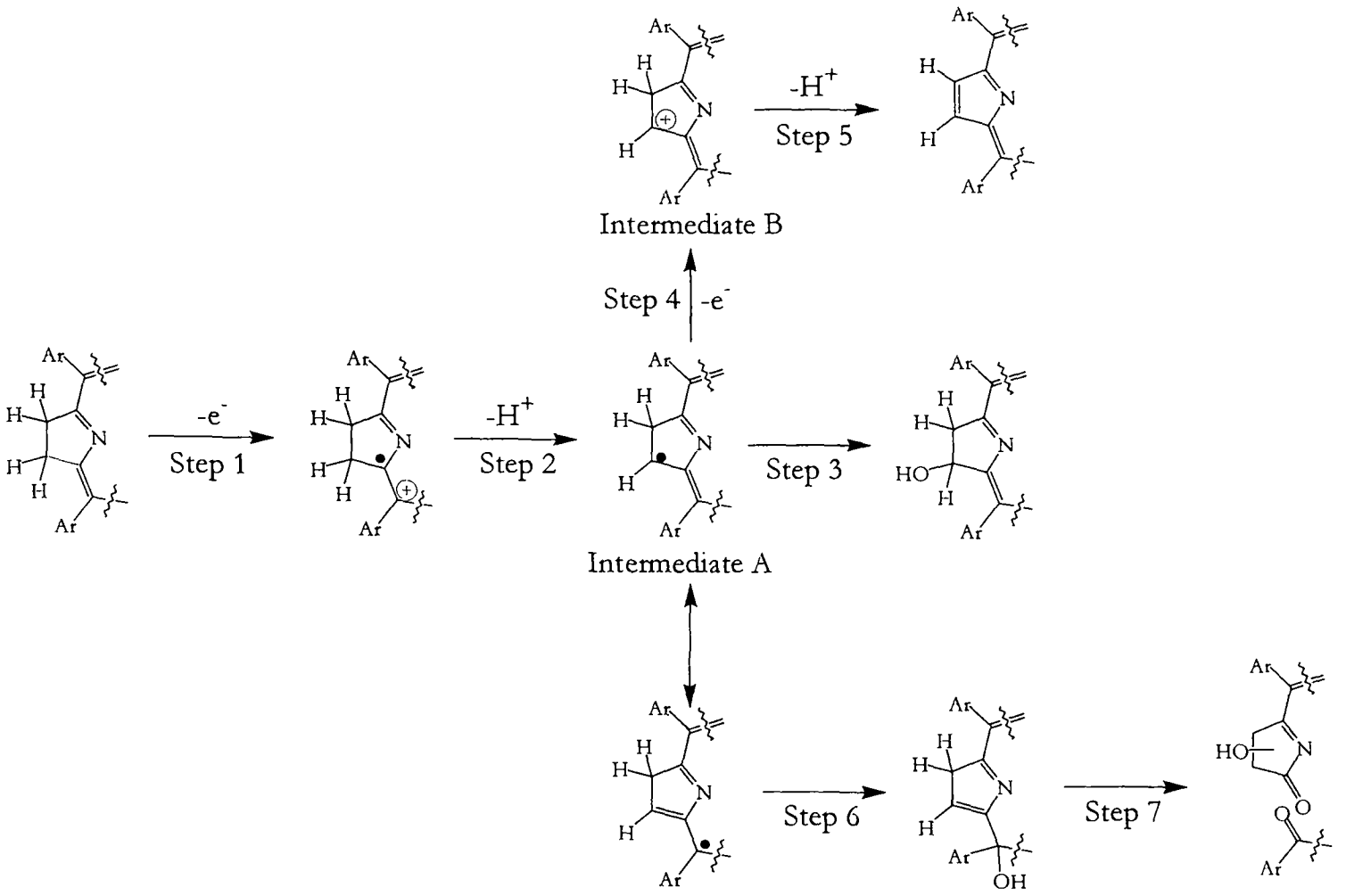

Figure **5.11**- proposed single electron transfer mechanism for the oxidation of a chlorin on silica. Ar= 3.5-di-*tert*-butylphenyl.

has already been noted that at relatively negative oxidation potentials the correlation between oxidation potential and hydroxylated products is slightly weak. This can now be explained by the choice of positions at which the hydroxyl radical can attack. As the competition will depend on subtle electronic factors rather than purely oxidation potential, and as the biliverdin product is not always isolated as it is very likely that it is susceptible to further oxidation on the silica, the result is the sporadic correlation of hydroxylated product with oxidation potential at more negative oxidation potentials.

It has also already been emphasised that the porphyrin product is not a result of dehydration of the hydroxy-chlorin product, and therefore the origin of the porphyrin product can be attributed to a second electron abstraction after step 2 from intermediate A and subsequent proton loss. It would also be possible to obtain hydroxylated product from this pathway through the quenching of the carbocation intermediate B with H_2O. However this can be discounted as a 'crossroads' in the mechanism is required by the correlations shown in Figure **5.10**; this conclusion is also supported by additional evidence of the oxidation of other substrates on silica and alumina, outlined in section **5.8.2**.

5.7.3 The role of oxygen

The final elusive part of the mechanism is the role that oxygen plays in this oxidation. Taking a lead from Mazur[168] (see section **5.8.3**) it is thought that the destination of the electron abstracted from the chlorin substrate is in fact molecular oxygen itself. Mazur describes this as a 'contact charge-transfer interaction'. Within the present mechanism this is described as an electron-transfer process to molecular oxygen, mediated by a surface active site.

Step 1 in Figure **5.11** therefore involves the reduction of molecular oxygen by the chlorin substrate:

$$\text{Step 1:} \qquad O_2 + e^- \rightarrow O_2^-$$

The importance of the 'contact charge-transfer interaction' is realised when the thermodynamics of the situation are examined. Under normal circumstances step 1 would be considered thermodynamically unfeasible, as $E_{1/2}(O_2/ O_2^-)$ = -870 mV[169] (in acetonitrile at pH 10). Hence reaction does not occur and is not expected to occur in solution under an oxygen atmosphere. However the 'contact charge-transfer interaction' induced by the surface overcomes this thermodynamic barrier. One way in which this might be achieved would be through the pre-organisation of the chlorin substrate and an oxygen molecule at the silica surface. It has been shown in Chapter Three (Section **3.5**) for the mechanism of nitration of aromatic compounds that an inner-sphere charge-transfer interaction between two neutral species is possible in a tightly-bound complex, and in the present situation the role of the surface might be to facilitate the formation of such a tightly-bound complex. But EPR measurements on aromatic substrates[177,178] absorbed onto silica described in Section **5.8.1** show the formation of π-cation radicals in the absence of oxygen, suggesting that the initial destination of the electron abstracted from the substrate is actually a surface site. Therefore it is more likely that the initial species that is formed in the present situation is a tightly-bound complex of the chlorin with a surface active site, from which electron-transfer is now feasible from the chlorin to the surface site.

Although this charge-transfer complex needs to be tightly-bound as significant charge-separation is certainly infeasible, this is not to say that the complex is unreactive. The surface active site is now formally negatively charged, and in this state it will be liable to oxidation by molecular oxygen physisorbed onto the surface ('XH_2' represents the chlorin substrate and 'AS' the active site):

$$\text{Step 1:} \qquad XH_2\ AS\ \cdot O{=}O\cdot \rightarrow XH_2^+\ AS^-\ \cdot O{=}O\cdot \rightarrow XH_2^+\ AS\text{-}O\text{-}O^-$$

Once again the final state has to be tightly-bound to stabilize the chlorin π-radical cation.

The overall effect is therefore a surface-mediated electron transfer from the chlorin substrate to molecular oxygen. From this point, deprotonation of the chlorin would be facile:

Step 2: XH_2^+ AS-O-O^- → $XH^{\cdot}$ AS-O-OH

The result of deprotonation is the formation of the chlorin radical intermediate 'A' (Figure **5.11**).

From intermediate 'A' two pathways are viable:

- radical-radical combination leading to a hydroxy-chlorin product (step 3)

The mechanism described in Figure **5.11** requires intermediate 'A' to combine with a hydroxyl radical to form the hydroxy-chlorin and biliverdin products. The simplest explanation for this hydroxyl radical is that it is actually the $HOO^{\cdot}$ radical that is the other product from step 2. The hydro-peroxy chlorin that would be the product of radical combination could then be oxidized in a second step to the observed hydroxy-chlorin product. However the conversion of a hydro-peroxy species to a hydroxy species on silica is relatively unprecedented.

A more plausible explanation comes from the consideration of the nature of the oxygen product from step 2. It is by no means a free radical; if anything it is better described as being covalently bound to the active site on the surface. In this way the hydroxylation reaction in step 3 might be considered as a hydroxyl transfer between the surface oxygen species and the substrate:

Step 3: $XH^{\cdot}$ AS-O-OH → XHOH [AS-$O^{\cdot}$ ↔ AS=O]

This idea should also be compared to the mechanism of porphyrin hydroxylation that occurs in the breakdown of heme in the body by heme oxygenase. The porphyrin hydroxylation proceeds with a hydroxyl transfer from an iron(III)-OOH intermediate to the meso position of the porphyrin periphery[163,164]. Whilst the nature of this transfer remains controversial, it *can* be interpreted in terms of the transfer of a hydroxyl radical with the iron stabilizing the remaining radical oxygen intermediate (Fe(IV)=O). This is analogous to the proposed mechanism of chlorin hydroxylation on silica, just with an intermolecular hydroxyl radical transfer in place of an intramolecular one.

- a second single electron oxidation leading to the porphyrin product (step 4)

On initial inspection, hydroxylation should in fact be a disfavoured pathway. This is because the intermediate 'A' will possess a lower oxidation potential than the parent chlorin starting material, as it is formally a radical placed in a non-bonding orbital stabilized by the adjacent

chlorin bonding system. However in order to obtain any hydroxylated products intermediate 'A' has to be oxidized at a slower rate than the starting material.

This paradox can be resolved if the state of the surface active site at the end of step 2 is considered. It is effectively covalently bound to an oxygen species, and therefore will certainly not be as powerfully Lewis acidic as in its unbound state in step 1. In this way there is a greater barrier to charge-transfer from intermediate 'A' than to charge-transfer from the parent chlorin, and it is only at more negative chlorin oxidation potentials that this second pathway leading to the porphyrin product becomes dominant.

5.8 Other observations of oxidation on silica and alumina

Many diverse observations of the oxidation of various substrates on silica and alumina have been reported[150,152,153,170-181]. An evaluation of these can be used to strengthen the case for the single electron transfer mechanism shown in Figure **5.11**. Implicit in this discussion is that the same mechanism is operating on silica and alumina. The results presented in Section **5.1** show the similar behaviour of the chlorin on the two substrates, and since this hydroxylation is such an unusual reaction it is not unreasonable to assume that the same basic mechanism for the formation of the hydroxylated product is operating on both substrates.

5.8.1 Evidence for the formation of radical cations on silica and alumina

It was noted forty years ago that certain aromatic compounds could be hydroxylated by grinding or shaking with silica[174,175]. This process was interpreted in terms of the formation of 'active sites' during grinding[174]; the polar substrates physisorbed onto these active sites then underwent a 'polar interaction' leading to a 'possible positive ion intermediate'; the formation of these active sites was attributed to metal ion impurities such as iron present in the silica.

This 'polar interaction' has been further elucidated by various physical studies of substrates absorbed onto silica and alumina surfaces. Early electron paramagnetic resonance (EPR) studies of various polyaromatic hydrocarbons on alumina and silica-alumina substrates suggested the formation of the radical cations of the absorbed species[176]. These observations have been confirmed by more recent EPR[177,178] and infra-red[179] studies. One of these studies[177] shows the importance of the polarity of the solvent from which the substrate is absorbed onto the surface on the formation of π-radical cation of the substrate. In addition the active sites on the surfaces of the silica and alumina substrates are identified as metal ion impurities, due to

Al(III) species occupying surface sites- impurities that are still present at low concentrations even in 'pure' silica. It was also observed that the presence of molecular oxygen reduced the intensity of the EPR signal, pointing to a surface active site-mediated electron transfer between the substrate and molecular oxygen[177].

5.8.2 Evidence against a carbocation intermediate

The quenching of a carbocation intermediate by water leading to the formation of a hydroxylated product, as can be observed in for example the oxidative degradation of guanine in DNA[180,181], can be discounted for the present oxidation by the observation of other oxidations on silica and alumina. The first example shows oxidation of a porphyrin on alumina[152] (Figure **5.12**). If this oxidation was to proceed through a carbocation intermediate, it would be expected that the secondary carbocation would facilely rearrange to the more stable tertiary carbocation. Since no rearrangement is reported, a carbocation intermediate can be considered unlikely.

Oxidations have also been observed where the reactive centre is in conjugation with a carbonyl group[182,183]. These are shown in Figure **5.13**. These seem somewhat different to all the previous examples as the systems do not contain polyaromatic hydrocarbons. However the carbonyl functionality means that these two systems are incompatible with carbocation intermediates.

5.8.3 Evidence concerning the involvement of molecular oxygen

The role of molecular oxygen in certain oxidations on silica and alumina has been investigated. Burns observed that the oxidation of his porphyrin substrate on alumina[153] (Figure **5.14**) did not proceed when carried out in an argon glove-box. He explained this observation in terms of the mechanism of the allomerization of chlorophyll[166]. The allomerization of chlorophyll is

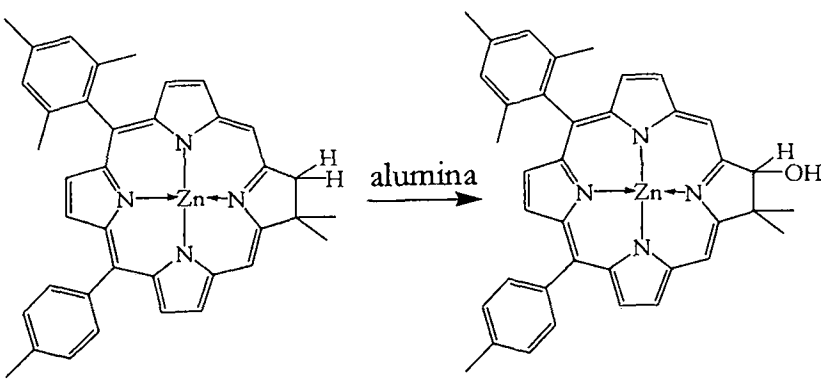

Figure **5.12**- Lindsey's oxidation of a chlorin on alumina.

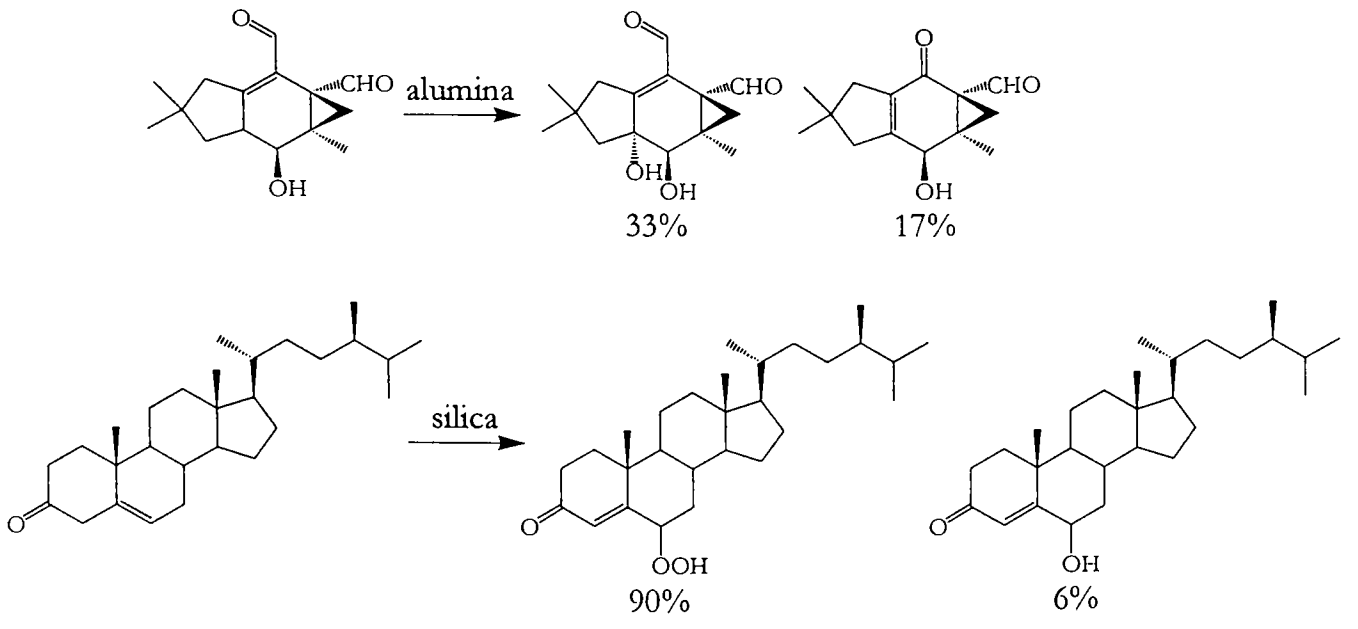

Figure **5.13**- further examples of oxidations on silica and alumina.

a hydroxylation reaction (also shown in Figure **5.14**) that thought to occur through an electron transfer from the enolate form of the porphyrin starting material to molecular oxygen. The reaction of the intermediate radical with a species derived from molecular oxygen is confirmed by ^{18}O-labelling studies. Therefore in the context of Burns's oxidation on alumina, the alumina is proposed to mediate an electron transfer between molecular oxygen and the porphyrin substrate.

One final piece of evidence supports a mechanism in which the solid support mediates electron transfer between the substrate and molecular oxygen. Mazur showed that 1,4-diphenylbutadiene was oxidized in the dark[168] (Figure **5.14**). It was proposed that a contact

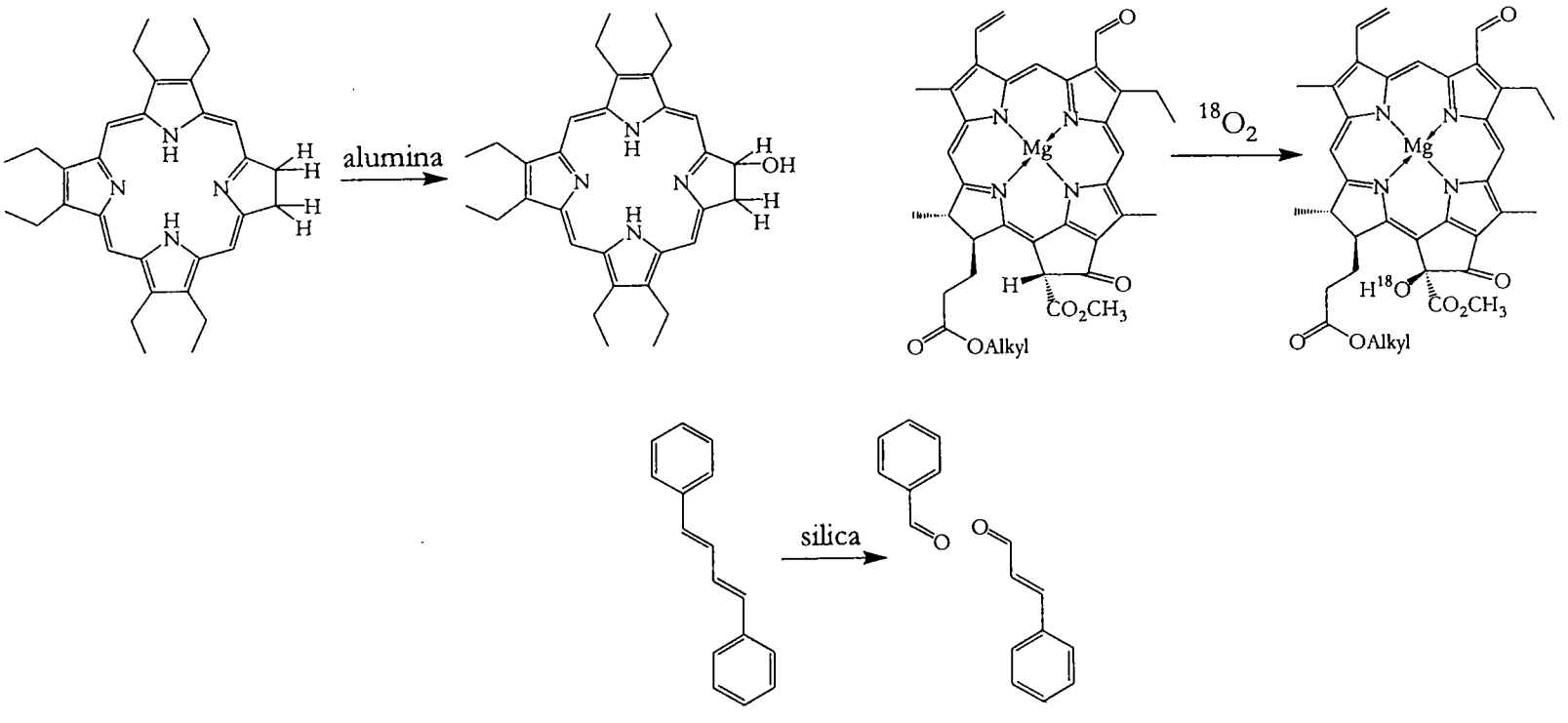

Figure **5.14**- the oxidation of various substrates that have been postulated to involve molecular oxygen. Clockwise from top left- Burns's oxidation; the allomerization of chlorophyll; and Mazur's oxidation.

charge-transfer interaction between the substrate and oxygen molecules leads to electron transfer between the two substrates; attack of the newly formed O_2^- onto the cation of the substrate might then lead to the observed products.

5.9 Application to the synthesis of porphyrin diones and tetra-ones

In order to demonstrate the utility of this methodology to the synthesis of porphyrin *alpha*-diones, oxidations of various hydroxy-chlorins by the Dess-Martin reagent were attempted. In general these oxidations were carried out by adding roughly ¾ of an equivalent of the Dess-Martin reagent to the pertinent substrate dissolved in dichloromethane at half hour intervals. The progress of the reaction was monitored closely by thin layer chromatography and when it was judged that the reaction had gone to completion, the reaction solution was passed through a plug of silica. Purification was then carried out by column chromatography.

5.9.1 Synthesis of the porphyrin *alpha*-dione

Firstly, the oxidation of the 2-hydroxychlorin (**62**) to 2,3-dioxochlorin **20** was successfully achieved in 80% yield. As a comparison the simple chlorin **46** was also oxidised by the Dess-Martin reagent; the porphyrin **45** was isolated in 79% yield. The Dess-Martin oxidation of the nickel hydroxy-chlorin **66** and the zinc hydroxy-chlorin **68** were also examined (Figure **5.15**). The oxidation of the nickel hydroxy-chlorin **66** proceeded with a 41% isolated yield of desired nickel dione product **78**. However the oxidation of the zinc hydroxy-chlorin **68** proceeded with the isolation only of the lactone product **79** in only 3% yield, with the remaining product remaining as baseline material on purification by column chromatography.

Therefore the oxidation of the free-base chlorin provides the best route to porphyrin *alpha*-diones. The overall transformation of the unfunctionalized porphyrin to the *alpha*-dione

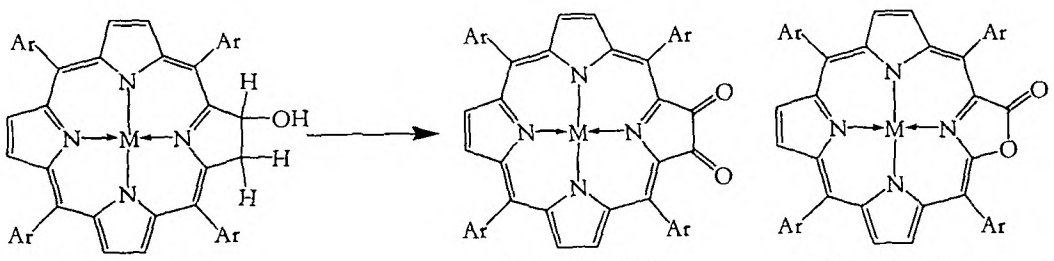

62, M= 2H
66, M= Ni
68, M= Zn

20, M= 2H
78, M= Ni

79, M= Zn

Figure **5.15**- oxidation of the hydroxy-chlorins with the Dess-Martin reagent. Ar= 3,5-di-*tert*-butylphenyl.

proceeds with a maximized yield of around 50% over three steps, which is comparable to previous, longer methodologies.

5.9.2 Synthesis of a single porphyrin tetra-one

In order to achieve the synthesis of a porphyrin tetra-one, the oxidation of the dihydroxy-bacteriochlorin **75** was examined. Only a 29% yield of desired tetra-one product **23** was isolated, with the rest of the reaction product remaining as baseline material on purification by column chromatography. Therefore the overall yield of transformation of the unfunctionalized porphyrin to the single porphyrin tetra-one is around 5% over 3 steps. On the face of it this is not as successful as previous methodologies. But in the oxidation step by silica around 70% of 'useful' by-products were also isolated, meaning that the overall 5% yield is not quite as bad as it might first seem.

5.9.3 Synthesis of a bis-porphyrin tetra-one

The synthesis of the bis-chlorin **60** was described in Chapter Four and now in order to synthesise the bis-porphyrin tetra-one it was subjected to various oxidation conditions on silica.

Initially **60** was placed on slightly deactivated silica (0.7 ml water per 100 ml silica) and solvent was removed. However 80% of the starting material was recovered, plus a small amount of more polar product. Therefore normal 'non-deactivated' silica was used, and this resulted in only a 19% recovery of starting material. A more polar band was isolated consisting of a mixture of products, but the poor solubility of the bis-chlorin meant that streaking on the column was a real problem and therefore isolation of pure products was not attempted. Instead direct oxidation with Dess-Martin periodinane of the mixture of product was attempted. A 29% yield of desired tetra-one product **21** was isolated along with a 16% isolated yield of the mono-functionalized dione product **80** (yields are over the two steps). This translates into a 15% yield of the desired tetra-one **21** from the unfunctionalized bis-porphyrin **14** over three steps, or 29% taking into account the recovery of starting material on the way. This compares very favourably with the one previous synthesis of the bis-porphyrin tetra-one[36], improving on it by up to a factor of five, and decreasing the number of steps for the functionalization from seven to only three.

5.10 Conclusions

It has been shown that the allylic oxidation of a chlorin can be usefully employed to functionalize porphyrins, and is specifically successful in the synthesis of the bis-porphyrin tetra-one **21**.

In addition the mechanism of this transformation has been elucidated as a surface-mediated electron-transfer from the chlorin substrate to molecular oxygen. This is a conceptually satisfying mechanistic conclusion. Chapters Two and Three invoked similar charge-transfer mechanisms to explain the observed reactivity of porphyrin substrates, but no definitive evidence could be provided for such mechanisms. In this instance good evidence has been provided for a charge-transfer interaction. This leads once again to the suggestion that the formation of charge-transfer complexes can be considered as a fingerprint of porphyrin chemistry.

Chapter Six

Synthesis and characterization of porphyrin arrays

Chapter Six
Synthesis and characterization of porphyrin arrays

It has been shown up to this point that several different strategies can be conceived for the synthesis of the building blocks to 1,4,5,8-tetraazaanthracene-bridged porphyrin arrays. The challenge that follows from these strategies is to use these building blocks to construct extended porphyrin arrays, and then to evaluate the properties of these porphyrin arrays.

6.1 Strategies for solubilizing porphyrin arrays

Crossley has only ever published the synthesis of a 1,4,5,8-tetraazaanthracene-bridged porphyrin array of four units' length[36]. The reasons for this have not been explicitly stated but it is very likely that as the size of the system increases its solubility decreases, making longer arrays insoluble. Crossley's strategy to solubilize his arrays was to substitute two *t*-butyl groups onto the phenyl rings of the tetraphenyl-porphyrin starting material. Osuka noted the limitations of this strategy, as when constructing his meso-meso singly-linked arrays he reached a limit of solubility at a length of eight porphyrins[21]. By changing to a solubilizing group incorporating long alkyl chains arrays of up to 1024 porphyrin units could be constructed. A similar strategy of incorporating long alkyl chains has also been used to synthesise Osuka's triply-linked porphyrin arrays[41], Sugiura's square dodecamer[29] and Anderson's butadiyne-linked arrays[184].

An alternative strategy for solubilizing a porphyrin array has been applied by Promarak to the 1,4,5,8-tetraazaanthracene-bridged system[37]. By incorporating a dendritic unit onto the

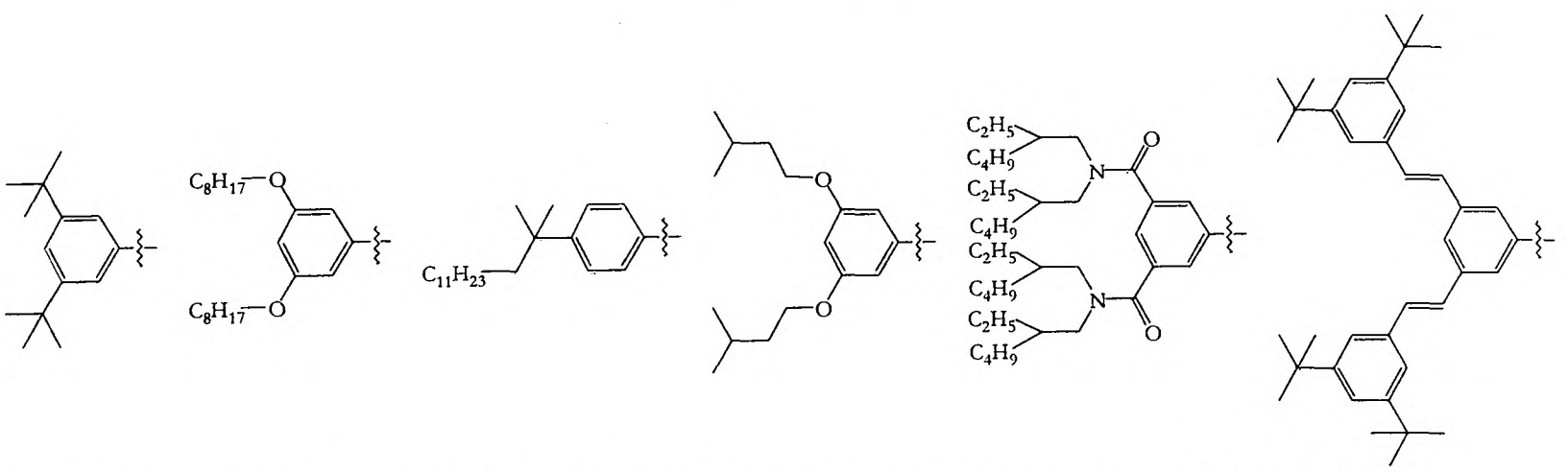

Figure **6.1**- solubilizing groups for the synthesis of extended porphyrin systems. From left to right: Crossley, Osuka, Osuka, Sugiura, Anderson and Promarak.

terminal positions of the array he showed that an array of 7 units' length could be constructed, nearly doubling Crossley's achievement.

Because of this success in the extension of the 1,4,5,8-tetraazaanthracene-bridged system it was decided to pursue this strategy to further extend these porphyrin arrays rather than to use the more popular strategy of using alkyl groups to aid solubility.

6.2 Functionalization of the dendritic porphyrin

6.2.1 Attempted synthesis of the dendritic porphyrin tetra-one

It was initially considered that the best route to an extended porphyrin array would be to synthesise the 'soluble' dendritic porphyrin tetra-one. For simplicity's sake this was attempted through the unregiospecific di-nitration of the porphyrin macrocycle, a route first described for the functionalization of the non-dendritic porphyrin by Narang[38,39] and then elucidated further by Crossley[82] and later Burn[89]. This route is illustrated in Figure **6.2**.

The first step of the synthesis leading to the copper dendritic nitro-porphyrin **85** has been demonstrated previously and was repeated in a similar yield (40%) with the addition of 1.5 equivalent of NO_2. Mono-nitration was also successful for the zinc porphyrin **83** in 22% yield. However when a second nitration was attempted on the copper porphyrin a significant proportion of starting material **85** was recovered (41%) even after the addition of 3 equivalents of NO_2. Equally when the direct di-nitration of the unfunctionalized zinc porphyrin **83** was attempted only baseline material was recovered on purification over silica, and attempted di-nitration of the nickel porphyrin **81** with 6 equivalents of NO_2 still led to the recovery of a small proportion of the mono-nitrated porphyrin **84** (7%).

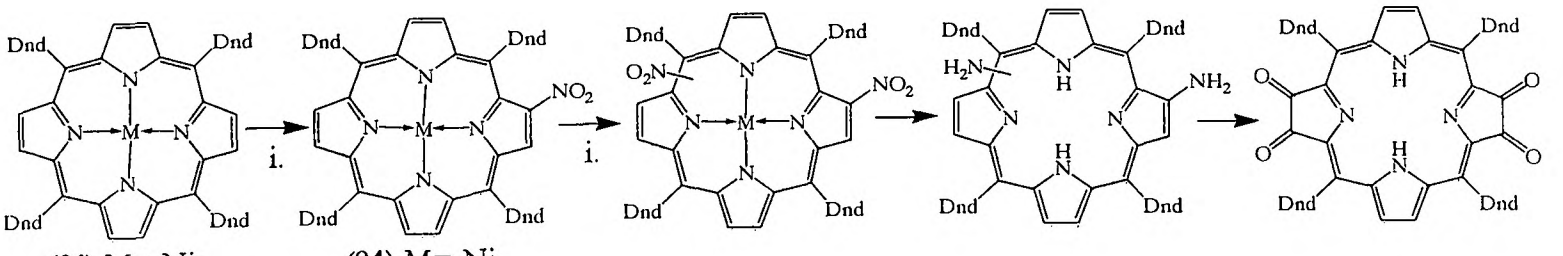

(**81**) M= Ni,
(**82**) M= Cu,
(**83**) M= Zn.

(**84**) M= Ni,
(**85**) M= Cu,
(**86**) M= Zn.

Figure **6.2**- proposed functionalization of the dendritic porphyrin **92**. i. NO_2 in light petroleum, CH_2Cl_2.

Dnd= 3,5-(3',5'-di-*tert*-butylstyryl)phenyl.

The attempted isolation of the di-nitrated porphyrins was further complicated by difficulties in purification and characterization. On purification these porphyrins streaked considerably on silica, so that the isolation of pure products from a mixture proved difficult. Equally samples that were thought to contain di-nitrated products could not be sufficiently structurally characterized. As the di-nitrated porphyrins exist as a mixture of six regioisomers ^{1}H NMR could not be used to prove the substitution on the porphyrin. Equally MALDI analysis of the products proved fruitless, as the nitro groups on the mono-nitrated products were observed to both significantly fragment and to pick up sodium ions in the spectra of the products, meaning that the parent ion peak of a pure di-nitrated product would be obscured by these other peaks.

Even with these difficulties in mind it is evident from the isolation of mono-nitrated products after the addition of a large excess of nitrogen dioxide that the dendritic porphyrin is reluctant to undergo a second nitration. This can be attributed to the mechanism of nitration. It has been speculated that this proceeds through the formation of a porphyrin π-cation radical *in situ* by reaction with a NO_2 molecule[92,185-188]. Then combination with either the NO_2^- anion or a second NO_2 molecule leads to the formation of the nitrated product. In the context of Chapters Two, Three and Four, this can be considered as another example of a porphyrin reacting through the formation of a charge-transfer complex. Table **6.1** shows how the dendritic copper porphyrin **82** has an oxidation potential a full 120 mV higher than the simple copper porphyrin **64**; and the effect of adding nitro groups to the porphyrin periphery is to increase that oxidation potential further. Therefore it can be speculated that

Unsubstituted/ dendritic porphyrin	**E(o1)/ mV**	**E(o2)/ mV**
Simple copper unsubstituted porphyrin **64**	220	580
Simple copper nitro porphyrin **95**	305	700
Dendritic copper unsubstituted **82**	360	-
Dendritic copper mono-nitro **85**	450	-
Dendritic nickel unsubstituted **81**	420	-
Dendritic zinc unsubstituted **83**	200	425

Table **6.1**- oxidation potentials of non-dendritic and dendritic, unsubstituted and nitrated porphyrins. Oxidation potentials are quoted relative to the ferrocene/ ferrocenium couple. It should be noted that at the concentrations that the electrochemistry was carried out the UV-VIS spectrum of the dendritic zinc unsubstituted porphyrin **83** showed evidence of significant aggregation.

the dendritic porphyrins are unwilling to undergo a second nitration because of their unfavourable oxidation potentials.

6.2.2 Synthesis of the dendritic porphyrin *alpha*-dione

Since the synthesis of the dendritic porphyrin tetra-one was not successful, it was decided to revert to the strategy of Promarak[37] and to incorporate two dendritic porphyrins as the end units of the porphyrin arrays. The overall methodology is explained in detail in Section **6.4.2** and is outlined in Figure **6.9**. Because of the large solubilizing groups that sit at either end of the array this type of array is referred to as a 'satellite' array.

Thus the dendritic porphyrin *alpha*-dione was synthesised in a 1 gram quantity by a previously established methodology (Figure **6.3**). The reaction sequence suffers from a low overall yield- 14% from the unfunctionalized dendritic porphyrin **87** and less than 0.5% from toluene (**87**)- although these yields were obtained before the adverse effect of the benzaldehyde oxime on the Dess-Martin oxidation was realised (see Section **6.3**).

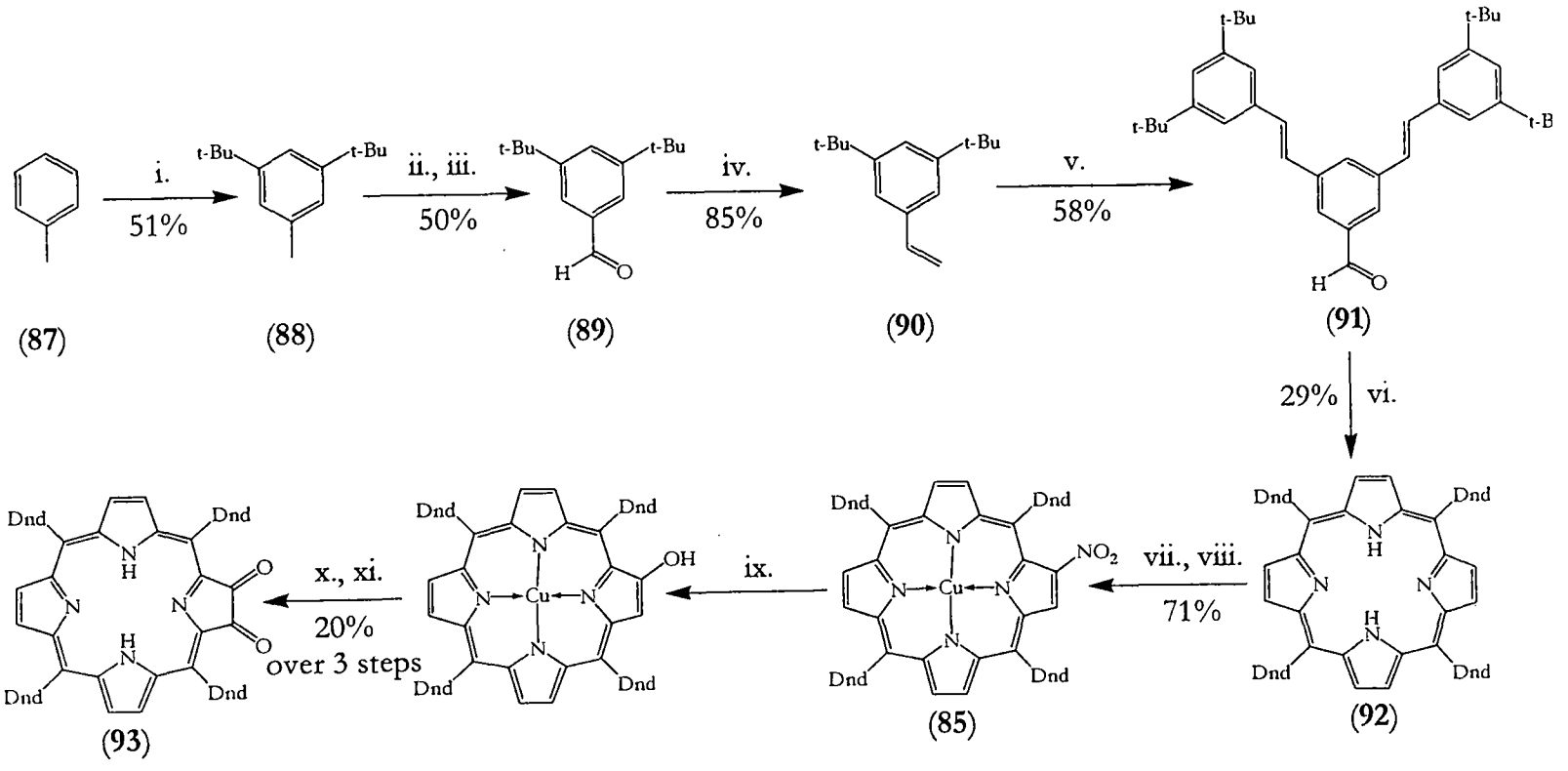

Scheme **6.2**- large-scale synthesis of the dendritic porphyrin *alpha*-dione. i. t-BuCl, $AlCl_3$; ii. *N*-bromosuccinimide, AIBN (cat.), $CHCl_3$, Δ_R; iii. HMTA, EtOH, Δ_R then conc. HCl; iv. Ph_3PCH_3I, t-BuOK, THF; v. 3,5-dibromobenzaldehyde, anhydrous Na_2CO_3, 2,6-di-*tert*-butyl-4-methylphenol, Hermann's catalyst, *N,N*-dimethylacetamide; vi. 1 eqv. pyrrole, trifluoroacetic acid, CH_2Cl_2 then DDQ; vii. $Cu(OAc)_2$, CH_2Cl_2/ MeOH, Δ_R; viii. 1.2 eqv. NO_2 in light petroleum, CH_2Cl_2, purification over alumina; ix. 10 eqv. benzaldehyde oxime, 11 eqv. NaH, DMSO/ THF, Δ_R; x. 1.5 eqv. Dess-Martin periodinane, CH_2Cl_2; xi. $(CH_3)_3SiI$, CH_2Cl_2.
Dnd= 3,5-(3',5'-di-*tert*-butylstyryl)phenyl.

6.3 Synthesis of the simple porphyrin tetra-one

It was initially thought that the quickest, easiest way to a porphyrin tetra-one unit would be through the di-nitration of the porphyrin macrocycle, outlined in Figure **6.4**. On a small scale this sequence has led to an overall yield of 15% of the tetra-one **23** from the starting porphyrin **45**, although previous attempts to scale-up this procedure had reduced this yield to only 5%[37].

Previous procedures[37] were followed precisely for this functionalization. Di-nitration of the copper porphyrin **64** was achieved successfully, and it was found that on a large scale a partial separation of the six regioisomers could be achieved as a proportion of the unwanted regioisomers ran ahead of the desired regioisomers on purification over silica. A proportion of the material was lost on demetallation of the macrocycle as it was difficult to prevent protonation of the porphyrin and the consequent formation of insoluble porphyrin derivatives. Despite this- and cracked glassware- 18.5 grams of partially separated free-base dinitro-porphyrin **94** was isolated, starting from 69 grams of porphyrin **45**. The final two steps were then carried out without purification of the intermediates, as described by Promarak[37]. Unfortunately barely 100 milligrams of the desired porphyrin tetra-one product **23** was isolated at the end of the sequence. The reasons for this very poor yield are not clear, but it is evident that this route to the porphyrin tetra-one is fraught with difficulty.

For this reason it was decided to revert to the methodology outlined in Chapters Four and Five in order to synthesise the bis-porphyrin tetra-one **21**. Building up a 1,4,5,8-tetraazaanthracene-bridged array with the bis-porphyrin tetra-one would also have the added advantage over the single porphyrin tetra-one **23** as the array will be lengthened by two units with each addition of a monomer unit rather than by just one. The precise route to the monomer unit is outlined in Figure **6.5**.

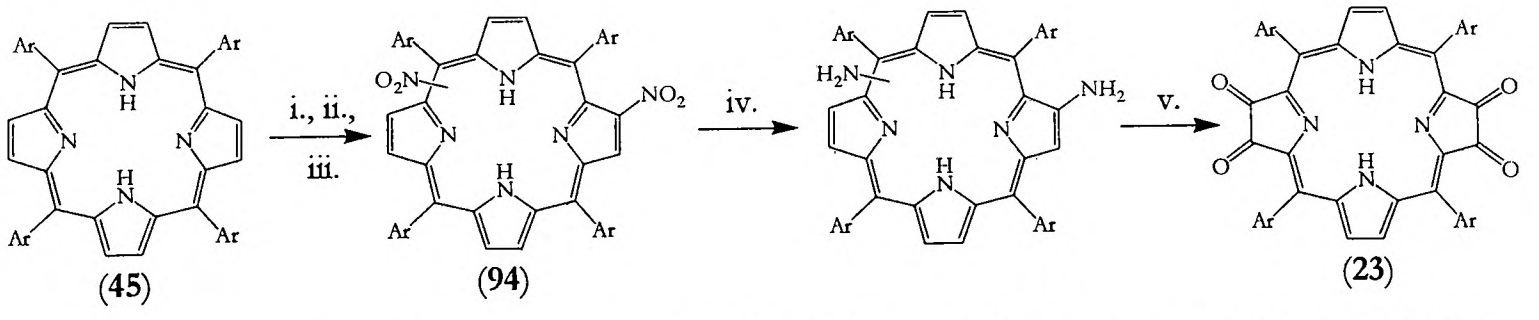

Figure **6.4**- the attempted large-scale synthesis of the simple porphyrin tetra-one. i. $Cu(OAc)_2$, CH_2Cl_2/ MeOH, Δ_R; ii. 2 eqv. NO_2 in light petroleum, CH_2Cl_2; iii. H_2SO_4, CH_2Cl_2; iv. $SnCl_2.2H_2O$, conc. HCl, CH_2Cl_2; v. 4 eqv. Dess-Martin periodinane, CH_2Cl_2. Ar = 3,5-di-*tert*-butylphenyl.

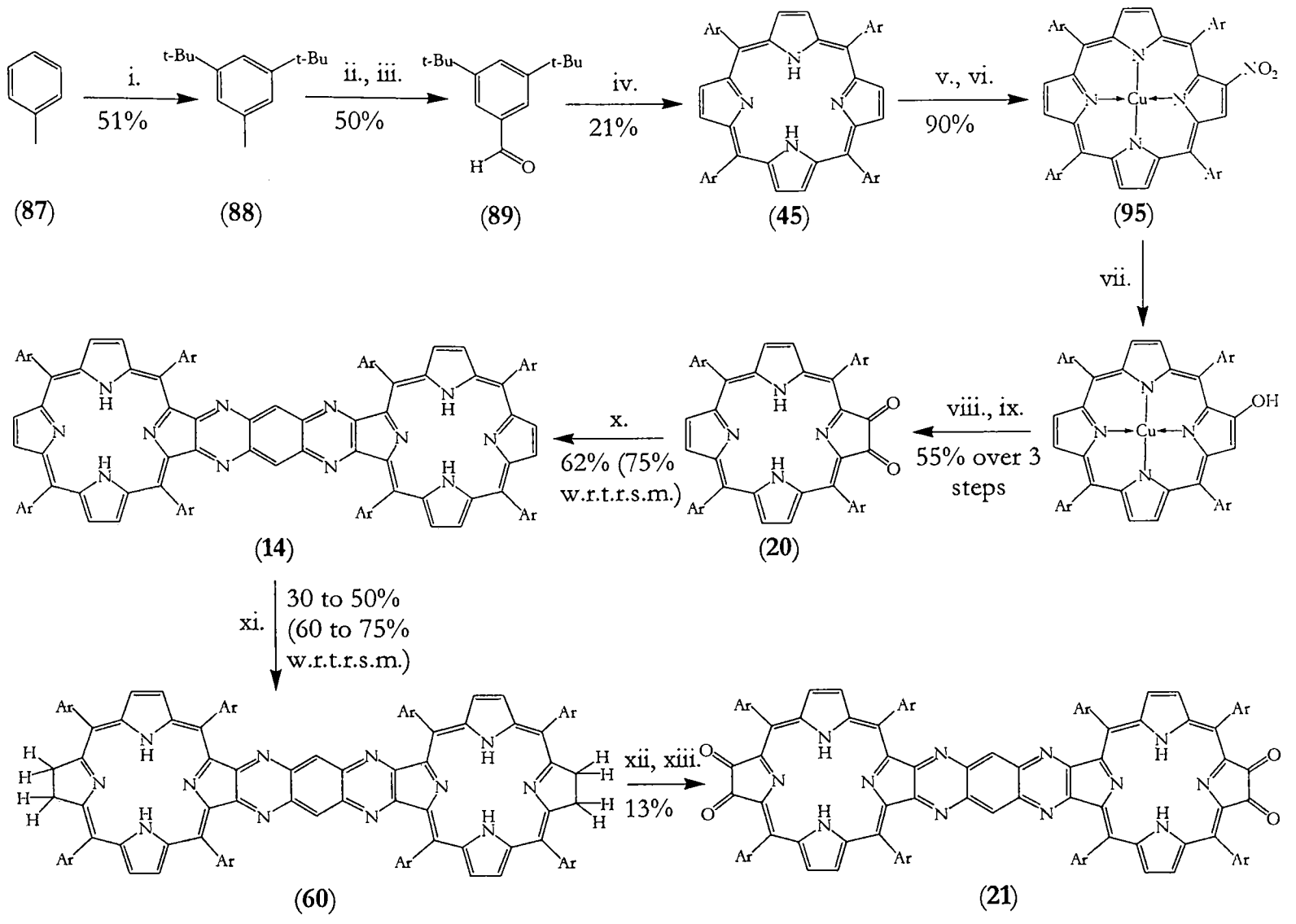

Figure **6.5**- the large-scale synthesis of the simple bis-porphyrin tetra-one. i. *t*-BuCl, $AlCl_3$; ii. *N*-bromosuccinimide, AIBN (cat.), $CHCl_3$, Δ_R; iii. HMTA, EtOH, Δ_R then conc. HCl; iv. 1 eqv. pyrrole, propionic acid, Δ_R; v. $Cu(OAc)_2$, CH_2Cl_2/ MeOH, Δ_R; vi. 1 eqv. NO_2 in light petroleum, CH_2Cl_2; vii. 11 eqv. benzaldehyde oxime, 10 eqv. NaH, DMSO/ THF, Δ_R; viii. H_2SO_4, CH_2Cl_2, then recrystallization from CH_2Cl_2/ MeOH; ix. 1.5 eqv. Dess-Martin periodinane, CH_2Cl_2; x. 0.36 eqv. 1,2,4,5-tetraaminobenzene tetrahydrochloride, pyridine, Δ_R; xi. *p*-toluenesulfonylhydrazide, anhydrous K_2CO_3, pyridine, 108^{0}C, the starting material is recovered by the oxidation with DDQ of other products isolated from the reaction mixture; xii. silica, substrate deposited from 1:8 dichloromethane: light petroleum, and then solvent removed from the system, 35^{0}C; xiii. 5 eqv. Dess-Martin periodinane, CH_2Cl_2. Ar = 3,5-di-*tert*-butylphenyl. 'w.r.t.s.m.' means with respect to recovery of starting materials.

The functionalization starts with the nitration of the simple copper porphyrin, and this was achieved with the separation of both starting material and over-nitrated products repeatedly on a 30 gram scale. Displacement of the nitro group with the anion of benzaldehyde oxime appeared to be successful even at a much higher substrate concentration than previously attempted[87]. Purification was not attempted at this point due to the instability of the products on silica. Demetallation also appeared to be successful, but when the products were then oxidized with the Dess-Martin periodinane reagent, typically only 10% of the desired porphyrin *alpha*-dione **20** was isolated with up to a further 60% of a slightly less polar product (yields are given over the three steps). The appearance of this slightly less polar

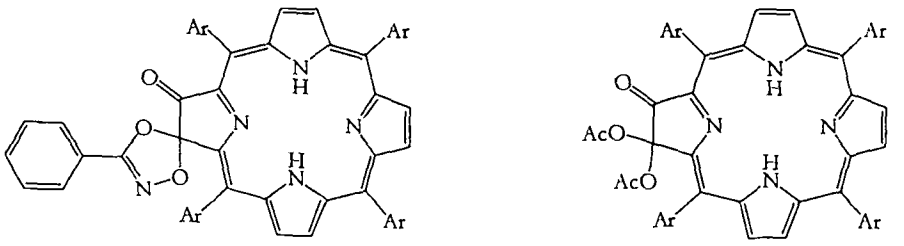

(96) (97)

Figure **6.6**- left- the product isolated from the attempted oxidation of the free-base hydroxy-porphyrin with the Dess-Martin periodinane in the presence of contaminating benzaldehyde oxime. Right- an analogous product isolated by Beavington from the attempted oxidation of the hydroxy-porphyrin with $Pb(OAc)_4$.
Ar = 3,5-di-*tert*-butylphenyl.

product was puzzling, but it was eventually identified as the novel chlorin structure in Figure **6.6**. Its structure was confirmed by its MALDI mass- 1212.5 where **96**H^+ requires 1212.8- and by the appearance of 17 protons in the aryl region of its ^1H NMR.

The formation of this product was traced to the presence of benzaldehyde oxime still remaining from the last-but-one step in the reaction sequence. It is a mechanistically interesting product as it is analogous to the product **97** isolated by Beavington[87] in the oxidation of the hydroxy-porphyrin with $Pb(OAc)_4$. Once the oxime had been removed by recrystallizing the intermediate hydroxy-porphyrin from dichloromethane/ methanol the course of the reaction reverted to what had been observed previously, and typically a 55% yield of porphyrin *alpha*-dione could be isolated (the yield is given over three steps).

With the successful preparation of the porphyrin *alpha*-dione **20**, condensation of **20** around 1,2,4,5-tetraaminobenzene led to the bis-porphyrin **14**. The optimum reaction conditions require the use of only 0.36 equivalents of 1,2,4,5-tetraaminobenzene[35] so when starting material was recovered at the end of reaction it could be recycled.

The synthesis of the bis-chlorin **60** was now attempted. The tendency of the reaction to over-reduce the bis-porphyrin as mentioned in Chapter Four seemed to be more prevalent on a larger scale, and so it was repeatedly necessary to oxidize any over-reduced material back to the starting bis-porphyrin **14** in order to recycle it. Once the bis-chlorin **60** was isolated, its oxidation by silica consistently resulted in the recovery of around 20% of the starting material (and by implication up to 80% of the desired hydroxylated products) as long as the diameter of the column used in this oxidation did not exceed 5 cm, suggesting that this oxidation can be successfully applied to a large-scale synthesis. However the next step involved oxidation by the Dess-Martin periodinane. On a 100 mg scale this had

reproducibly resulted in a 29% isolated yield of the tetra-one **21** from the bis-chlorin **60** (see Chapter Five). But on a 1.3 gram scale this was reduced to only 13%. In addition a further 13% of slightly impure bis-porphyrin *alpha*-dione **80** was isolated.

Following this sequence all the way through, starting from 31 grams of porphyrin **45**, 16 grams of porphyrin *alpha*-dione **20** was synthesised. This was converted into 10.3 grams of bis-porphyrin **14** and then 5.2 grams of bis-chlorin **60**. After oxidation on silica and by the Dess-Martin periodinane, 0.67 grams of bis-porphyrin tetra-one **21** was isolated.

6.4 Synthesis of porphyrin arrays

At last the synthesis of 1,4,5,8-tetraazaanthracene-bridged porphyrin arrays can be described. As the details of the characterization of these arrays are equally as important as the synthetic details, these are described separately in Section **6.5**.

6.4.1 Non-dendritic porphyrin arrays

So that arrays containing non-dendritic and dendritic solubilizing groups could be compared, initially two arrays without the dendritic solubilizing groups were synthesised. The simple tetramer was synthesised through the double condensation of the bis-porphyrin *alpha*-dione **22** onto 1,2,4,5-tetraaminobenzene. This reaction was carried out in a similar manner to synthesising the simple bis-porphyrin **14** (Figure **6.7**). However since the bis-porphyrin *alpha*-dione **80** was less soluble than the single porphyrin *alpha*-dione the reaction was carried out at a concentration of 31 μmolml^{-1} of the bis-porphyrin *alpha*-dione, equivalent to half that of the porphyrin *alpha*-dione for the synthesis of the bis-porphyrin **14**. Purification of the product also proved to be difficult. Initial attempted purification over silica with a 1:2 volume mixture of dichloromethane: light petroleum eluted two products, neither of which was identified as either the starting material or the desired tetramer product. But when the column was pumped through with chloroform, a third product was eluted. This was shown by thin layer chromatography to be *less* polar than either of the other two products, and was purified further with a 1:1 volume mixture of chloroform: light petroleum. Through an identical UV-VIS spectrum as that reported in the literature and the correct MALDI mass this was identified as the tetramer **22** (isolated yield 32% with respect to the bis-porphyrin *alpha*-dione starting material, or 45% with respect to the 1,2,4,5-tetraaminobenzene).

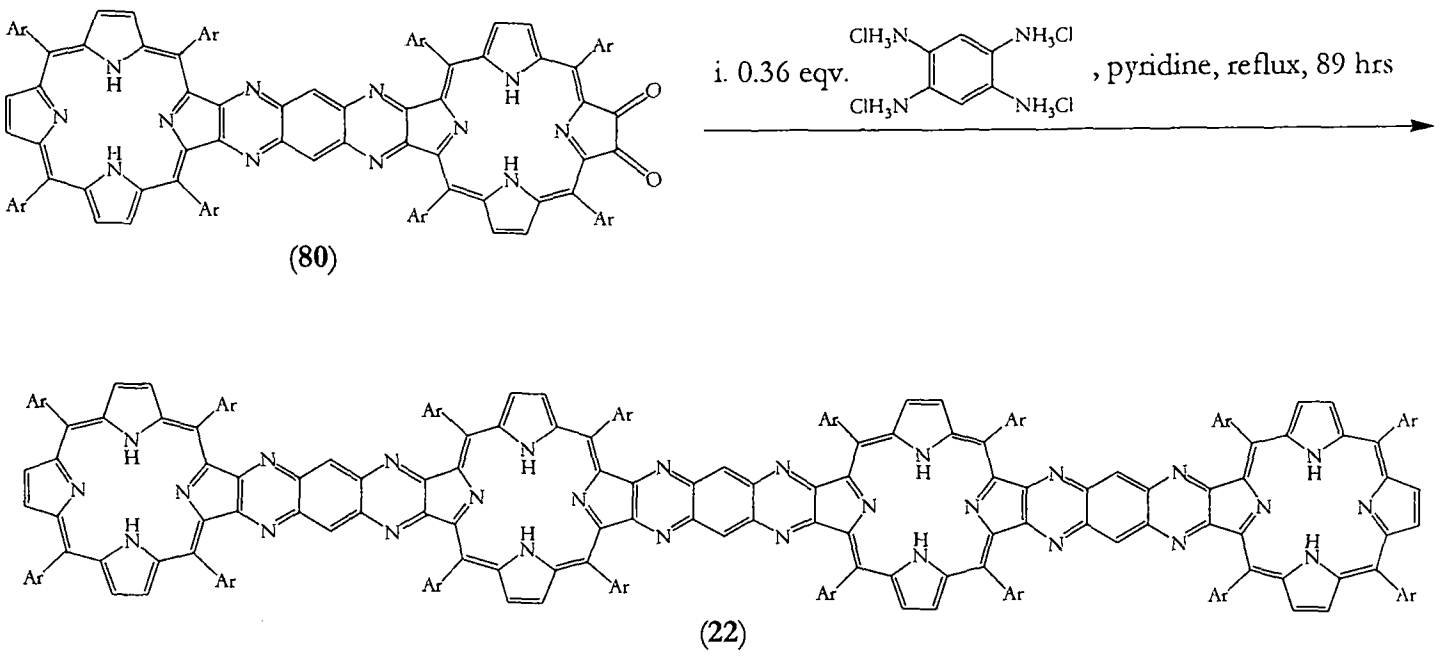

Figure 6.7- a new synthesis of the non-dendritic tetramer **22**. Ar= 3,5-di-*tert*-butylphenyl.

The non-dendritic hexamer **98** was synthesised through the condensation of the bis-porphyrin tetra-one **21** with an excess of 1,2,4,5-tetraaminobenzene. The intermediate bis-porphyrin condensate was capped with an excess of bis-porphyrin *alpha*-dione **80** (Figure **6.8**). The product from the condensation of the bis-porphyrin with 1,2,4,5-tetraaminobenzene proved quite insoluble and so the second part of the reaction was carried out with the bis-porphyrin tetra-one **21** at a concentration of only 5.5 μmolml^{-1}. The low yield of isolated product (only 8%) was further hampered by problems with the purification of the product over silica. It was observed that the product significantly streaked or did not move at all with a solvent mixture any less polar than about 1:1 chloroform: light petroleum. Hence purification had to be carried out at solvent polarities where the separation of the desired product from possible impurities was small.

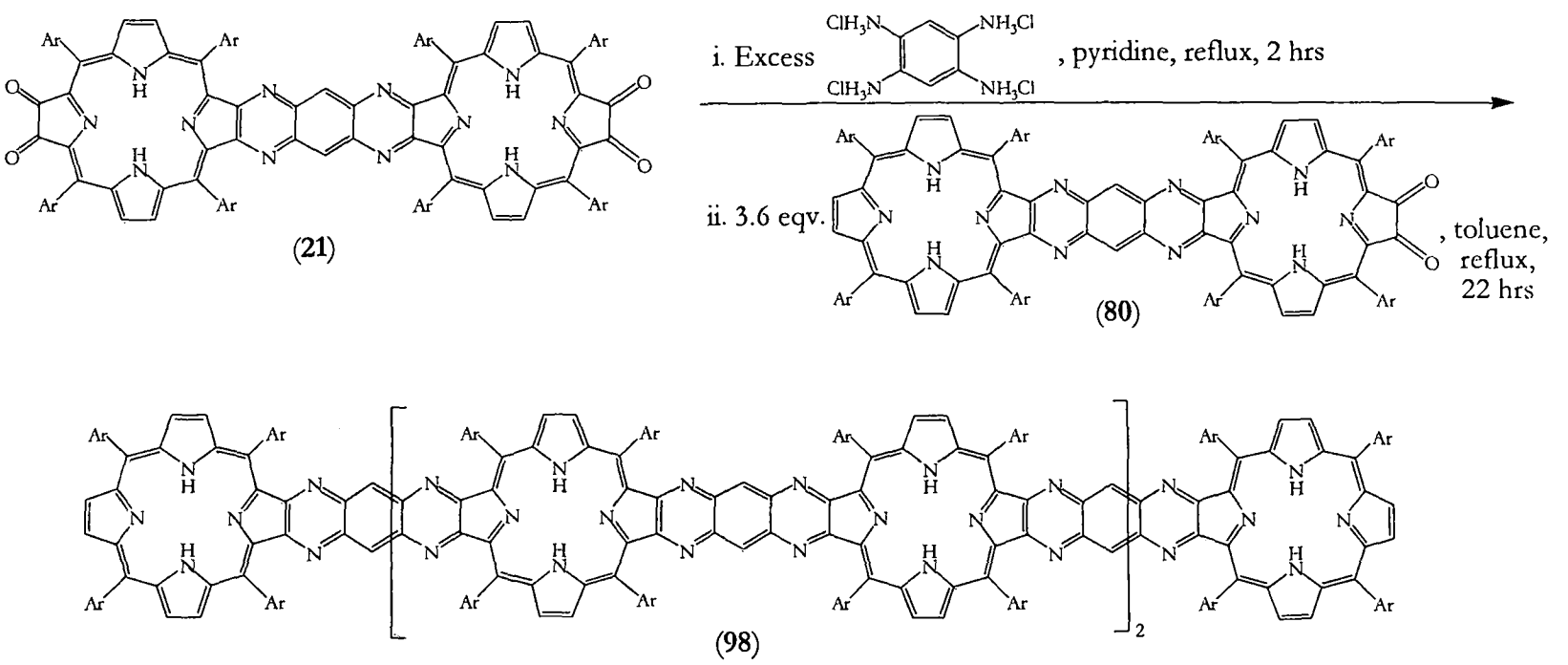

Figure **6.8**- synthesis of the non-dendritic hexamer **98**. Ar= 3,5-di-*tert*-butylphenyl.

6.4.2 Arrays containing a dendritic solubilizing group

With the successful synthesis of the two monomer units the synthesis of 'satellite' arrays incorporating the dendritic solubilizing unit could now be attempted. This was carried out in an iterative manner, as illustrated in Figure **6.9**. Typically, one equivalent of the porphyrin *alpha*-dione was condensed with a large excess of 1,2,4,5-tetraaminobenzene in pyridine; after two hours at reflux under argon the reaction was worked up and solvent was removed. The residue and at least 2¼ equivalents of the bis-porphyrin tetra-one were dissolved in a small amount of toluene, the system was placed under argon, and then heated to reflux for 19 hours[82]. Solvent was again removed and purification was carried out over silica. This iterative procedure was carried out three times, and yields for each iterative step are given in Table **6.2**. The sequence was finished with the capping of the 7mer porphyrin *alpha*-dione around the bis-porphyrin tetra-one unit **21** to give in theory the 16mer porphyrin array. This final condensation was carried out through the condensation of 2¼ equivalents of the 7mer porphyrin *alpha*-dione with an excess of 1,2,4,5-benzenetetraamine in pyridine; after work-up this was heated at reflux with one equivalent of bis-porphyrin tetra-one in toluene.

For the shorter arrays the solubility of the substrates in both pyridine and toluene were good. In this way for the synthesis of the 3mer, 5mer and 7mer porphyrin *alpha*-diones **99**, **100** and**101**, the second step of the reaction was carried out a concentration of bis-porphyrin tetra-one **21** of between 6.0 and 8.0 $\mu molml^{-1}$. This led to a reasonable yield of the desired porphyrin *alpha*-dione product, as showed in Table **6.2**. However the solubility of the 7mer *alpha*-dione in both solvents appeared to be poor, so that its condensation around the bis-porphyrin tetra-one **21** was carried out at a concentration of **21** of only 0.41 $\mu molml^{-1}$ in toluene. This undoubtedly contributed to the poor isolated yield of porphyrin array product from this final step.

Solubility also became an issue when purifying some of the product mixtures over silica. The first two reactions in the iterative sequence could be purified easily with various volume fractions of dichloromethane to light petroleum. In this way the unfunctionalized porphyrin arrays **102** and **103** were eluted first with a volume mixture of 1: 2.5 dichloromethane: light petroleum; the porphyrin *alpha*-diones **99** and **100** were eluted with a 1: 1.75 mixture of dichloromethane: light petroleum; and the bis-porphyrin tetra-one **21** was recovered with a 1: 1 mixture of dichloromethane: light petroleum. However when such purification was attempted for the crude product mixture from the third reaction in the iterative sequence, the 12mer porphyrin array **104** was not eluted and only a small amount of the 7mer *alpha*-

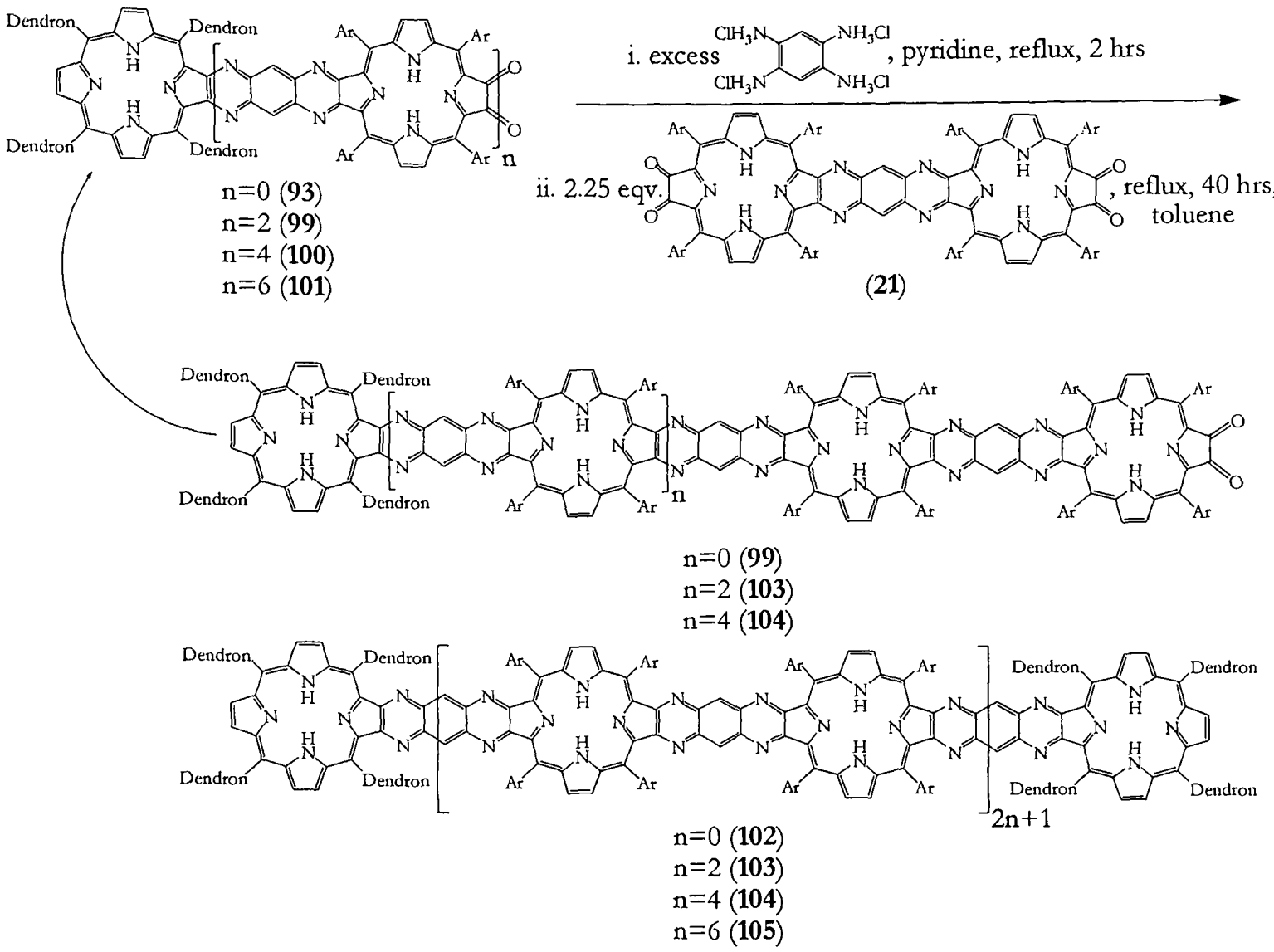

Figure **6.9**- iterative procedure for building up 1,4,5,8-tetraazaanthracene bridged porphyrin arrays. The starting material is a porphyrin *alpha*-dione with *n* 3,5-di-*tert*-butylphenyl-substituted porphyrins fused onto a dendritic porphyrin end group. The process is iterative, so that the *alpha*-dione product from one reaction becomes the starting material for the next reaction (shown by the curly arrow). See also Table **6.2**. Ar= 3,5-di-*tert*-butylphenyl and Dendron= 3,5-(3',5'-di-*tert*-butylstyryl)phenyl.

dione **101** was isolated. As for the non-dendritic tetramer this was taken as a sign of the insolubility of the substrates in dichloromethane, so the column was flushed through with

Number of porphyrins in porphyrin *alpha*-dione starting material	**Number of porphyrins in porphyrin *alpha*-dione product***	**Yield of porphyrin *alpha*-dione product (%)****	**Number of porphyrins in porphyrin array product**	**Yield of porphyrin array product (%)**	**Yield of the recovery of bis-porphyrin tetra-one 21**
(**93**) 1 (n= 0)	(**99**) 3	44	(**102**) 4	7	59
(**99**) 3 (n=2)	(**100**) 5	54	(**103**) 8	9	72
(**100**) 5 (n=4)	(**101**) 7	46	(**104**) 12	2	57
(**101**) 7 (n=6)	n/a	n/a	(**105**) 16	7	n/a

Table **6.2**- yields in the synthesis for the iterative procedure described by Figure **6.9**. The values of *n* correspond to those in Figure **6.9**. *Products not characterized because of: **possible anhydride impurity in the product (see text).

chloroform and the products re-purified in a volume mixture of 2:3 chloroform: light petroleum. From this second purification a small amount of 12mer porphyrin array **104** was isolated (2%) along with a considerable yield of the 7mer porphyrin *alpha*-dione **101** (46%). The 16mer porphyrin array **105** proved even more insoluble, so that purification over silica was attempted in 1:1 chloroform: light petroleum. However at this solvent polarity the separation of the desired product from possible impurities was small. This is an unsatisfactory situation as in the first step of the reaction sequence when the porphyrin *alpha*-dione is condensed with 1,2,4,5-tetraaminobenzene a small amount of over-reaction and dimerization of the substrate can also occur. Hence the small amount of a porphyrin array containing (N-2) units needs to be carefully separated from the main fraction of porphyrin array containing N units, which is not possible at such high solvent polarities.

In addition to solubility problems on purification it also proved impossible to completely purify the porphyrin *alpha*-dione intermediates, so they were not characterized. This was because it was noticed that a very slightly less polar band accompanied each sample of porphyrin *alpha*-dione. Whilst it was not possible to separate this less polar band from the main band, the appearance of this impurity was reconciled with the appearance of a small, significantly deshielded NH signal in the ^{1}H NMR. This appears at typically -1.4 ppm whereas the NH signal of the porphyrin *alpha*-dione appears at around -1.9 ppm.

A similar product was also identified as an impurity in the bis-porphyrin tetra-one **21** recovered from the condensation reactions. However in this case the impurity could be separated from the main product and it was identified as the anhydride structure shown in Figure **6.10**. It is probable that this product and the similar impurities in the porphyrin *alpha*-diones are a result of the oxidation of the porphyrin *alpha*-dione by residual oxygen in the system[90]. Indeed it was observed that when the system was not degassed thoroughly before heating to reflux, the proportion of this impurity in the recovered bis-porphyrin tetra-one **21** seemed to increase.

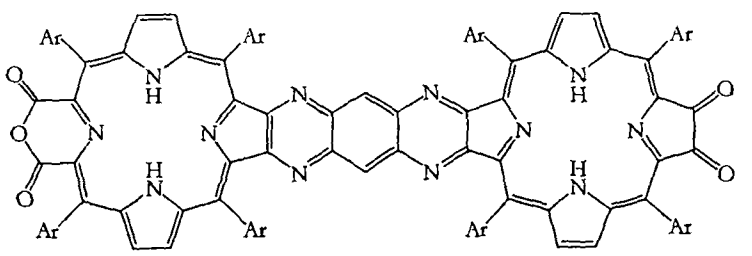

(106)

Figure **6.10**- the impurity isolated from the bis-porphyrin tetra-one **21** recovered from the condensation reactions. Ar= 3,5-di-*tert*-butylphenyl.

Hence this iterative procedure produced samples that should have corresponded with porphyrin arrays containing four, eight, twelve and sixteen porphyrins each.

6.5 Characterization of porphyrin arrays

A defining feature of the characterization of these porphyrin arrays is the apparent decomposition of the arrays under ambient laboratory conditions, simply by adding solvent and removing it from the sample. As detailed below, this process has unfortunately led to the incomplete characterization of several of the arrays. The likely cause of this decomposition is discussed further in Section **6.5.4**. Despite this two arrays, specifically the dendritic 12mer **104** and the non-dendritic tetramer **22**, have been well characterized. In addition to this decomposition process, attempts to reproduce the iterative build-up of the satellite arrays did not succeed as described in Section **6.5.5**, so several of the arrays have remained not fully characterized.

6.5.1 Non-dendritic arrays

The best place to start a discussion about the characterization of these arrays is with the non-dendritic tetramer **22**. Detailed characterization of **22** has been previously described by Crossley and Burn[36] so the characterization process in the present situation was focused on confirming the size of the array and the purity of the sample. Firstly, its ^{1}H NMR spectrum in chloroform was characterized by very broad signals. This can be attributed to considerable aggregation in solution at the concentration that the ^{1}H NMR was undertaken. In contrast its UV-VIS spectrum (shown in Figure **6.12**) proved much more informative, as it was identical to that previously described except that the extinction coefficient for the B band absorption was determined to be 574,000 $dm^{-3}mol^{-1}cm^{-1}$ instead of 430,000 $dm^{-3}mol^{-1}cm^{-1}$. The characteristic structure of the UV-VIS spectrum is further analyzed in Chapter Seven. The composition of the sample was further confirmed by MALDI-TOF analysis (Figure **6.11**) that showed one principle signal of the correct molecular weight, with very little other structure to the spectrum.

Finally the GPC analysis in THF is shown in Figure **6.11**. Whilst GPC gives a measure of the molecular weight and polydispersity of the sample, the actual GPC instrument is calibrated with samples of polystyrene. It is not certain that the samples of polystyrene and the porphyrin arrays will interact with the GPC column in the same way, so quantitative data

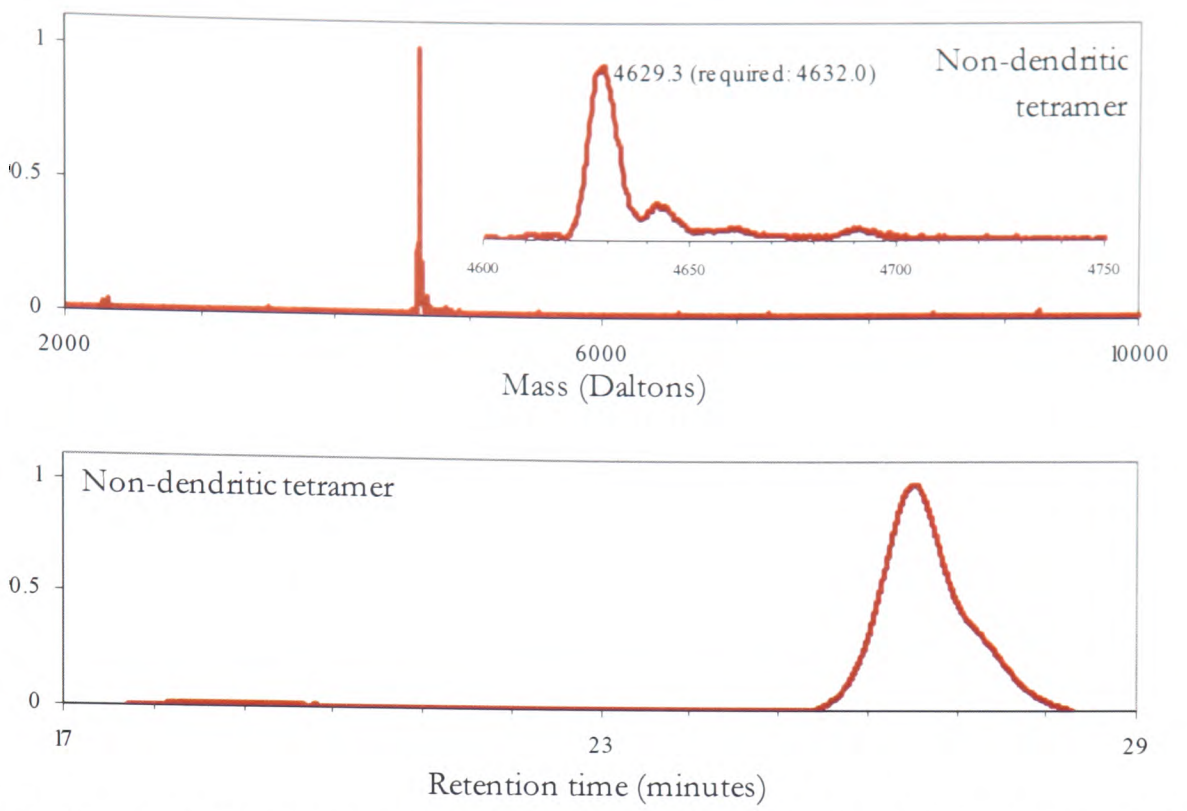

Figure **6.11**- Characterizing the non-dendritic tetramer **22**. From top to bottom- the MALDI from a 9-nitroanthracene matrix; and the GPC analysis. Both vertical axes are given in normalised units. The UV-VIS spectrum is given in Figure **6.12**.

derived from the GPC needs to be treated with caution. With this in mind, the main peak of the GPC trace has a mode molecular weight of 4700 and the whole peak has a polydispersity of 1.17- both figures are given relative to the polystyrene reference. However there appears to be a small shoulder on the main peak. If this shoulder is analyzed separately it is found to have a maximum at a molecular weight of around 1800, and constitute up to 4% of the total peak area with the UV detector set at 425 nm. It is unclear as to the cause of this shoulder. It should also be noted that **22** exhibited extremely low solubility in THF, and therefore it is likely that this GPC analysis will overestimate the proportion of any more soluble impurities present in the sample.

Therefore the MALDI and UV-VIS data confirm the identity of the non-dendritic tetramer, whilst the GPC analysis confirms that the sample is of low polydispersity.

This is a reasonably impressive set of characterization data that is in contrast with what is obtained for the non-dendritic hexameric array **98**. The first thing that was evident from handling the hexameric array was its lack of solubility in nearly all solvents. The most favourable solvent system was found to be chloroform, and even in this case stirring was required before the substrate dissolved significantly. As for the tetramer only broad signals were apparent in the ^{1}H NMR of the hexamer. The UV-VIS spectrum, shown in Figure **6.12** does exhibit the characteristic band structure established by the non-dendritic tetramer, but

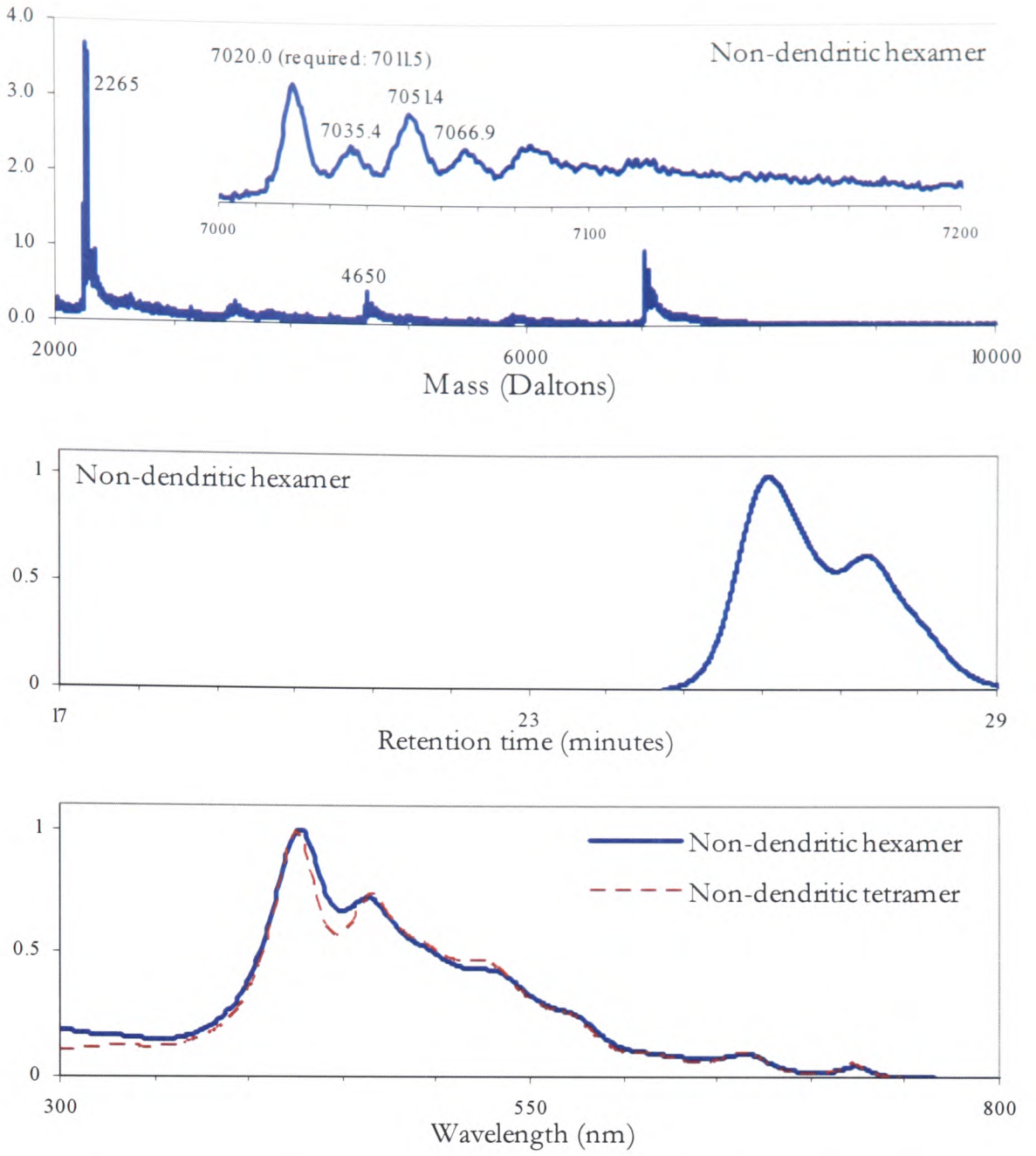

Figure **6.12**- Characterizing the non-dendritic hexamer **98**. From top to bottom- the MALDI from a 9-nitroanthracene matrix; the GPC analysis; and the UV-VIS spectrum. For comparison the UV-VIS spectrum of the non-dendritic tetramer is also illustrated. All vertical axes are given in normalised units; the strongest absorbance in the UV-VIS spectrum of the hexamer and the tetramer are normalised to the same value although the maximum extinction coefficient for the hexamer was recorded as 259,000 $dm^{-3}mol^{-1}cm^{-1}$ compared to of 574,000 $dm^{-3}mol^{-1}cm^{-1}$ the tetramer.

the sample actually shows a reduced splitting in the B band compared to that of the tetramer (c.f. Chapter Seven). The MALDI spectrum (Figure **6.12**) confirms that the sample does contain the hexamer, but it also suggests the presence of an impurity with molecular weight around 2265. The GPC analysis (Figure **6.12**) quantifies the relative abundance of this impurity. Analyzing the two distinct peaks in the trace separately, the main peak is found to have a maximum at a molecular weight of 7000 (relative to the polystyrene standard). The smaller peak is found to constitute 28% of the area under the graph (with the UV detector set at 425 nm) and to have a mode molecular weight of around 2400.

The MALDI spectrum also shows considerable structure to the parent ion signal of the hexamer. Peaks are clearly observed that correspond to the addition of one, two and three oxygens to the parent ion. It is unclear as to whether these peaks are an artefact of some oxidation process occurring in the ionization process during MALDI, or whether they actually indicate the presence of impurities in the substrate.

Overall therefore it is concluded that the sample of non-dendritic hexamer is of low purity. In addition the apparent decomposition of the hexamer during characterization- the results of which were evident after simply recording a ^{1}H NMR spectrum- meant that further analysis of the product could not be attempted (c.f. Section **6.5.4**).

6.5.2 ^{1}H NMR of dendritic satellite arrays

An initial evaluation of the dendritic satellite arrays was made by ^{1}H NMR as illustrated in Figure **6.13**. It is evident that on going from the tetramer **102** to the octamer **103**, and from the octamer **103** to the 12mer **104** that some of the resonances grow in intensity with respect to some others. The situation for the 16mer **105** will be examined later. Examining the β-pyrrolic protons first, it is evident that there are four types of β-pyrrolic environments. The two sets of protons above 9 ppm are significantly deshielded from the other resonances. The likely cause of this deshielding is ring-currents caused by the dendrons, and given that as the length of the array increases the relative intensity of these signals stays the same it is reasonable to assign these resonances to the H(2), H(3) and H(4) proton environments (Figure **6.13**). The only singlet in the β-pyrrolic region at 8.95 ppm is undoubtedly from the terminal H(1) protons, meaning that the 'lump' centred around 8.90 ppm is due to the H(5) and H(6) proton environments. And as the length of the array increases it is this 'lump' which grows in intensity relative to the other β-pyrrolic environments.

The protons on the 1,4,5,8-tetraazaanthracene bridge are well separated from other proton environments, appearing just above 8.6 ppm. It is observed that the relative intensity of this group of signals increases as the length of the array increases.

The aryl region is more difficult to assign because for each aryl environment there are two different types of proton. The confused signal between 7.3 and 7.6 ppm will most likely be due to the styryl protons and the protons on the surface phenyl groups of the dendrons. In total this should integrate to 80 protons. In addition the easiest thing to say about the other group of resonances- between 7.9 and 8.2 ppm- is that above the tetramer all the additional aryl environments are roughly equivalent, so that the *ortho* aryl protons appear at 8.15 ppm,

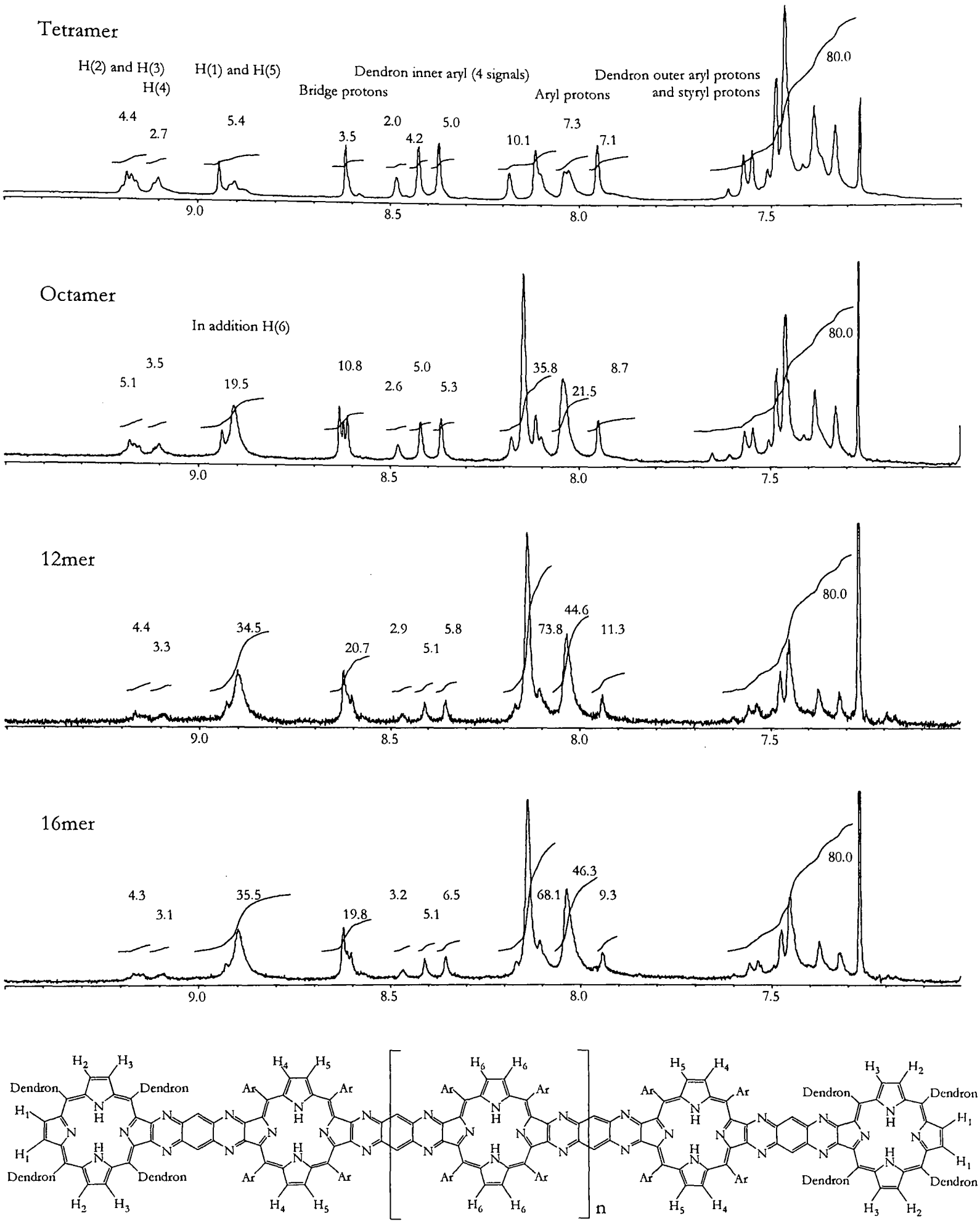

Figure **6.13**- aromatic region of the 400 MHz ^{1}H NMRs of the satellite tetramer (**102**), octamer (**103**), 12mer (**104**) and 16mer (**105**). The numbering system used for assignment of the peaks is given at the bottom. Ar= 3,5-di-*tert*-butylphenyl; Dendron= 3,5-(3',5'-di-*tert*-butylstyryl)phenyl.

and the *para* aryl protons appear at 8.05 ppm. It is observed that these signals grow in intensity as the length of the array also increases.

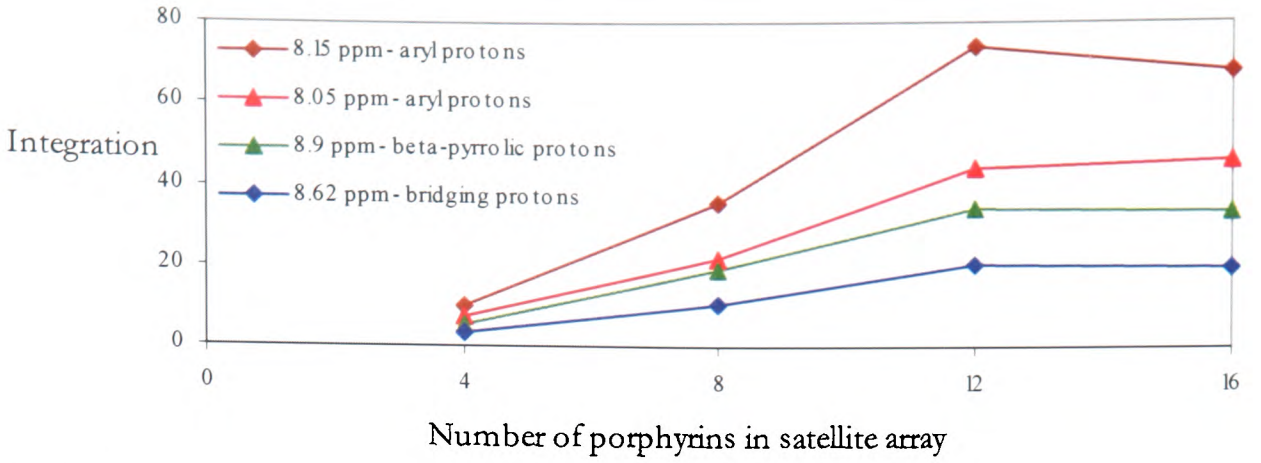

Figure **6.14**- integration of the relevant environments from the ^{1}H NMRs of Figure **6.13**. For each array the dendron signal between 7.3 and 7.6 ppm was set to integrate to 80 protons.

With this assignment in mind, it should be possible to make a quantitative estimation of the length of each array. However care has to be taken as it is apparent that the relative integration of one proton environment versus another is not self-consistent. For example the H(2) and H(3) environments represent eight protons, so should integrate to a tenth of the value of the dendron resonances between 7.3 and 7.6 ppm. This is clearly not the case for any of the arrays, and similar inconsistencies are also evident. If it assumed that protons in similar environments in different arrays can be legitimately compared with one another, then by setting the dendron signal between 7.3 and 7.6 ppm to integrate to a standard of 80 protons a comparison of the arrays can be made. This is done in Figure **6.14**. It is observed that in the sequence of the tetramer **102** to the octamer **103** and 12mer **104** there is a roughly linear increase in the magnitude of the integration of the β-pyrrolic environment centred around 8.9 ppm, the bridging proton environment centred around 8.62 ppm and the aryl environments centred around 8.15 ppm and 8.05 ppm. In this way it would appear that the number of porphyrins in each array is increasing linearly in the sequence tetramer< octamer< 12mer. However the integrations of the relative signals of the 12mer and 16mer appear to be very similar, suggesting that perhaps the sample of 16mer is not quite what it might claim to be.

6.5.3 Further characterization of the dendritic satellite arrays

The dendritic satellite arrays were then further characterized. The first sample to be analyzed was the tetramer **102**. A broad parent ion peak centred around 7200 was observed in its MALDI spectrum (required mass- 7164) showing the sample did indeed contain the desired tetramer. However analyzing the sample by thin layer chromatography at this point revealed that it had nearly completely decomposed into baseline material, so no further spectroscopy was carried out on the sample.

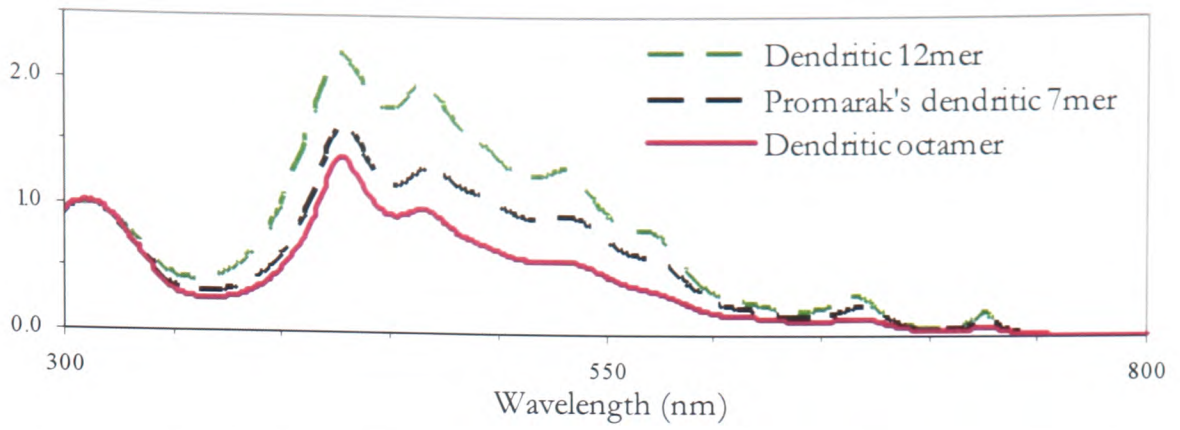

Figure **6.15**- Characterizing the dendritic octamer **103** by UV-VIS spectroscopy. For comparison the UV-VIS spectrum of the dendritic 12mer and Promarak's 7mer are also illustrated. The vertical axis is given in normalised units.

The octamer **103** suffered similar problems of decomposition. A UV-VIS spectrum of the sample was recorded which does show the band structure that was observed in the UV-VIS spectra of the non-dendritic arrays **22** and **98** (Figure **6.15**). However the spectrum is not consistent with an array containing eight porphyrin units as the intensity of absorption of the B band relative to the dendron is less than that of the 7mer synthesised by Promarak[37]. This can be explained if the array has already partially decomposed. Further spectroscopy was attempted on the sample, but by the time that this was carried out changes in the sample's UV-VIS spectrum (see Section **6.5.4**) and analysis by thin layer chromatography revealed that the sample had now fully decomposed.

Luckily, characterization of the 12mer array **104** proved much more successful. The MALDI spectrum run from a dithranol matrix appears a bit messy at first glance (Figure **6.16**). The parent ion peak is the most visible, but it is characterized by a very broad signal- even at half the peak height it seems to be practically 1000 Daltons wide. It was thought that this might be due to the use of an inappropriate matrix, but when the sample was re-run using a variety of other matrices- specifically 9-nitroanthracene, *alpha*-cyano-4-hydroxy cinnamic acid and 5,10,15,20-tetrakis(3',5'-di-*tert*-butylphenyl)porphyrin itself- or run without the use of a matrix, the same broad signal was observed on each occasion. In addition the MALDI shows many peaks of lower molecular weight. The relative size of these peaks compared to the parent ion peak is not an indication that these impurities constitute a significant proportion of the sample as it is very likely that the heavier parent ion is more reluctant to fly in the MALDI machine than the lighter impurities. However the actual identity of some of the peaks is a bit more worrying. For example the peak at 13,100 would correspond to either a satellite array containing nine porphyrin units or a porphyrin *alpha*-dione containing ten porphyrin units. The methodology in Figure **6.9** does not allow for either of these

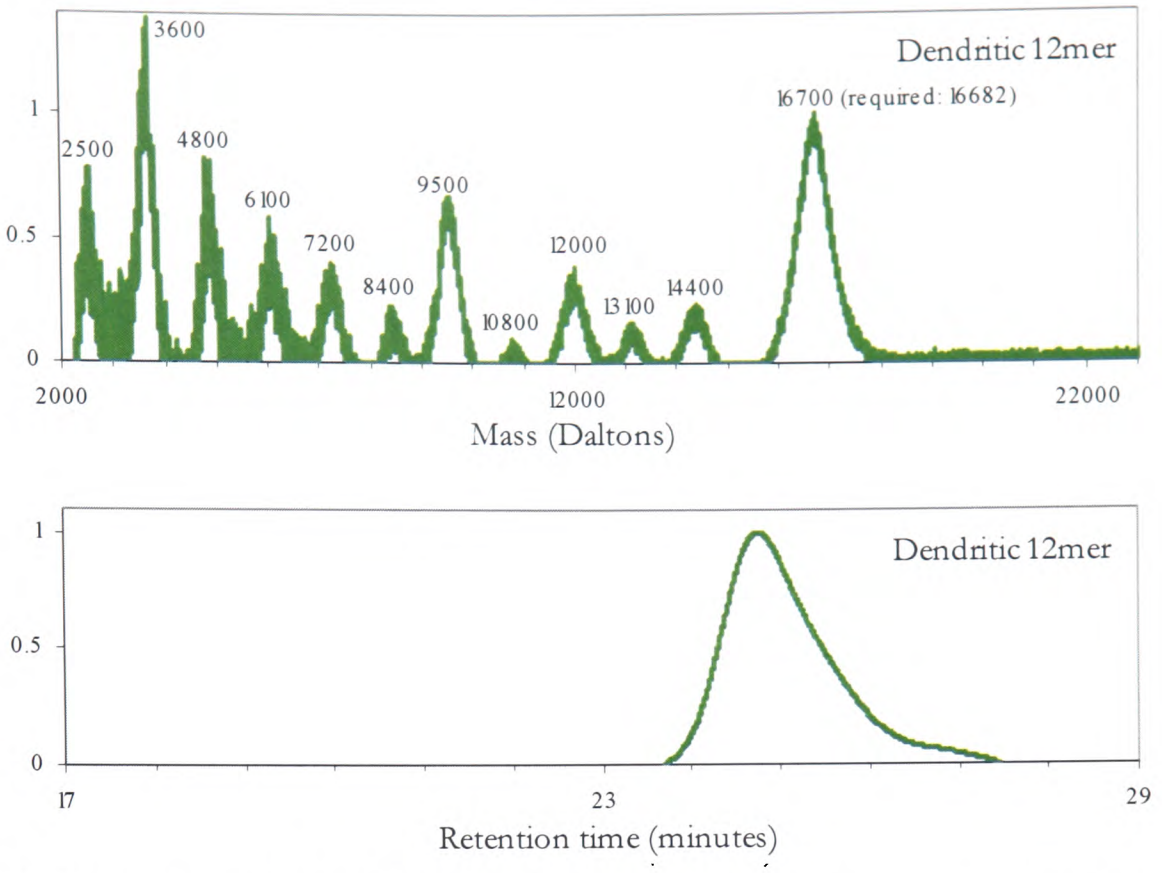

Figure **6.16**- Characterizing the dendritic 12mer **104**. From top to bottom- the MALDI from a dithranol matrix; and the GPC analysis. Both vertical axes are given in normalised units. The UV-VIS spectrum is given in Figure **6.15**.

products, suggesting that the array is subject to fragmentation somewhere along the reaction sequence or in the measurement itself.

Thus MALDI analysis of **104** gives a clear indication of the identity of the parent ion; and it is GPC analysis that gives a clear indication as to the purity of the substrate. This is also shown in Figure **6.16**. A relatively rounded, uniform peak is observed with only the presence of a small shoulder of low molecular weight material. When the whole peak is analyzed as one peak, a polydispersity of 1.31 is obtained with a mode molecular weight of 19900 (both relative to a polystyrene standard). When the small shoulder is analyzed as a separate peak it is found to constitute only 1% of the total area of the graph, and possesses a mode molecular weight of around 2000. In this way the GPC analysis shows that the impurities that are observed by MALDI constitute only a small proportion of the sample, and that the 12mer is of low polydispersity.

The UV-VIS spectrum (Figure **6.15**) also broadly supports the assignment of the structure of the 12mer. It is observed that the intensity of absorption of the B band relative to the dendron is significantly greater than that of Promarak's 7mer[37], indicating that there are significantly more non-dendronised porphyrins in the sample of 12mer than in Promarak's 7mer.

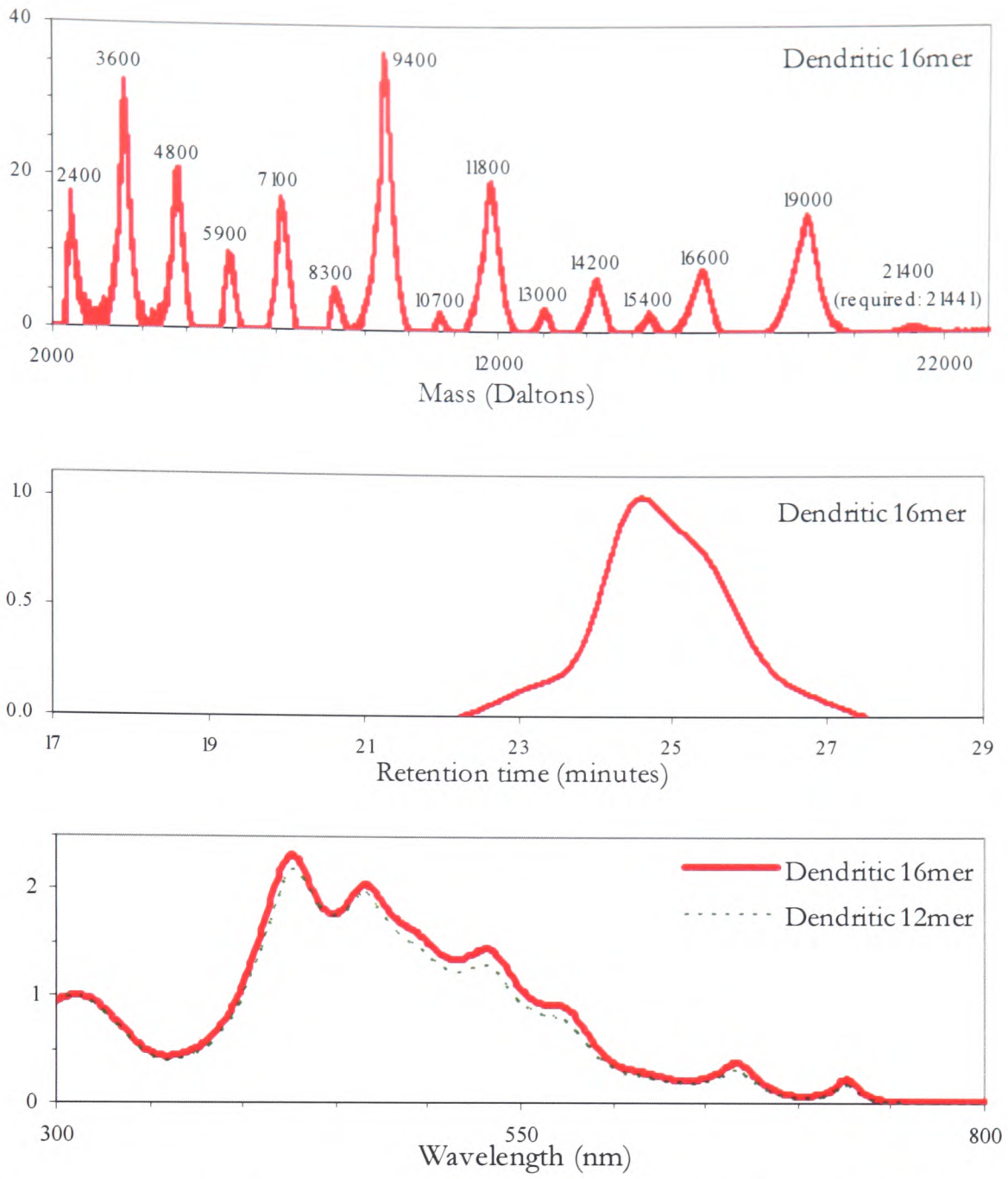

Figure **6.17**- Characterizing the non-dendritic 16mer **105**. From top to bottom- the MALDI from a dithranol matrix; the GPC analysis; and the UV-VIS spectrum. For comparison the UV-VIS spectrum of the dendritic 12mer is also illustrated. All vertical axes are given in normalised units.

Like the 12mer, the 16mer was well characterised without the significant decomposition of the sample. However as suggested by its ^{1}H NMR constitution of the 16mer was found not be as it might first seem. In fact it might be more appropriate to assign the 16mer as containing only 14 porphyrin units. All this is best illustrated by the GPC analysis (Figure **6.17**). The main peak of the GPC trace has two shoulders of lower molecular weight and one shoulder of higher molecular weight. When the trace is analyzed as one peak, a polydispersity of 1.63 and a mode molecular weight of 22,400 are obtained (relative to the polystyrene standard). This molecular weight corresponds to only two porphyrin units heavier than the molecular weight obtained by GPC for the 12mer, suggesting that the sample is more consistent with an array containing 14 porphyrin units rather than 16.

Whilst this determination of molecular weight from the GPC analysis is flawed because the porphyrin arrays might interact with the GPC column in a different manner to the polystyrene calibration, MALDI analysis suggests a similar conclusion to the GPC analysis. The MALDI spectrum (Figure **6.16**) shows a small parent ion peak corresponding to the molecular weight of the 16mer; but a much larger peak is observed for the peak corresponding to the 14mer. The 14 porphyrin product would originate from dimerization of the 7mer porphyrin *alpha*-dione when condensed with 1,2,4,5-tetraaminobenzene in pyridine in the first step of the reaction sequence. However relative proportions of products cannot be ascertained from the MALDI spectrum, and therefore the exact identity of the 16mer remains elusive.

Further analysis of the GPC trace reveals more information about the identity of impurities in the sample. When the small broad shoulder of higher molecular weight (i.e. shorter elution time) is analyzed by itself, it is found to constitute 2% of the sample by integration of the graph. The trace also suggests that the impurity possesses a molecular weight of 134,000. This is clearly not a realistic molecular weight given the methodology used to construct these arrays. Therefore this shoulder is probably a result of the aggregation of the high molecular weight arrays in solution.

Two shoulders are then apparent to the lower molecular weight side of the main peak. When the large shoulder is analyzed as one peak it is found to constitute roughly 10% of the sample by integration underneath the trace. The width of the shoulder corresponds to a molecular weight range of between 6,000 and 12,000. It is probable therefore that this peak corresponds to some porphyrin *alpha*-dione derivative. The smaller of the two shoulders constitutes only 3% of the sample with a molecular weight of around 2,300.

The UV-VIS spectrum (Figure **6.17**) also reflects the composition of the sample. The intensity of absorption of the B band relative to the dendron is only very slightly greater than that for the 12mer array. This can be explained by the majority of the sample containing the 14mer porphyrin array, with a small but significant impurity of lower molecular weight impurities containing relatively more of the dendron.

6.5.4 Decomposition of the arrays

Unfortunately it seems that these 1,4,5,8-tetaazaanthracene bridged arrays are unstable to ambient laboratory conditions. Thus the dendritic tetramer **102**, octamer **103** and the non-dendritic hexamer **98** remain not fully characterized. This decomposition process can be

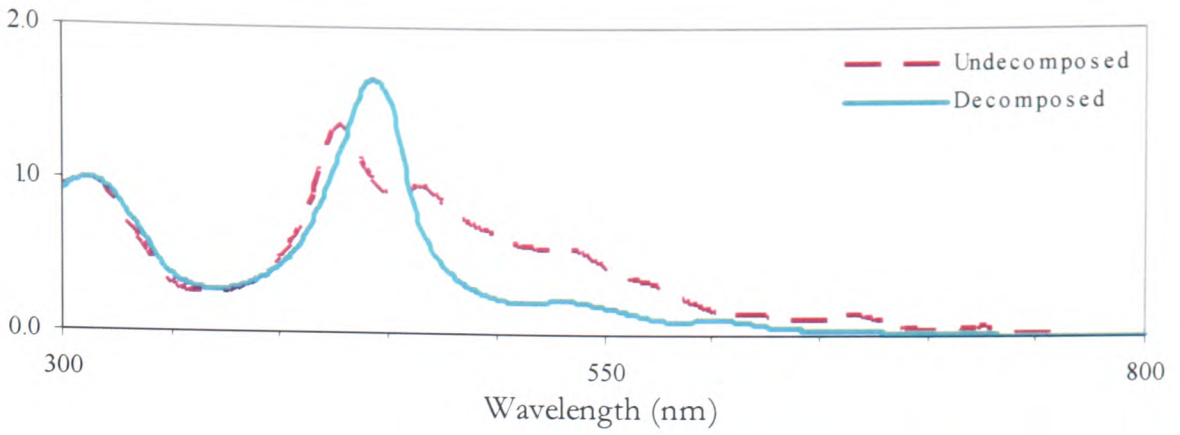

Figure **6.18**- the UV-VIS spectrum of the dendritic octamer **103** 'before' and after decomposition.

traced back to dissolving the substrates in either unstabilized chloroform or in un-dried THF. Intuitively therefore it is probable that this decomposition corresponds to some kind of hydrolysis process. Examining the decomposed product by thin layer chromatography it is observed to be of much greater polarity than the starting array; the *β*-pyrrolic and NH protons in the ^{1}H NMR now only exhibit broad signals, in addition to which new signals at around 4 and 5.5 ppm have appeared; and the UV-VIS spectrum is observed to radically change.

This change in the UV-VIS spectrum is illustrated in Figure **6.18** for the dendritic octamer. The UV-VIS spectrum of the initial sample is characterized by a distinct band structure; however when the sample has fully decomposed, the UV-VIS spectrum shows no splitting in the B band and a greatly reduced intensity of the Q bands. The presence of the dendron absorption at around 310 nm in the decomposed sample confirms that the dendron is not responsible for the decomposition process. In addition the fact that the usual B band/ Q band structure is still present suggests that it is not the porphyrin macrocycle that is decomposing. So by a process of elimination it is thought that the bridging units are subject to hydrolysis under ambient conditions. This would make chemical sense and would also fit in with the picture of the electronic structure of the arrays described in Chapter Seven where the porphyrin *β*-pyrrolic carbon-tetraazaanthracene nitrogen bonds in the bridging units are described as attaining nearly full double bond character.

6.5.5 Attempts to repeat the methodology- isolation of an unknown array

Because of the decomposition of some of the satellite arrays, an attempt was made to re-run this methodology on a similar scale. However the methodology failed on the first iterative cycle. As before the dendritic porphyrin *alpha*-dione was condensed with 1,2,4,5-tetraaminobenzene in pyridine; the reaction was worked up and the residue was combined

with the bis-porphyrin tetra-one **21** and heated to reflux in toluene for 19 hours. On purification some relatively non-polar products were isolated in small amounts and the excess bis-porphyrin tetra-one **21** was also recovered; a small amount of material was recovered with similar polarity to that of the tris-porphyrin *alpha*-dione **99**, but analysis by ^{1}H NMR revealed that this did not contain the desired tris-porphyrin *alpha*-dione **99**. So the methodology was repeated in total six times, but none of the desired tris-porphyrin *alpha*-dione was isolated on any occasion. The conditions for the reaction were varied slightly from run to run, so it can be conclusively stated that the apparent lack of reaction was not due to: decomposed or impure starting materials, as these were judged pure by ^{1}H NMR and thin layer chromatography; wet solvents, as when both the pyridine and the toluene were freshly distilled from calcium hydride no reaction was still evident; poorly deoxygenated systems, as consciously thoroughly degassing the system and then placing it under argon, and repeating the procedure four times for both steps of the reaction still lead to the isolation of none of the desired tris-porphyrin *alpha*-dione **99**; decomposition of the porphyrin *alpha*-dione on purification over silica, as when the solvents for column chromatography were deoxygenated by bubbling with nitrogen and light was rigorously excluded from the column still no porphyrin *alpha*-dione product was isolated; the system being too acidic in the second step of the reaction, thus disfavouring the formation of the porphyrin/ bridge imine bonds, as when the condensation in toluene was carried out with 1% pyridine added still no desired product was isolated.

However three variables were varied from the previous successful application of this methodology. Firstly it was thought best to try to minimize the amount of porphyrin dimer product resulting from the condensation of two porphyrin units onto one 1,2,4,5-tetraaaminobenzene unit in the first step of the reaction, so the first step was carried out with a larger excess of 1,2,4,5-tetraaminobenzene. Secondly, in order to favour the condensation in the second step of the reaction, the starting materials were dissolved in a smaller amount of toluene. Finally, in order to retard any decomposition during purification, solvents for purification were doped typically with around 1% triethylamine.

Although no tris-porphyrin *alpha*-dione was ever recovered from any of the reactions, some products of relatively low polarity that were initially thought could correspond to either the dendronised bis-porphyrin or the porphyrin tetramer **102** were recovered in small amounts. These fractions were combined and purified together, and very small quantities of two products of similar polarity were isolated. The more polar of these two products exhibited a

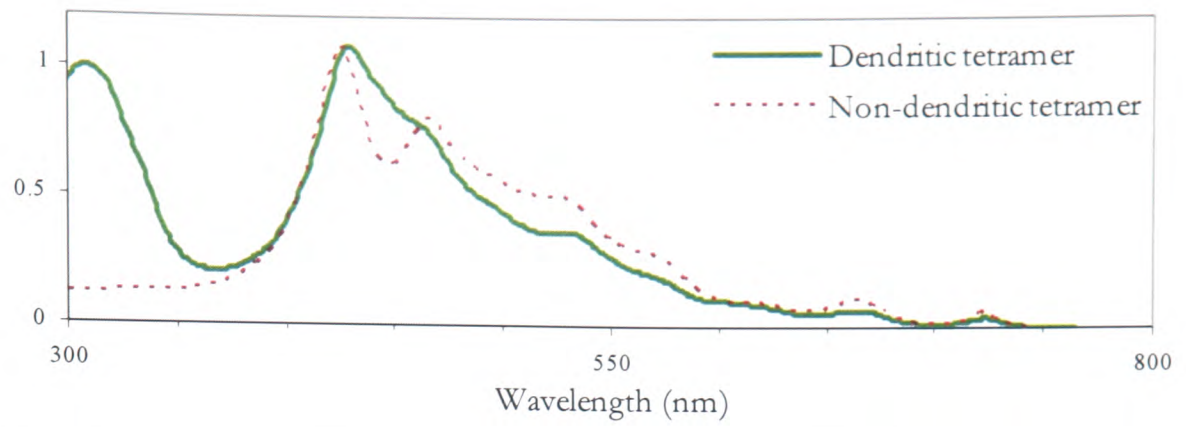

Figure **6.19**- UV-VIS spectrum of the unknown tetramer product. For comparison the UV-VIS spectrum of the non-dendritic tetramer **22** is also illustrated.

broad peak in the MALDI spectrum centred around 7200, where the dendritic tetramer requires a mass of 7164. Equally the ^{1}H NMR showed the right peaks in roughly the right proportions in roughly the correct positions to correspond to the tetramer **102**. However the resolution of the ^{1}H NMR was not good and it appeared by thin layer chromatography that a proportion of the sample had by this stage decomposed, complicating matters further.

At this point therefore it would appear that the sample is consistent with the structure of the tetramer **102**. But its UV-VIS spectrum -that was actually the first measurement recorded on the sample so that it would not be complicated by the effects of decomposition- does not show the characteristic band structure of a 1,4,5,8-tetaazaanthracene-bridged array (Figure **6.19**). Although the Q band region looks similar to those of similar arrays, no splitting is observed in the B band.

A similar set of observations is recorded for the less polar product. Its MALDI mass, measured accurately as 4785 (probably ±5 Daltons at the most), and its poorly resolved ^{1}H NMR suggest that the product is the dendronised bis-porphyrin (required mass- 4784). However its UV-VIS spectrum also shows no splitting in the B band, indicating that the product is not in fact the dendronised bis-porphyrin.

This is a puzzling set of results, and conclusions from them can only be tentatively drawn. Bearing in mind that the MALDI masses of the products conform very closely with the desired products, and that the ^{1}H NMRs seem to convey that the symmetry and the general substitution of the products are very similar to the desired products, then the most sensible thing to propose is that the 1,4,5,8-tetraazaanthracene bridge has been reduced. This is illustrated in Figure **6.20**. This would also explain the difference in the UV-VIS spectrum, as it has been shown by Crossley that chemical modification of the bridge can lead to a

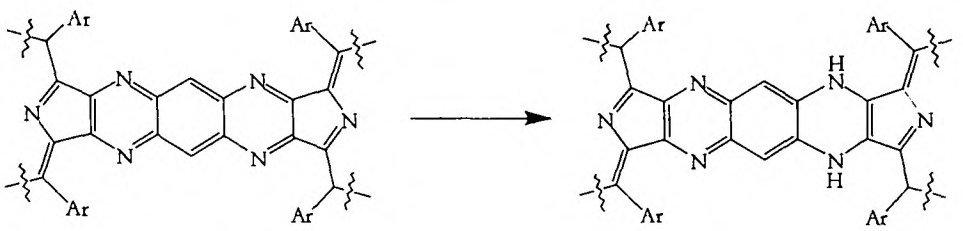

Figure **6.20**- a possible fate of the 1,4,5,8-tetraazaanthracene bridge.

cessation of the splitting in the B band without a significant change in the rest of the spectrum[189].

There are two explanations for the origin of this possible reductive pathway. The first is simply that over-zealous attempts to prevent the decomposition of the arrays by doping the solvents used for purification with triethylamine actually resulted in the reaction of the triethylamine with the substrate. The photoreduction of porphyrins with amines has precedent, although the reported reaction required irradiation for two days in a 25% solution of triethylamine in benzene[150]. The second explanation is that there is an active reductive pathway occurring in the reaction mixture that is causing this reduction process.

Most importantly, the lack of porphyrin *alpha*-dione products can also be reconciled with this possible reductive pathway, as the *alpha*-dione functionality would be very susceptible to any reductive process.

6.6 Conclusions for the synthesis of tetraazaanthracene-bridged arrays

The first problem that is encountered in the synthesis of tetraazaanthracene-bridged porphyrin arrays is the synthesis of the monomer units. For the construction of an extended array the simple bis-porphyrin tetra-one **21** is superior to the simple single porphyrin tetra-one **23** because the array is built up by two units at a time rather than just one. Equally it has been shown that the methods for the synthesis of the bis-porphyrin tetra-one are more reliable than those for the synthesis of the single porphyrin tetra-one.

For the synthesis of an extended porphyrin array a solubilizing group needs to be incorporated into the array. It has been shown in this chapter that by not using a solubilizing group only the tetrameric array can be synthesised and purified to a satisfactory standard. The group that has been used to solubilize the array has been a dendritic-based system. It has been shown that this solubilizing group, when incorporated onto the porphyrins occupying the terminal positions of the array, can successfully solubilize a

structure up to 12 porphyrin units long. However above this length this strategy is insufficient as the products are not soluble enough to enable adequate purification of the arrays.

It would be desirable therefore to synthesise a 'soluble porphyrin tetra-one.' Using the dendritic solubilizing group this has not proved successful. Therefore it can be concluded that the limit of this particular solubilizing group has been reached.

It has further been shown that the formation of the 1,4,5,8-tetraazaanthracene bridge does not always proceed smoothly, and this has had a major effect on the reproducibility of the methodology. In addition the fact that such side-reactions might be occurring emphasises the need for the porphyrin arrays to be soluble enough so that by-products can be successfully separated from the desired products.

Finally it has been possible to synthesise and satisfactorily characterize two porphyrin arrays. Firstly the non-dendritic tetramer has been synthesised by a new route in a relatively large quantity (over 150 mg). Then the dendritic 12mer satellite array has also been synthesised, and GPC analysis suggests that the product is of low polydispersity. Other arrays have been synthesised, but have decomposed before full characterization has been achieved.

Chapter Seven

Photophysical properties of porphyrin arrays

Chapter Seven
Photophysical properties of porphyrin arrays

Chapter Six has described the attempted synthesis of various 1,4,5,8-tetraazaanthracene bridged porphyrin arrays up to 16 porphyrin units' length. Unfortunately due to decomposition processes occurring during their characterization only the non-dendritic tetramer and the dendritic 12mer have been characterized as sufficiently pure products so that conclusions can be drawn from their photophysical spectra.

In addition to this Promarak synthesised an analogous series of dendritic 1,4,5,8-tetraazaanthracene bridged arrays[37]. Fortunately for him he did not observe any decomposition occurring during his characterization process and porphyrin arrays containing 3, 5 and 7 porphyrin units were each synthesised. Although GPC analysis of his products was not undertaken, the fact that the parent ion peaks in the respective MALDI spectra corresponded to the proposed product structures and the consistency shown in the increase in absorption in the UV-VIS spectra with the number of porphyrin units in the array (see Figure **7.4**) suggests that these products are of sufficient purity that their photophysical properties can be analyzed.

Therefore the aim of this final chapter is to examine the photophysical properties of these porphyrin arrays and to try and draw some conclusions of the feasibility of exploiting these arrays in field effect transistors or single molecule devices.

7.1 The UV-VIS spectrum of the dimer

This analysis of the photophysical properties of the porphyrin arrays starts at the simple bis-porphyrin dimer. The UV-VIS spectrum of the non-dendritic di-zinc bis-porphyrin **107** is given in Figure **7.1**. It can be superficially explained in terms of the B band/ Q band model described in Appendix One. The B band, centred at 442 nm, has been split into two components. Meanwhile two Q band is also split into two components, with band origins at around 535 nm and 700 nm.

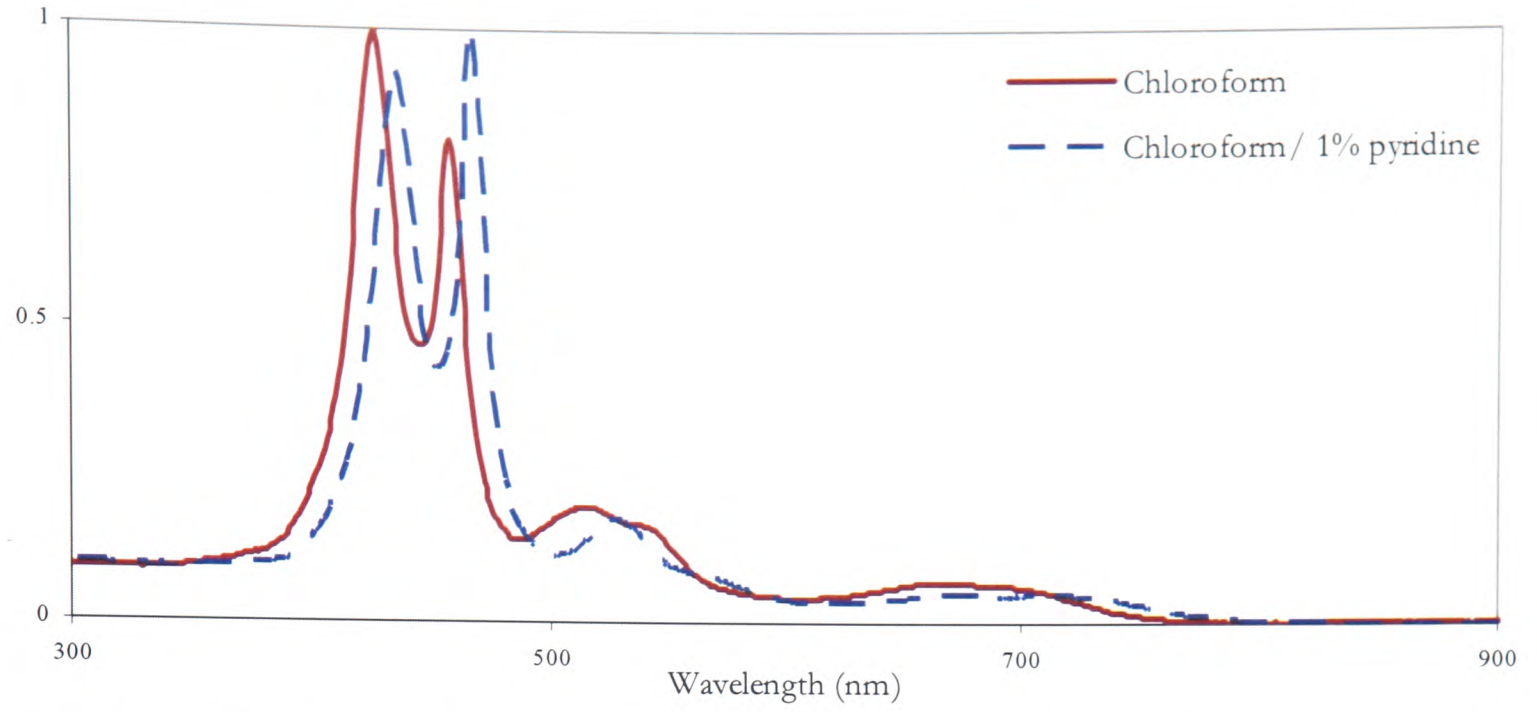

Figure **7.1**- the UV-VIS spectrum of the di-zinc bis-porphyrin **107** in chloroform and chloroform/ 1% pyridine. The intensities of absorption have been normalised.

The splitting in the B band could be cause by two electronic effects:

1. Exciton Coupling

As outlined in Appendix Two exciton coupling between neighbouring porphyrins can lead to a splitting of the B band. In this case the *x* components of the transition dipole moment orientate themselves in a head-to-tail alignment to one another, whereas the *y* components of the transition dipole moment orientate themselves alongside one another (Figure **7.2**). This will lead to a red shift in the allowed component of the *x*-transition of the B band and a blue shift in the allowed component of the *y*-transition of the B band. In this way a splitting of the B band occurs.

2. A reduction in the symmetry

As outlined in Appendix One, a reduction of the symmetry of the porphyrin environment can account for a splitting in the B band. This lowering of symmetry is emphasised by the appearance of two Q bands. An unsubstituted metallated porphyrin displays only one Q band, and even when the symmetry of the unsubstituted system is lifted often only one Q

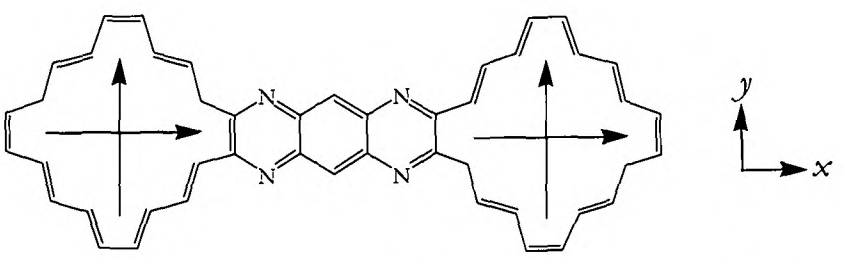

Figure **7.2**- orientation of the transition dipole moment in a planar bis-porphyrin dimer.

band is observed. Hence the appearance of two Q bands demonstrates the asymmetry of the system, and it might also account for the splitting in the B band.

In addition to these electronic effects, aggregation of porphyrins in solution can also lead to a splitting of the B band. It is important to consider this as previous photophysical studies on porphyrin arrays have shown that aggregation can have a significant effect. The usual way of assessing the effect of aggregation has been to metallate the porphyrin array with zinc and then to measure the differences between the absorption spectrum recorded in neat chloroform and in chloroform containing a small amount of pyridine[190]. This is because pyridine can co-ordinate to the zinc and better solvate the array than just chloroform by itself. Therefore aggregation is more likely to occur in neat chloroform, and significant changes in the UV-VIS spectra between the two solvent systems can be attributed to the effects of aggregation.

In this way the UV-VIS spectrum of the di-zinc bis-porphyrin **107** was measured in both neat chloroform and in chloroform doped with 1% pyridine. The respective UV-VIS spectra are shown in Figure **7.1**. It is evident that the spectra in the two solvent mixtures are not the same. The B band of the sample in the chloroform/ 1% pyridine solution is red-shifted by 9 nm with respect to the sample in neat chloroform, and both Q bands are red-shifted by 15 to 20 nm. In order to explain this shift in terms of excitonic coupling within an aggregate it would have to be assumed that the porphyrins are stacking directly on top of one another in an 'H' aggregate formation in neat chloroform. However the observation that the red shift in the Q bands is of equal or greater magnitude than the red shift in the B band is inconsistent with excitonic interactions within an H aggregate. This is because the magnitude of the excitonic interaction should be proportional to the transition dipole moment of the electronic transition, and therefore the effects of excitonic interaction would be expected to result in a much greater shift of the B band. Therefore the most likely cause for the slight red-shift in the spectrum on addition of pyridine is the coordination of pyridine to the zinc, making the metal centre more electropositive and destabilizing the bonding a_{2u} orbital[191]. In this way the HOMO-LUMO gap is observed to decrease.

It is therefore concluded that the effects of aggregation are not observed in the UV-VIS spectrum of the di-zinc bis-porphyrin **107**. Importantly the splitting of the B band is shown to be unequivocally not a consequence of aggregate formation.

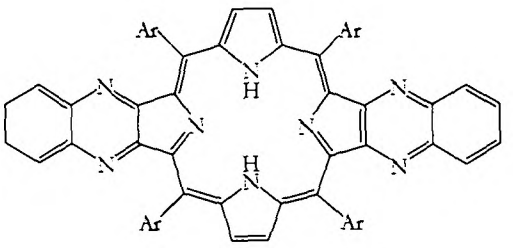

(**108**)

Figure **7.3**- the model monomer unit **108**. Ar=3,5-di-*tert*-butylphenyl.

7.2 Excitonic interactions within the B band

7.2.1 UV-VIS spectrum of the non-dendritic tetramer 22

Having discussed the effects contributing to the UV-VIS spectrum of the bis-porphyrin, the next challenge is to interpret the UV-VIS spectra of the longer arrays. A comparison of the UV-VIS spectrum of the non-dendritic tetramer **22** and the model monomer unit **108** is made in Figure **7.3**. **108** is considered to act as a monomer unit for an extended array as the porphyrin is di-functionalized at antipodal β-pyrrolic units.

The UV-VIS spectrum of the tetramer at first glance appears complicated, but as for the bis-porphyrin it can in fact be explained in terms of the normal B band/ Q band model. Firstly the B band, which is at 448 nm in the monomer, has been split into a lower energy component at 466 nm and a higher energy component at 425 nm. Then the two characteristic Q bands are also visible with origins at around 565 nm and at 722 nm. The first vibrational overtone to these bands is observed, at around 520 nm and 665 nm

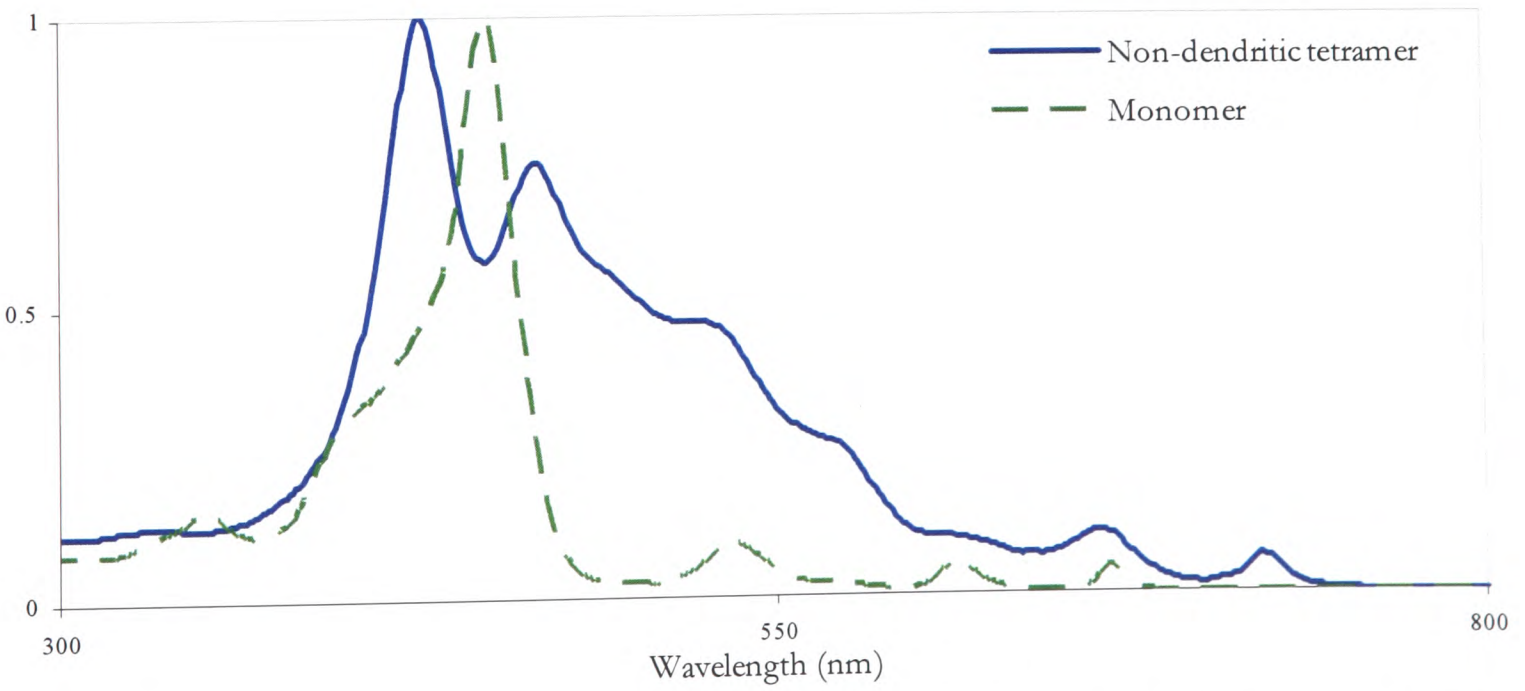

Figure **7.3**- a comparison of the UV-VIS spectra of the non-dendritic tetramer **22** in chloroform and the model monomer unit **108** in dichloromethane. The intensities of absorption have been normalised.

respectively. In addition, in contrast to the UV-VIS spectrum of an unsubstituted porphyrin, the second vibrational overtones to the Q bands are also visible at around 485 nm and at 608 nm respectively. It should be noted that the shoulder at around 485 nm might also be assigned to an electronic transition from porphyrin-centred orbitals to the tetraazaanthracene bridge-centred orbitals[189].

Therefore as for the bis-porphyrin, the tetramer shows a splitting of the B band. It is not clear as to the extent that which exciton coupling contributes to this splitting, but exciton coupling does contribute to other facets of the spectrum. Specifically, the intensities of the Q band absorptions are increased with respect to the monomer unit. This increase in intensity is greatest for the highest energy Q band absorptions; so for example the shoulder at around 520 nm is of half the intensity of absorption as the B band, whereas the respective absorption in the monomer unit is of about a tenth of the intensity of the B band. This phenomenon can be explained by 'intensity transfer' between the B and Q transition dipole moments, mediated by excitonic interactions[192]. The extent of this intensity transfer is theoretically dependent on the difference in energy between the donor and acceptor states, which is why it is observed that the magnitude of the increase in intensity amongst the Q band transitions is the greatest for the highest energy transitions.

An assessment of the effects of aggregation on the UV-VIS spectrum of the tetramer **22** was also attempted. Thus the synthesis of the non-dendritic tetra-zinc tetramer was attempted by heating the free-base tetramer **22** with a large excess of zinc diacetate in DMF. However only a mixture of mono-, di- and tri-substituted products was isolated, as evidenced by MALDI using the free-base tetramer as an internal standard.

7.2.2 UV-VIS spectra of satellite porphyrin arrays

In order to definitively establish the extent of exciton coupling in the UV-VIS spectra of 1,4,5,8-tetraazaanthracene bridged arrays, a whole series of porphyrin arrays of different lengths need to be considered. For this to be achieved, Promarak's 3-, 5- and 7-membered porphyrin arrays need to be included with the 12-membered porphyrin array described in Chapter Six in this analysis. Their representative UV-VIS spectra are shown in Figure **7.4**.

Initial inspection reveals that all the spectra are similar to that of the non-dendritic tetramer **22**, with identifiable B band Q bands. In fact the spectra are very similar not only to that of the tetramer, but also to one another. The splitting in the B band does not appear to increase significantly with an increasing number of porphyrin units in the array and the

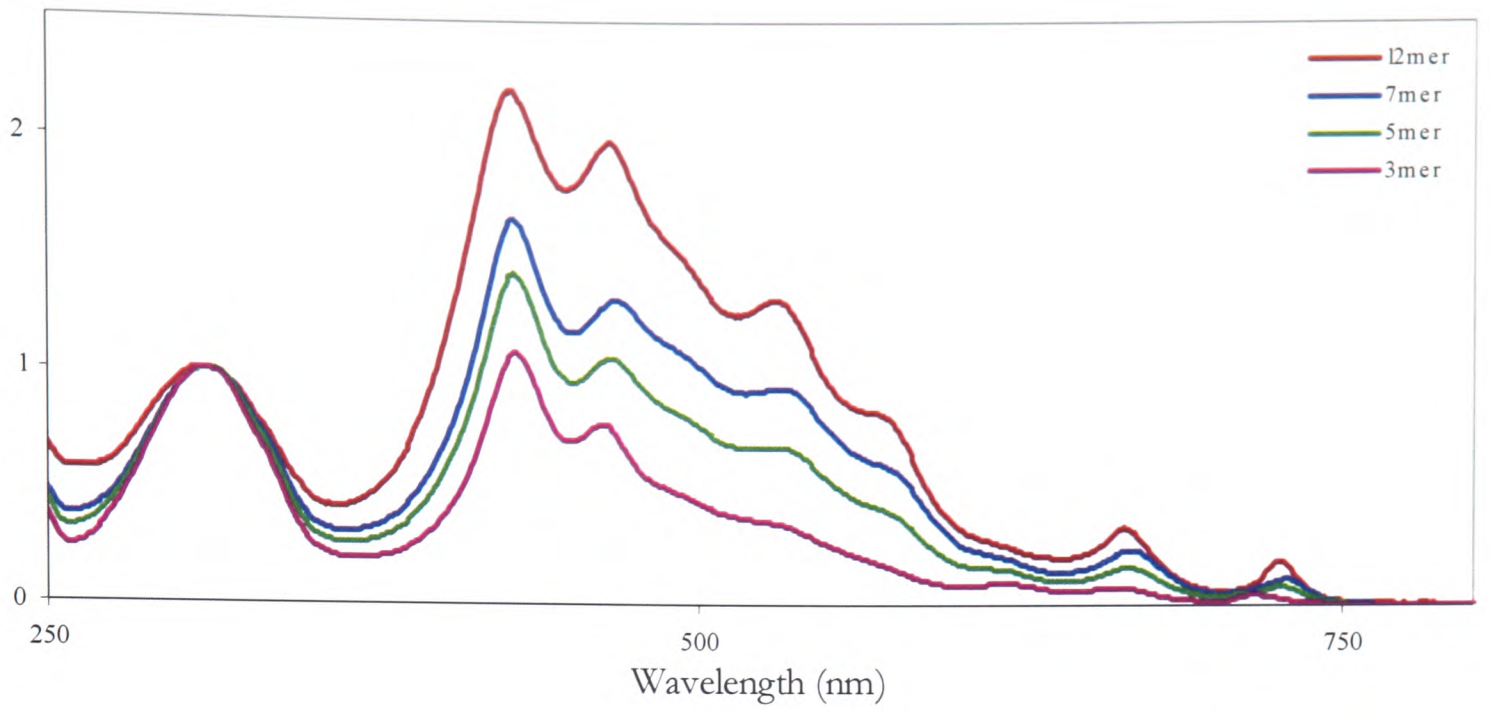

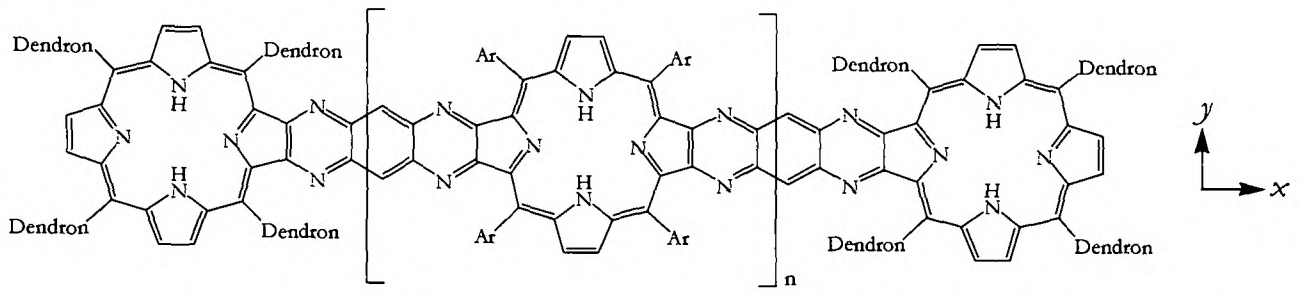

n=1- 3mer
n=3- 5mer
n=5- 7mer
n=10- 12mer

Figure **7.4**- Top- UV-VIS spectra of 1,4,5,8-tetraazanthracene bridged porphyrin arrays in dichloromethane, whose structure are shown below. The horizontal scale is the normalized absorption. Dendron= 3,5-(3',5'-di-*tert*-butylstyryl)phenyl; Ar= 3,5-di-*tert*-butylphenyl.

intensity of the Q bands seems to remain in proportion with the intensity of the B band. These are both indicative of only weak exciton coupling between neighbouring porphyrins. In order to exactly quantify the magnitude of exciton coupling then the splitting in the B band needs to be plotted against $\cos[\pi/(N+1)]$, according to Equation **A2.3** of Appendix Two:

$$\Delta E_N = \Delta E_0 \cos\left(\frac{\pi}{N+1}\right) \qquad \text{Equation } \mathbf{A2.3}$$

This is shown in Figure **7.5**. Implicit in this treatment is the assumption that Frenkel excitons are formed on photoexcitation; but as discussed in Section **7.3** this is a safe assumption.

The straight line relationship shown in Figure **7.5** for the magnitude of the splitting of the B band of the satellite arrays shows that exciton interaction energy ΔE_0 for the

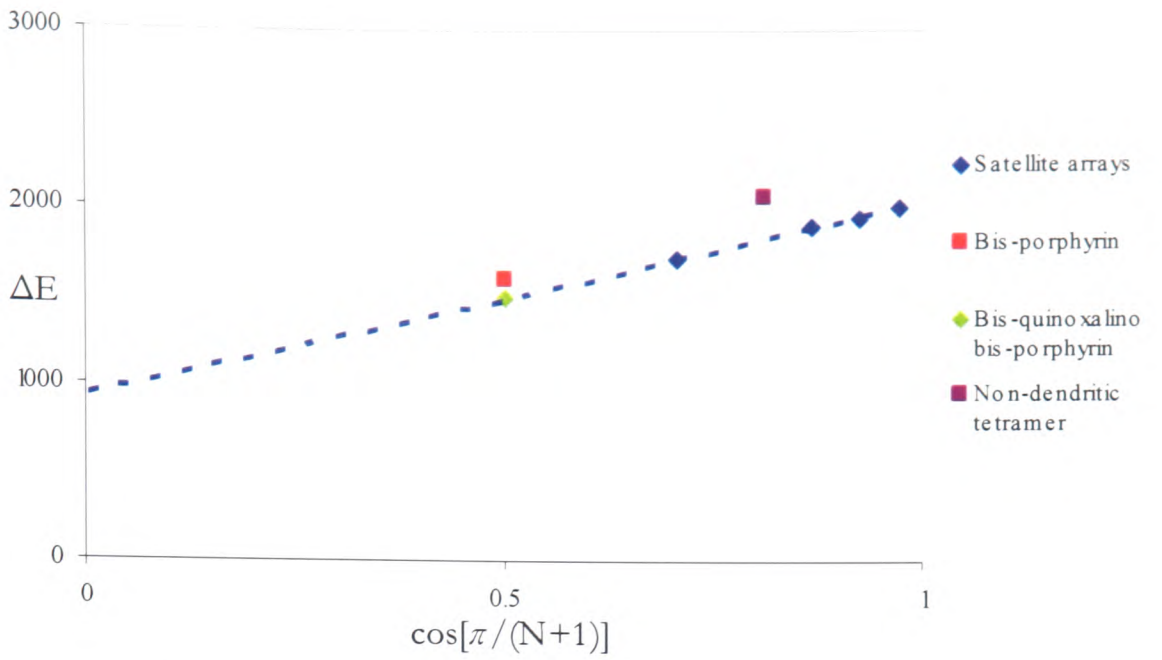

Figure **7.5**- magnitude of the splitting of the B band (ΔE) plotted against the cos[π/(N+1)] where N is the total number of porphyrin units in the array. The error in the measure of ΔE is approximately ±50 cm^{-1}, which is roughly represented by the height of the markers.

1,4,5,8-tetraazaanthracene bridged arrays equals 555 cm^{-1}. This is determined by halving gradient of the graph (1115 cm^{-1}). The gradient is halved since *both* the *x*-polarized and *y*-polarized components of the B band are shifted by ΔE_0 resulting in a total B band splitting of $2\Delta E_0$.

The relationship shown in Figure **7.5** differs from other porphyrin arrays described in Chapter One since the line of best fit does not cross the axes at their origins at their intersection. Instead when cos[π/(N+1)]= 0 then ΔE= 930 cm^{-1}. Several reasons for this can be hypothesised:

- A breakdown of the 'strong' coupling regime

Strictly speaking equation **A2.3** is only valid in a strong coupling regime where the magnitude of the exciton interaction is greater than the vibronic bandwidth of the electronic absorption. In this system this is clearly not the case. However it is unlikely that this is the actual cause of the deviation from equation **A2.3** as this equation has been successfully applied to similar porphyrin systems.

- The exciton interaction originating from the end units is stronger than from the inner units

If the magnitude of the exciton interaction between an end dendritic unit and the next-from-end unit is much greater than that between two inner units then the line in Figure **7.5** would

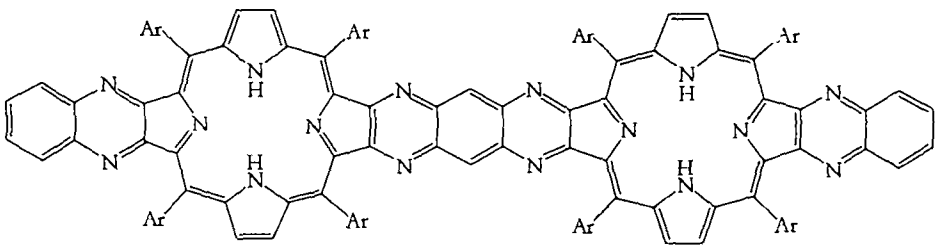

(**109**)

Figure **7.6**- the bis-quinoxalino bis-porphyrin model unit for the inner units of a porphyrin array. Ar= 3,5-di-*tert*-butylphenyl.

not cross the axes at their intersection. Whilst this difference in the magnitude in exciton interactions does not have a great theoretical backing, the hypothesis has been nonetheless tested by the synthesis of the model system bis-quinoxalino bis-porphyrin **109** (Figure **7.6**). It is considered to act as a model to the inner units of the array because each porphyrin is substituted at antipodal β-pyrrolic units in contrast to a terminal unit which is substituted at only one β-pyrrolic unit. The splitting in its B band was found to be a respectable 1495 cm^{-1}, showing that the deviation from equation **A2.3** is not due to an inequality in the exciton interaction between neighbouring porphyrin units in the array.

- Aggregation

The effects of aggregation would be expected to unpredictably affect the splitting of the B band as the length of the array increases. So the fact that all four arrays lie on the straight line in Figure **7.5** and fit in with this figure of 555 cm^{-1} for ΔE_0 suggests that aggregation is not playing the dominant role.

- The asymmetry of the system causing a splitting in the B band

As described in Appendix One and earlier in this chapter, a reduction in the symmetry of the porphyrin can lead to a splitting of the B band. In this case, since all other factors have been ruled out it is very likely that unaccounted splitting in the B band of 930 cm^{-1} is caused by the asymmetry of the system.

Figure **7.5** shows a good straight line relationship for the series of satellite arrays, but the values for the splittings of the B bands of the non-dendritic bis-porphyrin **14** and the tetramer **22** lie off this line. It is not particularly worrying that the bis-porphyrin **14** does not fit into the trend, as it would be expected that the magnitude of the splitting of the B band caused by the asymmetry of the porphyrin environment will differ in the dimer to that in an extended array. This is because both the porphyrins are substituted at only one β-pyrrolic unit rather than being di-substituted at antipodal β-pyrrolic units. Indeed when di-

substitution is imposed on the system in the bis-quinoxalino bis-porphyrin unit **109**, the energy splitting of the B band once again lies on the straight line.

The observation that the splitting in the B band of the non-dendritic tetramer **22** lies off the straight line is not such a trivial matter. In fact it not only lies off the straight line, but the magnitude of its splitting (2070 cm^{-1}) is greater than that predicted for an array of infinite length (2040 cm^{-1}, where $\cos[\pi/(N+1)]= 1$). This could be due to the fact that the tetramer's UV-VIS spectrum was recorded in chloroform rather than the usual dichloromethane for reasons of solubility. However a similar increase in the splitting of the B band of the zinc bis-porphyrin **107** is not observed when moving from dichloromethane to chloroform. Therefore the extra splitting of the B band might be better explained by a certain level of aggregation of the non-dendritic tetramer occurring in solution.

7.2.3 Magnitude of the exciton interaction

The magnitude of the exciton interaction energy in the satellite arrays has therefore been determined as 555 cm^{-1}. In the context of porphyrin arrays given in Chapter One this is a comparatively small value, especially compared to Osuka's value of 4300 cm^{-1} for his meso-meso directly linked arrays[193]. But this is not a wholly surprising result because of the large separation between neighbouring porphyrin units, decreasing the exciton interaction according to Equations **A2.1** and **A2.2** of Appendix Two.

7.3 Electronic delocalization along the array

Perhaps the most interesting question to ask of a porphyrin array is about the extent of electronic delocalization between neighbouring porphyrin units. However for the present system this is a difficult question to answer.

7.3.1 Physical measurements of the HOMO-LUMO gap

Initial inspection of the UV-VIS spectra of the satellite arrays reveals that the lowest energy absorbance moves to longer wavelengths as the length of the array is increased (Figure **7.7**). Thus the 3mer has its lowest energy absorbance at 716 nm, whereas the 12mer has its lowest energy absorbance at 725 nm. Following this kind of treatment to its logical end it would be concluded that there is a certain amount of electronic delocalization along the array because as the number of units in the array increases then the energy of the lowest energy absorbance

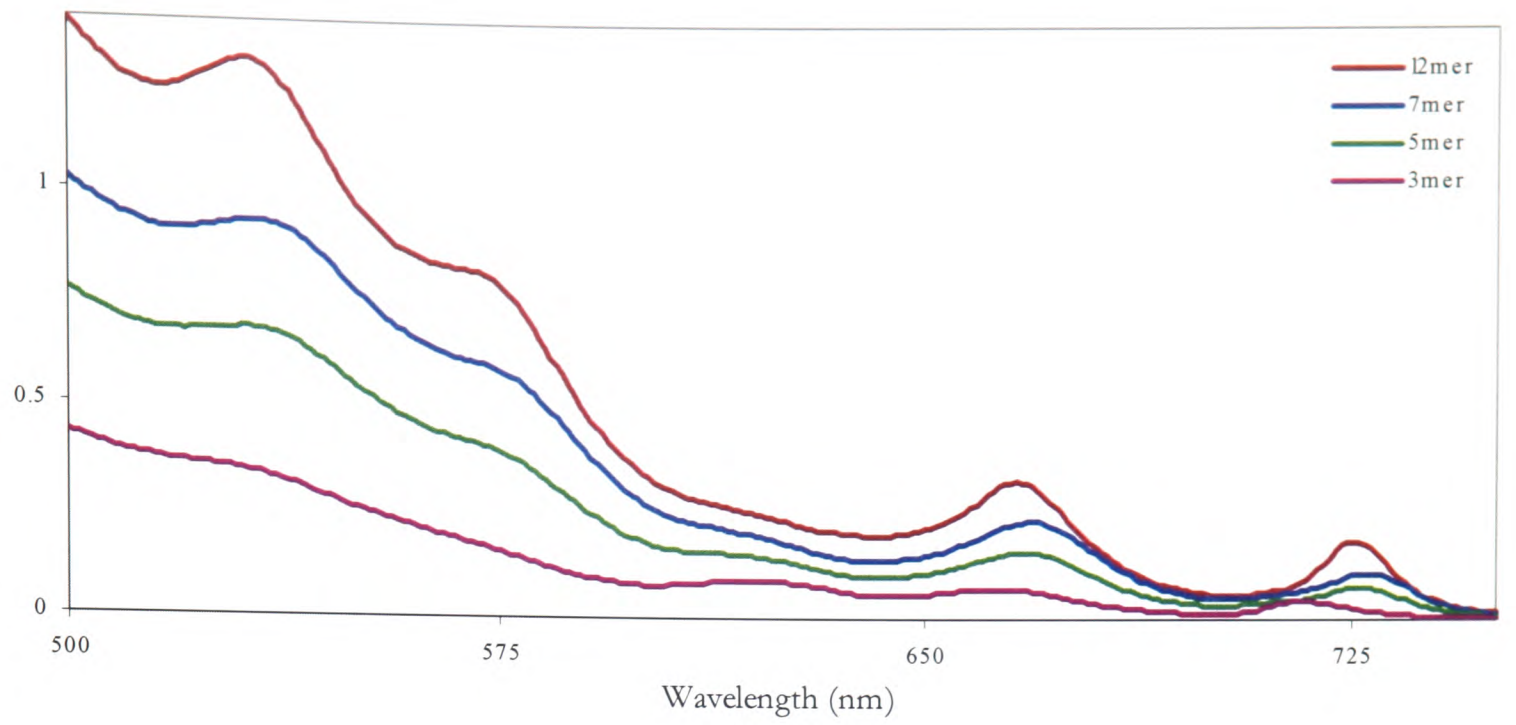

Figure **7.7**- the Q band region in the UV-VIS spectra of the satellite porphyrin arrays (c.f. Figure **7.4**). The horizontal scale is the normalized absorbance.

decreases. However there comes a point- at an array containing around 7 porphyrin units- where the electronic properties of the array become independent of the total number of porphyrin units in the array. This point would be called the 'effective conjugation length' of the array and it has been observed in other oligomeric systems[194,195].

However this superficial treatment is critically flawed. At a fundamental level as Appendix One sets out, the HOMO-LUMO gap of a porphyrin system cannot be determined directly from the energy of the lowest energy absorbance in the UV-VIS spectrum due to the effects of configurational interaction on the system. This means that all that can be determined for certain from the UV-VIS spectrum of a free-base porphyrin is the *average* gap between the HOMO-1 and the HOMO, and the LUMO and LUMO+1.

In addition, even if the assumption is made that the extent of configurational interaction is the same for each porphyrin array, there is a valid argument that the lowest energy absorption band is the wrong band to look at when considering the effects of delocalization *along* the backbone of the array. This is because according to Gouterman in a free-base porphyrin the lowest energy absorbance originates from the transition dipole polarized parallel to the NH axis[191], so in the case of Figure **7.4** it is polarized along the *y* axis. And it would be expected that the effects of delocalization along the array would manifest themselves in the transition dipole orientated parallel to the backbone of the array, so for Figure **7.4** in the direction of the *x* axis. This means that the absorption that might indicate

Porphyrin	B_y (nm)	B_x (nm)	Q_x (nm)	Q_y (nm)	B band centre (cm^{-1})	Q band centre (cm^{-1})	Lowest energy absorbance (cm^{-1})	B/ Q band centre (cm^{-1})
bis-porphyrin	426	457	545	676	22678	16571	14793	19624
bis-quinoxalino bis-porphyrin	440	471	545	700	21979	16317	14286	19148
3mer	429	463	568	716	22454	15786	13966	19120
5mer	429	467	568	726	22362	15690	13774	19026
7mer	428	467	568	727	22389	15680	13755	19035
12mer	427	467	566	725	22416	15730	13793	19073
Non-dendritic tetramer	425	466	566	722	22494	15759	13850	19127
ERROR	±0.5	±0.5	±5	±0.5	±26	±85	±10	±55

Table **7.1**- vital statistics for the UV-VIS spectra of various porphyrin arrays. The error quoted for the Q(1) band is exceptionally large as it only appears as a shoulder in several of the UV-VIS spectra.

electronic delocalization along the backbone of the array is the higher energy of the two Q bands, so for the satellite arrays the absorption centred around 570 nm.

So the most that can be obtained from the UV-VIS spectra is the average gap between the HOMO-1 and the HOMO, and the LUMO and LUMO+1. This information is given in Table **7.1**. Within the margins of error there is very little variation in this average gap between arrays of different lengths. This leads to the conclusion that within the limitations of this optical treatment that there is evidence of little, if any, delocalization along the backbone of the array.

Examination of the arrays through electrochemistry would provide more information about the exact extent of electronic delocalization along these porphyrin arrays. Indeed electrochemistry could provide a direct measurement of the HOMO-LUMO gap. Previously the simple bis-porphyrin **14** has been examined in this way with exactly these aims. Such investigations seemed to indicate electronic delocalization across the 1,4,5,8-tetraazaanthracene bridge[35,81]. This was further emphasised by a splitting in the 1st and 2nd reduction potentials of the bis-porphyrin **14**[35], where if the two porphyrins are not electronically communicating it is thought that they should be reduced at roughly the same potential. However the electrochemical measurements are not necessarily directly comparable with the optical measurements as there is often more of an incentive to delocalize an actual charge than an excitonic state. In addition to this there might be two more fundamental flaws in drawing conclusions from these electrochemical measurements.

Firstly, much care was taken in the optical measurements to try to assess the contribution of aggregation on the photophysical properties of the arrays. Electrochemical measurements are made at typically over 100 times the concentration of these photophysical measurements, so that the effects of aggregation would be much more likely to be observed in the electrochemical measurements. Secondly a splitting in the electrochemical reduction or oxidation potentials is not necessarily a sign of a high degree of ground state electronic communication between neighbouring porphyrins. This is best exemplified by Osuka's singly meso-meso porphyrin dimer (similar to **8**, with the remaining meso positions substituted by 3,5-di-*tert*-butylphenyl groups) where the two porphyrins are at right angles to one another. Therefore no significant ground state electronic communication is possible, and yet a splitting of the first and second oxidation potentials is still observed[196]. This suggests that judging significant ground-state electronic communication purely from the splitting in a porphyrin array's reduction and oxidation potentials is misleading.

7.3.2 Modelling the electronic structure of the array

So it appears that there is little, if any, electronic delocalization along the backbone of the 1,4,5,8-tetraazaanthracene bridged array. This conclusion is supported by a comparison with the photophysical properties of Osuka's triply-linked arrays and Anderson's butadiyne-linked arrays. Both of these systems show a significant red-shift of the UV-VIS spectrum with an increasing number of units in the array in contrast to the present system. So whilst the exciton on photoexcitation of these systems can be considered to have loosely-bound Mott-Wannier character[19,193], it would appear that the 1,4,5,8-tetrazaanthracene bridged system to be much better described in character by a tightly-bound Frenkel description.

These observations are almost counter-intuitive since it would be expected that conjugation would be favoured over the flat, rigid 1,4,5,8-tetraazaanthracene bridge structure. However thorough theoretical investigations into the electronic structure of these arrays by Noel Hush have revealed that this is not necessarily the case[109,197-199]. To illustrate this, the average calculated bond orders of each individual bond in the bis-porphyrin[197] unit are shown in Figure **7.8**. It is evident from this that the system is behaving as three practically *isolated* delocalized systems. So the electronic structure of the two porphyrin units is chlorin-like and is isolated from the bridge by two *alpha*-pyrrolic/ *β*-pyrrolic bonds that are essentially behaving as single bonds. The bridge itself is dominated by delocalization around the benzene ring, with the carbon-nitrogen imine bonds almost attaining full double bond character. On moving to an extended porphyrin array it can be elucidated that the electronic

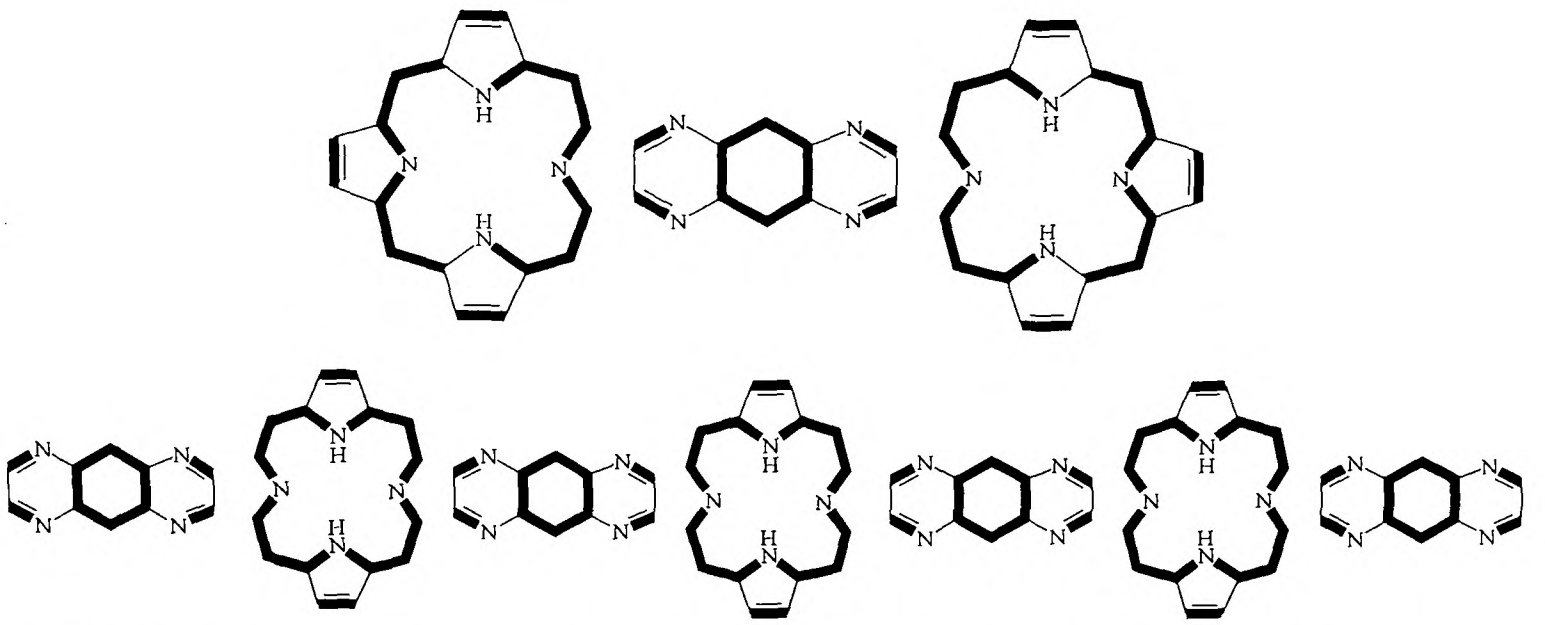

Figure 7.8- Top- calculated bond orders for the bis-porphyrin (adapted from Noel Hush). All bonds possess at least single bond character, so above this the bond order is pictorially represented as increasing in the series: no bond < single feint bond < single bold bond < double bold bond. Bottom- Hush's predictions applied to explain the electronic structure of an extended porphyrin array.

structure of the porphyrin would be similar to that of a bacteriochlorin. Hush ends up by concluding that a 1,4,5,8-tetraazaanthracene bridged porphyrin array is composed of a series weakly interacting chromophores[109,197].

Hush's theoretical treatment really puts into context the UV-VIS data. It cannot be definitively established exactly how weakly the chromophores are interacting. However it appears that there is next-to-no delocalization across the tetraazaanthracene bridge, and the chromophores seem quite happy to maintain their almost independent electronic structure.

7.4 Porphyrin arrays for FET devices

So with the syntheses of various porphyrin oligomers and an evaluation of their electronic properties, a final assessment of the suitability of 1,4,5,8-tetraazaanthracene bridged porphyrin arrays for exploitation in field effect transistors can be made.

The first factor to consider is that even for testing in an FET 100 mg of sample has to be prepared. It has been shown through the various attempts of synthesis that this is no easy task in itself. It has been possible in the current work to synthesise over 100 mg of the non-dendritic bis-porphyrin and non-dendritic tetramer; but attempts to synthesise similar amounts of the dendritic satellite arrays have failed. This is not to say that synthesis on such a scale is impossible, just with this slightly problematic porphyrin system it has proved

difficult. In addition, the susceptibility of these arrays to decompose has not contributed to either their characterization or their successful application in FET devices.

The more cerebral consideration is to examine the electronic suitability of these substrates in FET devices. In Chapter One it was revealed that a subtle interplay of electronic and morphological factors contribute to the mobility of charge in an FET device. For certain the rigidity of the 1,4,5,8-tetraazaanthracene bridge and the sheer length of each array (even the non-dendritic tetramer **22** is 56 Ångstroms[199] from end to end) are favourable morphological factors. However, the conclusion that the system is acting as a series of weakly interacting chromophores rather than as a more cooperative assembly suggests that intra-molecular charge transport along the array might not be necessarily more favourable than inter-molecular charge transport in a well-ordered molecular system. Indeed the porphyrins are rigidly held a huge 7 Ångstroms apart from one another, over which distance *in a worst case scenario* charge would be forced to hop from one chromophore to another. This having been said, the validity of applying conclusions derived from the photophysical analysis of these arrays to an essentially electrochemical situation is questionable. Equally some of Noel Hush's calculations talk favourably about the application of this type of array as a molecular wire[198,199]. So it is still a matter of debate as to whether these arrays are electronically suited to exploitation in a field effect transistor. Similar considerations are also valid in the examination of the application of 1,4,5,8-tetaazaanthracene bridged porphyrin arrays to single molecule devices.

The real challenge for these arrays will come in their testing in actual FET devices. The successful medium-scale synthesis of the non-dendritic tetramer **22** will allow such an evaluation, and should definitively establish whether these 1,4,5,8-tetraazaanthracene bridged porphyrin arrays are suitable as substrates for FET devices.

"The only regret I have about the transistor is its use in rock and roll"

W Brattain, co-inventor of the 'bipolar' transistor in 1948

Chapter Eight

New porphyrin architectures

Chapter Eight
New porphyrin architectures

During the course of any investigation a whole spectrum of new compounds are synthesised. Some do not really fit in with the overall direction of the investigation, but are important nonetheless. Two relevant systems are outlined here, and their importance is emphasised as new porphyrin architectures.

The first is the crown-ether porphyrin **110**. This has been synthesised from the nickel dihydroxy-chlorin **69** described in Chapter Five under previously established methodology of a crown-ether from a diol[200] (Figure **8.1**). It is an interesting product not only because it is the first example of a crown-ether directly appended onto a porphyrin, but also because of its potential application. It has the potential to act as a molecular sensor; it has the potential to act as a supramolecular handle on the porphyrin, so porphyrins can be assembled into larger architectures; equally it has the potential to bring two different metal ions very close to one another, giving rise to porphyrin systems with new optical and electrochemical properties.

The second example is the *seco*-porphyrin **112**. It was isolated from the attempted hydroxylation of the nickel(II) dibromo-quinoxaline **111**. Apart from an unremarkable distribution of the same products obtained from the hydroxylation of the nickel(II) monobromo-quinoxaline **33**, a distinctly apple green relatively non-polar product was also isolated. It was eventually identified as the *seco*-porphyrin structure shown in Figure **8.2** by its LDI mass and the appearance of two very deshielded protons in the ^{1}H NMR spectrum at 9.81 ppm. In addition the appearance of a strongly absorbing band at 700 nm in its UV-VIS spectrum is very reminiscent of a chlorin's UV-VIS spectrum. This is an unusual chromophore that has itself been the target of two separate synthetic investigations[90,201].

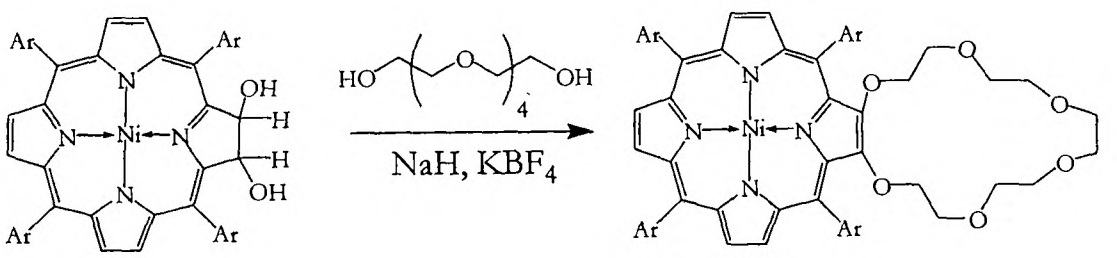

(69) (110)

Figure **8.1**- the synthesis of a crown-ether appended porphyrin. Ar= 3,5-di-*tert*-butylphenyl.

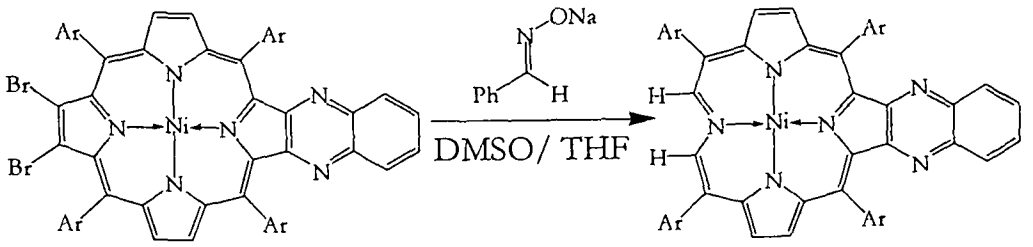

Figure 8.2- synthesis of a *seco*-porphyrin. Ar= 3,5-di-*tert*-butylphenyl.

How it is formed under the present circumstances is unclear, especially because this product was never isolated from any of the attempted hydroxylation reactions of any of the mono-halogenated-quinoxalines.

Chapter Nine
Experimental details

Chapter Nine
Experimental details

9.1 General procedures and instruments

9.1.1 Instruments

^{1}H NMR spectra of new compounds were recorded on either a Bruker AR-400 spectrometer (400 MHz), a Bruker DPX-400 spectrometer (400 MHz) or a Bruker AMX-500 spectrometer (500 MHz) as reported. ^{1}H NMR of previously synthesised compounds were recorded on either a Bruker DPX-200 spectrometer (200 MHz) or a Bruker DPX-400 spectrometer (400 MHz). ^{13}C spectra were recorded on either a Bruker AR-400 spectrometer (100 MHz) or a Bruker AMX-500 spectrometer (125 MHz) as reported. Chemical shifts (δ) are reported in parts per million (ppm) and are referenced to the residual solvent peak. Multiplicities are reported as broad (br), singlet (s), doublet (d), doublet of doublets (dd), doublet of double doublets (ddd), triplet (t), an AB quartet (ABq), an AB quartet coupling to a third resonance X (ABX) or multiplet (m). Coupling constants are reported in Hertz (Hz) and are given to the nearest 0.05 Hz.

Infrared spectra were recorded using KBr discs or in solution in chloroform as reported with a Perkin-Elmer Paragon 1000 IR spectrometer. UV-VIS spectra were measured either in spectrophotometric grade dichloromethane or chloroform as reported with a Perkin-Elmer Lambda 14P UV-VIS spectrometer. The absorption peaks are reported as wavelength (nm) ($\log(\varepsilon/dm^{-3}mol^{-1}cm^{-1})$). 'sh' refers to the appearance of a shoulder. Where substrates were judged not to be completely pure, extinction coefficients are quoted to one decimal place.

Laser Desorption Ionization Time of Flight (LDI-TOF) spectra were recorded on a Micromass Tofspec E spectrometer with no matrix unless otherwise stated. Samples with mass less than 5,000 Daltons were recorded in reflectron (high resolution) mode, whilst samples with mass greater than 5,000 Daltons were recorded in linear (low resolution) mode. Values for m/z are quoted in Daltons. Where the mass spectra occur as isotopic mixtures, the first (lightest) peak is reported.

Melting points were measured using a Gallenkamp melting point apparatus and are uncorrected. Microanalyses were performed by Mrs A Douglas in the Inorganic Chemistry Laboratory, University of Oxford.

Electrochemistry was performed on an EG&G Princeton Applied Research potentiostat/ galvanostat model 263A with a platinum working electrode, a platinum wire counter electrode and a Ag/ 0.1M $AgNO_3$ in acetonitrile reference electrode. A supporting electrolyte of 0.1M tetra *n*-butylammonium tetrafluoroborate that had been purified by recrystallization from ether/ ethyl acetate was used. Cyclic voltammograms were gathered at a scan rate of 60 mVs^{-1} in spectrophotometric grade dichloromethane. Potentials are quoted relative to the ferrocene/ ferrocenium couple in which the ferrocene had been purified by sublimation.

Gel permeation chromatography was performed using a Polymer Laboratories PL gel 20 mm Mixed-A column (600 mm+ 300 mm lengths, 7.5 mm diameter) calibrated with polystyrene narrow standards (mass range 1300- 15.4×10^6) at 30°C. The elutant was tetrahydrofuran and was eluted at a flow rate of 1.0 cm^3min^{-1}. The UV-VIS detector was set at 425 nm.

9.1.2 Solvents and reagents

Spectrophotometric grade petroleum spirit with a boiling point range of 60 to 80°C is referred to light petroleum. Acetone was dried by refluxing over calcium sulphate and then distilling from fresh calcium sulphate. Chloroform required for the halogenation reactions was washed with concentrated sulphuric acid and water before drying and distilling over sodium sulphate. It was then kept over activated 4Å molecular sieves (4-8 mesh) before use. Spectrophotometric grade dichloromethane (CH_2Cl_2) was used as supplied. Dimethylformamide (DMF) was dried over activated 4Å molecular sieves (4-8 mesh) before use. Ether refers to diethyl ether. Pyridine was distilled over potassium hydroxide pellets and kept over calcium hydride prior to use. Tetrahydrofuran was either of anhydrous grade and used as supplied, or dried by distillation over a sodium wire under argon, or dried by passing through a column of alumina. Where solvent mixtures are used, the proportions are given in terms of volume.

Thin layer chromatography was performed with Merck aluminium plates coated with silica gel F_{254}. Column chromatography was performed using either the gravity feed or flash chromatography technique, with ACROS Organics silica gel 0.035-0.07 mm. Grade I neutral

alumina (06300) was supplied from Fluka. Basic alumina (06290) and acidic alumina (06320) were also supplied from Fluka.

N-iodosuccinimide was re-crystallized from dichloromethane/ light petroleum three times before use. *N*-bromosuccinimide and *N*-chlorosuccinimide were re-crystallized from water three times before use.

9.2 Experimental details for Chapter Two

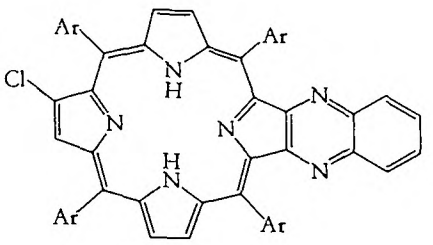

(25)

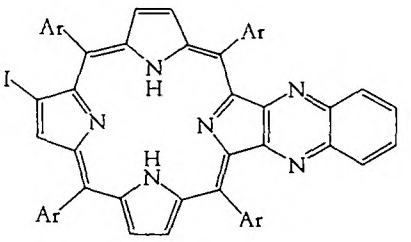

(27)

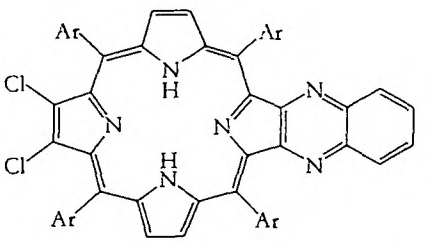

(28)

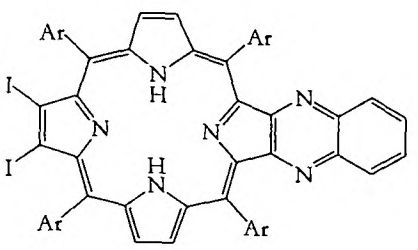

(30)

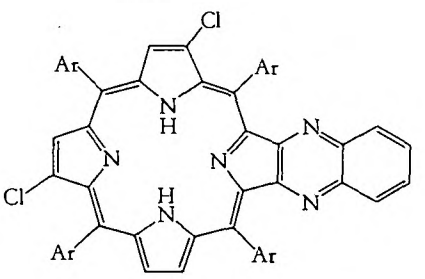

(31)

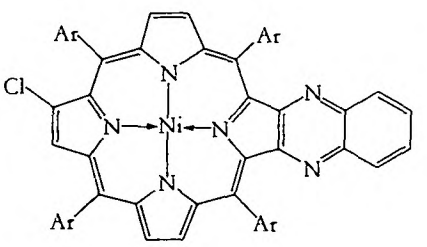

(32)

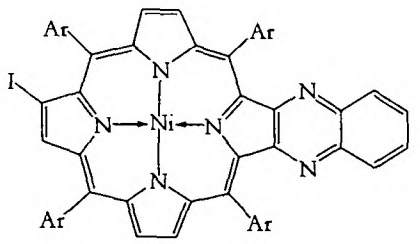

(34)

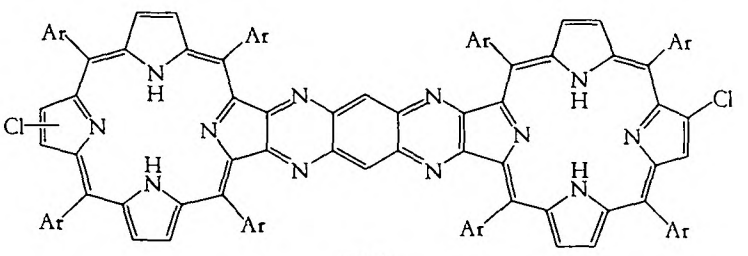

(35)

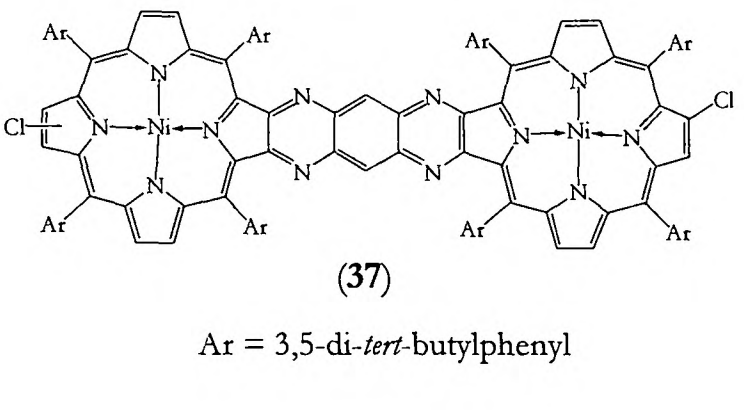

(37)

Ar = 3,5-di-*tert*-butylphenyl

9.2.1 Halogenations

The free-base quinoxalino-porphyrin **24**, the mono-bromo free-base and metallated quinoxalines **26** and **33**, the di-bromo free-base quinoxaline **29** and the di-bromo free-base and metallated bis-porphyrins **36** and **38** were prepared according to identical procedures and had identical spectra as those reported by Burn[81]

12-chloro-5,10,15,20-tetrakis(3',5'-di-*tert*-butylphenyl)quinoxalino[2,3-b]porphyrin (25)

5,10,15,20-tetrakis(3',5'-di-*tert*-butylphenyl)quinoxalino[2,3-b]porphyrin (**24**) (42 mg, 0.036 mmol) was dissolved in chloroform (10 ml) and brought to reflux. Iodine monochloride (14 mg, 0.086 mmol) dissolved in chloroform (0.4 ml) was added over 4 hours, at which point the system was allowed to cool. Saturated sodium thiosulphate solution (100 ml) was added and the organic layer separated. This was washed with more saturated sodium thiosulphate

solution (100 ml), dried over sodium sulphate and the solvent was removed. The product was purified by column chromatography (1:8 dichloromethane: light petroleum). The first main band was collected and identified as 12-chloro-5,10,15,20-tetrakis(3',5'-di-*tert*-butylphenyl)quinoxalino[2,3-b]porphyrin (**25**) (41 mg, 93%), a dark purple solid. υ_{max}(KBr) 3365 (NH), 2963, 1594, 1477, 1363, 1248, 801; λ_{max} (CH_2Cl_2)/nm (log(ε/$dm^{-3}mol^{-1}cm^{-1}$)) 299 (4.32), 338sh (4.39), 358 (4.44), 435 (5.27), 531 (4.31), 567sh (3.50), 600 (3.95), 653 (2.87); ^{1}H n.m.r. (400 MHz; $CDCl_3$) δ: -2.69 (1H, br s, NH) -2.56 (1H, br s, NH), 1.50-1.55 (72H, m, *t*-butyl H), 7.73-7.78 (2H, m, quinoxalino H), 7.81 (1H, dd $J_{2',4'}$ = $J_{6',4'}$ = 2.05 Hz, C(4')H), 7.81-7.86 (2H, m quinoxalino H), 7.83 (1H, dd $J_{2',4'}$ = $J_{6',4'}$ = 1.75 Hz, C(4')H), 7.94 (2H, dd $J_{2',4'}$ = $J_{6',4'}$ = 1.70 Hz, C(4')H), 7.96 (2H, d, $J_{4',2'}$ = $J_{4',6'}$ = 1.95 Hz, C(2')H and C(6')H), 7.97 (2H, d, $J_{4',2'}$ = $J_{4',6'}$ = 2.00 Hz, C(2')H and C(6')H), 7.98 (2H, d, $J_{4',2'}$ = $J_{4',6'}$ = 1.80 Hz, C(2')H and C(6')H), 8.07 (2H, d, $J_{4',2'}$ = $J_{4',6'}$ = 1.65 Hz, C(2')H and C(6')H), 8.07 (1H, s, C(12)H), 8.91 (1H, dd, $J_{\beta,\beta}$ = 5.20 Hz, $J_{NH,\beta}$ = 1.40 Hz, β-pyrrolic H), 8.94 (1H, dd, $J_{\beta,\beta}$ = 5.05 Hz, $J_{NH,\beta}$ = 1.55 Hz, β-pyrrolic H), 9.04 (1H, dd, $J_{\beta,\beta}$ = 5.25 Hz, $J_{NH,\beta}$ = 1.25 Hz, β-pyrrolic H), 9.07 (1H, dd, $J_{\beta,\beta}$ = 4.95 Hz, $J_{NH,\beta}$ = 1.25 Hz, β-pyrrolic H); *m*/*z* (LDI-TOF) 1198.5 (M^+, 100%); $C_{82}H_{95}N_6Cl$ requires 1198.7 (M^+).

12,13-dichloro-5,10,15,20-tetrakis(3',5'-di-*tert*-butylphenyl)quinoxalino[2,3-b] porphyrin (28) and 7,13-dichloro-5,10,15,20-tetrakis(3',5'-di-*tert*-butylphenyl)quinoxalino[2,3-b]porphyrin (31)

5,10,15,20-tetrakis(3',5'-di-*tert*-butylphenyl)quinoxalino[2,3-b]porphyrin (**24**) (130 mg, 0.11 mmol) and *N*-chlorosuccinimide (33 mg, 0.25 mmol) were dissolved in chloroform (10 ml) and pyridine (0.5 ml). The system was heated at the point of reflux for 3 hours, and then allowed to cool. Dichloromethane (50 ml) and hydrochloric acid (3M, 50 ml) were added to the reaction mixture; the organic layer was separated and washed with water (3×50 ml), saturated sodium bicarbonate solution (50 ml), brine (50 ml), dried over sodium sulphate, and solvent was removed. The product was purified by column chromatography (1:6 dichloromethane: light petroleum.) The first feint band was collected and evaporated to dryness to give 7,13-dichloro-5,10,15,20-tetrakis(3',5'-di-*tert*-butylphenyl)quinoxalino[2,3-b] porphyrin (**31**), a dark purple solid (6.4 mg, 5%.) υ_{max}($CHCl_3$) 3346 (NH), 2966, 1596, 1477, 1423, 1364, 1074, 908, 897; λ_{max} (CH_2Cl_2)/nm (log(ε/$dm^{-3}mol^{-1}cm^{-1}$)) 300(4.15), 336sh (4.26), 360 (4.33), 438 (5.07), 531 (4.16), 565sh (3.59), 655 (2.98); ^{1}H n.m.r. (400 MHz; $CDCl_3$) δ: -2.73 (1H, br s, NH), –2.36 (1H, br s, NH), 1.47 to 1.54 (72H, m, *t*-butyl H), 7.72-7.80 (4H,

m, quinoxalino H), 7.79 (1H, dd $J_{2',4'}$ = $J_{6',4'}$ = 1.90 Hz, C(4')H), 7.83 (1H, dd $J_{2',4'}$ = $J_{6',4'}$ = 1.70 Hz, C(4')H), 7.89 (2H, d, $J_{4',2'}$ = $J_{4',6'}$ = 2.20 Hz, C(2')H and C(6')H), 7.92 (1H, dd $J_{2',4'}$ = $J_{6',4'}$ = 1.70 Hz, C(4')H), 7.93-7.94 (5H, m, of which 4H, C(2')H and C(6')H and 1H, C(4')H), 8.01 (2H, d, $J_{4',2'}$ = $J_{4',6'}$ = 1.75 Hz, C(2')H and C(6')H), 8.58 (1H, s, C(12)H), 8.85 (1H, d, $J_{NH,\beta}$ = 2.25 Hz, C(8)H), 8.88 (1H, dd, $J_{\beta,\beta}$ = 5.30 Hz, $J_{NH,\beta}$ = 1.00 Hz, β-pyrrolic H), 9.04 (1H, dd, $J_{\beta,\beta}$ = 4.80 Hz, $J_{NH,\beta}$ = 1.40 Hz, β-pyrrolic H); an NOE difference experiment (500 MHz; $CDCl_3$)shows NOE's between the signal at 7.93-7.94 and those at 8.88 and 9.01; also between the signal at 8.01 and both 8.85 and 8.58; m/z (LDI-TOF) 1233.2 (M^+, 100%); $C_{82}H_{94}N_6Cl_2$ requires 1232.7 (M^+).

The second band was collected in fractions. The first fraction of the second band was evaporated to dryness to give 12,13-dichloro-5,10,15,20-tetrakis(3',5'-di-*tert*-butylphenyl)quinoxalino[2,3-b]porphyrin (**28**), a dark purple solid (12 mg, 9%.) υ_{max}(KBr) 3379 (NH), 2968, 1594, 1477, 1423, 1363, 1247, 1052, 801, 741, 704; λ_{max} (CH_2Cl_2)/nm (log(ε/$dm^{-3}mol^{-1}cm^{-1}$)) 300(4.19), 340sh (4.36), 360 (4.36), 437 (5.20), 533 (4.19), 600 (3.90), 658 (2.96); ^{1}H n.m.r. (400 MHz; $CDCl_3$) δ: -2.73 (2H, br s, NH), 1.49 and 1.52 (72H, s, *t*-butyl H), 7.74-7.79 (2H, m, quinoxalino H), 7.80-7.85 (2H, m, quinoxalino H), 7.82 (2H, dd $J_{2',4'}$ = $J_{6',4'}$ = 1.80 Hz, C(4')H), 7.93 (2H, dd $J_{2',4'}$ = $J_{6',4'}$ = 1.75 Hz, C(4')H), 7.95 (4H, d, $J_{4',2'}$ = $J_{4',6'}$ = 2.10 Hz, C(2')H and C(6')H), 7.97 (4H, d, $J_{4',2'}$ = $J_{4',6'}$ = 1.75 Hz, C(2')H and C(6')H), 8.91 (2H, dd, $J_{\beta,\beta}$ = 4.95 Hz, $J_{NH,\beta}$ = 1.65 Hz, β-pyrrolic H), 9.02 (2H, dd, $J_{\beta,\beta}$ = 5.20 Hz, $J_{NH,\beta}$ = 1.60 Hz, β-pyrrolic H); m/z (LDI-TOF) 1232.6 (M^+, 100%); $C_{82}H_{94}N_6Cl_2$ requires 1232.7 (M^+).

The second fraction of the second band was evaporated to dryness and was identified as 12-chloro-5,10,15,20-tetrakis(3',5'-di-*tert*-butylphenyl)quinoxalino[2,3-b]porphyrin (**25**), (40 mg, 30%) by an identical ^{1}H NMR as and co-chromatography against an authentic sample. The third band was collected and evaporated to dryness to recover the starting material (**24**) (24 mg, 18%).

12-iodo-5,10,15,20-tetrakis(3',5'-di-*tert*-butylphenyl)quinoxalino[2,3-b]porphyrin (27) and **12,13-diiodo-5,10,15,20-tetrakis(3',5'-di-*tert*-butylphenyl)quinoxalino[2,3-b] porphyrin** (**30**)

5,10,15,20-tetrakis(3',5'-di-*tert*-butylphenyl)quinoxalino[2,3-b]porphyrin (**24**) (195 mg, 0.17 mmol) was dissolved in DMF (10 ml) and brought to the point of reflux. Iodine (1.09 g, 4.3

mmol) was added over 5½ hours and then the system was allowed to cool. Ether (50 ml) and water (50 ml) were added and the organic layer was extracted, washed with saturated sodium thiosulphate solution (50 ml), water (4×50 ml), brine (50 ml), and dried over sodium sulphate. Solvent was removed and the product was purified by column chromatography (1:7 dichloromethane: light petroleum). The first band was collected and was evaporated to dryness to give 12-iodo-5,10,15,20-tetrakis(3',5'-di-*tert*-butylphenyl)quinoxalino[2,3-b] porphyrin (**27**) (102 mg, 47%), a dark purple solid. υ_{max}(KBr) 3369 (NH), 2963, 1594, 1477, 1363, 1261, 800, 710; λ_{max} (CH_2Cl_2)/nm (log(ε/$dm^{-3}mol^{-1}cm^{-1}$)) 299 (4.34), 346sh (443), 366sh (4.49), 414sh (5.10), 438 (5.38), 532 (4.38), 600 (4.10), 656 (3.03); ^{1}H n.m.r. (400 MHz; $CDCl_3$) δ: -2.69 (1H, br s, NH), -2.53 (1H, br s, NH), 1.49-1.55 (72H, m, *t*-butyl H), 7.74-7.77 (2H, m, quinoxalino H), 7.81-7.85 (4H, m, of which 2H, quinoxalino H and 2H, C(4')H), 7.93 (2H, dd $J_{2',4'}$ = $J_{6',4'}$ = 1.85 Hz, C(4')H), 7.96 (4H, ABq, $J_{4',2'}$ = $J_{4',6'}$ = 2.10 Hz, C(2')H and C(6')H), 7.97 (2H, d, $J_{4',2'}$ = $J_{4',6'}$ = 2.15 Hz, C(2')H and C(6')H), 8.08 (2H, d, $J_{4',2'}$ = $J_{4',6'}$ = 2.10 Hz, C(2')H and C(6')H), 8.93 (1H, dd, $J_{\beta,\beta}$ = 5.00 Hz, $J_{NH,\beta}$ = 1.50 Hz, *β*-pyrrolic H), 8.95 (1H, dd, $J_{\beta,\beta}$ = 4.95 Hz, $J_{NH,\beta}$ = 1.50 Hz, *β*-pyrrolic H), 9.02 (1H, dd, $J_{\beta,\beta}$ = 4.70 Hz, $J_{NH,\beta}$ = 1.65 Hz, *β*-pyrrolic H), 9.06 (1H, dd, $J_{\beta,\beta}$ = 5.20 Hz, $J_{NH,\beta}$ = 1.60 Hz, *β*-pyrrolic H); *m/z* (LDI-TOF) 1291.3 (M^+, 10%), 1162.5 (M^+, 100%); $C_{82}H_{95}N_6I$ requires 1290.7 (M^+), (M^+ - I) requires 1163.8.

The second band was collected and evaporated to dryness to recover starting material **24** (70 mg, 36%) which was co-chromatographed against and had an identical ^{1}H NMR spectrum as an authentic sample. The third band was collected and evaporated to dryness to give 12,13-diiodo-5,10,15,20-tetrakis(3',5'-di-*tert*-butylphenyl)quinoxalino[2,3-b]porphyrin (**30**), a purple-brown solid (36 mg, 15%.) υ_{max}(KBr) 3388 (NH), 2963, 1594, 1476, 1362, 1261, 800; λ_{max} (CH_2Cl_2)/nm (log(ε/$dm^{-3}mol^{-1}cm^{-1}$)) 304 (4.32), 334 (4.32), 451 (5.13), 543 (4.09), 608 (3.76), 685 (3.25); ^{1}H n.m.r. (400 MHz; $CDCl_3$) δ: -2.36 (2H, br s, NH), 1.51 and 1.58 (72H, s, *t*-butyl H), 7.73-7.77 (2H, m, quinoxalino H), 7.81-7.85 (2H, m, quinoxalino H), 7.87 (2H, dd, $J_{2',4'}$ = $J_{6',4'}$ = 1.85 Hz, C(4')H), 7.93 (2H, dd $J_{2',4'}$ = $J_{6',4'}$ = 1.65 Hz, C(4')H), 7.99 (4H, d, $J_{4',2'}$ = $J_{4',6'}$ = 1.75 Hz, C(2')H and C(6')H), 8.08 (4H, d, $J_{4',2'}$ = $J_{4',6'}$ = 1.75 Hz, C(2')H and C(6')H), 8.93 (2H, dd, $J_{\beta,\beta}$ = 5.03 Hz, $J_{NH,\beta}$ = 1.60 Hz, *β*-pyrrolic H), 9.01 (2H, dd, $J_{\beta,\beta}$ = 4.95 Hz, $J_{NH,\beta}$ = 1.60 Hz, *β*-pyrrolic H); *m/z* (LDI-TOF) 1417.4 (M^+, 100%), 1288.5 (M^+ - I, 60%), 1162.6(M^+ - 2I, 20%); $C_{82}H_{94}N_6I_2$ requires 1416.6 (M^+), (M^+ - I) requires 1289.7, (M^+ - 2I) requires 1162.8.

2,22-dichloro-5,10,15,20,25,30,35,40-octakis(3',5'-di-*tert*-butylphenyl)cycloeicosa[b] cycloeicosa[5,6]pyrazino[2,3-g]quinoxaline and **2,23-dichloro-5,10,15,20,25,30,35,40-octakis(3',5'-di-*tert*-butylphenyl)cycloeicosa[b]cycloeicosa[5,6]pyrazino[2,3-g] quinoxaline** (**35**)

5,10,15,20,25,30,35,40-octakis(3',5'-di-*tert*-butylphenyl)cycloeicosa[b]cycloeicosa[5,6] pyrazino[2,3-g]quinoxaline (**14**) (257 mg, 0.11 mmol) was dissolved in chloroform (30 ml) and was heated to reflux under a flowing stream of nitrogen. Iodine monochloride (89 mg, 0.55 mmol) in chloroform (1 ml) was added in five aliquots over 6 hours. The system was allowed to cool and saturated sodium thiosulphate solution (100 ml) was added. The organic layer was extracted and washed with saturated sodium thiosulphate solution again (100 ml), dried over sodium sulphate and the solvent removed. The product was purified by column chromatography (1:8 dichloromethane: light petroleum). The first main band was collected and identified as a mixture of 2,22-dichloro-5,10,15,20,25,30,35,40-octakis(3',5'-di-*tert*-butylphenyl)cycloeicosa[b]cycloeicosa[5,6]pyrazino[2,3-g]quinoxaline and 2,23-dichloro-5,10,15,20,25,30,35,40-octakis(3',5'-di-*tert*-butylphenyl)cycloeicosa[b]cycloeicosa[5,6] pyrazino[2,3-g]quinoxaline (**35**) (170 mg, 64%), a dark brown solid. υ_{max}(KBr) 3369(NH), 2961, 1594, 1477, 1363, 1248, 1205, 1173, 1070, 1011, 802, 710; λ_{max} (CH_2Cl_2)/nm (log(ε/$dm^3mol^{-1}cm^{-1}$)) 250 (4.47), 332sh (4.43), 429 (5.35), 458 (5.29), 529sh (4.59), 610sh (4.14), 622 (4.19), 672sh (3.66); ^{1}H n.m.r. (400 MHz; $CDCl_3$) δ: -2.54 (2H, br s, NH), -2.40 (2H, br s, NH), 1.52 to 1.60 (144H, m, *t*-butyl H), 7.80 (2H, dd $J_{2',4'} = J_{6',4'}$ = 1.60 Hz, C(4')H), 7.82 (2 H, dd $J_{2',4'} = J_{6',4'}$ = 1.75 Hz, C(4')H), 7.95 (4H, d, $J_{4',2'} = J_{4',6'}$ = 1.60 Hz, C(2')H and C(6')H), 8.00 (4H, dd, $J_{2',4'} = J_{6',4'}$ = 1.70 Hz, C(4')H), 8.05 (4H, d, $J_{4',2'} = J_{4',6'}$ = 2.10 Hz, C(2')H and C(6')H), 8.08 (4H, d, $J_{4',2'} = J_{4',6'}$ = 1.90 Hz, C(2')H and C(6')H), 8.09 (4H, d, $J_{4',2'} = J_{4',6'}$ = 2.00 Hz, C(2')H and C(6')H), 8.58 (2H, m, bridging H), 8.65 (2H, s, C(3)H and C (23)H), 8.83 to 8.92 (8H, m, β-pyrrolic H); COSY shows coupling between the NH proton signals and the multiplet at 8.83 to 8.93; *m/z* (LDI-TOF) 2319.1 (M^+, 100%); $C_{158}H_{184}N_{12}Cl_2$ requires 2319.4 (M^+).

9.2.2 Metallation of halogenated porphyrins with nickel(II)

(12-chloro-5,10,15,20-tetrakis(3',5'-di-*tert*-butylphenyl)quinoxalino[2,3-b]porphinato) nickel(II) (**32**)

12-chloro-5,10,15,20-tetrakis(3',5'-di-*tert*-butylphenyl)quinoxalino[2,3-b]porphyrin (**25**) (120 mg, 0.10 mmol) and nickel acetate tetrahydrate (76 mg, 0.31 mmol) were dissolved in DMF

(20 ml) and heated at the point of reflux for 3 hours. The system was allowed to cool and ether (100 ml) and water (150 ml) were added. The organic layer was separated, washed with distilled water (4×100 ml), brine (100 ml) and dried over sodium sulphate. Solvent was removed and the product was purified by column chromatography (2:3 dichloromethane: light petroleum). The main band was collected and evaporated to dryness to give (12-chloro-5,10,15,20-tetrakis(3',5'-di-*tert*-butylphenyl)quinoxalino[2,3-b]porphinato)nickel(II) (**32**), a dark purple solid (120 mg, 96%.) υ_{max}(KBr) 2962, 1594, 1477, 1363, 1247, 946, 821, 807, 795; λ_{max} (CH_2Cl_2)/nm (log(ε/$dm^3mol^{-1}cm^{-1}$)) 291 (4.29), 258 (4.42), 410 (4.81), 451 (4.89), 529sh (3.75), 560 (4.01), 604 (3.93); ^{1}H n.m.r. (400 MHz; $CDCl_3$) δ: 1.42-1.46 (72H, m, *t*-butyl H), 7.66 (3H, m, of which 1H, C(4')H and 2H, C(2')H and C(6')H), 7.68 (2H, d, $J_{4',2'} = J_{4',6'}$ = 1.70 Hz, C(2')H and C(6')H), 7.69 (2H, d, $J_{4',2'} = J_{4',6'}$ = 2.10 Hz, C(2')H and C(6')H), 7.70 (1H, dd $J_{2',4'} = J_{6',4'}$ = 1.90 Hz, C(4')H), 7.73-7.77 (2H, m, quinoxalino H), 7.78 (2H, d, $J_{4',2'} = J_{4',6'}$ = 1.80 Hz, C(2')H and C(6')H), 7.79-7.82 (4H, m, of which 2H, C(4')H and 2H, quinoxalino H), 8.54 (1H, s, C(12)H), 8.74 and 8.90 (2H, ABq, $J_{\beta,\beta}$ = 4.85 Hz, *β*-pyrrolic H), 8.88 and 8.89 (2H, ABq, $J_{\beta,\beta}$ = 4.95 Hz, *β*-pyrrolic H); *m/z* (LDI-TOF) 1254.4 (M^+, 100%); $C_{82}H_{93}N_6NiCl$ requires 1254.7 (M^+).

(12-iodo-5,10,15,20-tetrakis(3',5'-di-*tert*-butylphenyl)quinoxalino[2,3-b]porphinato) nickel(II) (34)

12-iodo-5,10,15,20-tetrakis(3',5'-di-*tert*-butylphenyl)quinoxalino[2,3-b]porphyrin (**27**) (50 mg, 0.039 mmol) and nickel acetate tetrahydrate (330 mg, 1.3 mmol) were dissolved in DMF (15 ml) and heated at the point of reflux for 3 hours. The system was allowed to cool and ether (100 ml) and water (100 ml) were added. The organic layer was extracted and washed with water (4×100 ml), brine (100 ml), dried over sodium sulphate and the solvent was removed. The product was purified by column chromatography (2:3 dichloromethane: light petroleum.) The main band was collected and identified as (12-iodo-5,10,15,20-tetrakis(3',5'-di-*tert*-butylphenyl)quinoxalino[2,3-b]porphinato)nickel(II) (**34**) (29 mg, 55%), a dark purple/ brown solid. Found: C, 72.9%; H, 7.1%; N, 6.6%; $C_{82}H_{93}N_6NiI$ requires C, 73.1%; H, 7.0%; N, 6.2%; υ_{max}(KBr) 2962, 1594, 1477, 1362, 1247, 943, 793; λ_{max} (CH_2Cl_2)/nm (log(ε/$dm^3mol^{-1}cm^{-1}$)) 291 (4.25), 360 (4.36), 412 (4.77), 456 (4.87), 524sh (3.74), 562 (4.03), 604 (3.86); ^{1}H n.m.r. (400 MHz; $CDCl_3$) δ: 1.42-1.48 (72H, m, *t*-butyl H), 7.66 (2H, d, $J_{4',2'} = J_{4',6'}$ = 1.75 Hz, C(2')H and C(6')H), 7.68 (2H, d, $J_{4',2'} = J_{4',6'}$ = 2.05 Hz, C(2')H and C(6')H), 7.69-7.72 (2H, m, C(4')H), 7.69 (2H, d, $J_{4',2'} = J_{4',6'}$ = 1.95 Hz, C(2')H and C(6')H), 7.73-7.77 (2H, m, quinoxalino H), 7.79-7.82 (6H, m, of which 2H, C(4')H, 2H, quinoxalino H and 2H,

C(2')H and C(6')H), 8.73 and 8.92 (2H, ABq, $J_{\beta,\beta}$ = 5.25 Hz, β-pyrrolic H), 8.87 and 8.89 (2H, ABq, $J_{\beta,\beta}$ = 4.85 Hz, β-pyrrolic H), 9.00 (1H, s, C(12)H); m/z (LDI-TOF) 1347.4 (M^+, 100%), 1218.4 (M^+- I, 80%); $C_{82}H_{93}N_6NiI$ requires 1346.6 (M^+), $C_{82}H_{93}N_6Ni$, 1219.6 (M^+- I).

[2,22-dichloro-5,10,15,20,25,30,35,40-octakis(3',5'-di-*tert*-butylphenyl)cycloeicosa[b] cycloeicosa[5,6]pyrazino[2,3-g]quinoxalino]nickel(II) and **[2,23-dichloro-5,10,15,20,25,30,35,40-octakis(3',5'-di-*tert*-butylphenyl)cycloeicosa[b]cycloeicosa[5,6] pyrazino[2,3-g]quinoxalino]nickel(II)** (**37**)

35 (141mg, 0.060 mmol) and nickel(II) diacetate tetrahydrate (219mg, 0.88 mmol) were dissolved in DMF (21 ml) and heated at the point of reflux under nitrogen for four hours. The system was allowed to cool and ether (100 ml) and water (100 ml) were added. The organic layer was extracted and washed with water (4×100 ml) brine (100 ml) dried over sodium sulphate and solvent removed. The product was purified by column chromatography (1:2 dichloromethane: light petroleum). The main band was identified as an inseparable mixture of [2,22-dichloro-5,10,15,20,25,30,35,40-octakis(3',5'-di-*tert*-butylphenyl)cycloeicosa[b]cycloeicosa[5,6]pyrazino[2,3-g]quinoxalino]nickel(II) and [2,23-dichloro-5,10,15,20,25,30,35,40-octakis(3',5'-di-*tert*-butylphenyl)cycloeicosa[b]cycloeicosa[5,6] pyrazino[2,3-g]quinoxalino]nickel(II) (**37**) (140 mg, 94%), a dark brown solid. υ_{max}(KBr) 2959, 1594, 1476, 1462, 1362, 1295, 1247, 1209, 1089, 1044, 1017, 946, 818, 793; λ_{max} (CH_2Cl_2)/nm (log(ε/$dm^{-3}mol^{-1}cm^{-1}$)) 295sh (4.61), 328 (4.64), 431 (5.43), 450 (5.41), 504sh (4.89), 536 (4.95), 663 (4.42), 721sh (4.07); ^{1}H n.m.r. (400 MHz; $CDCl_3$) δ: 1.46 to 1.50 (144H, m, *t*-butyl H), 7.67 (6H, m, aryl H), 7.73 to 7.74 (8H, m, aryl H), 7.79 (4H, m, aryl H), 7.84 (4H, m, aryl H), 8.49 (2H, s, β-pyrrolic H), 8.56 (2H, m, β-pyrrolic H), 8.63 (2H, m, β-pyrrolic H), 8.66 (4H, m, β-pyrrolic H), 8.84 (2H, d, $J_{\beta,\beta}$ = 4.60 Hz, β-pyrrolic H); m/z (LDI-TOF) 2431.3 (M^+, 100%); $C_{158}H_{180}N_{12}Cl_2Ni_2$ requires 2431.3 (M^+).

9.3 Experimental details for Chapter Three

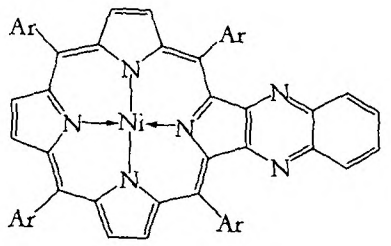

(39)

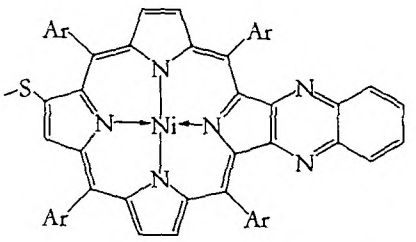

(42)

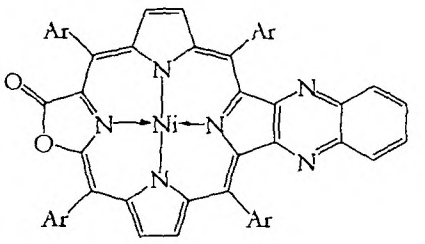

(43)

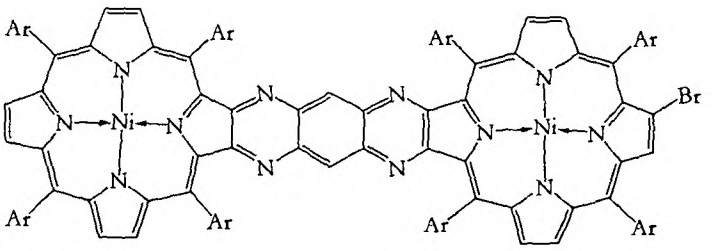

(44)

Ar= 3,5-di-*tert*-butylphenyl.

Hydroxylation of the iodo-quinoxaline ***34***

(5,10,15,20-tetrakis(3',5'-di-*tert*-butylphenyl)quinoxalino[2,3-b]porphinato)nickel(II) (**39**) and **(13-oxo-12-oxa-tetrakis(3',5'-di-*tert*-butylphenyl)quinoxalino[2,3-b]) porphinato)nickel(II)** (**43**)

Sodium hydride (60% dispersion in mineral oil) (16 mg, 0.40 mmol) and DMSO (10 ml) were stirred under nitrogen at 80°C for 50 minutes to give a clear, pale yellow solution. Heat was removed, benzaldehyde oxime (36 mg, 0.30 mmol) was added and the solution stirred for a further 5 minutes. This was then transferred under nitrogen to a solution of (12-iodo-5,10,15,20-tetrakis(3',5'-di-*tert*-butylphenyl)quinoxalino[2,3-b]porphinato)nickel(II) (**34**) (29 mg, 0.022 mmol) in dry tetrahydrofuran (dried by distillation over sodium wire, 10ml) and heated at reflux in the dark for 16.5 hours. The system was allowed to cool and ether (75 ml) and water (100 ml) were added to the reaction mixture. The organic layer was extracted and washed with water (5×100 ml), brine (100ml) and dried over sodium sulphate. Solvent was removed and the residue was purified by column chromatography in the dark (1:5 dichloromethane: petroleum spirit.) The first band was collected and evaporated to dryness to give a dark purple solid (5,10,15,20-tetrakis(3',5'-di-*tert*-butylphenyl)quinoxalino[2,3-b] porphinato)nickel(II) (**39**) (15 mg, 56%.) υ_{max}(KBr) 2962, 1594, 1476, 1363, 1247, 1012, 796, 713; λ_{max} (CH_2Cl_2)/nm (log(ε/$dm^3mol^{-1}cm^{-1}$)) 287 (4.29), 356 (4.42), 408 (4.88), 447 (4.89), 558 (3.97), 602 (4.01); ^{1}H n.m.r. (400 MHz; $CDCl_3$) δ: 1.49 (36H, s, *t*-butyl H),1.53 (36H, s, *t*-butyl H), 7.77 (2H, dd $J_{2',4'} = J_{6',4'}$ = 2.00 Hz, C(4')H), 7.78-7.82 (2H, m, quinoxalino H), 7.78

(4H, d, $J_{4',2'}$ = $J_{4',6'}$ = 1.40 Hz, C(2')H and C(6')H), 7.85-7.89 (4H, m, of which 2H, C(4')H and 2H, quinoxalino H), 7.91 (2H, d, $J_{4',2'}$ = $J_{4',6'}$ = 1.75 Hz, C(2')H and C(6')H), 8.76 (2H, s, C(12)H and C(13)H), 8.83 and 8.98 (4H, ABq, $J_{\beta,\beta}$ = 5.30 Hz, β-pyrrolic H); m/z (LDI-TOF) 1221.0 (M^+, 100%); $C_{82}H_{95}N_6Ni$ requires 1220.7 (M^+).

The second much more polar, green band was collected and evaporated to dryness to give (13-oxo-12-oxatetrakis(3',5'-di-*tert*-butylphenyl)quinoxalino[2,3-b]chlorinato)porphyrin (**43**) (3.0 mg, 11%), a dark green solid. υ_{max}(KBr) 2962, 1780 (CO), 1595, 1476, 1361, 1297, 1247, 1041, 797, 772, 710; λ_{max} (CH_2Cl_2)/nm (log(ε/$dm^3mol^{-1}cm^{-1}$)) 303 (4.21), 347 (4.38), 414sh (4.70), 447 (4.84), 532 (3.74), 599 (3.78), 748sh (2.83); ^{1}H n.m.r. (400 MHz; $CDCl_3$) δ: 1.43-1.47 (72H, m, *t*-butyl H), 7.64 (2H, d, $J_{4',2'}$ = $J_{4',6'}$ = 1.45 Hz, C(2')H and C(6')H), 7.66-7.70 (2H, m, quinoxalino H), 7.68 (2H, d, $J_{4',2'}$ = $J_{4',6'}$ = 2.00 Hz, C(2')H and C(6')H), 7.70 (2H, d, $J_{4',2'}$ = $J_{4',6'}$ = 1.70 Hz, C(2')H and C(6')H), 7.74-7.80 (2H, m, quinoxalino H), 7.75-7.78 (4H, m, of which 2H, C(4')H and 2H, C(2')H and C(6')H), 7.83 (1H, dd $J_{2',4'}$ = $J_{6',4'}$ = 1.70 Hz, C(4')H), 7.84 (1H, dd $J_{2',4'}$ = $J_{6',4'}$ = 1.70 Hz, C(4')H), 8.48 and 8.72 (2H, ABq, $J_{\beta,\beta}$ = 4.80 Hz, β-pyrrolic H), 8.58 and 8.84 (2H, ABq, $J_{\beta,\beta}$ = 4.95 Hz, β-pyrrolic H); m/z (LDI-TOF) 1239.0 (M^+, 100%); $C_{81}H_{92}N_6NiO_2$ requires 1238.7 (M^+).

Hydroxylation of the bromo-quinoxaline ***33***

[12-methylthio-5,10,15,20-tetrakis(3',5'-di-*tert*-butylphenyl)quinoxalino[2,3-b] porphinato]nickel(II) (42)

Sodium hydride (60% dispersion in mineral oil) (22 mg, 0.56 mmol) and DMSO (8 ml) were stirred under nitrogen at 80°C for 50 minutes to give a clear, pale yellow solution. Heat was removed, benzaldehyde oxime (53 mg, 0.44 mmol) was added and the solution stirred for a further 5 minutes. This was then transferred under nitrogen to a solution of (12-bromo-5,10,15,20-tetrakis(3',5'-di-*tert*-butylphenyl)quinoxalino[2,3-b]porphinato)nickel(II) (**33**) (48 mg, 0.037 mmol) in dry tetrahydrofuran (dried by distillation over sodium wire, 8 ml) and heated at reflux in the dark for 17 hours. The system was allowed to cool and ether (75 ml) and water (100 ml) were added to the reaction mixture. The organic layer was extracted and washed with water (5×100 ml), brine (100ml) and dried over sodium sulphate. Solvent was removed and the residue was purified by column chromatography in the dark (1:5 dichloromethane: petroleum spirit). The main band was identified as (5,10,15,20-tetrakis(3',5'-di-*tert*-butylphenyl)quinoxalino[2,3-b]porphinato)nickel(II) (**39**) (19 mg, 43%) by an identical ^{1}H NMR as and co-chromatography against an authentic sample. The second

and third bands were of similar polarity and therefore had to be carefully separated. The second band was identified as [12-methylthio-5,10,15,20-tetrakis(3',5'-di-*tert*-butylphenyl)quinoxalino[2,3-b]porphinato]nickel(II) (**42**) (1.0 mg, 2%), a dark brown solid. υ_{max}(KBr) 2961, 1594, 1476, 1362, 1298, 1282, 1247, 1064, 1026, 946, 899, 880, 821, 791, 762, 711, 609; λ_{max} (CH_2Cl_2)/nm (log(ε/$dm^3mol^{-1}cm^{-1}$)) 296 (3.97), 345 (3.98), 414 (4.54), 451 (4.47), 569 (3.57), 626 (3.61); ^{1}H n.m.r. (500 MHz; $CDCl_3$) δ: 1.43 to 1.48 (72H, m, *t*-butyl H), 2.52 (3H, s, methyl H), 7.66 (2H, d, $J_{4',2'} = J_{4',6'} = 1.30$ Hz, C(2')H and C(6')H), 7.70 (4H, d, $J_{4',2'} = J_{4',6'} = 1.40$ Hz, C(2')H and C(6')H), 7.71 (2H, dd, $J_{2',4'} = J_{6',4'} = 1.85$ Hz, C(4')H),7.73 to 7.75 (2H, m, quinoxalino H), 7.80 to 7.83 (4H of which 2H are quinoxalino H and 2H are C(4')H, m), 7.85 (2H, d, $J_{4',2'} = J_{4',6'} = 1.85$ Hz, C(2')H and C(6')H), 8.29 (1H, s, C(13)H), 8.70 (1H, d, $J_{\beta,\beta} = 5.15$ Hz, *β*-pyrrolic H), 8.81 (1H, d, $J_{\beta,\beta} = 4.95$ Hz, *β*-pyrrolic H), 8.88 (1H, d, $J_{\beta,\beta} = 4.85$ Hz, *β*-pyrrolic H), 8.90 (1H, d, $J_{\beta,\beta} = 5.00$ Hz, *β*-pyrrolic H); HMQC reveals the ^{13}C signal of the methyl group at 17.9 ppm; *m/z* (LDI-TOF) 1267.3 (M^+, 100%); $C_{83}H_{96}N_6NiS$ requires 1266.7 (M^+).

The third band was identified as (12-hydroxy-5,10,15,20-tetrakis(3',5'-di-*tert*-butylphenyl)quinoxalino[2,3-b]porphinato)nickel(II) (**40**) (8.8 mg, 19%) by having identical ^{1}H NMR and IR spectra to that of an authentic sample[81] The fourth band was identified as (12-oxo-13-oxa-5,10,15,20-tetrakis(3',5'-di-*tert*-butylphenyl)quinoxalino[2,3-b]porphinato) nickel(II) (**43**) (3.0 mg, 6%) by having an identical ^{1}H NMR as and co-chromatography against an authentic sample. The fifth band was identified as (12,13-dioxo-5,10,15,20-tetrakis(3',5'-di-*tert*-butylphenyl)quinoxalino[2,3-b]porphinato)nickel(II) (**41**) (6.5 mg, 14%) by having identical ^{1}H NMR and IR spectra to that of an authentic sample[81].

Hydroxylation of the chloro-quinoxaline ***32***

The same procedure for the hydroxylation of the bromo-quinoxaline **33** was followed, except THF was dried by passing through a column of alumina rather than by distillation over sodium wire. Yields after purification by column chromatography are given in Table **3.1**.

Table 3.2- *Hydroxylation of the bromo-quinoxaline* ***33*** *varying the proportion of benzaldehyde oxime*

The same procedures for the hydroxylation of the bromo-quinoxaline **33** were followed. At the appropriate point a greater proportion of benzaldehyde oxime was added to the sodium hydride dissolved in DMSO, as detailed in Table **3.2**. Products were purified by column

chromatography, so quoted yields are isolated yields of pure products. Results are given in Table **3.2**.

Table 3.3- *Hydroxylation of the bromo-quinoxaline* **33** *in the presence of radical inhibitors*

The same procedures for the hydroxylation of the bromo-quinoxaline **33** were followed. The pertinent radical inhibitor was added to the substrate dissolved in THF before the addition of the sodium benzaldoximate/ DMSO mixture. Products were purified by column chromatography, so quoted yields are isolated yields of pure products. Results are given in Table **3.3**. For the reaction with 1,1-diphenylethylene, the hydroxylated quinoxaline **40** had to be further recrystallised from dichloromethane/ acetonitrile because of the presence of aromatic impurities in the originally isolated product.

Table 3.4- *Attempted hydroxylation of the bromo-quinoxaline* **33** *by variously substituted oximes*

The same procedures for the hydroxylation of the bromo-quinoxaline **33** with the unsubstituted benzaldehyde oxime were followed, just with the unsubstituted oxime being replaced by the relevantly-substituted oxime. Products were purified by column chromatography, so quoted yields are isolated yields of pure products. Results are given in Table **3.4**.

Attempted hydroxylation of the di-chloro bis-porphyrin bis-nickel **37** *by benzaldehyde oxime*

Sodium hydride (60% dispersion in mineral oil) (59 mg, 1.5 mmol) and DMSO (21 ml) were stirred under nitrogen at 80°C for 50 minutes to give a clear, pale yellow solution. Heat was removed, benzaldehyde oxime (310 mg, 2.6 mmol) was added and the solution stirred for a further 5 minutes. This was then transferred under nitrogen to a solution of antipodal functionalized (di-chloro-bis-porphinato)nickel(II) (**37**) (122 mg, 0.050 mmol) in dry tetrahydrofuran (dried by passing through a column of alumina, 21 ml) and heated at reflux in the dark for 17 hours. The system was allowed to cool and ether (75 ml) and water (100 ml) were added to the reaction mixture. The organic layer was extracted and washed with water (5×100 ml), brine (100ml) and dried over sodium sulphate. Solvent was removed and the residue was purified by column chromatography in the dark (1:6 dichloromethane: petroleum spirit). The first band was identified as the starting material **37** (98 mg, 80%) by an identical ^{1}H NMR as and co-chromatography against an authentic sample. The second band overlapped with the tail-end of the first, and because both products were observed to streak on purification over silica it was not isolated in pure form. However its LDI spectrum

and the integration of the β-pyrrolic region relative to the aryl region in the ^{1}H NMR suggested that it contained a proportion of partially de-chlorinated product.

Attempted hydroxylation of the di-bromo bis-porphyrin bis-nickel **38** *by benzaldehyde oxime*

[2-bromo-5,10,15,20,25,30,35,40-octakis(3',5'-di-*tert*-butylphenyl)cycloeicosa[b] cycloeicosa[5,6]pyrazino[2,3-g]quinoxalino]nickel(II) (44)

The same procedures for the hydroxylation of the di-chloro bis-porphyrin **37** with benzaldehyde oxime were followed. Products were purified by column chromatography (1:6 dichloromethane: light petroleum). From the attempted hydroxylation of di-bromo bis-porphyrin bis-nickel(II) **38** (17 mg, 0.0068 mmol) the first band eluted was identified as the starting material **38** (12 mg, 71%) which was co-chromatographed against and had an identical ^{1}H NMR and LDI spectrum and an authentic sample. The second band was identified as [2-bromo-5,10,15,20,25,30,35,40-octakis(3',5'-di-*tert*-butylphenyl)cycloeicosa[b]cycloeicosa[5,6]pyrazino[2,3-g]quinoxalino]nickel(II) (**44**) (4.5 mg, 26%), a dark brown solid. $\upsilon_{max}(CHCl_3)$ 2965, 1595, 1473, 1464, 1364, 1297, 1265, 1092, 1018, 943, 909, 819; λ_{max} (CH_2Cl_2)/nm (log(ε/dm^{-3}mol^{-1}cm^{-1})) 318 (4.43), 429 (5.22), 449 (5.21), 512sh (4.70), 536 (4.75), 664 (4.24); ^{1}H n.m.r. (400 MHz; $CDCl_3$) δ: 1.43 to 1.47 (144H, m, *t*-butyl H), 7.64 to 7.66 (3H, m, aryl H), 7.69 to 7.71 (7H, m, aryl H), 7.73 to 7.75 (4H, m, aryl H), 7.76 (2H, d, $J_{4',2'} = J_{4',6'} = 1.40$ Hz, C(2')H and C(6')H), 7.81 to 7.82 (8H, m, aryl H), 8.53 to 8.56 (2H, m, β-pyrrolic H), 8.59 (1H, d, $J_{\beta,\beta} = 5.20$ Hz, β-pyrrolic H), 8.61 to 8.63 (6H, m, β-pyrrolic H), 8.65 (1H, d, $J_{\beta,\beta} = 5.25$ Hz, β-pyrrolic H), 8.68 (2H, d, $J_{\beta,\beta} = 4.50$ Hz, β-pyrrolic H), 8.82 (1H, d, $J_{\beta,\beta} = 5.20$ Hz, β-pyrrolic H); *m/z* (LDI-TOF) 2442.3 (MH^+, 100%); $C_{158}H_{181}N_{12}Ni_2Br$ requires 2442.2 (MH^+).

Attempted hydroxylation of the di-chloro bis-porphyrin bis-nickel **37** *by 3-bromo-benzaldehyde oxime and 3-nitro-benzaldehyde oxime*

The same procedures for the hydroxylation of di-chloro bis-porphyrin bis-nickel **37** with the unsubstituted benzaldehyde oxime were followed, just with the unsubstituted oxime being replaced by the appropriately substituted oxime. Products were purified by column chromatography, so quoted yields are isolated yields of pure products. Results are given in Section **3.4**.

9.4 Experimental details for Chapter Four

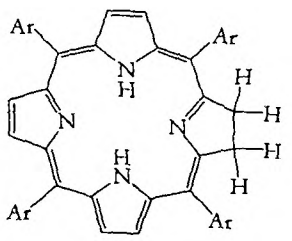
(46)

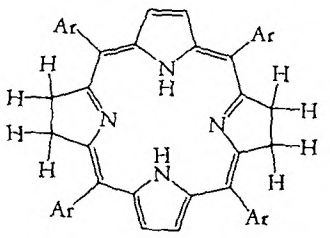
(47)

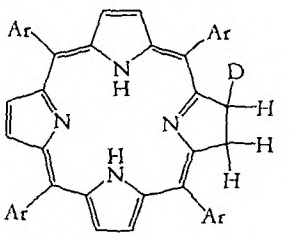
(48)

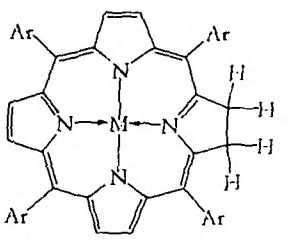
(49) M = Ni,
(50) M = Cu,
(51) M = Zn

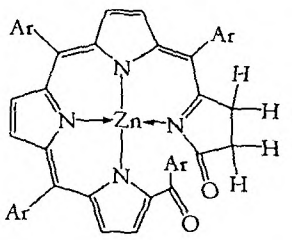
or
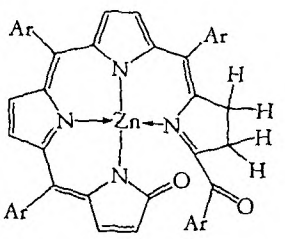
(52)

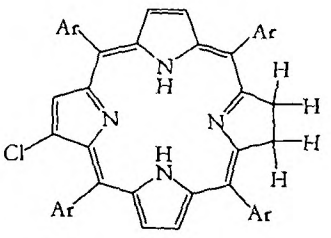
(53)

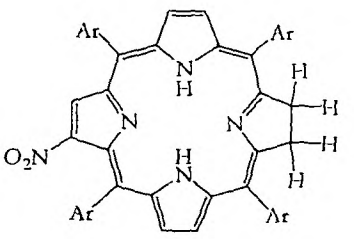
(54)

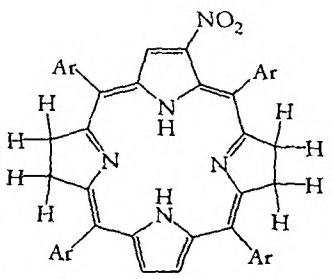
(55)

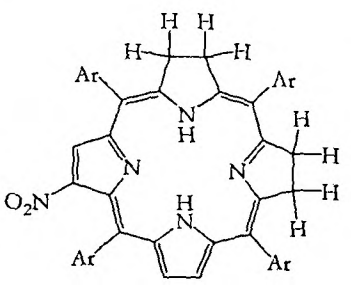
(56)

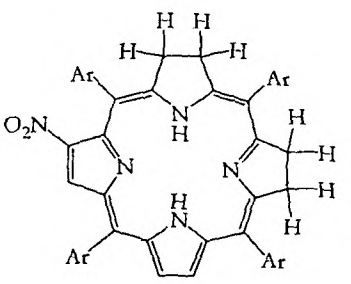
(57)

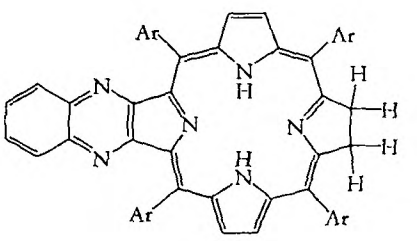
(58)

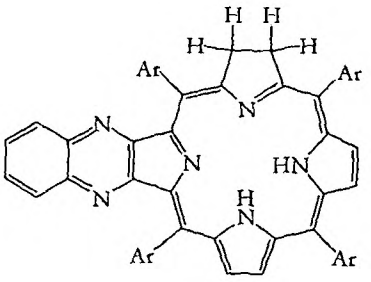
(59)

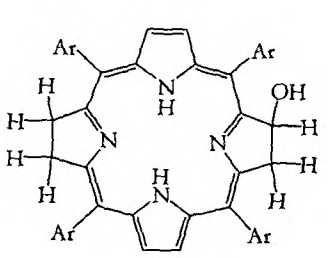
(61)

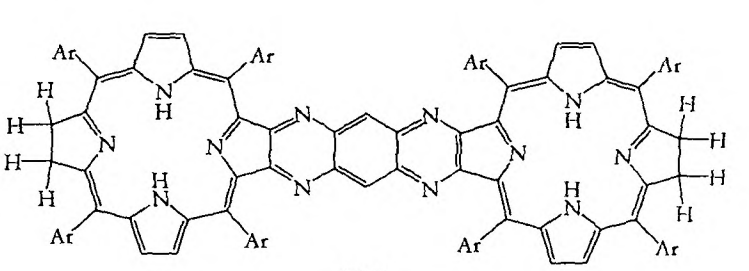
(60)

Ar= 3,5-di-*tert*-butylphenyl

9.4.1 Free-base unfunctionalized chlorins

2,3-dihydro-5,10,15,20-tetrakis(3',5'-di-*tert*-butylphenyl)porphyrin (46) and **2-deutero-2,3-dihydro-5,10,15,20-tetrakis(3',5'-di-*tert*-butylphenyl)porphyrin** (48)

Typically 5,10,15,20-tetrakis(3',5'-di-*tert*-butylphenyl)porphyrin (**45**) (815 mg, 0.77 mmol) was dissolved in THF (50 ml) at room temperature and diborane (7.0 ml, 1 moldm^{-3} in THF, 7.0 mmol) was added. The system was stirred under a nitrogen atmosphere in the dark for 3 hours at which point the solution had turned from dark red to dark brown. Water (100 ml) and ether (100 ml) were added to the reaction mixture and the organic layer was extracted, washed with water (4×100 ml), brine (50 ml), dried over sodium sulphate and the solvent was removed. The residue was purified by column chromatography (1:4 dichloromethane: light petroleum). The main brown band was collected and identified as 2,3-dihydro-

5,10,15,20-tetrakis(3',5'-di-*tert*-butylphenyl)porphyrin (**46**), a dark purple solid (560 mg, 69%, 0% impurity of porphyrin (**45**) by ^{1}H NMR). Found: C 85.7, H 8.9, N 5.5; $C_{76}H_{96}N_4$ requires C 85.7, H 9.1, N 5.3; υ_{max}(KBr)/cm^{-1} 3350 (NH), 2962, 1592 and 1581, 1475, 1363, 1287, 1246, 1039, 944, 880, 796, 714; λ_{max} (CH_2Cl_2)/nm (log (ε/dm^{3}mol^{-1}cm^{-1})) 289sh (4.15), 296 (4.15), 311 (4.15), 373 (4.43), 409sh (5.04), 421 (5.23), 489sh (3.62), 523 (4.08), 549 (3.99), 598 (3.69), 652 (4.39); ^{1}H n.m.r. (400 MHz; $CDCl_3$) δ: -1.32 (2H, br s, NH), 1.52 (36H, s, *t*-butyl H), 1.54 (36H, s, *t*-butyl H), 4.22 (4H, s, C(2)H_2, and C(3)H_2), 7.71 (2H, dd, $J_{2',4'} = J_{6',4'}$ = 1.65 Hz, C(4')H), 7.76 (2H, dd, $J_{2',4'} = J_{6',4'}$ = 1.85 Hz, C(4')H), 7.77 (4H, d, $J_{4',2'} = J_{4',6'}$ = 1.75 Hz, C(2')H and C(6')H), 8.04 (4H, d, $J_{4',2'} = J_{4',6'}$ = 1.95 Hz, C(2')H and C(6')H), 8.28 and 8.67 (4H, ABq, $J_{\beta,\beta}$ = 4.70 Hz, C(7)H, C(8)H, C(17)H and C(18)H), 8.54 (2H, s, C(12)H and C(13)H); *m/z* (LDI-TOF) 1064.8 (M^+, 100%); $C_{76}H_{96}N_4$ requires 1064.8 (M^+).

When D_2O was added to quench the boron-porphyrin complex, 2-deutero-2,3-dihydro-5,10,15,20-tetrakis(3',5'-di-*tert*-butylphenyl)porphyrin (**48**) was isolated as a dark brown solid. υ_{max}(KBr)/cm^{-1} 3350 (NH), 2963, 1591 and 1580, 1474, 1363, 1245, 796, 714; λ_{max} (CH_2Cl_2)/nm (log (ε/dm^{3}mol^{-1}cm^{-1})) 288sh (4.22), 297 (4.23), 311 (4.23), 375 (4.48), 405sh (5.05), 421 (5.30), 487sh (3.62), 523 (4.16), 550 (4.08), 598 (3.76), 652 (4.45); ^{1}H n.m.r. (400 MHz; $CDCl_3$) δ: -1.35 (2H, br s, NH), 1.49 (36H, s, *t*-butyl H), 1.51 (36H, s, *t*-butyl H), 4.18 (2H, br s, C(3)H_2), 4.19 (1H, br s, C(2)H), 7.69 (2H, dd, $J_{2',4'} = J_{6',4'}$ = 2.00 Hz, C(4')H), 7.74 (2H, dd, $J_{2',4'} = J_{6',4'}$ = 1.90 Hz, C(4')H), 7.75 (4H, d, $J_{4',2'} = J_{4',6'}$ = 1.95 Hz, C(2')H and C(6')H), 8.01 (4H, d, $J_{4',2'} = J_{4',6'}$ = 1.80 Hz, C(2')H and C(6')H), 8.25 and 8.65 (4H, ABq, $J_{\beta,\beta}$ = 4.60 Hz, C(7)H, C(8)H, C(17)H and C(18)H), 8.51 (2H, s, C(12)H and C(13)H); *m/z* (LDI-TOF) 1065.7 (M^+, 100%); $C_{76}H_{95}N_4D$ requires 1065.8 (M^+). The LDI spectrum suggests that there is a proportion of the *4H*-chlorin **46** as an impurity.

46 was also prepared by dissolving 5,10,15,20-tetrakis(3',5'-di-*tert*-butylphenyl)porphyrin (520 mg, 0.48 mmol) in pyridine (25 ml), heating to 110°C under a flowing stream of nitrogen and adding *p*-toluenesulfonylhydrazine (1.40 g, 7.5 mmol) and anhydrous potassium carbonate (2.10 g, 14.9 mmol) over 5½ hours. The system was allowed to cool, ether (100 ml) and water (100 ml) were added, the organic layer was extracted, washed with aqueous hydrochloric acid (3M, 2×100 ml), water (100 ml), aqueous saturated sodium bicarbonate solution (100 ml), brine (100 ml), dried over sodium sulphate and the solvent was removed. The product was purified by column chromatography (1:1 dichloromethane: light petroleum.) The main band was collected to yield 2,3-dihydro-tetrakis(3',5'-di-*tert*-

butylphenyl)porphyrin (490 mg, 95%) that contained approximately 87% chlorin (**46**) and 13% bacteriochlorin (**47**) as judged by integration of the ^{1}H NMR of the product.

2,3,12,13-tetrahydro-5,10,15,20-tetrakis(3',5'-di-*tert*-butylphenyl)porphyrin (47)

5,10,15,20-tetrakis(3',5'-di-*tert*-butylphenyl)porphyrin (**45**) (780 mg, 0.73 mmol) in pyridine (80 ml), was heated to 110°C under a flowing stream of nitrogen and had added *p*-toluenesulfonylhydrazine (8.30 g, 44.3 mmol) and anhydrous potassium carbonate (9.9g, 71.2 mmol) added to it over 5½ hours. The system was allowed to cool, ether (100 ml) and water (100 ml) were added, the organic layer was extracted, washed with aqueous hydrochloric acid (3M, 2×100 ml), water (100 ml), aqueous saturated sodium bicarbonate solution (100 ml), brine (100 ml), dried over sodium sulphate and the solvent was removed. The product was purified by column chromatography (1:6 dichloromethane: light petroleum). The first band was collected to give 2,3,12,13-tetrahydro-5,10,15,20-tetrakis(3',5'-di-*tert*-butylphenyl)porphyrin (**47**) (0.50 g, 65%), a green solid. Found C 85.8, H 8.9, N 5.5; $C_{76}H_{98}N_4$ requires C 85.5, H 9.3, N 5.3; υ_{max}(KBr)/cm^{-1} 3392 (NH), 2961, 1586, 1474, 1364, 1243, 1107, 1020, 865, 789, 750, 699, 592; λ_{max} (CH_2Cl_2)/nm (log (ε/dm^{3}mol^{-1}cm^{-1})) 357 (4.75), 378 (4.86), 462 (3.43), 420 (3.91), 525 (4.45), 617 (3.30), 675 (3.54), 740 (4.75); ^{1}H n.m.r. (400 MHz; $CDCl_3$) δ: -1.23 (2H, br s, NH), 1.49 (72H, s, *t*-butyl H), 4.03 (8H, s, $CH(2)_2$, $CH(3)_2$, $CH(12)_2$, and $CH(13)_2$), 7.66 (4H, dd, $J_{2',4'} = J_{6',4'}$ = 1.85 Hz, C(4')H), 7.72 (8H, d, $J_{4',2'} = J_{4',6'}$ = 2.05 Hz, C(2')H and C(6')H), 8.04 (4H, d, $J_{NH,\beta}$ = 4.95 Hz, C(7)H, C(8)H, C(17)H and C(18)H); *m/z* (LDI-TOF) 1066.7 (M^+, 100%); $C_{76}H_{98}N_4$ requires 1066.8 (M^+).

9.4.2 Metallated chlorins

[2,3-dihydro-5,10,15,20-tetrakis(3',5'-di-*tert*-butylphenyl)porphinato]nickel(II) (49)

2,3-dihydro-5,10,15,20-tetrakis(3',5'-di-*tert*-butylphenyl)porphyrin (**46**) (104 mg, 0.097 mmol, 0% porphyrin impurity by ^{1}H NMR) and $Ni(OAc)_2.4H_2O$ (55 mg, 0.22 mmol) were dissolved in DMF (15 ml) and heated at the point of reflux under nitrogen in the dark for 2¼ hours. The system was allowed to cool and ether (100 ml) and water (100 ml) were added. The organic layer was extracted and washed with water (4×50 ml), brine (50 ml), dried over sodium sulphate and the solvent was removed. The product was purified by column chromatography (1:2 dichloromethane: light petroleum). [2,3-dihydro-5,10,15,20-tetrakis(3',5'-di-*tert*-butylphenyl)porphinato]nickel(II) (**49**) was isolated as a green/ blue solid (87 mg, 80%, 4% (porphinato)nickel(II) impurity **63** by ^{1}H NMR). Found C 81.1, H 8.5, N

5.0; $C_{76}H_{94}N_4Ni$ requires C 81.3, H 8.5, N 5.0. υ_{max}(KBr)/cm^{-1} 2962, 1594 (single peak), 1476, 1363, 1280, 1246, 1062, 1011, 899, 881, 829, 792, 714; λ_{max} (CH_2Cl_2)/nm (log (ε/ $dm^3mol^{-1}cm^{-1}$)) 356sh (4.2), 419 (5.3), 500sh (3.8), 526 (3.8), 579 (4.1), 617 (4.5), 739 (3.4), 775 (3.1); ^{1}H n.m.r. (400 MHz; $CDCl_3$) δ: 1.40 (36H, s, *t*-butyl H), 1.43 (36H, s, *t*-butyl H), 3.81 (4H, s, $CH(2)_2$, and $CH(3)_2$), 7.47(4H, d, $J_{4',2'} = J_{4',6'} = 1.80$ Hz, C(2')H and C(6')H), 7.54 (2H, dd, $J_{2',4'} = J_{6',4'} = 1.70$ Hz, C(4')H), 7.63 (2H, dd, $J_{2',4'} = J_{6',4'} = 1.75$ Hz, C(4')H), 7.73 (4H, d, $J_{4',2'} = J_{4',6'} = 1.65$ Hz, C(2')H and C(6')H), 8.09 and 8.38 (4H, ABq, $J_{\beta,\beta} = 4.85$ Hz, C(7)H, C(8)H, C(17)H and C(18)H), 8.22 (2H, s, C(12)H and C(13)H); *m/z* (LDI-TOF) 1120.8 (M^+, 100%); $C_{76}H_{94}N_4Ni$ requires 1120.7 (M^+).

[2,3-dihydro-5,10,15,20-tetrakis(3',5'-di-*tert*-butylphenyl)porphinato]copper(II) (**50**)

2,3-dihydro-5,10,15,20-tetrakis(3',5'-di-*tert*-butylphenyl)porphyrin (**46**) (94 mg, 0.088 mmol, 0% porphyrin impurity by ^{1}H NMR) and $Cu(OAc)_2.H_2O$ (40 mg, 0.20 mmol) were dissolved in dichloromethane (15 ml) and methanol (5 ml) and brought to reflux in the dark for 1¼ hours. The system was allowed to cool and solvent was removed. The product was purified by column chromatography (1:2 dichloromethane: light petroleum). [2,3-dihydro-5,10,15,20-tetrakis(3',5'-di-*tert*-butylphenyl)porphinato]copper (II) (**50**) was isolated as a green/ blue solid (88 mg, 89%). υ_{max}(KBr)/cm^{-1} 2961, 1592 (single peak), 1476, 1363, 1345, 1278, 1247, 1069, 1004, 977, 880, 827, 796, 714; λ_{max} (CH_2Cl_2)/nm (log (ε/$dm^3mol^{-1}cm^{-1}$)) 397sh (4.73), 417 (5.44), 510 (3.75), 551 (3.78), 579 (4.00), 617 (4.56); *m/z* (LDI-TOF) 1126.1 (M^+, 100%); $C_{76}H_{94}N_4Cu$ requires 1125.7 (M^+).

[2,3-dihydro-5,10,15,20-tetrakis(3',5'-di-*tert*-butylphenyl)porphinato]zinc(II) (**51**) and **[2,3-dihydro-5,10,15,20-tetrakis(3',5'-di-*tert*-butylphenyl)biliverdo]zinc(II)** (**52**)

2,3-dihydro-5,10,15,20-tetrakis(3',5'-di-*tert*-butylphenyl)porphyrin (**46**) (577 mg, 0.54 mmol, 0% porphyrin impurity) and $Zn(OAc)_2.2H_2O$ (298 mg, 1.4 mmol) were dissolved in dichloromethane (130 ml) and methanol (50 ml). The system was degassed, placed under argon, brought to reflux in the dark for 1 hour and then the solvent was removed. The crude product was recrystallised four times from dichloromethane/ methanol. The precipitate was identified as [2,3-dihydro-5,10,15,20-tetrakis(3',5'-di-*tert*-butylphenyl)porphinato]zinc (II) (**51**), a purple solid (584 mg, 96%, 5% (porphinato)zinc(II) (**65**) impurity by ^{1}H NMR). υ_{max}(KBr)/cm^{-1} 2963, 1591 and 1579, 1475, 1362, 1342, 1272, 1246, 1064, 1001, 970, 879, 796, 713; λ_{max} (CH_2Cl_2)/nm (log (ε/$dm^3mol^{-1}cm^{-1}$)) 312 (4.2), 377 (4.3), 399sh (4.6), 421 (5.3), 467 (3.9), 524 (3.8), 554 (3.8), 587 (3.9), 622 (4.5), 739 (3.6); ^{1}H

n.m.r. (400 MHz; $CDCl_3$) δ: 1.50 (36H, s, *t*-butyl H), 1.52 (36H, s, *t*-butyl H), 4.91 (4H, s, $CH(2)_2$, and $CH(3)_2$), 7.68 (2H, dd, $J_{2',4'} = J_{6',4'} = 1.75$ Hz, C(4')H), 7.73 (4H, d, $J_{4',2'} = J_{4',6'} = 1.60$ Hz, C(2')H and C(6')H), 7.74 (2H, dd, $J_{2',4'} = J_{6',4'} = 1.85$ Hz, C(4')H), 7.99 (4H, d, $J_{4',2'} = J_{4',6'} = 1.85$ Hz, C(2')H and C(6')H), 8.16 and 8.60 (4H, ABq, $J_{\beta,\beta} = 4.40$ Hz, C(7)H, C(8)H, C(17)H and C(18)H), 8.46 (2H, s, C(12)H and C(13)H); *m/z* (LDI-TOF) 1126.8 (M^+, 100%); $C_{76}H_{94}N_4Zn$ requires 1126.7 (M^+).

Solvent was removed from the filtrate, and the residue was purified by column chromatography (1:8 dichloromethane: light petroleum). The product was identified as [2,3-dihydro-5,10,15,20-tetrakis(3',5'-di-*tert*-butylphenyl)biliverdo]zinc(II) (**52**), a dark brown solid (8.1 mg, 1%.) $\upsilon_{max}(CHCl_3)/cm^{-1}$ 2966, 1690 (CO), 1592, 1527, 1456, 1365, 1061, 1012, 908, 828; λ_{max} (CH_2Cl_2)/nm (log ($\varepsilon/dm^3mol^{-1}cm^{-1}$)) 290 (4.43), 368 (4.50), 426sh (4.47), 466 (4.66), 547 (3.91), 752sh (4.02), 817 (4.13); ^{1}H n.m.r. (400 MHz; $CDCl_3$) δ: 1.36 to 1.40 (72H, m, *t*-butyl H), 1.74 (1H, ddd, $J_{C(3)H,C(3)H} = 18.00$ Hz, $J_{C(2)H,C(3)H} = 9.60$ Hz, $J_{C(2)H,C(3)H} = 3.95$ Hz, C(3)H), 1.90 (1H, ddd, $J_{C(3)H,C(3)H} = 17.80$ Hz, $J_{C(2)H,C(3)H} = 9.00$ Hz, $J_{C(2)H,C(3)H} = 4.30$ Hz, C(3)H), 2.33 (1H, ddd, $J_{C(2)H,C(2)H} = 18.70$ Hz, $J_{C(3)H,C(2)H} = 9.60$ Hz, $J_{C(3)H,C(2)H} = 4.35$ Hz, C(2)H), 2.59 (1H, ddd, $J_{C(2)H,C(2)H} = 18.80$ Hz, $J_{C(3)H,C(2)H} = 9.10$ Hz, $J_{C(3)H,C(2)H} = 3.90$ Hz, C(2)H), 6.54 (1H, d, $J_{\beta,\beta} = 5.30$ Hz, *β*-pyrrolic H), 6.61 (1H, d, $J_{\beta,\beta} = 5.05$ Hz, *β*-pyrrolic H), 6.87 (1H, d, $J_{\beta,\beta} = 4.65$ Hz, *β*-pyrrolic H), 6.88 (1H, d, $J_{\beta,\beta} = 4.35$ Hz, *β*-pyrrolic H), 6.93 (1H, d, $J_{\beta,\beta} = 4.15$ Hz, *β*-pyrrolic H), 7.00 (1H, d, $J_{\beta,\beta} = 4.20$ Hz, *β*-pyrrolic H), 7.21* (1H, m, C(2')H and C(6')H), 7.26* (1H, m, C(2')H and C(6')H), 7.36* (1H, m, C(2')H and C(6')H), 7.38 (1H, m, C(4')H), 7.45 (1H, m, C(4')H), 7.51* (2H, m, C(2')H and C(6')H), 7.55 (1H, m, C(4')H), 7.59* (1H, m, C(2')H and C(6')H), 7.61 (1H, m, C(4')H), 7.87 (2H, m, C(2')H and C(6')H); * shows peaks that only appear at 233K; the low temperature and high temperature ^{1}H NMR spectra were not exactly identical, but this was not investigated further; ^{13}C n.m.r. (125 MHz; $CDCl_3$) δ: 28.8 (CH_2), 31.2 (CH_2), 31.3 to 31.5 (*t*-butyl CH_3), 34.7 to 34.9 (*t*-butyl C), 112 to 175 (unsaturated C), 187.7 (CO), 188.6 (CO); HMBC as described in the text; *m/z* (MALDI-TOF from an *alpha*-cyano-4-hydroxy cinnamic acid matrix) 1158.7 (M^+, 100%); $C_{76}H_{94}N_4O_2Zn$ requires 1158.6 (M^+).

9.4.3 Functionalized chlorins

2,3-dihydro-12-chloro-5,10,15,20-tetrakis(3',5'-di-*tert*-butylphenyl)porphyrin (53)

2,3-dihydro-5,10,15,20-tetrakis(3',5'-di-*tert*-butylphenyl)porphyrin (**46**) (233 mg, 0.20 mmol) and *N*-chlorosuccinimide (28 mg, 0.21 mmol) were dissolved in chloroform (25 ml) and

pyridine (1 ml) and were heated at reflux under nitrogen for 3 hours. The system was allowed to cool. Ether (100 ml) and aqueous hydrochloric acid (3M, 50 ml) were added and the organic layer was extracted, washed with aqueous hydrochloric acid (3M, 50 ml), water (100 ml), saturated aqueous sodium bicarbonate solution (100 ml), brine (100 ml), dried over sodium sulphate and the solvent was removed. The product was purified by column chromatography (1:8 dichloromethane: light petroleum). The first main band was identified as 2,3-dihydro-12-chloro-5,10,15,20-tetrakis(3',5'-di-*tert*-butylphenyl)porphyrin (**53**), a dark purple solid (23 mg, 10%). $\upsilon_{max}(CHCl_3)/cm^{-1}$ 3367 (NH), 2966, 1592 and 1581, 1477, 1364, 1265, 1249, 1068, 950, 882, 714; λ_{max} $(CH_2Cl_2)/nm$ (log $(\varepsilon/dm^3mol^{-1}cm^{-1})$) 293 (4.19), 312 (4.21), 373 (4.42), 412sh (5.20), 424 (5.31), 526 (4.12), 550 (4.01), 597 (3.84), 650 (4.33); ^1H n.m.r. (400 MHz; $CDCl_3$) δ: -1.60 (1H, br s, NH), -1.44 (1H, br s, NH), 1.47 to 1.49 (72H, m, *t*-butyl H), 4.13 to 4.16 (4H, m, $CH(2)_2$, and $CH(3)_2$), 7.67 (2H, dd, $J_{2',4'} = J_{6',4'} = 1.80$ Hz, C(4')H), 7.71 to 7.72 (5H, m, aryl H), 7.73 (1H, dd, $J_{2',4'} = J_{6',4'} = 2.00$ Hz, C(4')H), 7.83 (2H, d, $J_{4',2'} = J_{4',6'} = 1.45$ Hz, C(2')H and C(6')H), 7.94 (2H, d, $J_{4',2'} = J_{4',6'} = 1.65$ Hz, C(2')H and C(6')H), 8.19 (1H, dd, $J_{\beta,\beta} = 5.00$ Hz, $J_{NH,\beta} = 1.75$ Hz, β-pyrrolic H), 8.23 (1H, dd, $J_{\beta,\beta} = 5.00$ Hz, $J_{NH,\beta} = 1.25$ Hz, β-pyrrolic H), 8.38 (1H, s, C(13)H), 8.54 (1H, dd, $J_{\beta,\beta} = 4.65$ Hz, $J_{NH,\beta} = 1.05$ Hz, β-pyrrolic H), 8.57 (1H, d, $J_{\beta,\beta} = 4.80$ Hz, β-pyrrolic H); *m/z* (LDI-TOF) 1099.3 (MH^+, 100%); $C_{76}H_{95}N_4Cl$ requires 1099.7 (MH^+).

The second band collected was identified as 5,10,15,20-tetrakis(3',5'-di-*tert*-butylphenyl)porphyrin (**45**) (193 mg, 83%) which was co-chromatographed against and had an identical ^1H NMR as an authentic sample.

2,3-dihydro-12-nitro-5,10,15,20-tetrakis(3',5'-di-*tert*-butylphenyl)porphyrin (**54**), **2,3,12,13-tetrahydro-7-nitro-5,10,15,20-tetrakis(3',5'-di-*tert*-butylphenyl)porphyrin** (**55**), **2,3,7,8-tetrahydro-13-nitro-5,10,15,20-tetrakis(3',5'-di-*tert*-butylphenyl)porphyrin** (**56**) and **2,3,7,8-tetrahydro-12-nitro-5,10,15,20-tetrakis(3',5'-di-*tert*-butylphenyl)porphyrin** (**57**)

2-nitro-5,10,15,20-tetrakis(3',5'-di-*tert*-butylphenyl)porphyrin (508 mg, 0.46 mmol) was dissolved in pyridine (40 ml) and heated to 110°C under a flowing stream of nitrogen and had *p*-toluenesulfonylhydrazine (4.0 g, 21.4 mmol) and anhydrous potassium carbonate (3.5 g, 29.6 mmol) added to it over 5½ hours. The system was allowed to cool, ether (100 ml) and water (100 ml) were added, the organic layer was extracted, washed with aqueous hydrochloric acid (3M, 2×100 ml), water (100 ml), aqueous saturated sodium bicarbonate

solution (100 ml), brine (100 ml), dried over sodium sulphate and the solvent was removed. The product was purified by column chromatography (1:4 dichloromethane: light petroleum). The first band was identified as 2,3,12,13-tetrahydro-5,10,15,20-tetrakis(3',5'-di-*tert*-butylphenyl)porphyrin (**47**) (62 mg, 12%) which was co-chromatographed against and had an identical ^{1}H NMR as an authentic sample. The second band was identified as 2,3-dihydro-5,10,15,20-tetrakis(3',5'-di-*tert*-butylphenyl)porphyrin (**46**) (33 mg, 7%) and co-chromatographed and had an identical ^{1}H NMR as an authentic sample. The third band was identified as 2,3-dihydro-12-nitro-5,10,15,20-tetrakis(3',5'-di-*tert*-butylphenyl)porphyrin (**54**) (199 mg, 39%), a dark brown solid. Found C 81.9, H 8.9, N 6.2; $C_{76}H_{95}N_5O_2$ requires C 82.2, H 8.6, N 6.3. υ_{max}(KBr)/cm^{-1} 3365 (NH), 2962, 1592 and 1582, 1524, 1476, 1364, 1265, 1248, 1068, 926, 901, 881, 852, 798, 713; λ_{max} (CH_2Cl_2)/nm (log (ε/dm^{3}mol^{-1}cm^{-1})) 296 (4.41), 374 (4.69), 420sh (4.98), 440 (5.13), 535 (4.15), 548 (4.17), 596 (4.08), 645 (4.00), 741 (3.67); ^{1}H n.m.r. (400 MHz; $CDCl_3$) δ: -0.87 (2H, br s, NH), 1.50 (18H, s, *t*-butyl H), 1.51 (18H, s, *t*-butyl H), 1.53 (18H, s, *t*-butyl H), 1.54 (18H, s, *t*-butyl H), 4.14 (4H, s, $CH(2)_2$, and $CH(3)_2$), 7.72 (7H, m, aryl H), 7.79 (1H, dd, $J_{2',4'} = J_{6',4'} = 1.75$ Hz, C(4')H), 7.98 (2H, d, $J_{4',2'} = J_{4',6'} = 1.85$ Hz, C(2')H and C(6')H), 8.02 (2H, d, $J_{4',2'} = J_{4',6'} = 2.20$ Hz, C(2')H and C(6')H), 8.20 and 8.60 (2H, ABX, $J_{\beta,\beta} = 4.90$ Hz, $J_{NH,\beta} = 1.70$ Hz, β-pyrrolic H), 8.24 and 8.75 (2H, ABX, $J_{\beta,\beta} = 4.80$ Hz, $J_{NH,\beta} = 1.60$ Hz, β-pyrrolic H), 8.76 (1H, s, C(13)H); COSY also reveals the NH-β pyrrolic proton patterns; *m*/*z* (MALDI-TOF from a dithranol matrix) 1110.8 (MH^+, 100%); $C_{76}H_{95}N_5O_2$ requires 1110.8 (MH^+).

The fourth, fifth and sixth bands overlapped with one another and were further purified by column chromatography over silica (1:3 dichloromethane: light petroleum). The fourth band was identified as 2,3,12,13-tetrahydro-7-nitro-5,10,15,20-tetrakis(3',5'-di-*tert*-butylphenyl)porphyrin (**55**) (8 mg, 2%), a dark red solid. υ_{max}($CHCl_3$)/cm^{-1} 3371 (NH), 2968, 1592, 1515, 1475, 1364, 1345, 1262, 1100, 1050, 1023, 903; λ_{max} (CH_2Cl_2)/nm (log (ε/dm^{3}mol^{-1}cm^{-1})) 363 (4.53), 416sh (4.00), 546 (4.04), 621 (3.36), 677 (3.67), 743 (4.21); ^{1}H n.m.r. (400 MHz; $CDCl_3$) δ: 0.53 (1H, br s, NH), 0.63 (1H, d, $J_{\beta,NH} = 2.45$ Hz, NH), 1.41 to 1.43 (72H, m, *t*-butyl H), 3.66 to 3.68 (2H, m, chlorin H), 3.74 to 3.78 (6H, m, chlorin H), 7.49 (1H, dd, $J_{2',4'} = J_{6',4'} = 1.85$ Hz, C(4')H), 7.54 to 7.56 (8H, m, aryl H), 7.59 to 7.61 (3H, m, aryl H), 7.84 and 7.86 (2H, ABX, $J_{\beta,\beta} = 5.10$ Hz, $J_{NH,\beta} = 1.95$ Hz, C(17)H and C(18)H), 7.89 (1H, d, $J_{NH,\beta} = 3.10$ Hz, C(8)H); COSY also reveals the NH-β pyrrolic proton patterns; *m*/*z* (MALDI-TOF from a dithranol matrix) 1111.7 (M^+, 90%), 1112.7 (MH^+, 100%); $C_{76}H_{97}N_5O_2$ requires 1111.8 (M^+).

The fifth band was identified as 2,3,7,8-tetrahydro-13-nitro-5,10,15,20-tetrakis(3',5'-di-*tert*-butylphenyl)porphyrin (**56**) (10 mg, 2%), a dark blue solid. $\upsilon_{max}(CHCl_3)/cm^{-1}$ 3372 (NH), 3019 and 2966, 1591 (broad), 1495, 1477, 1363, 1095, 1051, 1019, 954; λ_{max} $(CH_2Cl_2)/nm$ (log $(\varepsilon/dm^3mol^{-1}cm^{-1})$) 278 (4.32), 384 (4.66), 395sh (4.64), 412sh (4.63), 553 (3.95), 598sh (4.00), 651 (4.19); ^1H n.m.r. (400 MHz; $CDCl_3$) δ: 1.38 to 1.40 (72H, m, *t*-butyl H), 3.20 to 3.28 (4H, m, chlorin H), 3.35 (4H, s, chlorin H), 7.01 and 7.62 (2H, ABQ, $J_{\beta,\beta}$ = 4.60 Hz, C(17)H and C(18)H), 7.27 (2H, d, $J_{4',2'}$ = $J_{4',6'}$ = 1.15 Hz, C(2')H and C(6')H), 7.40 (2H, d, $J_{4',2'}$ = $J_{4',6'}$ = 1.95 Hz, C(2')H and C(6')H), 7.41 (2H, d, $J_{4',2'}$ = $J_{4',6'}$ = 1.80 Hz, C(2')H and C(6')H), 7.42 (1H, s, C(12)H), 7.48 (1H, dd, $J_{2',4'}$ = $J_{6',4'}$ = 1.75 Hz, C(4')H), 7.50 (1H, dd, $J_{2',4'}$ = $J_{6',4'}$ = 1.75 Hz, C(4')H), 7.51 (1H, dd, $J_{2',4'}$ = $J_{6',4'}$ = 1.80 Hz, C(4')H), 7.54 (1H, dd, $J_{2',4'}$ = $J_{6',4'}$ = 1.80 Hz, C(4')H), 7.64 (2H, d, $J_{4',2'}$ = $J_{4',6'}$ = 1.50 Hz, C(2')H and C(6')H); COSY shows no NH-β pyrrolic proton couplings, and it is assumed that the NH protons signals are obscured by the 72H *t*-butyl H signal; *m/z* (MALDI-TOF from a dithranol matrix) 1111.7 (M^+, 85%), 1112.7 (MH^+, 100%); $C_{76}H_{97}N_5O_2$ requires 1111.8 (M^+).

The sixth band was identified as 2,3,7,8-tetrahydro-12-nitro-5,10,15,20-tetrakis(3',5'-di-*tert*-butylphenyl)porphyrin (**57**) (12.5 mg, 2%), a dark blue solid. $\upsilon_{max}(CHCl_3)/cm^{-1}$ 3377 (NH), 3019 and 2966, 1592 and 1574, 1509, 1477, 1362, 1264, 1001, 908; λ_{max} $(CH_2Cl_2)/nm$ (log $(\varepsilon/dm^3mol^{-1}cm^{-1})$) 274 (4.30), 371sh (4.53), 393sh (4.63), 413 (4.65), 511sh (3.79), 546 (3.93), 586 (4.07), 627 (4.31), 686sh (3.35); ^1H n.m.r. (400 MHz; $CDCl_3$) δ: 1.37 to 1.41 (72H, m, *t*-butyl H), 3.16 (4H, m, $C(2)H_2$ and $C(3)H_2$), 3.31 (2H, m, $C(7)H_2$), 3.51 (2H, m, $C(8)H_2$), 6.90 and 7.47 (2H, ABq, $J_{\beta,\beta}$ = 4.75 Hz, C(17)H and C(18)H), 7.26 (2H, d, $J_{4',2'}$ = $J_{4',6'}$ = 1.50 Hz, C(2')H and C(6')H), 7.36 (1H, dd, $J_{2',4'}$ = $J_{6',4'}$ = 1.90 Hz, C(4')H), 7.37 (2H, d, $J_{4',2'}$ = $J_{4',6'}$ = 2.10 Hz, C(2')H and C(6')H), 7.40 (2H, d, $J_{4',2'}$ = $J_{4',6'}$ = 1.50 Hz, C(2')H and C(6')H), 7.40 (1H, dd, $J_{2',4'}$ = $J_{6',4'}$ = 2.00 Hz, C(4')H), 7.49 (1H, dd, $J_{2',4'}$ = $J_{6',4'}$ = 1.75 Hz, C(4')H), 7.49 (1H, m, C(4')H), 7.61 (2H, d, $J_{4',2'}$ = $J_{4',6'}$ = 1.50 Hz, C(2')H and C(6')H), 7.80 (1H, s, C(13)H); COSY shows no NH-β pyrrolic proton couplings, and it is assumed that the NH protons signals are obscured by the 72H *t*-butyl H signal; NOE difference experiments show the following NOEs: between 3.16 ($C(2)H_2$ and $C(3)H_2$) and the doublets at 7.26 and 7.37; between 3.31 ($C(7)H_2$) and the doublet at 7.26; between 3.51 ($C(8)H_2$) and the doublet at 7.40; and between the singlet at 7.80 (C(13)H) and the doublet at 7.61; *m/z* (MALDI-TOF from a dithranol matrix) 1111.7 (M^+, 70%), 1112.7 (MH^+, 100%); $C_{76}H_{97}N_5O_2$ requires 1111.8 (M^+).

12,13-dihydro-5,10,15,20-tetrakis(3',5'-di-*tert*-butylphenyl)quinoxalino[2,3-b]porphyrin (**58**) and **7,8-dihydro-5,10,15,20-tetrakis(3',5'-di-*tert*-butylphenyl)quinoxalino[2,3-b] porphyrin** (**59**)

5,10,15,20-tetrakis(3',5'-di-*tert*-butylphenyl)quinoxaline (**24**) (325 mg, 0.28 mmol) was dissolved in pyridine (20 ml) and heated to 110°C under nitrogen and had *p*-toluenesulfonylhydrazine (3.4 g, 18.4 mmol) and anhydrous potassium carbonate (3.6 g, 26 mmol) added over six hours. The system was allowed to cool, ether (100 ml) and water (100 ml) were added, the organic layer was extracted, washed with aqueous hydrochloric acid (3M, 2×100 ml), water (100 ml), aqueous saturated sodium bicarbonate solution (100 ml), brine (100 ml), dried over sodium sulphate and the solvent was removed. The product was purified by column chromatography (1:6 dichloromethane: light petroleum). The first band was identified as 12,13-dihydro-5,10,15,20-tetrakis(3',5'-di-*tert*-butylphenyl)quinoxalino[2,3-b] porphyrin (**58**) (231 mg, 71%), a dark brown solid. υ_{max}(KBr)/cm^{-1} 3388 (NH), 2962, 1592 and 1579, 1476, 1363, 1247, 1226, 1161, 1113, 917, 900, 795; λ_{max} (CH_2Cl_2)/nm (log (ε/dm^{3}mol^{-1}cm^{-1})) 257 (4.53), 292 (4.46), 350 (4.57), 422 (5.35), 519 (4.32), 554 (4.18), 631 (4.04), 689 (5.01); ^{1}H n.m.r. (400 MHz; $CDCl_3$) δ: -1.59 (2H, br s, NH), 1.53 (36H, s, *t*-butyl H), 1.55 (36H, s, *t*-butyl H), 4.28 (4H, s, CH(12)$_2$, and CH(13)$_2$), 7.73 to 7.76 (2H, m, quinoxalino H), 7.75 (2H, m, C(4')H), 7.83 (4H, d, $J_{4',2'} = J_{4',6'} = 1.35$ Hz, C(2')H and C(6')H), 7.83 to 7.86 (2H, m, quinoxalino H), 7.95 (2H, dd, $J_{2',4'} = J_{6',4'} = 1.50$ Hz, C(4')H), 7.97 (4H, d, $J_{4',2'} = J_{4',6'} = 1.30$ Hz, C(2')H and C(6')H), 8.38 and 8.86 (4H, ABX, $J_{\beta\beta} = 4.95$ Hz, $J_{NH,\beta} = 1.75$ Hz, C(7)H, C(8)H, C(17)H and C(18)H); *m/z* (LDI-TOF) 1166.7 (M^+, 100%); $C_{82}H_{98}N_6$ requires 1166.8 (M^+).

The second band was identified as 7,8-dihydro-5,10,15,20-tetrakis(3',5'-di-*tert*-butylphenyl)quinoxalino[2,3-b]porphyrin (**59**), a black solid. υ_{max}(KBr)/cm^{-1} 3314 (NH), 2962, 1593 and 1581, 1477, 1363, 1261, 1098, 1022, 876, 797, 712; λ_{max} (CH_2Cl_2)/nm (log (ε/dm^{3}mol^{-1}cm^{-1})) 302 (4.45), 332sh (4.40), 4.06 (5.15), 455sh (4.62), 481 (4.70), 568 (4.16), 593 (4.12), 614sh (3.99), 670 (3.99); ^{1}H n.m.r. (400 MHz; $CDCl_3$) δ: 1.43 to 1.48 (72H, m, *t*-butyl H), 3.94 (2H, m, chlorin H), 4.10 (2H, m, chlorin H), 7.60 (2H, d, $J_{4',2'} = J_{4',6'} = 1.60$ Hz, C(2')H and C(6')H), 7.70 (1H, m, C(4')H), 7.80 (3H, m, C(2')H and C(6')H and β-pyrrolic H), 7.82 (1H, dd, $J_{2',4'} = J_{6',4'} = 1.85$ Hz, C(4')H), 7.92 (2H, d, $J_{4',2'} = J_{4',6'} = 1.55$ Hz, C(2')H and C(6')H), 8.21 and 8.24 (2H, ABq, $J_{\beta\beta} = 4.40$ Hz, β-pyrrolic H), 8.25 (1H, m, β-pyrrolic H); it is assumed that the NH peaks are obscured by the 72H *t*-butyl peak; COSY

shows the appropriate β-pyrrolic couplings, and the position of the β-pyrrolic proton at 7.80; *m/z* (LDI-TOF) 1167.0 (M^+, 100%); $C_{82}H_{98}N_6$ requires 1166.8 (M^+).

2,3,22,23-tetrahydro-5,10,15,20,25,30,35,40-octakis(3',5'-di-*tert*-butylphenyl) cycloeicosa[b]cycloeicosa[5,6]pyrazino[2,3-g]quinoxaline (60)

2,3,22,23-tetrahydro-5,10,15,20,25,30,35,40-octakis(3',5'-di-*tert*-butylphenyl)cycloeicosa[b] cycloeicosa[5,6]pyrazino[2,3-g]quinoxaline (**14**) (912 mg, 0.40 mmol) was dissolved in pyridine (140 ml) and heated to 108°C under nitrogen and had *p*-toluenesulfonylhydrazine (3.87 g, 20.8 mmol) and anhydrous potassium carbonate (8.90 g, 64.7 mmol) added over 4½ hours. The system was allowed to cool, ether (200 ml) and water (200 ml) were added, the organic layer was extracted, washed with aqueous hydrochloric acid (3M, 2×100 ml), water (100 ml), aqueous saturated sodium bicarbonate solution (100 ml), brine (100 ml), dried over sodium sulphate and the solvent was removed. The product was purified by column chromatography (1:4 dichloromethane: light petroleum.) The first band was collected and identified as 2,3,22,23-tetrahydro-5,10,15,20,25,30,35,40-octakis(3',5'-di-*tert*-butylphenyl)cycloeicosa[b]cycloeicosa[5,6]pyrazino[2,3-g]quinoxaline (**60**) (460 mg, 50%). υ_{max}(KBr)/cm^{-1} 3392 (NH), 2961, 1592 and 1578, 1476, 1363, 1248, 1207, 1167, 1074, 946, 907, 806 and 795, 718; λ_{max} (CH_2Cl_2)/nm (log (ε/$dm^3mol^{-1}cm^{-1}$)) 257 (4.46), 294 (4.45), 420 (5.26), 454 (5.37), 520sh (4.59), 557 (4.40), 607sh (4.04), 656sh (3.98), 692 (4.16), 723 (4.18), 747 (4.39); ^{1}H n.m.r. (400 MHz; $CDCl_3$) δ: -1.57 (2H, br s, NH), 1.49 to 1.56 (144H, m, *t*-butyl H), 4.17 (8H, s, C(2)H_2, C(3)H_2, C(22)H_2, C(23)H_2, 7.69 (4H, dd, $J_{2',4'} = J_{6',4'} = 1.70$ Hz, C(4')H), 7.75 (8H, d, $J_{4',2'} = J_{4',6'} = 1.65$ Hz, C(2')H and C(6')H), 7.92 (4H, dd, $J_{2',4'} = J_{6',4'} = 1.95$ Hz, C(4')H), 8.00 (8H, d, $J_{4',2'} = J_{4',6'} = 1.65$ Hz, C(2')H and C(6')H), 8.28 and 8.60 (8H, ABX, $J_{\beta\beta} = 4.80$ Hz, $J_{NH,\beta} = 1.90$ Hz, C(7)H, C(8)H, C(17)H, C(18)H, C(27)H, C(28)H, C(37)H and C(38)H), 8.49 (2H, s, C(41)H and C(42)H); *m/z* (LDI-TOF) 2255.2 (M^+, 100%); $C_{158}H_{190}N_{12}$ requires 2255.5 (M^+).

The substrate remaining on the column was then eluted by dichloromethane and solvent removed. The dark brown residue was redissolved in dichloromethane and had dichloro-dicyano-quinone (65 mg, 0.29 mmol) added to it. The mixture was stirred for 45 minutes, and then the product passed through a plug of silica eluting with ethyl acetate. The product was purified by column chromatography (1:2 dichloromethane: light petroleum). The first main band was identified as 2,3,22,23-tetrahydro-5,10,15,20,25,30,35,40-octakis(3',5'-di-*tert*-butylphenyl)cycloeicosa[b]cycloeicosa[5,6]pyrazino[2,3-g]quinoxaline (**14**) (257 mg, 28%)

which was co-chromatographed against and had an identical ^{1}H NMR as an authentic sample.

2-hydroxy-2,3,12,13-tetrahydro-5,10,15,20-tetrakis(3',5'-di-*tert*-butylphenyl)porphyrin (61)

2-hydroxy-2,3-dihydro-5,10,15,20-tetrakis(3',5'-di-*tert*-butylphenyl)porphyrin (**62**) (126 mg, 0.12 mmol), was dissolved in pyridine (15 ml) and heated to 110°C under a flowing stream of nitrogen and had *p*-toluenesulfonylhydrazine (1.66 g, 8.4 mmol) and anhydrous potassium carbonate (1.25g, 9.0 mmol) added to it over six hours. The system was allowed to cool, ether (100 ml) and water (100 ml) were added, the organic layer was extracted, washed with aqueous hydrochloric acid (3M, 2×100 ml), water (100 ml), aqueous saturated sodium bicarbonate solution (100 ml), brine (100 ml), dried over sodium sulphate and the solvent was removed. The product was purified by column chromatography (2:5 dichloromethane: light petroleum with a couple of drops of triethylamine). The second band was collected and identified as 2-hydroxy-2,3,12,13-tetrahydro-5,10,15,20-tetrakis(3',5'-di-*tert*-butylphenyl) porphyrin (**61**) (72 mg, 57%), a green solid. υ_{max}(KBr)/cm^{-1} 3562 (OH), 3392 (NH), 2961, 1590 and 1583, 1475, 1363, 1246, 1108, 1018, 872, 790, 753, 715, 589; λ_{max} (CH_2Cl_2)/nm (log (ε/dm^{3}mol^{-1}cm^{-1})) 358sh (4.90), 379 (4.99), 410sh (4.55), 421 (4.67), 461 (3.48), 494 (3.78), 525 (4.62), 600 (3.44), 652 (3.99), 723 (4.86); ^{1}H n.m.r. (400 MHz; $CDCl_3$) δ: -1.50 (1H, br s, NH), -1.45 (1H, br s, NH), 1.45 to 1.48 (72H, m, *t*-butyl H), 2.39 (1H, d, $J_{C(2)H,OH}$ = 2.45 Hz, OH), 3.95 (1H, d, $J_{C(3)H,C(3)H}$ = 18.45 Hz, C(3)H), 4.05 (4H, s, $C(12)H_2$, $C(13)H_2$) 4.31 (1H, dd, $J_{C(3)H,C(3)H}$ = 18.20 Hz, $J_{C(2)H,C(3)H}$ = 8.20 Hz, C(3)H), 6.27 (1H, d, $J_{C(3)H,C(2)H}$ = 8.10 Hz, C(2)H), 7.65 (5H, m, aryl H), 7.68 (1H, m, aryl H), 7.70 (1H, dd, $J_{2',4'}$ = $J_{6',4'}$ = 1.65 Hz, C(4')H), 7.71 (1H, dd, $J_{2',4'}$ = $J_{6',4'}$ = 1.75 Hz, C(4')H), 7.75 (1H, m, aryl H), 7.81 (1H, m, aryl H), 8.03 and 8.05 (2H, ABX, $J_{\beta,\beta}$ = 4.75 Hz, $J_{NH,\beta}$ = 1.80 Hz, β-pyrrolic H), 8.09 and 8.14 (2H, ABX, $J_{\beta,\beta}$ = 4.60 Hz, $J_{NH,\beta}$ = 1.90 Hz, β-pyrrolic H); *m/z* (LDI-TOF) 1083.1 (M^+, 95%), 1084.2 (MH^+, 100%); $C_{76}H_{98}N_4O$ requires 1082.8 (M^+).

9.5 Experimental details for chapter Five

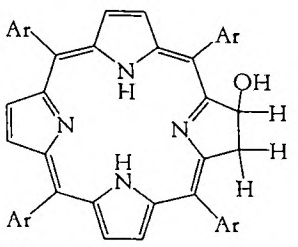

(62)

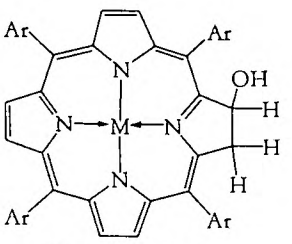

(66) M = Ni,
(67) M = Cu,
(68) M = Zn

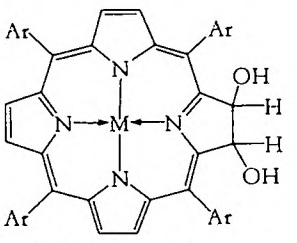

(69) M = Ni,
(70) M = Cu

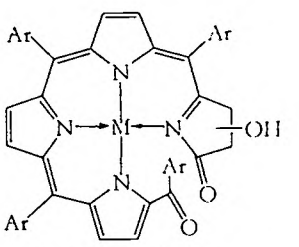

(71) M = Ni,
(72) M = Cu

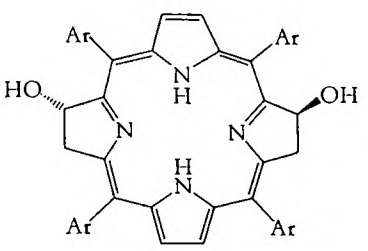

(74a)

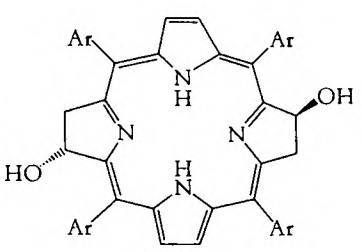

(74b)

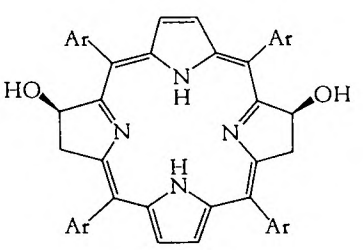

(75a)

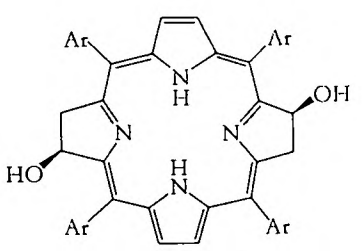

(75b)

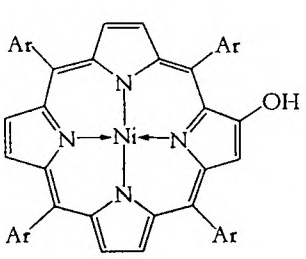

(73)

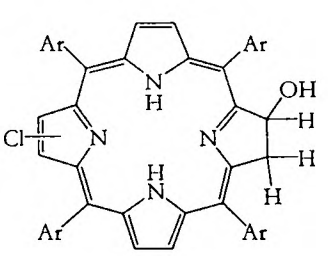

(76)

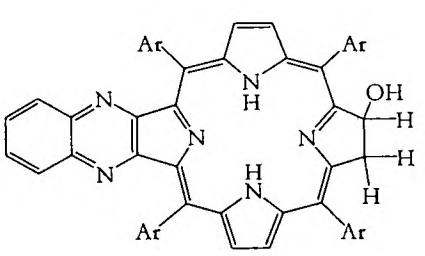

(77)

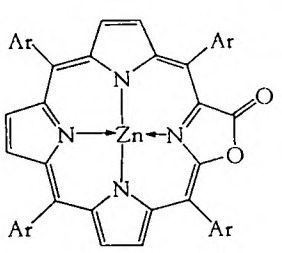

(79)

Ar= 3,5-di-*tert*-butylphenyl.

9.5.1 Unsubstituted chlorins

2-hydroxy-2,3-dihydro-5,10,15,20-tetrakis(3',5'-di-*tert*-butylphenyl)porphyrin (62)

2,3-dihydro-5,10,15,20-tetrakis(3',5'-di-*tert*-butylphenyl)porphyrin (**46**) was dissolved in the relevant solvent and loaded onto the column, also prepared from the relevant solvent. If appropriate, solvent was then pumped off the column by hand. After the appropriate period of time 1:4 dichloromethane: light petroleum was used to elute the starting material (**46**) and porphyrin (**45**) in the same band, and the product 2-hydroxy-2,3-dihydro-5,10,15,20-tetrakis(3',5'-di-*tert*-butylphenyl)porphyrin (**62**) was eluted with dichloromethane. As porphyrin **45** and chlorin **46** were not separable by column chromatography their respective yields were determined by integration of β-pyrrolic and NH peaks in the ^{1}H NMR of the front-running product. 2-hydroxy-2,3-dihydro-5,10,15,20-tetrakis(3',5'-di-*tert*-butylphenyl)porphyrin (**62**) was isolated as a purple/ brown solid. υ_{max}(KBr) 3564 (OH), 3350 (NH), 2963, 1592 and 1578, 1476, 1636, 1246, 953, 797, 715; λ_{max} (CH_2Cl_2)/nm (log (ε/$dm^3mol^{-1}cm^{-1}$)) 251 (4.04), 270sh (4.07), 287sh (4.12), 300 (4.14), 312 (4.14), 375sh (4.38), 418 (4.98), 484sh (3.59), 520 (4.04), 547 (4.04), 592 (3.74), 644 (4.25); ^{1}H n.m.r. (400 MHz;

$CDCl_3$) δ: -1.72 (1H, br s, NH), -1.69 (1H, br s, NH), 1.48-1.52 (72H, m, t-butyl H), 2.55 (1H, d, $J_{C(2)H,\ OH}$ = 2.65 Hz, OH), 4.14 (1H, dd, $J_{C(3')H,\ C(3)H}$ = 18.25 Hz, $J_{C(2)H,\ C(3)H}$ = 1.55 Hz, C(3)H), 4.50 (1H, dd, $J_{C(3)H,\ C(3')H}$ = 18.00 Hz, $J_{C(2)H,\ C(3')H}$ = 8.10 Hz, C(3')H), 6.48 (1H, dt, $J_{C(3')H,\ C(2)H}$ = 8.20 Hz, $J_{C(3)H,\ C(2)H} \approx J_{OH,\ C(2)H} \approx$ 2.1 Hz, C(2)H), 7.70 (2H, d, $J_{4',2'} = J_{4',6'}$ = 1.65 Hz, C(2')H and C(6')H), 7.74 (1H, dd $J_{2',4'} = J_{6',4'}$ = 1.95 Hz, C(4')H), 7.75 (1H, dd $J_{2',4'} = J_{6',4'}$ = 1.70 Hz, C(4')H), 7.76 (1H, dd $J_{2',4'} = J_{6',4'}$ = 1.85 Hz, C(4')H), 7.87 (1H, dd $J_{2',4'} = J_{6',4'}$ = 1.80 Hz, C(4')H), 7.93 (1H, m, C(2')H and C(6')H), 7.95 (1H, m, C(2')H and C(6')H), 7.97 (1H, m, C(4')H), 8.01-8.02 (2H, m, C(2')H and C(6')H), 8.07 (1H, m, C(4')H), 8.33 (1H, d, $J_{\beta,\beta}$ = 4.85 Hz, β-pyrrolic H), 8.37 (1H, d, $J_{\beta,\beta}$ = 4.55 Hz, β-pyrrolic H), 8.55 and 8.57 (2H, ABq, $J_{\beta,\beta}$ = 4.70 Hz, C(12)H and C(13)H), 8.71 (2H, d, $J_{\beta,\beta}$ = 4.90 Hz, β-pyrrolic H); *m/z* (LDI-TOF) 1080.6 (M^+, 100%); $C_{76}H_{96}N_4O$ requires 1080.8 (M^+).

In experiment F of Table **5.1**, solvent was degassed by bubbling argon through individual flasks of dichloromethane and light petroleum; these were then mixed in the appropriate proportions by transferring to a third flask through a cannula under argon.

Reaction of hydroxy-chlorin ***62*** *on silica*

2-hydroxy-2,3-dihydro-5,10,15,20-tetrakis(3',5'-di-*tert*-butylphenyl)porphyrin (**62**) (65 mg, 0.060 mmol) was dissolved in solvent and placed onto a column of silica (1:8 dichloromethane: light petroleum). Solvent was removed from the column by hand and the substrate was then left for 3 hours at 32°C. The starting material **62** was eluted with dichloromethane (65 mg, 100%).

Reaction of hydroxy-chlorin ***62*** *on alumina*

2-hydroxy-2,3-dihydro-5,10,15,20-tetrakis(3',5'-di-*tert*-butylphenyl)porphyrin (**62**) (87 mg, 0.082 mmol) was dissolved in solvent and placed onto a column of alumina (1:8 dichloromethane: light petroleum.) The substrate was left for 2 hours at 20°C with solvent remaining on the column at which point 5,10,15,20-tetrakis(3',5'-di-*tert*-butylphenyl)porphyrin (**45**) (37 mg, 43%) was eluted with 1:8 dichloromethane and the starting material was recovered with methanol (41 mg, 48%).

[2-hydroxy-2,3-dihydro-5,10,15,20-tetrakis(3',5'-di-*tert*-butylphenyl)porphinato] nickel(II) (**66**), **[2,3-dihydroxy-2,3-dihydro-5,10,15,20-tetrakis(3',5'-di-*tert*-butylphenyl) porphinato]nickel(II)** (**69**) and **[hydroxy-2,3-dihydro-5,10,15,20-tetrakis(3',5'-di-*tert*-butylphenyl)biliverdo]nickel(II)** (**71**)

Silica (100 ml) was thoroughly mixed with water (2 ml) and then used to prepare a column (1:8 dichloromethane: light petroleum). [2,3-dihydro-5,10,15,20-tetrakis(3',5'-di-*tert*-butylphenyl)porphinato]nickel(II) (**49**) (575 mg, 0.51 mmol, 0% porphyrin impurity by ^{1}H NMR) was dissolved in solvent and placed onto the column. Solvent was then pumped off the column by hand. The substrate was left for 3 hours at 21°C, after which time products were eluted by adding further solvent. The first band eluted was identified as [5,10,15,20-tetrakis(3',5'-di-*tert*-butylphenyl)porphinato]nickel(II) (**63**) (221 mg, 38%), a red-purple solid that had identical ^{1}H NMR, LDI-TOF and IR spectra as an authentic sample [REF]. The second band was identified as [2-hydroxy-2,3-dihydro-5,10,15,20-tetrakis(3',5'-di-*tert*-butylphenyl)porphinato]nickel(II) (**66**) (136 mg, 23%), a dark blue solid. υ_{max}(KBr) 3573 (OH), 2962, 1593, 1477, 1363, 1285, 1247, 1010, 899, 881, 827, 792, 714; λ_{max} (CH_2Cl_2)/nm (log (ε/dm^{3}mol^{-1}cm^{-1})) 351sh (4.07), 418 (5.23), 503 (3.70), 572sh (3.97), 607 (4.43); ^{1}H n.m.r. (400 MHz; $CDCl_3$) δ: 1.37-1.63 (72H, m, *t*-butyl H), 1.88 (1H, d, $J_{C(2)H,\ OH}$ = 2.90 Hz, OH), 3.90 (1H, dd, $J_{C(3')H,\ C(3)H}$ = 16.65 Hz, $J_{C(2)H,\ C(3)H}$ = 6.90 Hz, C(3)H), 4.00 (1H, dd, $J_{C(3)H,\ C(3')H}$ = 16.65 Hz, $J_{C(2)H,\ C(3')H}$ = 1.65 Hz, C(3')H), 5.85 (1H, br d, $J_{C(3')H,\ C(2)H}$ = 6.55 Hz, C(2)H), 6.98* (1H, br, C(2')H and C(6')H), 7.10* (1H, br, C(2')H and C(6')H), 7.40* (2H, m, C(2')H and C(6')H), 7.56 (1H, dd, $J_{2',4'}$ = $J_{6',4'}$ = 1.85 Hz, C(4')H), 7.59 (1H, $J_{2',4'}$ = $J_{6',4'}$ = 1.75 Hz, C(4')H), 7.64 (2H, dd, $J_{2',4'}$ = $J_{6',4'}$ = 1.75 Hz, C(4')H), 8.04* (1H, br, C(2')H and C(6')H), 8.07* (1H, br, C(2')H and C(6')H), 8.11* (2H, br, C(2')H and C(6')H), 8.16 and 8.43 (2H, ABq, $J_{\beta,\beta}$ = 4.90 Hz, β-pyrrolic H), 8.17 and 8.43 (2H, ABq, $J_{\beta,\beta}$ = 5.20 Hz, β-pyrrolic H), 8.28 and 8.30 (2H, ABq, $J_{\beta,\beta}$ = 4.90 Hz, β-pyrrolic H); * shows the resonances that do not appear in the room temperature ^{1}H NMR spectrum; COSY shows the relevant β-pyrrolic coupling patterns; *m/z* (LDI-TOF) 1137.1 (M^+, 100%); $C_{76}H_{94}NiN_4O$ requires 1136.7 (M^+).

The third band was identified as [2,3-dihydroxy-2,3-dihydro-5,10,15,20-tetrakis(3',5'-di-*tert*-butylphenyl)porphinato]nickel(II) (**69**) (104 mg, 18%), a dark blue solid. υ_{max}(KBr) 3580 (OH), 2962, 1593, 1477, 1363, 1293, 1247, 1010, 899, 882, 828, 793, 715; λ_{max} (CH_2Cl_2)/nm (log (ε/dm^{3}mol^{-1}cm^{-1})) 350sh (4.14), 418 (5.16), 502(3.73), 578sh (3.99), 606 (4.35); ^{1}H n.m.r. (400 MHz; $CDCl_3$) δ: 1.56 (72H, m, *t*-butyl H), 1.92 (2H, d, $J_{C(2)H,\ C(2)OH}$ = $J_{C(3)H,\ C(3)OH}$ = 3.10

Hz, C(2)OH and C(3)OH), 5.71 (2H, d, $J_{C(2)OH,C(2)H}$ =$J_{C(3)OH,C(3)H}$ 3.60 Hz, C(2)H and C(3)H), 7.05* (2H, br, C(2')H and C(6')H), 7.35* (2H, br, C(2')H and C(6')H), 7.60 (2H, dd, $J_{2',4'}$ = $J_{6',4'}$ = 1.70 Hz, C(4')H), 7.64 (2H, $J_{2',4'}$ = $J_{6',4'}$ = 2.15 Hz, C(4')H), 8.05* (2H, br, C(2')H and C(6')H), 8.10* (2H, br, C(2')H and C(6')H), 8.15 and 8.43 (4H, ABq, $J_{\beta,\beta}$ = 5.15 Hz, C(7)H, C(8)H, C(17)H and C(18)H), 8.29 (2H, s, C(12)H and C(13)H), * shows the resonances that do not appear in the room temperature ^{1}H NMR; COSY shows the relevant β-pyrrolic coupling patterns; *m/z* (LDI-TOF) 1153.1 (M^+, 100%); $C_{76}H_{94}NiN_4O_2$ requires 1152.7 (M^+).

The fourth band was only eluted very slowly with dichloromethane. It was identified as [(2 or 3)-hydroxy-2,3-dihydro-tetrakis(3',5'-di-*tert*-butylphenyl)biliverdo]nickel(II) (**71**) (31 mg, 5%). υ_{max}(KBr) 3568 (OH from keto-enol tautomerisation), 2962, 1724 (CO), 1704(CO), 1593, 1529, 1475, 1364, 1252 and 1247, 1014, 827, 882, 714; λ_{max} (CH_2Cl_2)/nm (log (ε/$dm^3mol^{-1}cm^{-1}$)) 313 (4.35), 349 (4.36), 422sh (4.52), 451 (4.64), 504sh (3.80), 753 (4.17); ^{1}H n.m.r. (400 MHz; $CDCl_3$) δ: 1.39 to 1.44 (72H, M, *t*-butyl H), 1.63 (1H, d, $J_{C(3)H, C(3)OH}$ = 1.85 Hz, C(3)OH), 2.16 (1H, dd, $J_{C(2)H, C(2)H}$ = 18.40 Hz, $J_{C(3)H, C(2)H}$ = 4.40 Hz, C(2)H), 2.73 (1H, dd, $J_{C(2)H, C(2)H}$ = 17.70 Hz, $J_{C(3)H, C(2)H}$ = 8.65 Hz, C(2)H), 4.95 (1H, ddd, $J_{C(2)H, C(3)H}$ = 8.40 Hz, $J_{C(2)H, C(3)H}$ = 3.95 Hz, $J_{C(3)OH, C(3)H}$ = 1.80 Hz, C(3)H), 7.03 (1H, d, $J_{\beta,\beta}$ = 4.50 Hz, *β*-pyrrolic H), 7.16 (1H, d, $J_{\beta,\beta}$ = 4.90 Hz, *β*-pyrrolic H), 7.24 (1H, d, $J_{\beta,\beta}$ = 4.35 Hz, *β*-pyrrolic H), 7.38 (1H, d, $J_{\beta,\beta}$ = 5.05 Hz, *β*-pyrrolic H), 7.50 (1H, d, $J_{\beta,\beta}$ = 5.10 Hz, *β*-pyrrolic H), 7.66 (1H, d, $J_{\beta,\beta}$ = 4.65 Hz, *β*-pyrrolic H), 7.46 to 7.67 (10H, m, aryl H), 7.89 (2H, d, $J_{4',2'}$ = $J_{4',6'}$ = 2.05 Hz, C(2')H and C(6')H); the ^{1}H NMR spectrum at 233K and 298K were not identical, but this was not investigated further; ^{13}C n.m.r. (125 MHz; $CDCl_3$) δ: 30 to 34 (*t*-butyl C), 38 (CH_2), 70 (HCOH), 115 to 166 (unsaturated C), 183 (NCO), 186 (CO); HMBC as described in the text; *m/z* (MALDI-TOF from an *alpha*-cyano-4-hydroxy cinnamic acid matrix) 1169.8 (MH^+, 100%); $C_{76}H_{94}N_4NiO_3$ requires 1169.7 (MH^+).

Attempted formation of a propylidene acetal from nickel di-hydroxy chlorin ***69***

[2-hydroxy-5,10,15,20-tetrakis(3',5'-di-*tert*-butylphenyl)porphinato]nickel(II) (**73**)

[2,3-dihdyroxy-2,3-dihydro-5,10,15,20-tetrakis(3',5'-di-*tert*-butylphenyl)porphinato]nickel(II) (**69**) (66 mg, 0.057 mmol) was dissolved in dry acetone (20 ml) and had anhydrous zinc chloride (24 mg, 0.18 mmol) added to it. The system was brought to reflux under argon for 3 hours and then allowed to cool. Solvent was removed, and the ^{1}H NMR of the crude product showed no evidence for the formation of a propylidene acetal. The product was purified by column chromatography (1:3 dichloromethane: light petroleum). The first band

eluted was identified as [2-hydroxy-5,10,15,20-tetrakis(3',5'-di-*tert*-butylphenyl)porphinato] nickel(II) (**73**) (33 mg, 51%), a bright red/ purple solid. υ_{max}(KBr) 3486 (OH), 2961, 1620, 1592, 1462, 1387, 1362, 1297, 1247, 1172, 1078, 1009, 935, 800, 716; λ_{max} (CH_2Cl_2)/nm (log (ε/$dm^3mol^{-1}cm^{-1}$)) 287sh (4.24), 323sh (4.11), 415 (5.30), 529 (4.25), 566 (3.84); ^{1}H n.m.r. (400 MHz; $CDCl_3$) δ: 1.47 to 1.48 (72H, m, *t*-butyl H), 6.01 (1H, s, C(2)OH), 7.70 (1H, dd, $J_{2',4'} = J_{6',4'} = 1.90$ Hz, C(4')H), 7.72 (2H, m, C(4')H), 7.83 (2H, d, $J_{4',2'} = J_{4',6'} = 1.35$ Hz, C(2')H and C(6')H), 7.86 (1H, dd, $J_{2',4'} = J_{6',4'} = 1.75$ Hz, C(4')H), 7.88 (2H, d, $J_{4',2'} = J_{4',6'} = 1.60$ Hz, C(2')H and C(6')H), 7.88 (2H, d, $J_{4',2'} = J_{4',6'} = 1.60$ Hz, C(2')H and C(6')H), 7.90 (2H, d, $J_{4',2'} = J_{4',6'} = 1.50$ Hz, C(2')H and C(6')H), 7.93 (1H, s, C(3)H), 8.65 (1H, d, $J_{\beta,\beta} = 4.95$ Hz, β-pyrrolic H), 8.75 (1H, d, $J_{\beta,\beta} = 4.70$ Hz, β-pyrrolic H), 8.78 (2H, m, β-pyrrolic H), 8.80 (1H, d, $J_{\beta,\beta} = 5.40$ Hz, β-pyrrolic H), 8.81 (1H, d, $J_{\beta,\beta} = 4.85$ Hz, β-pyrrolic H); *m/z* (LDI-TOF) 1135.1 (M^+, 100%); $C_{76}H_{92}N_4NiO$ requires 1134.7 (MH^+).

The second band was identified as the starting material **69** (31 mg, 47%).

Reaction of nickel hydroxy-chlorin ***66*** *on silica*

Silica (100 ml) was thoroughly mixed with water (2 ml) and then used to prepare a column (1:8 dichloromethane: light petroleum). [2-hydroxy-2,3-dihydro-5,10,15,20-tetrakis(3',5'-di-*tert*-butylphenyl)porphinato]nickel(II) (**66**) (34 mg, 0.030 mmol) was dissolved in solvent and placed onto the column. Solvent was pumped off the column by hand. The substrate was left for 2½ hours at 28°C at which point the starting material (**66**) (22 mg, 63%) was eluted followed by [2,3-dihydroxy-2,3-dihydro-5,10,15,20-tetrakis(3',5'-di-*tert*-butylphenyl)porphinato]nickel(II) (**69**) (8 mg, 23%.) These were identified by their ^{1}H NMRs and co-chromatography with authentic samples.

[hydroxydihydro-5,10,15,20-tetrakis(3',5'-di-*tert*-butylphenyl)porphinato]copper(II) (**67**), **[dihydroxydihydro-5,10,15,20-tetrakis(3',5'-di-*tert*-butylphenyl)porphinato] copper(II)** (**70**) and **[hydroxydihydro-5,10,15,20-tetrakis(3',5'-di-*tert*-butylphenyl) biliverdo]copper(II)** (**72**)

Silica (100 ml) was thoroughly mixed with water (2 ml) and then used to prepare a column (1:8 dichloromethane: light petroleum). [2,3-dihydro-5,10,15,20-tetrakis(3',5'-di-*tert*-butylphenyl)porphinato]copper(II) (**49**) (208 mg, 0.18 mmol, no porphyrin impurity by LDI or thin layer chromatography) was dissolved in solvent and placed onto the column. Solvent was pumped off the column by hand. The substrate was left for 2¾ hours at 21°C, after which time products were eluted by adding further solvent. The first band eluted was

identified as [5,10,15,20-tetrakis(3',5'-di-*tert*-butylphenyl)porphinato]copper(II) (**64**) (86 mg, 41%) that had identical IR and LDI spectra to those of an authentic sample. The second band was identified as [hydroxydihydro-5,10,15,20-tetrakis(3',5'-di-*tert*-butylphenyl) porphinato]copper(II) (**67**) (55 mg, 26%), a blue/ green solid. υ_{max}(KBr) 3556 (OH), 2961, 1593, 1493, 1248, 1069, 1007, 791, 715; λ_{max} (CH_2Cl_2)/nm (log (ε/$dm^3mol^{-1}cm^{-1}$)) 393sh (4.40), 416 (5.31), 510 (3.56), 572 (3.84), 606 (4.22); *m/z* (LDI-TOF) 1142.1 (M^+, 100%); $C_{76}H_{94}CuN_4O$ requires 1141.7 (M^+).

The third band was identified as [dihydroxydihydro-5,10,15,20-tetrakis(3',5'-di-*tert*-butylphenyl)porphinato]copper(II) (**70**) (60 mg, 28%), a blue/ green solid. υ_{max}(KBr) 3570 (OH), 2961, 1592, 1363, 1290, 1247, 1064, 1004, 899, 827, 797, 716; λ_{max} (CH_2Cl_2)/nm (log (ε/$dm^3mol^{-1}cm^{-1}$)) 387sh (4.50), 415 (5.39), 508 (3.68), 575 (4.00), 604 (4.48); *m/z* (LDI-TOF) 1158.1 (M^+, 100%); $C_{76}H_{94}CuN_4O_2$ requires 1157.7 (M^+).

The fourth band was identified as [hydroxydihydro-5,10,15,20-tetrakis(3',5'-di-*tert*-butylphenyl)biliverdo]copper(II) (**72**) (4 mg, 2%), a brown solid. υ_{max}($CHCl_3$) 3604 (OH), 2967, 1710 (CO), 1592, 1540, 1462, 1422, 1364, 1062, 1015, 896, 827; λ_{max} (CH_2Cl_2)/nm (log (ε/$dm^3mol^{-1}cm^{-1}$)) 281 (4.55), 369 (4.58), 426sh (4.65), 458 (4.75), 535 (4.05), 575sh (3.90), 627sh (3.86), 703 (4.11), 808 (4.19); *m/z* (MALDI-TOF from a dithranol matrix) 1196.7 (MNa^+, 90%), 1174.7 (MH^+, 100%), 956.9 (M^+- $C_{15}H_{21}O$, 45%); $C_{76}H_{94}CuN_4O_3$ requires 1196.7 (MNa^+), 1174.7 (MH^+), 956.5 (M^+- $C_{15}H_{21}O$).

[2-hydroxy-2,3-dihydro-5,10,15,20-tetrakis(3',5'-di-*tert*-butylphenyl)porphinato] zinc(II) (**68**)

Silica (100 ml) was thoroughly mixed with water (2 ml) and then used to prepare a column (1:8 dichloromethane: light petroleum). [2,3-dihydro-5,10,15,20-tetrakis(3',5'-di-*tert*-butylphenyl)porphinato]zinc(II) (**51**) (128 mg, 0.11 mmol, 5% (porphinato)zinc(II) impurity by ^{1}H NMR) was dissolved in solvent and placed onto the column completely covered in foil. Solvent was pumped off the column by hand. The substrate was left for 3 hours at 22°C, after which time products were eluted by adding further solvent. The first band eluted was identified as a mixture of [5,10,15,20-tetrakis(3',5'-di-*tert*-butylphenyl)porphinato]zinc(II) (**65**) (46 mg, 38%) and [2,3-dihydro-5,10,15,20-tetrakis(3',5'-di-*tert*-butylphenyl) porphinato]zinc(II) (**51**) (7 mg, 6%). Products were identified by ^{1}H NMR and by co-chromatography against authentic samples; the proportion of each product was also identified by ^{1}H NMR. The second band was identified as [2-hydroxy-2,3-dihydro-

5,10,15,20-tetrakis(3',5'-di-*tert*-butylphenyl)porphinato]zinc(II) (**68**) (51 mg, 42%), a dark purple solid. υ_{max}(KBr) 3356 (OH), 2962, 1591 and 1578, 1476, 1362, 1343, 1247, 1064, 1001, 899, 881, 824, 795, 715; λ_{max} (CH_2Cl_2)/nm (log (ε/$dm^3mol^{-1}cm^{-1}$)) 298 (4.27), 401sh (4.70), 417 (5.36), 482 (3.54), 520 (3.83), 561sh (3.63), 582 (4.09), 612 (4.53), 706 (3.09); ^{1}H n.m.r. (400 MHz; $CDCl_3$) δ: 1.47 to 1.52 (72H, m, *t*-butyl H), 2.59 (1H, d, $J_{C(2)H,\ C(2)OH}$ = 2.50 Hz, C(2)OH), 4.11 (1H, dd, $J_{C(3)H,\ C(3)H}$ = 18.15 Hz, $J_{C(2)H,\ C(3)H}$ = 1.95 Hz, C(3)H), 4.45 (1H, dd, $J_{C(3)H,\ C(3)H}$ = 18.25 Hz, $J_{C(2)H,\ C(3)H}$ = 8.40 Hz, C(3)H), 6.39 (1H, dt, $J_{C(3)H,C(2)H}$ = 8.50 Hz, $J_{C(3)H,\ C(2)H} \approx J_{C(2)OH,\ C(2)H}$ = 2.15 Hz, C(2)H), 7.68 (2H, d, $J_{4',2'} = J_{4',6'}$ = 1.65 Hz, C(2')H and C(6')H), 7.72 to 7.74 (3H, m, aryl H), 7.84 (1H, dd, $J_{2',4'} = J_{6',4'}$ = 1.65 Hz, C(4')H), 7.87 (1H, m, aryl H), 7.93 (1H, dd, $J_{2',4'} = J_{6',4'}$ = 1.75 Hz, C(4')H), 7.94 (1H, dd, $J_{2',4'} = J_{6',4'}$ = 1.70 Hz, C(4')H), 7.97 (2H, d, $J_{4',2'} = J_{4',6'}$ = 1.75 Hz, C(2')H and C(6')H), 8.02 (1H, dd, $J_{2',4'} = J_{6',4'}$ = 1.75 Hz, C(4')H), 8.21 (1H, d, $J_{\beta,\beta}$ = 4.70 Hz, *β*-pyrrolic H), 8.26 (1H, d, $J_{\beta,\beta}$ = 4.55 Hz, *β*-pyrrolic H), 8.52 (1H, d, $J_{\beta,\beta}$ = 4.40 Hz, *β*-pyrrolic H), 8.54 (1H, d, $J_{\beta,\beta}$ = 4.45 Hz, *β*-pyrrolic H), 8.64 (1H, d, $J_{\beta,\beta}$ = 4.35 Hz, *β*-pyrrolic H), 8.65 (1H, d, $J_{\beta,\beta}$ = 4.50 Hz, *β*-pyrrolic H); *m/z* (LDI-TOF) 1143.3 (MH^+, 100%); $C_{76}H_{94}ZnN_4O$ requires 1143.7 (MH^+).

9.5.2 Substituted chlorins

***cis*- and *trans*-2,12-dihydroxy-2,3,12,13-tetrahydro-5,10,15,20-tetrakis(3',5'-di-*tert*-butylphenyl)porphyrin and *cis*- and *trans*-2,13-dihydroxy-2,3,12,13-tetrahydro-5,10,15,20-tetrakis(3',5'-di-*tert*-butylphenyl)porphyrin** (*trans* forms are **74a** and **74b**; *cis* forms are **75a** and **75b**).

Silica (200 ml) was thoroughly mixed with water (4 ml) and then used to prepare a column (1:8 dichloromethane: light petroleum.) 2,3,12,13-tetrahydro-5,10,15,20-tetrakis(3',5'-di-*tert*-butylphenyl)porphyrin (**47**) (514 mg, 0.48 mmol) was dissolved in solvent and placed onto the column. Solvent was pumped off the column by hand. The substrate was left for 2½ hours at 30°C, after which time products were eluted by adding further solvent. The first band was identified as the starting material 2,3,12,13-tetrahydro-5,10,15,20-tetrakis(3',5'-di-*tert*-butylphenyl)porphyrin (**47**) (60 mg, 12%) by an identical ^{1}H NMR to and co-chromatography against an authentic sample. The second band was identified as 2,3-dihydro-5,10,15,20-tetrakis(3',5'-di-*tert*-butylphenyl)porphyrin (**46**) (233 mg, 45%) by an identical ^{1}H NMR to and co-chromatography against an authentic sample.

The third band was collected and was re-columned in 2:5 dichloromethane: light petroleum. It was found to contain two products of nearly identical polarity. The slightly less polar

product was identified as 2-hydroxy-2,3-dihydro-5,10,15,20-tetrakis(3',5'-di-*tert*-butylphenyl)porphyrin (**62**) (68 mg, 13%) by an identical ^{1}H NMR to and co-chromatography against an authentic sample. The slightly more polar product was identified as a roughly equimolar mixture of *trans*-2,13-dihydroxy-2,3,12,13-tetrahydro-5,10,15,20-tetrakis(3',5'-di-*tert*-butylphenyl)porphyrin (**74a**) and *trans*-2,12-dihydroxy-2,3,12,13-tetrahydro-5,10,15,20-tetrakis(3',5'-di-*tert*-butylphenyl)porphyrin (**74b**) (33 mg, 6%), a red/ brown solid. Because of its similar polarity to the hydroxy-chlorin **62**, the hydroxy-chlorin **62** made up roughly a 10% impurity of the product (estimated by integration of the NH peaks). This is accounted for in the ^{1}H NMR, the UV spectra and quoted yields. The ^{1}H NMR spectrum is assigned separately to the two different isomers; this is based on the assignment of the *cis* isomers where the slight difference in abundance of the two isomers allows for the differentiation of the two isomers. $\upsilon_{max}(CHCl_3)$ 3695 (OH), 3360 (NH), 2966, 1591, 1477, 1365, 908, 725, 706; λ_{max} (CH_2Cl_2)/nm (log (ε/dm^{3}mol^{-1}cm^{-1})) 244 (3.92), 358sh (4.64), 379 (4.93), 496 (3.61), 525 (4.39), 644 (3.83), 707 (4.60); ^{1}H n.m.r. (400 MHz; $CDCl_3$) 2,12-dihydroxy δ: -1.87 (2H, br s, NH), 1.43 to 1.52 (72H, m, *t*-butyl H), 2.39 (2H, d, $J_{C(2)H,\ C(2)OH} = J_{C(12)H,\ C(12)OH}$ = 1.90 Hz, C(2)OH and C(12)OH), 3.99 (2H, br d, $J_{C(3)H,\ C(3)H} = J_{C(13)H,\ C(13)H}$ = 17.65 Hz, C(3)H and C(13)H), 4.31 (2H, dd, $J_{C(3)H,\ C(3)H} = J_{C(13)H,\ C(13)H}$ = 17.85 Hz, $J_{C(2)H,\ C(3)H} = J_{C(12)H,\ C(13)H}$ = 7.60 Hz, C(3)H and C(13)H), 6.33 (2H, br d, $J_{C(3)H,C(2)H} = J_{C(13)H,C(12)H}$ = 8.40 Hz, C(2)H and C(12)H), 7.61 to 7.92 (12H, m, aryl H), 8.16 and 8.20 (4H, ABX, $J_{\beta,\beta}$ = 4.40 Hz, $J_{NH,\beta}$ = 1.65 Hz, C(7)H, C(8)H, C(17)H and C(18)H); 2,13-dihydroxy δ: -1.64 (1H, s, NH), -1.53 (1H, s, NH), 1.43 to 1.52 (72H, m, *t*-butyl H), 2.45 (2H, d, $J_{C(2)H,\ C(2)OH} = J_{C(13)H,\ C(13)OH}$ = 2.20 Hz, C(2)OH and C(13)OH), 3.99 (2H, br d, $J_{C(3)H,\ C(3)H} = J_{C(12)H,\ C(12)H}$ = 17.65 Hz, C(3)H and C(12)H), 4.38 (2H, dd, $J_{C(3)H,\ C(3)H} = J_{C(12)H,\ C(12)H}$ = 17.65 Hz, $J_{C(2)H,\ C(3)H} = J_{C(13)H,\ C(12)H}$ = 8.05 Hz, C(3)H and C(12)H), 6.28 (2H, br d, $J_{C(3)H,C(2)H} = J_{C(12)H,C(13)H}$ = 8.40 Hz, C(2)H and C(13)H), 7.61 to 7.92 (12H, m, aryl H), 8.07 (2H, d, $J_{NH,\beta}$ = 1.70 Hz, β-pyrrolic H), 8.20 (2H, d, $J_{NH,\beta}$ = 1.90 Hz, β-pyrrolic H); COSY shows coupling between the NH at -1.53 and the doublet at 8.06, between the NH at -1.64 and the signal centred around 8.20, and between the NH at -1.87 and the ABX system at 8.16 and 8.20; *m/z* (LDI-TOF) 1099.3 (M^+, 100%); $C_{76}H_{98}N_4O_2$ requires 1098.8 (M^+).

The fourth band was identified as a mixture of *cis*-2,13-dihydroxy-2,3,12,13-tetrahydro-5,10,15,20-tetrakis(3',5'-di-*tert*-butylphenyl)porphyrin (**75a**) and *cis*-2,12-dihydroxy-2,3,12,13-tetrahydro-5,10,15,20-tetrakis(3',5'-di-*tert*-butylphenyl)porphyrin (**75b**) (50.2 mg, 9%), a red/ brown solid. Integration of the NH and β-pyrrolic signals in the ^{1}H NMR show this to be

roughly a 60:40 mixture of the 2,12 to the 2,13 isomer, and the signals from each isomer could therefore be differentiated by examining individual integrations. Whilst these products were eluted as a pure sample as judged by thin layer chromatography and ^{1}H NMR, exposure to ambient laboratory conditions lead to partial dehydration of the product to give the 2-hydroxy chlorin **62**. This is accounted for in the UV spectrum. $\upsilon_{max}(CHCl_3)$ 3555(OH), 3389 (NH), 2966, 1590, 1476, 1365, 1263, 1111, 1030, 900; λ_{max} (CH_2Cl_2)/nm (log (ε/ $dm^3mol^{-1}cm^{-1}$)) 379 (4.97), 461 (3.47), 492 (3.64), 525 (4.42), 645 (3.74), 706 (4.61); ^{1}H n.m.r. (400 MHz; $CDCl_3$) 2,12-dihydroxy δ: -1.82 (2H, br s, NH), 1.44 to 1.49 (72H, m, *t*-butyl H), 2.39 (2H, d, $J_{C(2)H,\ C(2)OH} = J_{C(12)H,\ C(12)OH}$ = 1.95 Hz, C(2)OH and C(12)OH), 4.02 (2H, dd, $J_{C(3)H,\ C(3)H} = J_{C(13)H,\ C(13)H}$ = 17.95 Hz, $J_{C(2)H,\ C(3)H} = J_{C(12)H,\ C(13)H}$ = 2.00 Hz, C(3)H and C(13)H), 4.33 (2H, dd, $J_{C(3)H,\ C(3)H} = J_{C(13)H,\ C(13)H}$ = 18.20 Hz, $J_{C(2)H,\ C(3)H} = J_{C(12)H,\ C(13)H}$ = 8.25 Hz, C(3)H and C(13)H), 6.32 (2H, br d, $J_{C(3)H,C(2)H} = J_{C(13)H,C(12)H}$ = 8.00 Hz, C(2)H and C(12)H), 7.60 to 7.93 (12H, m, aryl H), 8.15 and 8.18 (4H, ABX, $J_{\beta,\beta}$ = 4.20 Hz, $J_{NH,\beta}$ = 1.75 Hz, C(7)H, C(8)H, C(17)H and C(18)H); 2,13-dihydroxy δ: -1.63 (1H, s, NH), -1.53 (1H, s, NH), 1.44 to 1.49 (72H, m, *t*-butyl H), 2.42 (2H, d, $J_{C(2)H,\ C(2)OH} = J_{C(13)H,\ C(13)OH}$ = 1.80 Hz, C(2)OH and C(13)OH), 3.95 (2H, dd, $J_{C(3)H,\ C(3)H} = J_{C(12)H,\ C(12)H}$ = 18.60 Hz, $J_{C(2)H,\ C(3)H} = J_{C(13)H,\ C(12)H}$ = 1.95 Hz, C(3)H and C(12)H), 4.34 (2H, dd, $J_{C(3)H,\ C(3)H} = J_{C(12)H,\ C(12)H}$ = 18.25 Hz, $J_{C(2)H,\ C(3)H} = J_{C(13)H,\ C(12)H}$ = 8.50 Hz, C(3)H and C(12)H), 6.28 (2H, br d, $J_{C(3)H,C(2)H} = J_{C(12)H,C(13)H}$ = 8.15 Hz, C(2)H and C(13)H), 7.60 to 7.93 (12H, m, aryl H), 8.06 (2H, d, $J_{NH,\beta}$ = 1.95 Hz, β-pyrrolic H), 8.19 (2H, d, $J_{NH,\beta}$ = 1.55 Hz, β-pyrrolic H); COSY shows coupling between the NH at -1.53 and the doublet at 8.06, between the NH at -1.63 and the signal centred around 8.19, and between the NH at -1.82 and the ABX system at 8.06 and 8.19; *m/z* (LDI-TOF) 1099.2 (M^+, 100%); $C_{76}H_{98}N_4O_2$ requires 1098.8 (M^+).

Oxidation of 2-hydroxy-2,3,12,13-tetrahydroporphyrin ***61*** *on silica*

Silica (200 ml) was thoroughly mixed with water (4 ml) and then used to prepare a column (1:8 dichloromethane: light petroleum). 2-hydroxy-2,3,12,13-tetrahydro-5,10,15,20-tetrakis(3',5'-di-*tert*-butylphenyl)porphyrin (**61**) (482 mg, 0.45 mmol) was dissolved in solvent and placed onto the column. Solvent was pumped off the column by hand. The substrate was left for 2½ hours at 30°C, after which time products were eluted by adding further solvent. The first band was identified as 2,3-dihydro-5,10,15,20-tetrakis(3',5'-di-*tert*-butylphenyl)porphyrin (**46**) (50 mg, 11%) by an identical ^{1}H NMR as and co-chromatography against an authentic sample. The second band was found to contain two fractions of very similar polarity and was re-columned (2:5 dichloromethane: light

petroleum.) The first fraction was identified as 2-hydroxy-2,3-dihydro-5,10,15,20-tetrakis(3',5'-di-*tert*-butylphenyl)porphyrin (**62**) (202 mg, 41%) by an identical ^{1}H NMR as and co-chromatography against an authentic sample. The second fraction was identified as a roughly equimolar mixture of *trans*-2,12-dihydroxy-2,3,12,13-tetrahydro-5,10,15,20-tetrakis(3',5'-di-*tert*-butylphenyl)porphyrin (**74a**) and *trans*-2,13-dihydroxy-2,3,12,13-tetrahydro-5,10,15,20-tetrakis(3',5'-di-*tert*-butylphenyl)porphyrin (**74b**) (60 mg, 12%) by an identical ^{1}H NMR as and co-chromatography against an authentic sample. The third band was identified as a roughly equimolar mixture of *cis*-2,12-dihydroxy-2,3,12,13-tetrahydro-5,10,15,20-tetrakis(3',5'-di-*tert*-butylphenyl)porphyrin (**75a**) and *cis*-2,13-dihydroxy-2,3,12,13-tetrahydro-5,10,15,20-tetrakis(3',5'-di-*tert*-butylphenyl)porphyrin (**75b**) (60 mg, 12%) by an identical ^{1}H NMR as and co-chromatography against an authentic sample.

(12- and 13)-chloro-2-hydroxy-2,3-dihydro-5,10,15,20-tetrakis(3',5'-di-*tert*-butylphenyl) porphyrin (**76**)

Silica (100 ml) was thoroughly mixed with 2 ml water and used to prepare a column (1:8 dichloromethane: light petroleum). 2,3-dihydro-12-chloro-5,10,15,20-tetrakis(3',5'-di-*tert*-butylphenyl)porphyrin (**53**) (17 mg, 0.015 mmol) was dissolved in solvent and placed onto the column. Solvent was pumped off the column by hand. The substrate was left for 3 hours at 30°C, after which time products were eluted by adding further solvent. The first band was eluted from the column and was identified as the starting material **53** (13 mg, 74%) by co-chromatography against an authentic sample and by its ^{1}H NMR. The second band was identified as an equimolar mixture of 12- and 13-chloro-2-hydroxy-2,3-dihydro-5,10,15,20-tetrakis(3',5'-di-*tert*-butylphenyl)porphyrin (**76**) (1.1 mg, 6%). $\upsilon_{max}(CHCl_3)$ 3550 (OH), 3360 (NH), 2966, 1593, 1477, 1427, 1394, 1364, 1248, 1068, 1010, 958, 924, 900, 883; λ_{max} (CH_2Cl_2)/nm (log $(\varepsilon/dm^3mol^{-1}cm^{-1})$) 255 (4.62), 312 (4.60), 375sh (4.81), 421 (5.58), 522 (4.51), 548 (4.39), 591 (4.19), 643 (4.58); as the compound exists as two roughly equimolar regioisomers, in the ^{1}H NMR the integration to 1H is taken as one proton in one of the regioisomers; ^{1}H n.m.r. (400 MHz; $CDCl_3$) δ: -1.94 (2H, br, s), -1.84 (1H, br, NH), -1.77 (1H, br, NH), 1.46 to 1.50 (144H, m, *t*-butyl H), 3.10 (2H, m, C(2)OH), 4.11 (2H, d, $J_{C(3)H,\ C(3)H} \approx$ 17.30 Hz, C(3)H), 4.47 (2H, dd, $J_{C(3)H,\ C(3)H}$ = 18.25 Hz, $J_{C(2)H,\ C(3)H}$ = 8.15 Hz, C(3)H), 6.45 (2H, dd, $J_{C(3)H,\ C(2)H} \approx J_{C(2)OH,\ C(2)H}$ = 5.05 Hz, C(2)H), 7.70 to 7.78 (12H, m, aryl H), 7.84 to 7.85 (4H, m, aryl H), 7.91 to 8.04 (8H, m, aryl H), 8.27 (1H, m, *β*-pyrrolic H), 8.32 (2H, m, *β*-pyrrolic H), 8.36 (1H, m, *β*-pyrrolic H), 8.43 (1H, s, C(12)H or C(13)H), 8.54 (1H, s, C(12)H

or C(13)H), 8.62 to 8.65 (4H, m, β-pyrrolic H); m/z (LDI-TOF) 1115.1 (M^+, 100%); $C_{76}H_{95}ClN_4O$ requires 1114.7 (M^+).

Attempted oxidation of nitro-chlorin ***54***

Silica (100 ml) was thoroughly mixed with 2 ml water and used to prepare a column (1:8 dichloromethane: light petroleum). 2,3-dihydro-12-nitro-5,10,15,20-tetrakis(3',5'-di-*tert*-butylphenyl)porphyrin (**54**) (28 mg, 0.025 mmol) was dissolved in solvent and placed onto the column. Solvent was pumped off the column by hand. The substrate was left for 3 hours at 30°C, after which time products were eluted by adding further solvent. One band was eluted from the column and was identified as the starting material **54** (28 mg, 100%) by co-chromatography against an authentic sample and by its ^{1}H NMR.

12-hydroxy-12,13-dihydro-5,10,15,20-tetrakis(3',5'-di-*tert*-butylphenyl)quinoxalino [2,3-b]porphyrin (**77**)

Silica (100 ml) was thoroughly mixed with water (2 ml) and then used to prepare a column (1:8 dichloromethane: light petroleum.) 12,13-dihydro-5,10,15,20-tetrakis(3',5'-di-*tert*-butylphenyl)quinoxalino[2,3-b]porphyrin (**58**) (77 mg, 0.066 mmol) was dissolved in solvent and placed onto the column. Solvent was pumped off the column by hand. The substrate was left for 3 hours at 30°C, after which time products were eluted by adding further solvent. The first band was identified as a mixture of 5,10,15,20-tetrakis(3',5'-di-*tert*-butylphenyl)quinoxalino[2,3-b]porphyrin (**24**) (7.3 mg, 9%) and 12,13-dihydro-5,10,15,20-tetrakis(3',5'-di-*tert*-butylphenyl)quinoxalino[2,3-b]porphyrin (**58**) (15 mg, 20%). Proportions of each product were identified by integration of the NH and β-pyrrolic protons in the ^{1}H NMR. The second band was identified as 12-hydroxy-12,13-dihydro-5,10,15,20-tetrakis(3',5'-di-*tert*-butylphenyl)quinoxalino[2,3-b]porphyrin (**77**) (37 mg, 47%), a dark brown solid. υ_{max}(KBr) 3568 (OH), 3385 (NH), 1593 and 1578, 1476, 1363, 1248, 1226, 1161, 1114, 921, 900, 796, 753; λ_{max} (CH_2Cl_2)/nm (log (ε/dm^{3}mol^{-1}cm^{-1})) 258(4,37), 283 (4,30), 349 (4,34), 421 (5.16), 517 (4.17), 622 (3.91), 677 (4.68); ^{1}H n.m.r. (400 MHz; $CDCl_3$) δ: -1.95 (1H, br s, NH), -1.90 (1H, br s, NH), 1.44 to 1.55 (72H, m, *t*-butyl H), 2.56 (1H, d, $J_{C(12)H,\ C(12)OH}$ = 2.90 Hz, C(12)OH), 4.18 (1H, dd, $J_{C(13)H,\ C(13)H}$ = 18.10 Hz, $J_{C(12)H,\ C(13)H}$ = 1.80 Hz, C(13)H), 4.52 (1H, dd, $J_{C(13)H,\ C(13)H}$ = 18.15 Hz, $J_{C(12)H,\ C(13)H}$ = 8.20 Hz, C(13)H), 6.50 (1H, dt, $J_{C(13)H,C(12)H}$ = 8.30 Hz, $J_{C(13)H,\ C(12)H} \approx J_{C(12)OH,\ C(12)H}$ = 2.30 Hz, C(12)H), 7.70 to 7.74 (2H, m, quinoxalino H), 7.73 (2H, d, $J_{4',2'} = J_{4',6'}$ = 1.50 Hz, C(2')H and C(6')H), 7.78 to 7.82 (2H, m, quinoxalino H), 7.79 (1H, m, aryl H), 7.87 (1H, m, aryl H), 7.90 to 7.92 (5H, m, aryl H), 7.97

(1H, m, aryl H), 7.98 (2H, m, aryl H), 8.39 (1H, d, $J_{\beta,\beta}$ = 4.85 Hz, $J_{NH,\beta}$ = 1.75 Hz, β-pyrrolic H), 8.45 (1H, d, $J_{\beta,\beta}$ = 4.95 Hz, $J_{NH,\beta}$ = 1.70 Hz, β-pyrrolic H), 8.85 (1H, d, $J_{\beta,\beta}$ = 5.15 Hz, $J_{NH,\beta}$ = 1.85 Hz, β-pyrrolic H), 8.87 (1H, d, $J_{\beta,\beta}$ = 4.90 Hz, $J_{NH,\beta}$ = 1.65 Hz, β-pyrrolic H); m/z (LDI-TOF) 1183.0 (M^+, 100%); $C_{82}H_{98}N_6O$ requires 1182.8 (M^+).

9.5.3 Oxidations to the *alpha*-dione.

*Oxidation to 2,3-dioxo-5,10,15,20-tetrakis(3',5'-di-tert-butylphenyl)porphyrin (**20**)*

2-hydroxy-2,3-dihydro-5,10,15,20-tetrakis(3',5'-di-*tert*-butylphenyl)porphyrin (**62**) (291 mg, 0.27 mmol) was dissolved in dichloromethane (75 ml) and had Dess-Martin periodinane (504 mg, 1.19 mmol) added to it over 2 hours. The reaction solution was passed through a silica plug, eluting with ethyl acetate, and the solvent was removed. The product was purified by column chromatography (2:5 dichloromethane: light petroleum.) The main band was identified as 2,3-dioxo-5,10,15,20-tetrakis(3',5'-di-*tert*-butylpheyl)porphyrin (**20**) (236 mg, 80%), which had an identical ^{1}H NMR and co-chromatographed against an authentic sample (see Chapter Six).

*Oxidation of 2,3-dihydro-chlorin **46** by Dess-Martin periodinane*

2,3-dihydro-5,10,15,20-tetrakis(3',5'-di-*tert*-butylphenyl)porphyrin (**46**) (91 mg, 0.085 mmol) was dissolved in dichloromethane (15 ml) and had Dess-Martin periodinane (101 mg, 0.24 mmol) added to it. The system was stirred at room temperature for 40 minutes and then passed through a plug of silica, eluting with 1:1 dichloromethane: light petroleum. Solvent was removed to give 5,10,15,20-tetrakis(3',5'-di-*tert*-butylphenyl)porphyrin (**45**) (72 mg, 79%) which had an identical ^{1}H NMR and co-chromatographed against an authentic sample.

*2,3-dioxo-5,10,15,20-tetrakis(3',5'-di-tert-butylphenyl)porphinato]nickel(II) (**78**)*

[2-hydroxy-2,3-dihydro-5,10,15,20-tetrakis(3',5'-di-*tert*-butylphenyl)porphinato]nickel(II) (**66**) (68 mg, 0.060 mmol) was dissolved in dichloromethane (20 ml) and had Dess-Martin periodinane (150 mg, 0.35 mmol) added to it over 1½ hours. The reaction was followed by thin layer chromatography, which was complicated by an unidentified by-product having a similar R_f value to that of the starting material. The mixture was passed through a plug of silica, eluting with ethyl acetate, and the solvent was removed. The product was purified by column chromatography (1:2 dichloromethane: light petroleum). The main band was collected and identified as 2,3-dioxo-5,10,15,20-tetrakis(3',5'-di-*tert*-

butylphenyl)porphinato]nickel(II) (**78**) (28 mg, 41%), which had an identical ^{1}H NMR and co-chromatographed against an authentic sample[81].

[2-oxo-3-oxa-5,10,15,20-tetrakis(3',5'-di-*tert*-butylphenyl)porphinato]zinc (II) (**79**)

[2-hydroxy-2,3-dihydro-5,10,15,20-tetrakis(3',5'-di-*tert*-butylphenyl)porphinato]zinc (II) (**68**) (51 mg, 0.045 mmol) was dissolved in dichloromethane (20 ml) and had Dess-Martin periodinane (42 mg, 0.098 mmol) added to it over 1 hour. The reaction was followed by thin layer chromatography and was then passed through a plug of silica, eluting with ethyl acetate. Solvent was removed and the product was purified by column chromatography (1:2 dichloromethane: light petroleum.) The first main band was collected and identified as [2-oxo-3-oxa-5,10,15,20-tetrakis(3',5'-di-*tert*-butylphenyl)porphinato]zinc (II) (**79**) (1.5 mg, 3%), a dark green solid. $\upsilon_{max}(CHCl_3)$ 2964, 1759 and 1711 (CO), 1592, 1465, 1364, 865; λ_{max} (CH_2Cl_2)/nm (log (ε/dm^{3}mol^{-1}cm^{-1})) 315 (3.95), 405sh (4.40), 425 (5.13), 520 (3.42), 560 (3.74), 603 (4.03); ^{1}H n.m.r. (400 MHz; $CDCl_3$) δ: 1.49 to 1.50 (72H, m, *t*-butyl H), 7.70 to 7.73 (4H, m, C(4')H), 7.80 (2H, d, $J_{4',2'} = J_{4',6'}$ = 1.75 Hz, C(2')H and C(6')H), 7.90 (2H, m, C(2')H and C(6')H), 7.97 (2H, d, $J_{4',2'} = J_{4',6'}$ = 2.10 Hz, C(2')H and C(6')H), 7.98 (2H, d, $J_{4',2'} = J_{4',6'}$ = 1.65 Hz, C(2')H and C(6')H), 8.59 (1H, d, $J_{\beta,\beta}$ = 4.50 Hz, β-pyrrolic H), 8.67 (1H, d, $J_{\beta,\beta}$ = 4.65 Hz, β-pyrrolic H), 8.73 to 8.75 (3H, m, β-pyrrolic H), 8.81 (1H, d, $J_{\beta,\beta}$ = 4.70 Hz, β-pyrrolic H); *m/z* (LDI-TOF) 1143.0 (M^+, 100%); $C_{75}H_{94}ZnN_4O_2$ requires 1142.6 (M^+).

*Oxidation to 2,3,12,13-tetraoxo-5,10,15,20-tetrakis(3',5'-di-tert-butylphenyl)porphyrin (**23**)*

The more polar mixture of dihydroxy-bacteriochlorins **75** (50 mg, 0.046 mmol) was dissolved in dichloromethane (20 ml) and had Dess-Martin periodinane (97.2 mg, 0.23 mmol) added to it over 1½ hours. The reaction was followed closely by thin layer chromatography. The mixture was passed through a plug of silica, eluting with ethyl acetate, and the solvent was removed. The product purified by column chromatography (1:2 dichloromethane: light petroleum.) The first main band was identified as 2,3,12,13-tetraoxo-5,10,15,20-tetrakis(3',5'-di-*tert*-butylphenyl)porphyrin (**23**) (14.7 mg, 29%), by an identical ^{1}H NMR and IR spectrum to an authentic sample (see Chapter Six).

2,3-dioxo-5,10,15,20,25,30,35,40-octakis(3',5'-di-*tert*-butylphenyl)cycloeicosa[b]cycloeicosa[5,6]pyrazino[2,3-g]quinoxaline (**80**) *and the bis-porphyrin tetra-one (**21**)*

2,3,22,23-tetrahydro-5,10,15,20,25,30,35,40-octakis(3',5'-di-*tert*-butylphenyl)cycloeicosa[b] cycloeicosa[5,6]pyrazino[2,3-g]quinoxaline (**60**) (85 mg, 0.038 mmol) was dissolved in solvent, and loaded onto a column of silica (1:8 dichloromethane: light petroleum.) The solvent was pumped off the column by hand. The substrate was left for 3 hours at 28°C, at which point products were eluted by adding more solvent. The first band collected was identified as the starting material **60** (16.0 mg, 19%). The rest of the products were eluted from the column with ethyl acetate and solvent removed. The dark brown residue was dissolved in dichloromethane (20 ml) and had Dess-Martin periodinane (183 mg, 0.43 mmol) added to it over 2 hours. The reaction was followed closely by thin layer chromatography. The mixture was passed through a plug of silica, eluting with ethyl acetate and the solvent was removed. The product was purified by column chromatography (1:2 dichloromethane: light petroleum). The first band was identified as 2,3-dioxo-5,10,15,20,25,30,35,40-octakis(3',5'-di-*tert*-butylphenyl)cycloeicosa[b]cycloeicosa[5,6]pyrazino[2,3-g]quinoxaline (**80**) (13 mg, 16%), a dark brown solid. υ_{max}(KBr) 3397 (NH), 3342 (NH), 2961, 1733 (CO), 1593, 1475, 1363, 1260, 1206, 1070, 1028, 801, 719; λ_{max} (CH_2Cl_2)/nm (log (ε/$dm^3mol^{-1}cm^{-1}$)) 330sh (4.49), 426 (5.36), 449sh (5.28), 621 (4.16), 680sh (3.97), 706 (3.92), 746sh (3.80); ^{1}H n.m.r. (400 MHz; $CDCl_3$) δ: -2.32 (2H, br s, NH), -1.90 (2H, br s, NH), 1.55 to 1.58 (144H, m, *t*-butyl H), 7.76 (4H, m, C(4')H), 7.78 (2H, m, C(4')H), 7.82 (2H, m, C(4')H), 7.99 (4H, m, C(2')H and C(6')H), 8.03 (4H, m, C(2')H and C(6')H), 8.08 (4H, m, C(2')H and C(6')H), 8.10 (4H, m, C(2')H and C(6')H), 8.56 (2H, s, C(22)H and C(23)H), 8.64 and 8.74 (4H, ABq, $J_{\beta,\beta}$ = 4.95 Hz, C(7)H, C(8)H, C(17)H and C(18)H), 8.77 (2H, s, C(41)H and C(42)H), 8.89 and 8.97 (4H, ABq, $J_{\beta,\beta}$ = 4.60 Hz, C(27)H, C(28)H, C(37)H and C(38)H); COSY shows the relevant β-pyrrolic proton couplings; COSY also shows coupling between the NH proton at -1.90 and the β-pyrrolic protons at 8.64 and 8.73; *m/z* (MALDI-TOF from dithranol) 2281.8 (M^+, 100%); $C_{158}H_{184}N_{12}O_2$ requires 2281.5 (M^+).

The second band was identified as 2,3,22,23-tetraoxo-5,10,15,20,25,30,35,40-octakis(3',5'-di-*tert*-butylphenyl)cycloeicosa[b]cycloeicosa[5,6]pyrazino[2,3-g]quinoxaline (**80**) (26 mg, 29%). It was identified by having an identical ^{1}H NMR and IR spectrum to an authentic sample (see Chapter Six).

9.6 Experimental details for Chapter Six

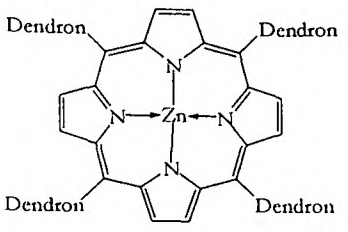

(83)

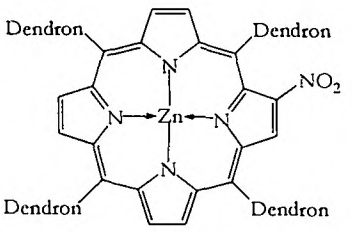

(86)

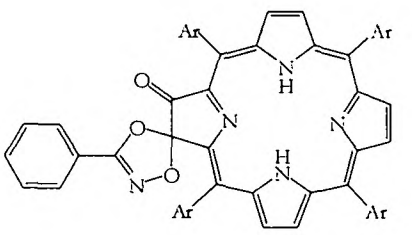

(96)

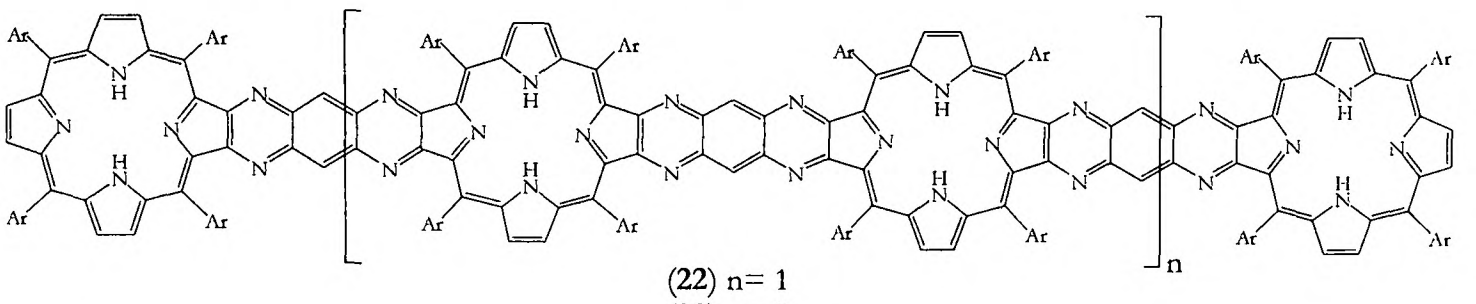

(22) n= 1
(98) n= 2

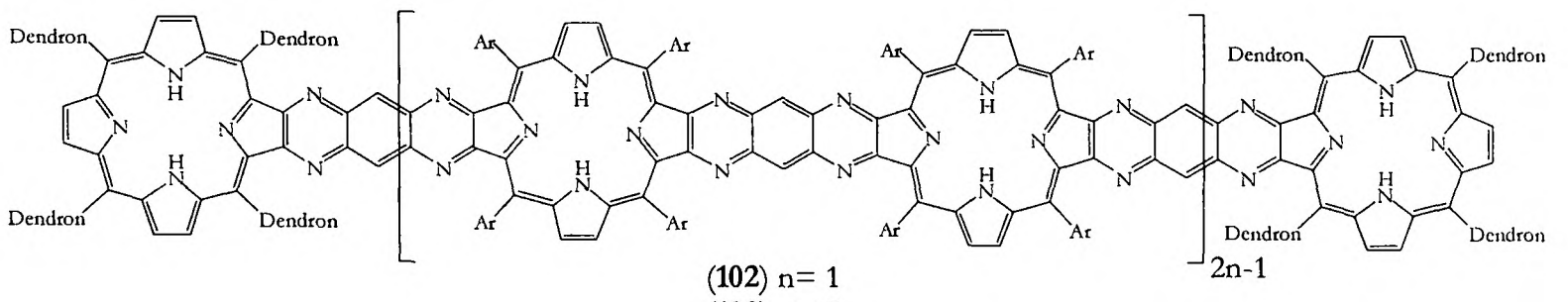

(102) n= 1
(103) n= 2
(104) n= 3
(105) n= 4

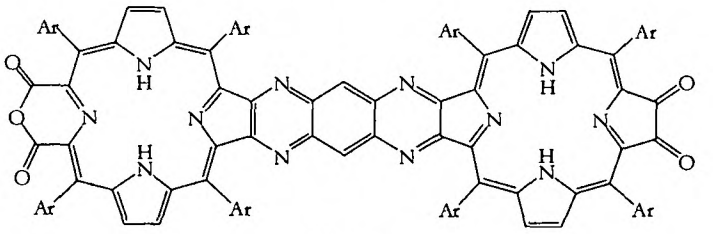

(106)

Ar = 3,5-di-*tert*-butylphenyl; Dendron = 3,5(3',5'-di-*tert*-butylstyryl)phenyl

9.6.1 Attempted synthesis of the dendritic porphyrin tetra-one

[5,10,15,20-tetrakis(3',5'-bis(3'',5''-di-tert-butylstyryl)phenyl)porphinato]nickel(II) (**81**), *[5,10,15,20-tetrakis(3',5'-bis(3'',5''-di-tert-butylstyryl)phenyl)porphinato]copper(II)* (**82**), and *[2-nitro-5,10,15,20-tetrakis(3',5'-bis(3'',5''-di-tert-butylstyryl)phenyl)porphinato]copper(II)* (**85**)

These products were synthesised by the method of Promarak[37]. Their structures were confirmed by co-chromatography against and by having identical ^{1}H NMRs as authentic samples, or in the case of the copper(II) derivatives by co-chromatography against and by having identical MALDI spectra (from a dithranol matrix) as authentic samples[37].

[5,10,15,20-tetrakis(3',5'-bis(3'',5''-di-*tert*-butylstyryl)phenyl)porphinato]zinc(II) (83)

5,10,15,20-tetrakis(3',5'-bis(3'',5''-di-*tert*-butylstyryl)phenyl)porphyrin (**92**) (245 mg, 0.11 mmol) and zinc diacetate dihydrate (152 mg, 0.69 mmol) were dissolved in dichloromethane (50 ml) and methanol (15 ml) and heated at the point of reflux for 2 hours. The solvent was removed and the product was purified by recrystallization from dichloromethane/ methanol. The product was identified as [5,10,15,20-tetrakis(3',5'-bis(3'',5''-di-*tert*-butylstyryl)phenyl) porphinato]zinc(II) (**83**), a red/ purple solid. υ_{max}(KBr) 2961, 1593, 1477, 1459, 1445, 1247, 1204, 1006, 958, 874, 798, 705, 535; λ_{max} (CH_2Cl_2)/nm (log(ε/$dm^3mol^{-1}cm^{-1}$)) 312 (5.23), 409sh (4.68), 430 (5.75), 513 (3.58), 551 (4.35), 589 (3.65), 635* (2.74), 696 (2.77), 773 (2.82), 868 (2.90) where * indicates an absorption whose intensity of absorption changes with concentration; ^{1}H n.m.r. (400 MHz; $CDCl_3$) δ: 1.36 (144H, s, *t*-butyl H), 7.38 (8H, m, C(4'')H), 7.44 (32H, m, C(2'')H, C(6'')H, C(7'')H and C(8'')H), 8.15 (4H, m, C(4')H), 8.38 (8H, d, $J_{4',2'} = J_{4',6'} = 1.15$ Hz, C(2')H and C(6')H), 9.19 (8H, s, *β*-pyrrolic H); *m/z* (LDI-TOF) 2389.1 (M^+, 100%); $C_{172}H_{204}N_4Zn$ requires 2389.5 (M^+).

[2-nitro-5,10,15,20-tetrakis(3',5'-bis(3'',5''-di-*tert*-butylstyryl)phenyl)porphinato] zinc(II) (86)

[5,10,15,20-tetrakis(3',5'-bis(3'',5''-di-*tert*-butylstyryl)phenyl)porphinato]zinc(II) (**83**) (101 mg, 0.042 mmol) was dissolved in dichloromethane (10 ml) and had 7 aliquots of nitrogen dioxide solution (0.1 ml, 0.071 $mmolml^{-1}$) added to it at 5 minute intervals. The solution was then passed through a plug of silica and the solvent was removed. The product was purified by column chromatography over silica (1:3 dichloromethane: light petroleum). The first band eluted was identified as the starting material **83** (10 mg, 10%) by co-chromatography against and having an identical ^{1}H NMR as an authentic sample. The second band was identified as [2-nitro-5,10,15,20-tetrakis(3',5'-bis(3'',5''-di-*tert*-butylstyryl)phenyl)porphinato] zinc(II) (**86**) (22 mg, 22%), a brown solid. υ_{max}(KBr) 2962, 1593, 1523 (NO_2), 1476, 1363, 1264, 1247, 1203, 1009, 961, 874, 799, 739, 705, 536; λ_{max} (CH_2Cl_2)/nm (log(ε/ $dm^3mol^{-1}cm^{-1}$)) 309 (5.32), 390sh (4.56), 440 (5.41), 526sh (3.75), 560 (4.30), 603 (4.10); ^{1}H n.m.r. (400 MHz; $CDCl_3$) δ: 1.35 (144H, s, *t*-butyl H), 7.36 (2H, dd, $J_{2'',4''} = J_{6'',4''} = 1.90$ Hz, C(4'')H), 7.38 (6H, m, C(4'')H), 7.40 to 7.47 (32H, m, C(2'')H, C(6'')H, C(7'')H and C(8'')H), 8.11 (1H, m, C(4')H), 8.15 (3H, dd, $J_{2',4'} = J_{6',4'} = 1.60$ Hz, C(4')H), 8.30 (4H, m, C(2')H and C(6')H), 8.32 (4H, m, C(2')H and C(6')H), 9.13 (5H, m, *β*-pyrrolic H), 9.21 (1H, d, $J_{\beta,\beta} = 4.80$ Hz, *β*-pyrrolic H), 9.43 (1H, s, C(3)H); *m/z* (MALDI-TOF from an *alpha*-cyano-4-hydroxy

cinnamic acid matrix) 2434.7 (M^+, 20%), 2418.6 (M^+- O, 20%), 2402.5 (M^+- 2O, 100%); $C_{172}H_{203}N_5O_2Zn$ requires 2434.5 (M^+).

Attempted di-nitration of the dendritic nickel(II) porphyrin ***81***

[5,10,15,20-tetrakis(3',5'-bis(3'',5''-di-*tert*-butylstyryl)phenyl)porphinato]nickel(II) (**81**) (65 mg, 0.027 mmol) was dissolved in dichloromethane (5 ml) and had 20 aliquots of nitrogen dioxide solution (0.2 ml, 0.033 $mmolml^{-1}$) added to it at 5 minute intervals. The solution was passed through a plug of silica and the solvent was removed. The product was purified by column chromatography (1:3 dichloromethane: light petroleum). Although no separation was apparent by eye the products were collected in fractions. The only fraction to be positively identified was the first fraction, as [2-nitro-5,10,15,20-tetrakis(3',5'-bis(3'',5''-di-*tert*-butylstyryl)phenyl)porphinato]nickel(II) (**84**) (4.5 mg, 7%) by co-chromatography against and an identical ^1H as an authentic sample[37].

Attempted second nitration of the dendritic copper(II) nitro-porphyrin ***85***

[2-nitro-5,10,15,20-tetrakis(3',5'-bis(3'',5''-di-*tert*-butylstyryl)phenyl)porphinato]copper(II) (**85**) (24 mg, 0.0099 mmol) was dissolved in dichloromethane (5 ml) and had 9 aliquots of nitrogen dioxide solution (0.1 ml, 0.033 $mmolml^{-1}$) added to it at 5 minute intervals. The solution was passed through a plug of silica and the solvent was removed. The product was purified by column chromatography (1:3 dichloromethane: light petroleum). The only main fraction was identified as the starting material (**85**) (9.9 mg, 41%) by co-chromatography against and an identical MALDI spectrum from an *alpha*-cyano-4-hydroxy cinnamic acid matrix as an authentic sample[37].

Attempted di-nitration of the zinc porphyrin ***83***

[5,10,15,20-tetrakis(3',5'-bis(3'',5''-di-*tert*-butylstyryl)phenyl)porphinato]zinc(II) (**83**) (113 mg, 0.047 mmol) was dissolved in dichloromethane (10 ml) and had 8 aliquots of nitrogen dioxide solution (0.1 ml, 0.11 $mmolml^{-1}$) added to it at 5 minute intervals. The solution was passed through a plug of silica eluting with ethyl acetate and the solvent was removed. The product was purified by column chromatography (dichloromethane). No product was eluted.

9.6.2 Synthesis of the dendritic porphyrin *alpha*-dione

3,5-(3',5'-di-*tert*-butylstyryl)benzaldehyde (91)

The method of Pillow was followed for the preparation of **91**[202]. The structure of the intermediates and the product were confirmed by co-chromatography against and identical ^{1}H NMRs as authentic samples. Yields for the preparation of this product are given in Scheme **6.2**.

2,3-dioxo-5,10,15,20-tetrakis(3',5'-bis(3'',5''-di-*tert*-butylstyryl)phenyl)porphyrin (93)

The method of Promarak was followed for the preparation of **X**[37]. The one difference being the [2-nitro-5,10,15,20-tetrakis(3',5'-bis(3'',5''-di-*tert*-butylstyryl)phenyl)porphinato]copper(II) (**85**) was purified over alumina (1:4 dichloromethane: light petroleum) instead of over silica. The structures of the intermediates and the product were confirmed by co-chromatography against and identical ^{1}H NMRs as authentic samples, or for the products containing copper by co-chromatography against and identical IR spectra as authentic samples[37]. Yields for the preparation of this product are given in Scheme **6.2**.

9.6.3 Preparation of the simple porphyrin tetra-one

*Attempted preparation of 2,3,12,13-tetraoxo-5,10,15,20-tetrakis(3',5'-di-tert-butylphenyl)porphyrin (**23**)*

The method of Promarak was followed for the attempted preparation of **23**[37]. The structures of the intermediates and the small amount of product were confirmed by co-chromatography against and identical ^{1}H NMRs as authentic samples, or for the products containing copper by co-chromatography against and identical IR spectra as authentic samples[37]. Yields for the preparation of this product are discussed in Section **6.3**.

*Preparation of 2,3-dioxo-bis-porphyrin **20** and 2,3,22,23-tetraoxo-bis-porphyrin **21***

Although the synthesis of the bis-porphyrin **14** has been reported previously[35], it is described again here as the synthesis was carried out on a larger scale than previously attempted. The functionalization of the bis-porphyrin **14** was then carried out as described in Chapters Four and Five.

3,5-di-*tert*-butyltoluene (88)

3,5-di-*tert*-butylphenyltoluene (**88**) was prepared by the method of Geuze[203] in 51% yield, boiling point typically 75 to 85°C, 2 mmHg (lit. 98°C, 5.7 mmHg). It also had an identical ^{1}H NMR as that of an authentic sample.

3,5-di-*tert*-butylbenzaldehyde (89)

3,5-di-*tert*-butylphenylbenzaldehyde (**89**) was prepared by the method of Newman and Fang Lee[204] in 50% yield. It had a melting point of 82°C (lit. 84 to 85°C).

5,10,15,20-tetrakis(3',5'-di-*tert*-butylphenyl)porphyrin (45)

3,5-di-*tert*-butylbenzaldehyde (**89**) (121 g, 0.56 mol) was dissolved in propionic acid (1750 ml) and was brought to the point of reflux for 15 minutes. Heat was removed and then pyrrole (38.5 ml, 0.56 mol) was added slowly over 15 minutes. At this point the yellow solution had turned black. The system was then heated at reflux for a further 2 hours and allowed to cool overnight. The product mixture was filtered and the filtrate was washed with water (500 ml), methanol (500 ml), water (500 ml), and methanol (500 ml). The filtrate was then recrystallised from dichloromethane/ methanol. It was identified as 5,10,15,20-tetrakis(3',5'-di-*tert*-butylphenyl)porphyrin (**45**) (31.0 g, 21%) by an identical ^{1}H NMR as and co-chromatography against an authentic sample[37].

[2-nitro-5,10,15,20-tetrakis(3',5'-di-*tert*-butylphenyl)porphinato]copper(II) (95)

5,10,15,20-tetrakis(3',5'-di-*tert*-butylphenyl)porphyrin (**45**) (31.0 g, 29.2 mmol) and copper diacetate monohydrate (16.1 g, 80.1 mmol) were dissolved in dichloromethane (1500 ml) and methanol (250 ml) and brought to the point of reflux for 2 hours. The system was allowed to cool and then filtered. The filtrate was redissolved in dichloromethane (1750 ml) and had 5 aliquots (12.5 ml) of a solution of nitrogen dioxide in light petroleum (0.55 $mmolml^{-1}$) added to it at 5 minute intervals. The progress of the reaction was monitored carefully by thin layer chromatography. The system was then passed through a plug of silica and solvent was removed. The product was purified by column chromatography (1:6 dichloromethane: light petroleum). The main band was collected and identified as [2-nitro-5,10,15,20-tetrakis(3',5'-di-*tert*-butylphenyl)porphinato]copper(II) (**95**) (30.7 g, 90%) by an identical IR spectrum as and co-chromatography against an authentic sample[37].

2,3-dioxo-5,10,15,20-tetrakis(3',5'-di-tert-butylphenyl)porphyrin (20) and **2-oxo-3-(4''-phenyl-2'',5''-dioxo-3''-azole)-5,10,15,20-tetrakis(3',5'-di-*tert*-butylphenyl)porphyrin** (96)

Sodium hydride (8.9 g, 60% dispersion in mineral oil, 0.22 mol) was dissolved in freshly distilled dimethyl sulphoxide (1600 ml) by stirring it at 80°C for 45 minutes under nitrogen. Heat was removed and benzaldehyde oxime (20.0 g, 0.17 mol) was added. The system was

stirred for a further 5 minutes and then transferred under nitrogen to a solution of [2-nitro-5,10,15,20-tetrakis(3',5'-di-*tert*-butylphenyl)porphinato]copper(II) (**95**) (17.1 g, 14.6 mmol) dissolved in THF (1600 ml). The system was heated at reflux under a flowing stream of nitrogen for 2 hours and then allowed to cool. Ether (1000 ml) and *then* water (1000 ml) were added and the organic layer was extracted. This was washed with water (4×500 ml), brine (500 ml), dried over sodium sulphate and solvent removed. This intermediate product was recrystallised from dichloromethane/ methanol. It was then redissolved in dichloromethane (2400 ml) and had Dess-Martin periodinane (6.8 g, 16 mmol) added to it and was stirred at room temperature for 30 minutes. The solution was passed through a plug of silica and solvent was removed. The product was purified by column chromatography (1:2 dichloromethane: light petroleum). It was identified as 2,3-dioxo-5,10,15,20-tetrakis(3',5'-di-*tert*-butylphenyl)porphyrin (**20**) (8.75 g, 55%) by co-chromatography against an authentic sample, and an identical ^{1}H NMR as that reported in the literature[87].

If the intermediate product was not recrystallised from dichloromethane/ methanol before the addition of the Dess-Martin periodinane then 2-oxo-3-(4''-phenyl-2'',5''-dioxo-3''-azole)-5,10,15,20-tetrakis(3',5'-di-*tert*-butylphenyl)porphyrin (**96**) was eluted as the major product slightly before the 2,3-dioxo-porphyrin **20**. υ_{max}(KBr) 3352 (NH), 2962, 1749 (CO), 1593, 1476, 1427, 1393, 1363, 1348, 1280, 1247, 1202, 1087, 1069, 1049, 1021, 1002, 989, 920, 900, 881, 801, 718; λ_{max} (CH_2Cl_2)/nm (log(ε/dm^{-3}mol^{-1}cm^{-1})) 305sh (4.23), 371sh (4.60), 425 (5.11), 446 (4.95), 541 (3.96), 578 (4.00), 605 (4.00), 657 (3.97); ^{1}H n.m.r. (400 MHz; $CDCl_3$) δ: -2.05 (1H, br s, NH), -1.90 (1H, br s, NH), 1.44 to 1.55 (72H, m, *t*-butyl H), 7.35 (2H, dd, $J_{2'',3''}$ = $J_{4'',3''}$ = 7.55 Hz, C(3'')H), 7.42 to 7.47 (3H, m, C(2'')H and C(4'')H), 7.58 (1H, m, aryl H), 7.60 (1H, m, aryl H), 7.71 to 7.75 (2H, m, aryl H), 7.76 (1H, dd, $J_{2',4'}$ = $J_{6',4'}$ = 1.60 Hz, aryl H), 7.78 (1H, dd, $J_{2',4'}$ = $J_{6',4'}$ = 1.85 Hz, C(4')H), 7.79 (1H, dd, $J_{2',4'}$ = $J_{6',4'}$ = 1.90 Hz, C(4')H), 7.88 (1H, dd, $J_{2',4'}$ = $J_{6',4'}$ = 1.50 Hz, C(4')H), 7.93 (1H, dd, $J_{2',4'}$ = $J_{6',4'}$ = 1.65 Hz, C(4')H), 7.97 (1H, dd, $J_{2',4'}$ = $J_{6',4'}$ = 1.60 Hz, C(4')H), 8.00 (1H, m, aryl H), 8.01 (1H, m, aryl H), 8.02 (1H, m, aryl H), 8.09 (1H, m, aryl H), 8.39 (1H, dd, $J_{\beta,\beta}$ = 4.90 Hz, $J_{NH,\beta}$ = 1.80 Hz, β-pyrrolic H), 8.62 to 8.65 (3H, m, β-pyrrolic H), 8.66 (1H, d, $J_{\beta,\beta}$ = 4.90 Hz, β-pyrrolic H), 8.78 (1H, dd, $J_{\beta,\beta}$ = 5.05 Hz, $J_{NH,\beta}$ = 1.60 Hz, β-pyrrolic H), 8.81 (1H, dd, $J_{\beta,\beta}$ = 4.85 Hz, $J_{NH,\beta}$ = 1.45 Hz, β-pyrrolic H); *m/z* (MALDI-TOF from a dithranol matrix) 1212.5 (MH^+, 25%), 1095.7 (MH^++2H- C_7H_5N, 100%), 1093.8 (MH^+, 80%); $C_{83}H_{97}N_5O_3$ requires 1212.8 (MH^+).

*5,10,15,20,25,30,35,40-octakis(3',5'-di-tert-butylphenyl)cycloeicosa[b]cycloeicosa[5,6]pyrazino[2,3-g] quinoxaline (**14**)*

2,3-dioxo-5,10,15,20-tetrakis(3',5'-di-*tert*-butylphenyl)porphyrin (**20**) (8.8 g, 8.0 mmol) and 1,2,4,5-tetraminobenzene tetrahydrochloride (803 mg, 2.8 mmol) were dissolved in dry pyridine (136 ml), stirred under a flowing stream of nitrogen for 30 minutes and then heated at reflux under a flowing stream of nitrogen for 19 hours. The system was allowed to cool and then filtered. The solid was redissolved in ether (500 ml) and washed with aqueous hydrochloric acid (3M, 2×200 ml), water (200 ml), saturated aqueous sodium bicarbonate solution (200 ml), brine (200 ml), dried over sodium sulphate and the solvent was removed. The product was then recrystallised from dichloromethane/ methanol. Meanwhile the filtrate had ether (500 ml) and aqueous hydrochloric acid (3M, 200 ml) added to it and the organic layer was extracted. This was washed with aqueous hydrochloric acid (3M, 200 ml), water (200 ml), saturated aqueous sodium bicarbonate solution (200 ml), brine (200 ml), dried over sodium sulphate and the solvent was removed. The product was purified by column chromatography (1:3 dichloromethane: light petroleum). The first band was combined with the first product isolated from the solid fraction from the filtration and identified as 5,10,15,20,25,30,35,40-octakis(3',5'-di-*tert*-butylphenyl)cycloeicosa[b]cycloeicosa [5,6]pyrazino[2,3-g]quinoxaline (**14**) (5.62 g, 62% with respect to the porphyrin *alpha*-dione, or 88% with respect to the 1,2,4,5-tetraaminobenzene) by having an identical LDI mass and ^{1}H NMR as reported in the literature[35]. The second band was identified as the starting material **20** (1.50 g, 17%) by co-chromatography against and having an identical ^{1}H NMR as an authentic sample.

9.6.4 Preparation of porphyrin arrays

Non-dendritic tetrakis porphyrin 22

2,3-dioxo-5,10,15,20,25,30,35,40-octakis(3',5'-di-*tert*-butylphenyl)cycloeicosa[b] cycloeicosa[5,6]pyrazino[2,3-g]quinoxaline (**80**) (505 mg, 0.22 mmol) and 1,2,4,5-tetraaminobenzene tetrahydrochloride (21.8 mg, 0.077 mmol) were dissolved in pyridine (7.2 ml) and stirred under a flowing stream of nitrogen for 30 minutes. The system was heated at reflux, still under a flowing stream of nitrogen, for 89 hours and then allowed to cool. Ether (500 ml) and aqueous hydrochloric acid (3M, 500 ml) were added to the system, and the organic layer was extracted. This was washed with aqueous hydrochloric acid (3M, 250 ml), water (4×250 ml), aqueous saturated sodium bicarbonate solution (250 ml), brine (250 ml), dried over sodium sulphate and the solvent was removed. The product was purified by

column chromatography (1:2 dichloromethane: light petroleum, then 1: 1.75 dichloromethane: light petroleum). Two bands were eluted, and then the product was eluted by flushing the column with chloroform. The product was re-purified over silica (1:1 chloroform: light petroleum) and then recrystallised from chloroform/ acetonitrile. It was identified as the non-dendritic tetramer **22** (165 mg, 32% with respect to the bis-porphyrin *alpha*-dione starting material, or 45% with respect to the 1,2,4,5-tetraaminobenzene), a dull brown solid. Characterization details are given in Chapter Six.

Non-dendritic hexamer 98

2,3,22,23-tetraoxo-5,10,15,20,25,30,35,40-octakis(3',5'-di-*tert*-butylphenyl)cycloeicosa[b] cycloeicosa[5,6]pyrazino[2,3-g]quinoxaline (**21**) (23 mg, 0.0099 mmol) and 1,2,4,5-tetraaminobenzene tetrahydrochloride (155 mg, 0.55 mmol) were dissolved in pyridine (10 ml) and degassed and placed under argon three times. The system was then heated at reflux for 2 hours, and allowed to cool. Ether (100 ml) and water (100 ml) were added to the system, and the organic layer was extracted. This was washed with water (3×100 ml), aqueous hydrochloric acid (3M, 2×100 ml), water (100 ml), aqueous saturated sodium bicarbonate solution (100 ml), brine (100 ml), dried over sodium sulphate and the solvent was removed. The brown residue and 2,3-dioxo-5,10,15,20,25,30,35,40-octakis(3',5'-di-*tert*-butylphenyl)cycloeicosa[b]cycloeicosa[5,6]pyrazino[2,3-g]quinoxaline (**80**) (82 mg, 0.036 mmol) were dissolved in toluene (5 ml) and degassed and placed under argon four times. The system was heated at reflux for 22 hours and then solvent was removed. The product was purified by column chromatography (1:1 chloroform: light petroleum) and the very first distinctly red band was collected. The product was identified as the non-dendritic hexamer **98** (6 mg, 8%), a dark red solid. λ_{max} ($CHCl_3$)/nm (log(ε/$dm^3mol^{-1}cm^{-1}$)) 327sh (4.6), 428 (5.4), 464 (5.3), 496sh (5.1), 522sh (5.0), 567sh (4.8), 615sh (4.4), 665 (4.4), 723 (4.1). Further details of characterization are given in Chapter Six.

Tris-porphyrin *alpha*-dione 99 and dendritic tetrakis porphyrin 102

2,3-dioxo-5,10,15,20-tetrakis(3',5'-bis(3'',5''-di-*tert*-butylstyryl)phenyl)porphyrin (**93**) (236 mg, 0.10 mmol) and 1,2,4,5-tetraaminobenzene tetrahydrochloride (294 mg, 1.0 mmol) were dissolved in pyridine (28 ml) and degassed and placed under argon three times. The system was then heated at reflux for 2 hours allowed to cool. Ether (100 ml) and water (100 ml) were added to the system, and the organic layer was extracted. This was washed with water (3×100 ml), aqueous hydrochloric acid (3M, 2×100 ml), water (100 ml), aqueous saturated sodium bicarbonate solution (100 ml), brine (100 ml), dried over sodium sulphate and the

solvent was removed. The brown residue and 2,3,22,23-tetraoxo-5,10,15,20,25,30,35,40-octakis(3',5'-di-*tert*-butylphenyl)cycloeicosa[b]cycloeicosa[5,6]pyrazino[2,3-g]quinoxaline (**21**) (515 mg, 0.22 mmol) were dissolved in toluene (28 ml) and degassed and placed under argon four times. The system was heated at reflux for 19 hours and then the solvent was removed. The product was purified by column chromatography (1: 2.25 then 1: 1.75 then 1: 1.25 dichloromethane: light petroleum). The first band was identified as the tetrakis porphyrin **102** (30.6 mg, 7%). Details of its characterization are given in Chapter Six. The second band was identified as the tris-porphyrin *alpha*-dione **99** (209 mg, 44%). The product was not characterized as possible small amounts of contaminating anhydride product were evident by ^{1}H NMR, as evidenced by the appearance of an erroneous signal in the NH region at around -1.38 ppm. The third band was identified as 2,3,22,23-tetraoxo-5,10,15,20,25,30,35,40-octakis(3',5'-di-*tert*-butylphenyl)cycloeicosa[b]cycloeicosa[5,6]pyrazino[2,3-g]quinoxaline (**21**) (306 mg, 59%).

5mer-porphyrin *alpha*-dione 100 and dendritic octamer 103

The 3mer porphyrin *alpha*-dione (**99**) (209 mg, 0.044 mmol) and 1,2,4,5-tetraaminobenzene tetrahydrochloride (270 mg, 0.95 mmol) were dissolved in pyridine (25 ml) and degassed and placed under argon three times. The system was then heated at reflux for 2 hours allowed to cool. Ether (100 ml) and water (100 ml) were added to the system, and the organic layer was extracted. This was washed with water (3×100 ml), aqueous hydrochloric acid (3M, 2×100 ml), water (100 ml), aqueous saturated sodium bicarbonate solution (100 ml), brine (100 ml), dried over sodium sulphate and the solvent was removed. The brown residue and 2,3,22,23-tetraoxo-5,10,15,20,25,30,35,40-octakis(3',5'-di-*tert*-butylphenyl)cycloeicosa[b] cycloeicosa[5,6]pyrazino[2,3-g]quinoxaline (**21**) (290 mg, 0.13 mmol) were dissolved in toluene (20 ml) and degassed and placed under argon four times. The system was heated at reflux for 19 hours and then the solvent was removed. The product was purified by column chromatography (1: 2.25 then 1: 1.75 then 1: 1.25 dichloromethane: light petroleum). The first band was identified as the octakis-porphyrin **103** (18.7 mg, 9%). Details of its characterization are given in Chapter Six. The second band was identified as the 5mer-porphyrin *alpha*-dione **100** (169 mg, 54%). The product was not characterized as possible small amounts of contaminating anhydride product were evident by ^{1}H NMR, as evidenced by the appearance of an erroneous signal in the NH region at around -1.38 ppm. The third band was identified as 2,3,22,23-tetraoxo-5,10,15,20,25,30,35,40-octakis(3',5'-di-*tert*-butylphenyl)cycloeicosa[b]cycloeicosa[5,6]pyrazino[2,3-g]quinoxaline (**21**) (210 mg, 72%).

7mer-porphyrin *alpha*-dione 101 and dendritic 12mer 104

The 5mer porphyrin *alpha*-dione (**100**) (143 mg, 0.020 mmol) and 1,2,4,5-tetraaminobenzene tetrahydrochloride (410 mg, 1.44 mmol) were dissolved in pyridine (30 ml) and degassed and placed under argon three times. The system was then heated at reflux for 2 hours allowed to cool. Dichloromethane (100 ml) and water (100 ml) were added to the system, and the organic layer was extracted. This was washed with water (3×100 ml), aqueous hydrochloric acid (3M, 2×100 ml), water (100 ml), aqueous saturated sodium bicarbonate solution (100 ml), brine (100 ml), dried over sodium sulphate and the solvent was removed. The brown residue and 2,3,22,23-tetraoxo-5,10,15,20,25,30,35,40-octakis(3',5'-di-*tert*-butylphenyl) cycloeicosa[b]cycloeicosa[5,6]pyrazino[2,3-g]quinoxaline (**21**) (209 mg, 0.090 mmol) were dissolved in toluene (15 ml) and degassed and placed under argon four times. The system was heated at reflux for 19 hours and then the solvent was removed. The product was purified by column chromatography (1: 2.25 then 1: 1.75 then 1: 1.25 dichloromethane: light petroleum). The column was then flushed with chloroform, and the products were re-purified (2:3 chloroform: light petroleum). The first band was identified as the 12mer porphyrin **104** (3.2 mg, 2%). λ_{max} (CH_2Cl_2)/nm (log(ε/$dm^3mol^{-1}cm^{-1}$)) 308 (5.73), 427 (6.06), 465 (6.02), 490sh (5.91), 530 (5.84), 567 (5.64), 611sh (5.18), 666 (5.26), 725 (5.02). Further details of its characterization are given in Chapter Six.

The second band was identified as the 7mer-porphyrin *alpha*-dione **101** (87 mg, 46%). The product was not characterized as possible significant amounts of contaminating anhydride product were evident by ^{1}H NMR, as evidenced by the appearance of an erroneous signal in the NH region at around -1.38 ppm. The third band was identified as 2,3,22,23-tetraoxo-5,10,15,20,25,30,35,40-octakis(3',5'-di-*tert*-butylphenyl)cycloeicosa[b]cycloeicosa[5,6] pyrazino[2,3-g]quinoxaline (**21**) (120 mg, 57%).

Dendritic 16mer 105

The 7mer porphyrin *alpha*-dione (**101**) (87 mg, 0.0074 mmol) and 1,2,4,5-tetraaminobenzene tetrahydrochloride (590 mg, 2.1 mmol) were dissolved in pyridine (45 ml) and degassed and placed under argon three times. The system was then heated at reflux for 2 hours allowed to cool. Dichloromethane (100 ml) and water (100 ml) were added to the system, and the organic layer was extracted. This was washed with water (3×100 ml), aqueous hydrochloric acid (3M, 2×100 ml), water (100 ml), aqueous saturated sodium bicarbonate solution (100 ml), brine (100 ml), dried over sodium sulphate and the solvent was removed. The brown residue and 2,3,22,23-tetraoxo-5,10,15,20,25,30,35,40-octakis(3',5'-di-*tert*-butylphenyl)

cycloeicosa[b]cycloeicosa[5,6]pyrazino[2,3-g]quinoxaline (**21**) (7 mg, 0.0030 mmol) were dissolved in toluene (7.5 ml) and degassed and placed under argon four times. The system was heated at reflux for 19 hours and then the solvent was removed. The product was purified by column chromatography (1: 1 chloroform: light petroleum). The first band was identified as the 16mer porphyrin **105** (5.9 mg, 7%). Details of its characterization are given in Chapter Six.

2,3-dioxo-22,23a-dioxo-18a-homo-17oxa-5,10,15,20,25,30,35,40-octakis(3',5'-di-*tert*-butylphenyl)cycloeicosa[b]cycloeicosa[5,6]pyrazino[2,3-g]quinoxaline (**106**)

On each iteration of the sequence, a small band was isolated that ran slightly in front of the recovered bis-porphyrin tetra-one **21** on purification over column chromatography (1: 1.25 dichloromethane: light petroleum). This was difficult to obtain in a pure form and was often discarded, but when it was eventually isolated in a pure form it was identified as 2,3-dioxo-22,23a-dioxo-18a-homo-17oxa-5,10,15,20,25,30,35,40-octakis(3',5'-di-*tert*-butylphenyl) cycloeicosa[b]cycloeicosa[5,6]pyrazino[2,3-g]quinoxaline (**106**), a dark brown solid. $\upsilon_{max}(CHCl_3)$ 3400 (NH), 2964, 1791 and 1734 (OCOCO), 1724 (COCO), 1594, 1476, 1464, 1364, 1296, 1265, 1069; λ_{max} (CH_2Cl_2)/nm ($\log(\varepsilon/dm^3mol^{-1}cm^{-1})$) 319 (4.67), 429 (5.34), 450 (5.35), 561sh (4.55), 605sh (4.55), 656 (4.25), 717 (4.25), 754 (3.91); ^{1}H n.m.r. (400 MHz; $CDCl_3$) δ: -1.91 (2H, br s, NH), -1.38 (2H, br s, NH), 1.51 (36H, s, *t*-butyl H), 1.52 (36H, s, *t*-butyl H), 1.57 (36H, s, *t*-butyl H), 1.58 (36H, s, *t*-butyl H), 7.75 (2H, dd, $J_{2',4'} = J_{6',4'} = 1.75$ Hz, C(4')H), 7.76 (4H, d, $J_{4',2'} = J_{4',6'} = 2.10$ Hz, C(2')H and C(6')H), 7.79 (2H, dd, $J_{2',4'} = J_{6',4'} = 1.75$ Hz, C(4')H), 7.89 (4H, d, $J_{4',2'} = J_{4',6'} = 1.85$ Hz, C(2')H and C(6')H), 7.97 (2H, dd, $J_{2',4'} = J_{6',4'} = 1.80$ Hz, C(4')H), 7.99 (2H, m, aryl H), 8.00 (2H, d, $J_{4',2'} = J_{4',6'} = 2.10$ Hz, C(2')H and C(6')H), 8.01 to 8.02 (4H, m, aryl H), 8.49 (2H, dd, $J_{\beta,\beta} = 5.15$ Hz, $J_{NH,\beta} = 2.10$ Hz, β-pyrrolic H), 8.55 (2H, m, bridging H), 8.65 (2H, dd, $J_{\beta,\beta} = 4.85$ Hz, $J_{NH,\beta} = 1.75$ Hz, β-pyrrolic H), 8.68 (2H, dd, $J_{\beta,\beta} = 4.85$ Hz, $J_{NH,\beta} = 1.70$ Hz, β-pyrrolic H), 8.74 (1H, dd, $J_{\beta,\beta} = 5.45$ Hz, $J_{NH,\beta} = 1.75$ Hz, β-pyrrolic H), 8.76 (1H, dd, $J_{\beta,\beta} = 5.00$ Hz, $J_{NH,\beta} = 1.70$ Hz, β-pyrrolic H); COSY shows coupling between the NH at -1.91 and the β-pyrrolic protons around 8.65 and 8.75 ppm, and also between the NH at -1.38 and the β-pyrrolic protons around 8.50 and 8.65 ppm; *m/z* (MALDI-TOF from a dithranol matrix) 2328.3 (MH^+, 25%), 2330.3 ($(MH+2H)^+$, 100%); $C_{158}H_{182}N_{12}O_5$ requires 2328.4 (MH^+).

9.7 Experimental Details for Chapter Seven

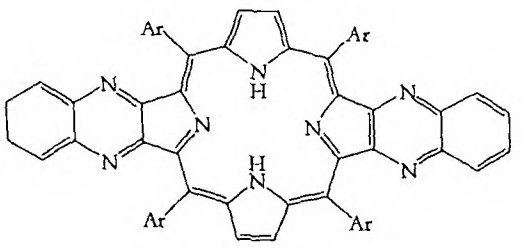

(**108**)

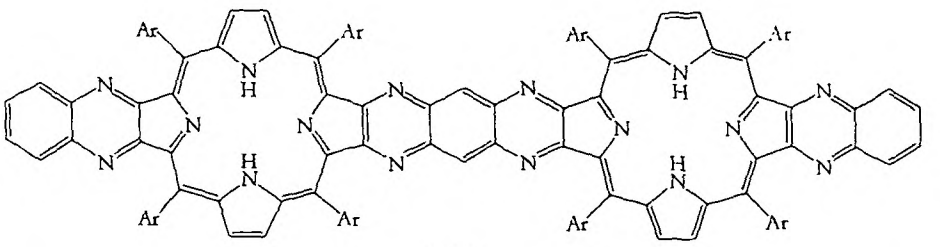

(**109**)

Ar = 3,5-di-*tert*-butylphenyl

[5,10,15,20,25,30,35,40-octakis(3',5'-di-*tert*-butylphenyl)cycloeicosa[b]cycloeicosa[5,6] pyrazino[2,3-g]quinoxalino]bis-zinc(II) (107)

5,10,15,20,25,30,35,40-octakis(3',5'-di-*tert*-butylphenyl)cycloeicosa[b]cycloeicosa[5,6] pyrazino[2,3-g]quinoxaline (**14**) (126 mg, 0.057 mmol) and zinc diacetate dihydrate (291 mg, 1.3 mmol) were dissolved in dichloromethane (25 ml) and methanol (5 ml) were heated to reflux for 2½ hours. Solvent was removed and the product was re-crystallized from dichloromethane/ methanol. The product was identified as [5,10,15,20,25,30,35,40-octakis(3',5'-di-*tert*-butylphenyl)cycloeicosa[b]cycloeicosa[5,6]pyrazino[2,3-g]quinoxalino]bis-zinc(II) (**107**) (114 mg, 86%) by having an identical ^{1}H NMR and LDI mass spectrum to those of an authentic sample[81].

5,10,15,20-tetrakis(3',5'-di-*tert*-butylphenyl)bis-quinoxalino[2,3-b],[12,13-b]porphyrin (108)

2,3,12,13-tetraoxo-5,10,15,20-tetrakis(3',5'-di-*tert*-butylphenyl)porphyrin (**23**) (85 mg, 0.076 mmol) and 1,2-diaminobenzene (247 mg, 2.3 mmol) were dissolved in dichloromethane (20 ml) and stirred for 5 hours. The solvent was removed and the product was purified by column chromatography (1:3 dichloromethane: light petroleum). The poor solubility of the product in dichloromethane was noted during purification. The only main band was identified as 5,10,15,20-tetrakis(3',5'-di-*tert*-butylphenyl)bis-quinoxalino[2,3-b],[12,13-b] porphyrin (**108**) (39 mg, 45%), a dark brown solid. υ_{max}(KBr) 3387 (NH), 2962, 1595, 1477, 1363, 1298, 1247, 1224, 1153, 1107, 901, 877, 801, 763, 699; λ_{max} (CH_2Cl_2)/nm (log(ε/dm^{-3}mol^{-1}cm^{-1})) 253 (4.46), 287 (4.25), 353 (4.44), 395sh (4.71), 448 (5.26), 534 (4.24), 567 (3.69), 614 (4.01), 668 (3.96); ^{1}H n.m.r. (400 MHz; $CDCl_3$) δ: -2.45 (2H, br s, NH), 1.53 (72H, s, *t*-butyl H), 7.77 to 7.79 (4H, m, quinoxalino H), 7.86 to 7.89 (4H, m, quinoxalino H), 7.98 (4H, dd $J_{2',4'} = J_{6',4'} = 1.80$ Hz, C(4')H), 8.03 (8H, d, $J_{4',2'} = J_{4',6'} = 1.55$ Hz, C(2')H

and C(6')H), 9.14 (4H, d, $J_{NH,\beta}$ = 1.80 Hz, β-pyrrolic H); COSY shows the coupling between the NH protons and the β-pyrrolic protons; m/z (LDI-TOF) 1266.3 (M^+, 100%); $C_{88}H_{98}N_8$ requires 1266.8 (M^+).

5,10,15,20,25,30,35,40-octakis(3',5'-di-*tert*-butylphenyl)bis-quinoxalino[2,3-b], [22,23-b]cycloeicosa[b]cycloeicosa[5,6]pyrazino[2,3-g]quinoxaline(109)

2,3,22,23-tetraoxo-5,10,15,20,25,30,35,40-octakis(3',5'-di-*tert*-butylphenyl)cycloeicosa[b] cycloeicosa[5,6]pyrazino[2,3-g]quinoxaline(**21**) (34 mg, 0.015 mmol) and 1,2-diaminobenzene (65 mg, 0.60 mmol) were dissolved in dichloromethane (15 ml) and stirred for 5 hours. Solvent was removed and the product was purified by column chromatography (1:2 dichloromethane: light petroleum). The main band was identified as 5,10,15,20,25,30,35,40-octakis(3',5'-di-*tert*-butylphenyl)bis-quinoxalino[2,3-b],[22,23-b]cycloeicosa[b]cycloeicosa[5,6] pyrazino[2,3-g]quinoxaline (**109**) (27 mg, 78%), a dark brown solid. υ_{max}(KBr) 3391 (NH), 2961, 1595, 1477, 1363, 1297, 1248, 1206, 1156, 1114, 1077, 801, 762; λ_{max} (CH_2Cl_2)/nm (log(ε/dm^{-3}mol^{-1}cm^{-1})) 257 (4.65), 344 (4.55), 440 (5.27), 471 (5.37), 545sh (4.67), 623sh (3.89), 646 (4.05), 687sh (3.62), 700 (3.98); ^{1}H n.m.r. (400 MHz; $CDCl_3$) δ: -2.31 (4H, br s, NH), 1.52 (72H, s, *t*-butyl H), 1.62 (72H, s, *t*-butyl H), 7.76 to 7.78 (4H, m, quinoxalino H), 7.85 to 7.88 (4H, m, quinoxalino H), 7.97 (4H, dd, $J_{2',4'} = J_{6',4'}$ = 1.75 Hz, C(4')H), 8.02 (8H, d, $J_{4',2'} = J_{4',6'}$ = 1.40 Hz, C(2')H and C(6')H), 8.04 (4H, dd, $J_{2',4'} = J_{6',4'}$ = 1.75 Hz, C(4')H), 8.14 (8H, d, $J_{4',2'} = J_{4',6'}$ = 1.40 Hz, C(2')H and C(6')H), 8.64 (2H, s, bridging H), 8.94 and 9.09 (8H, ABX, $J_{\beta,\beta}$ = 4.95 Hz, $J_{NH,\beta}$ = 1.80 Hz, β-pyrrolic H); COSY shows the appropriate β-β pyrrolic couplings and β-pyrrolic-NH couplings; m/z (LDI-TOF) 2455.4 (M^+, 100%); $C_{170}H_{190}N_{16}$ requires 2455.5 (M^+).

9.8 Experimental Details for Chapter Eight

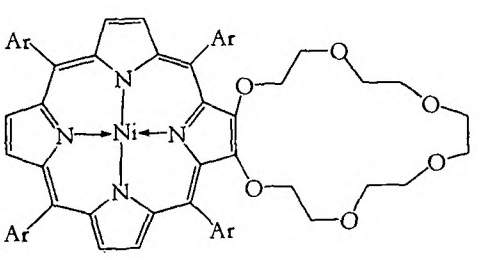

(**110**)

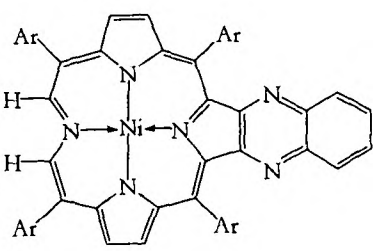

(**112**)

Ar = 3,5-di-*tert*-butylphenyl

[2,3-(2", 5", 8", 11", 14", 17"-hexaoxo-cyclooctadecane)-5,10,15,20-tetrakis(3',5'-di-*tert*-butylphenyl)porphinato]nickel(II) (110)

Sodium hydride (8.8 mg, 0.22 mmol) and potassium tetrafluoroborate (9.25 mg, 0.073 mmol) were dissolved in THF (6 ml), degassed and placed under nitrogen. The system was brought to reflux, and a solution of [2,3-dihydroxy-2,3-dihydro-5,10,15,20-tetrakis(3',5'-di-*tert*-butylphenyl)porphinato]nickel(II) (**69**) (85 mg, 0.074 mmol) and pentaethyleneglycol bis(toluene-*p*-sulfonate) (40 mg, 0.073 mmol) in THF (6 ml) was added over seven hours. Reflux was maintained for a further 14 hours, at which point the system was allowed to cool. Ether (100 ml) and water (100 ml) were added and the organic layer was extracted. This was washed with water (4×100 ml), dried over sodium sulphate and the solvent was removed. The product was purified by column chromatography (dichloromethane, then 1:1 dichloromethane: ethyl acetate). The fourth product eluted with 1:1 dichloromethane: ethyl acetate was identified as [2,3-(2", 5", 8", 11", 14", 17"-hexaoxo-cyclooctadecane)-5,10,15,20-tetrakis(3',5'-di-*tert*-butylphenyl)porphinato]nickel(II) (**110**), (17.9 mg, 18%), a dark red solid. $\upsilon_{max}(CHCl_3)$ 2966, 1593, 1523, 1477, 1394, 1294, 1247, 1100, 1013, 938, 899, 883, 826; λ_{max} (CH_2Cl_2)/nm $(\log(\varepsilon/dm^3mol^{-1}cm^{-1}))$ 289 (4.14), 312sh (4.09), 417 (5.59), 531 (4.14), 567 (3.78); ^{1}H n.m.r. (400 MHz; $CDCl_3$) δ: 1.45 (36H, s, *t*-butyl H), 1.49 (36H, s, *t*-butyl H), 3.45 (2H, t, $J_{crown,\ crown}$ = 5.85 Hz, crown ether H), 3.54 to 3.70 (16H, m, crown ether H), 4.29 (2H, t, $J_{crown,\ crown}$ = 6.05 Hz, crown ether H), 7.66 (1H, dd, $J_{2',4'} = J_{6',4'}$ = 1.95 Hz, C(4')H), 7.68 (2H, d, $J_{4',2'} = J_{4',6'}$ = 1.65 Hz, C(2')H and C(6')H), 7.70 to 7.72 (2H, m, C(4')H), 7.81 (1H, m, C(4')H), 7.85 (2H, d, $J_{4',2'} = J_{4',6'}$ = 2.10 Hz, C(2')H and C(6')H), 7.87 (2H, d, $J_{4',2'} = J_{4',6'}$ = 1.55 Hz, C(2')H and C(6')H), 7.88 (2H, d, $J_{4',2'} = J_{4',6'}$ = 1.75 Hz, C(2')H and C(6')H), 8.70 (1H, d, $J_{\beta\beta}$ = 4.85 Hz, *β*-pyrrolic H), 8.71 (1H, d, $J_{\beta\beta}$ = 4.85 Hz, *β*-pyrrolic H), 8.76 (2H, s, C(12)H and C(13)H), 8.76 (1H, d, $J_{\beta\beta}$ = 5.00 Hz, *β*-pyrrolic H), 8.79 (1H, d, $J_{\beta\beta}$ = 4.95 Hz, *β*-pyrrolic H); the C(7)H, C(8)H, C(17)H and C(18)H have four distinct signals- this suggests that the porphyrin macrocycle might be ruffled; *m*/*z* (LDI-TOF) 1354.3 (MH^+, 100%); $C_{86}H_{110}N_4O_6Ni$ requires 1353.8 (MH^+).

[5,10,15,20-tetrakis(3',5'-di-*tert*-butylphenyl)quinoxalino[2,3-b]*seco*porphinato] nickel(II) (112)

Sodium hydride (60% dispersion in mineral oil) (51 mg, 1.3 mmol) was dissolved in DMSO (30 ml) by stirring it at 80°C under nitrogen for 50 minutes. Heat was removed and benzaldehyde oxime (290 mg, 2.4 mmol) was added. After five more minutes stirring, this was transferred under nitrogen to a solution of [12,13-dibromo-5,10,15,20-tetrakis(3',5'-di-

tert-butylphenyl)quinoxalino[2,3-b]porphinato]nickel(II) (**111**) (150 mg, 0.11 mmol) (prepared by the method of Burn[81]) dissolved in dry THF (distilled over sodium wire) (30 ml). The mixture was heated at reflux under a flowing stream of nitrogen for 20 hours and then allowed to cool. Ether (75 ml) and water (100 ml) were added to the reaction mixture and then the organic layer was extracted and washed with water (5×100 ml), brine (100ml) and dried over sodium sulphate. Solvent was removed and the residue was purified by column chromatography in the dark (1:5 dichloromethane: petroleum spirit). The first band was collected and evaporated to dryness and identified as [5,10,15,20-tetrakis(3',5'-di-*tert*-butylphenyl)quinoxalino[2,3-b]porphinato]nickel(II) (**39**) (10 mg, 8%) by an identical ^{1}H NMR and LDI spectrum as and co-chromatography against an authentic sample. The third band was collected and evaporated to dryness to give [5,10,15,20-tetrakis(3',5'-di-*tert*-butylphenyl)quinoxalino[2,3-b]*seco*porphinato]nickel(II) (**112**) (3.2 mg, 2%), a dark green solid. $\upsilon_{max}(CHCl_3)$ 2966, 1594, 1478, 1364, 1249, 1036, 878; λ_{max} (CH_2Cl_2)/nm $(\log(\varepsilon/dm^3mol^{-1}cm^{-1}))$ 352 (4.53), 405sh (4.61), 442 (4.84), 498sh (4.22), 600 (3.99), 651sh (4.01), 700 (4.35); ^{1}H n.m.r. (400 MHz; $CDCl_3$) δ: 1.42 (36H, s, *t*-butyl H), 1.45 (36H, s, *t*-butyl H), 7.60 (2H, dd, $J_{2',4'} = J_{6',4'} = 1.85$ Hz, C(4')H), 7.67-7.70 (2H, m, quinoxalino H), 7.67 (8H, d, $J_{4',2'} = J_{4',6'} = 1.70$ Hz, C(2')H and C(6')H), 7.72-7.76 (2H, m, quinoxalino H), 7.77 (2H, dd, $J_{2',4'} = J_{6',4'} = 1.85$ Hz, C(4')H), 8.34 and 8.73 (4H, ABq, $J_{A,B} = 5.00$ Hz, C(7)H, C(8)H, C(17)H and C(18)H), 9.81 (2H, s, C(11)H and C(12)H; *m/z* (LDI-TOF) 1196.6 (M^+, 100%); $C_{89}H_{94}N_6Ni$ requires 1196.7 (M^+).

The fourth band was collected and identified as [12-hydroxy-5,10,15,20-tetrakis(3',5'-di-*tert*-butylphenyl)quinoxalino[2,3-b]porphinato]nickel(II) (**40**) (21 mg, 16%) by an identical ^{1}H NMR as and co-chromatography against an authentic sample. The fifth band was collected and identified as [13-oxo-12-oxa-5,10,15,20-tetrakis(3',5'-di-*tert*-butylphenyl)quinoxalino[2,3-b]porphinato]nickel(II) (**43**) (22 mg, 16%) by an identical ^{1}H NMR as and co-chromatography against an authentic sample. The sixth band was collected and identified as [12,13-dioxo-5,10,15,20-tetrakis(3',5'-di-*tert*-butylphenyl)quinoxalino[2,3-b]porphinato] nickel(II) (**41**) (7.4 mg, 6%) by an identical ^{1}H NMR as and co-chromatography against an authentic sample.

9.9 Electrochemistry

9.9.1 Chapter Five electrochemistry

Note that the horizontal and vertical scales are the same for each measurement.

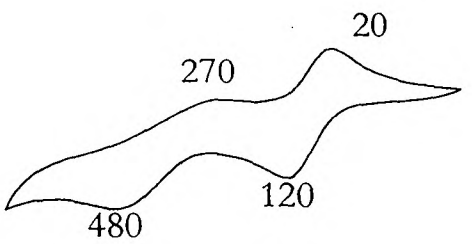

Free-base chlorin **46**

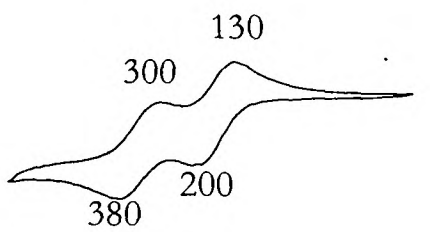

Hydroxy-chlorin **62**

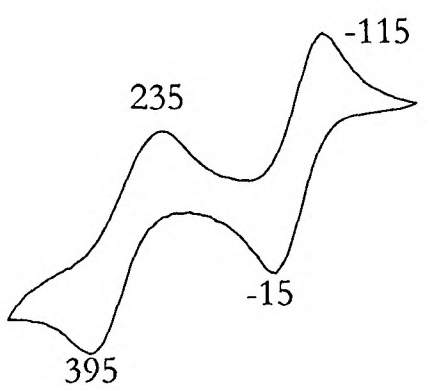

Nickel chlorin **49**

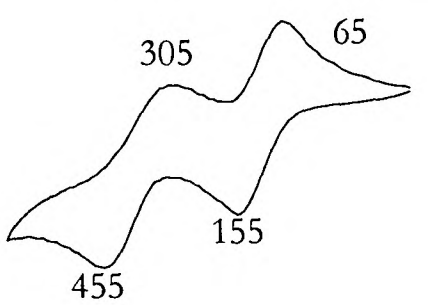

Nickel hydroxy-chlorin **66**

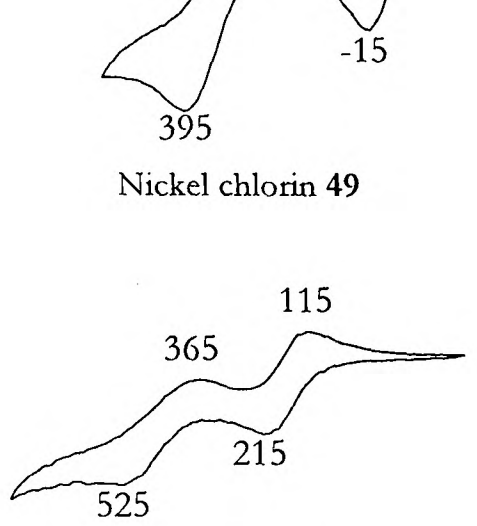

Nickel dihydroxy-chlorin **69**

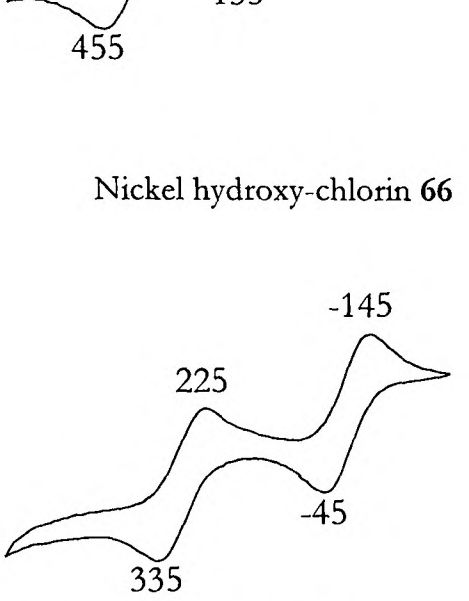

Copper chlorin **50**

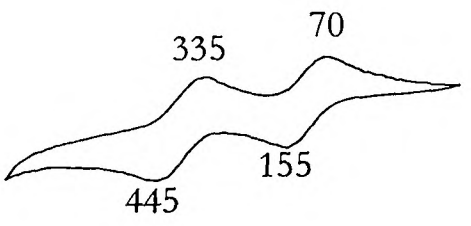

Copper hydroxy-chlorin **67**

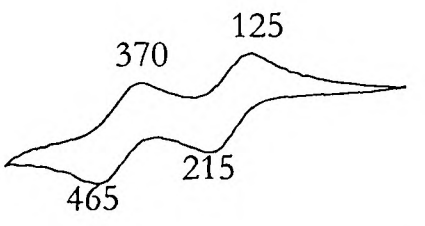

Copper dihydroxy-chlorin **70**

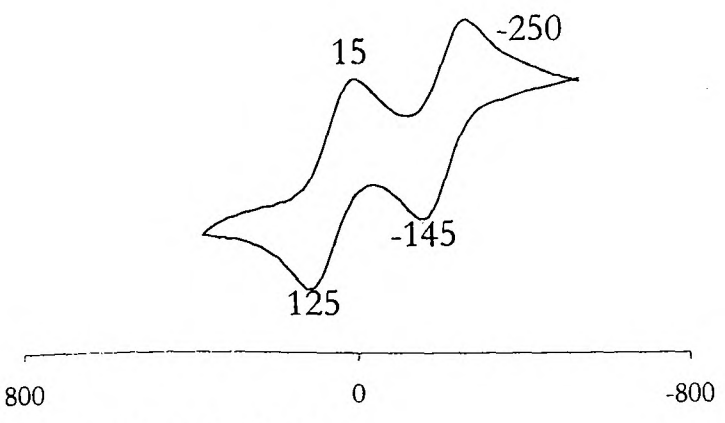

Zinc chlorin **51**

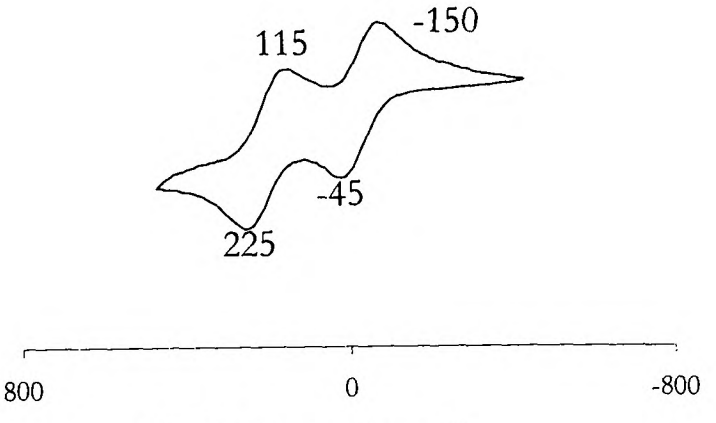

Zinc hydroxy-chlorin **68**

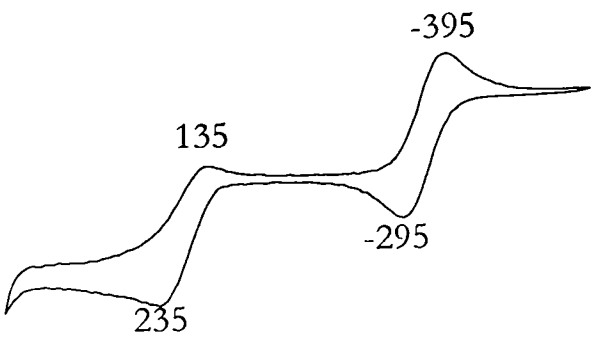

Bacteriochlorin **47**

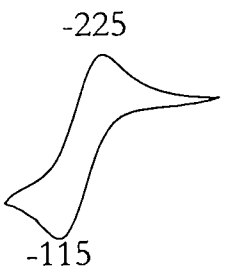

Hydroxy-bacteriochlorin **61**

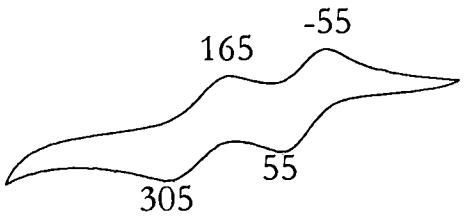

Quinoxalino chlorin **58**

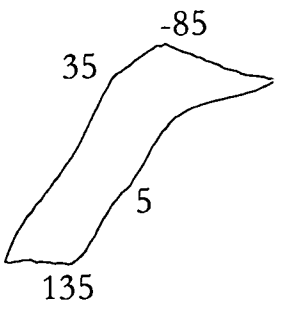

Bis-porphyrin bis-chlorin **60**

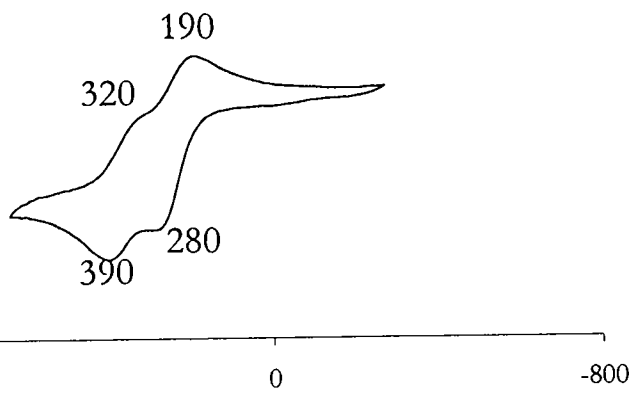

Nitro-chlorin **54**

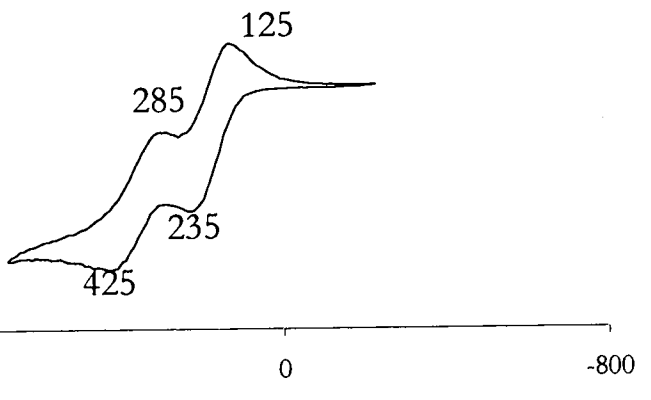

Chloro-chlorin **53**

9.9.2 Chapter Six electrochemistry

Again, the horizontal and vertical scales are the same for each measurement.

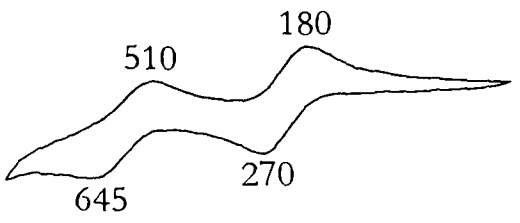

Non-dendritic copper porphyrin **64**

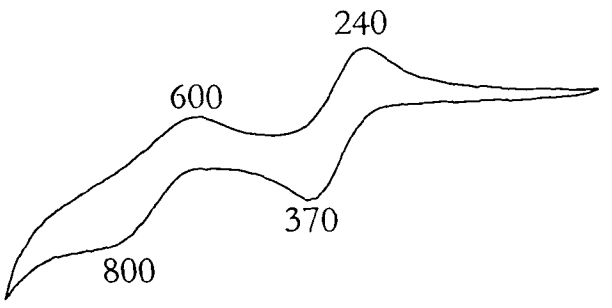

Non-dendritic copper nitro-porphyrin **95**

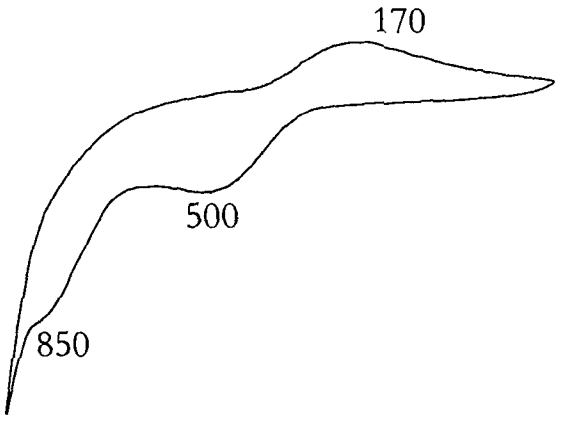

Dendritic copper porphyrin **82**

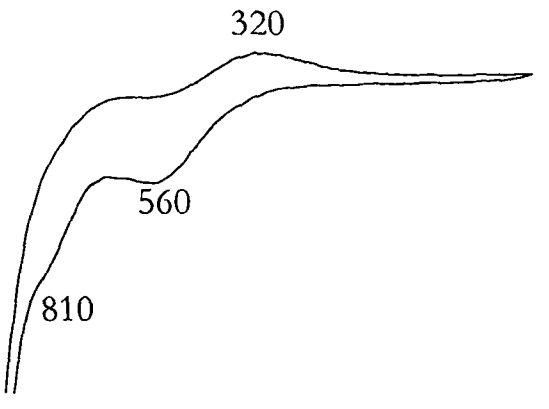

Dendritic copper nitro-porphyrin **85**

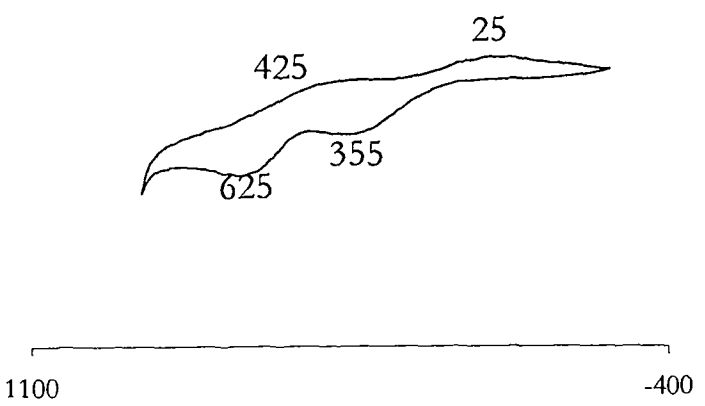

Dendritic zinc porphyrin **83**

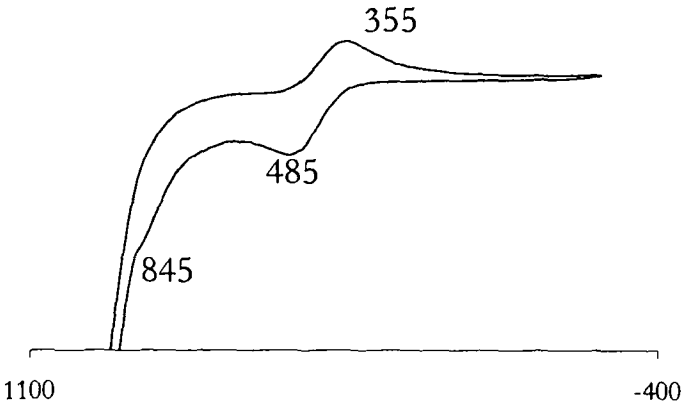

Dendritic nickel porphyrin **81**

Appendix One

Methods of porphyrin characterization

Appendix One
Methods of porphyrin characterization

One of the major challenges of synthetic porphyrin chemistry is to justify the structure of a porphyrin product. This is especially the case for porphyrins since the aim of synthesising a porphyrin is often to study its photophysical and electronic properties, while at the same time these photophysical and electronic properties are used to justify the structure of the product. Therefore it is very useful to examine the methods by which a porphyrin can be characterised, and what conclusions can be drawn from each method.

A1.1 NMR spectroscopy

NMR spectroscopy is a very powerful technique in organic chemistry as a whole, but when applied to synthetic porphyrin systems it can be taken beyond simply examining the nuclear environment and used to learn more about the symmetry of the porphyrin, ring currents around the porphyrin macrocycle that reflect its electronic structure, and even applied to the deduction of the regiochemistry of substitution around the porphyrin periphery. These broad ideas are illustrated by examining the ^{1}H NMR spectrum of two porphyrins (Figure **A1.1**).

The porphyrin **45**'s ^{1}H NMR spectrum is shown in Figure **A1.2**. On initial inspection the spectrum illustrates typical chemical shift values for the different types of protons in the porphyrin. The NHs are significantly shielded well below 0 ppm; the *t*-butyl protons appear at around 1.5 ppm; the aromatic protons on the meso phenyl groups appear around 8 ppm; and finally the β-pyrrolic protons are deshielded at around 9 ppm.

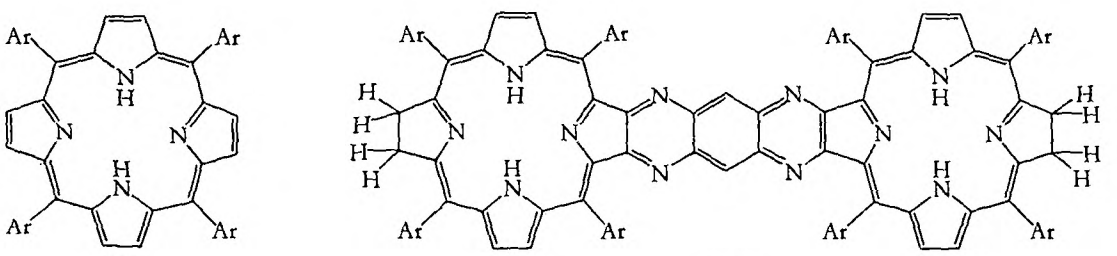

Figure **A1.1**- structures of porphyrins used to illustrate the application of NMR spectroscopy. Ar= 3,5-di-*tert*-butylphenyl.

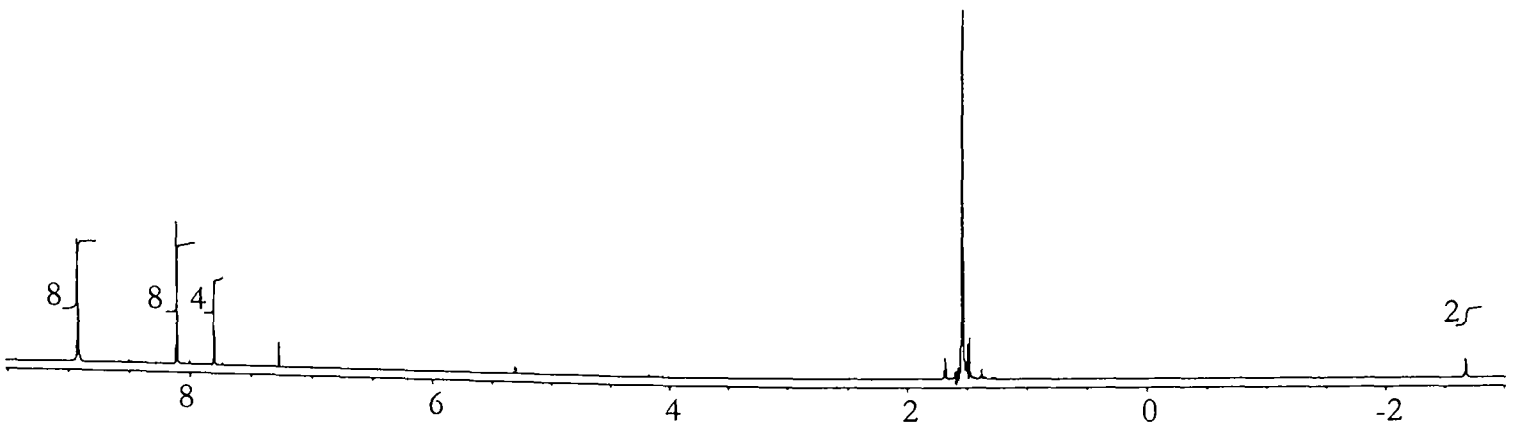

Figure **A1.2**- ^{1}H NMR spectrum of the simple porphyrin **45**

Closer inspection reveals that all eight β-pyrrolic protons appear at the same resonance, whilst in the free-base porphyrin structure there should be two proton environments. This is due to NH tautomerisation occurring faster than the NMR timescale causing a coalescence of the two β-pyrrolic environments[107]:

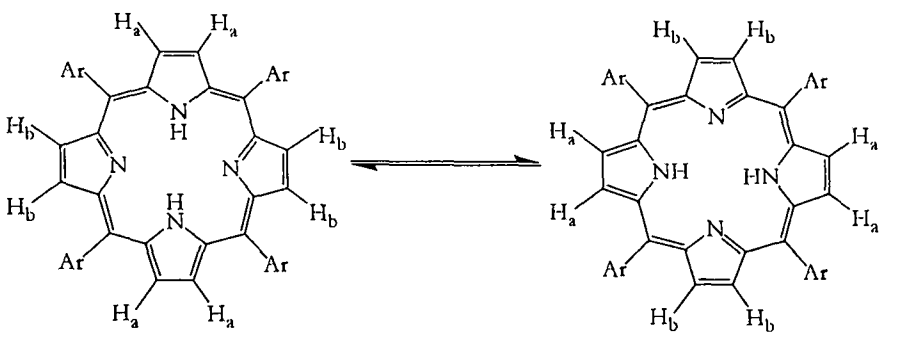

In this way the two β-pyrrolic proton environments appear as one coalesced signal.

Comparing the ^{1}H NMR of the bis-chlorin **60** (Figure **A1.3**) with the porphyrin **45** several differences are immediately apparent:

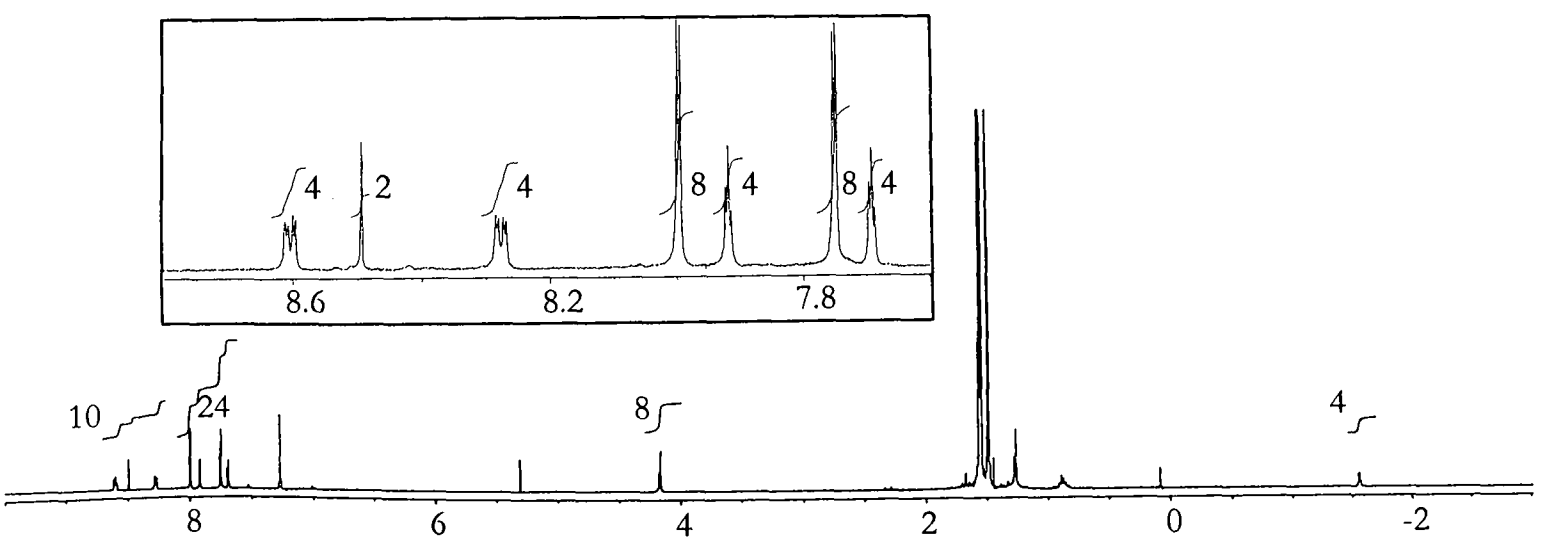

Figure **A1.3**- ^{1}H NMR spectrum of the bis-chlorin **60**. The insert is the expanded region of the unsaturated proton environments.

- Firstly the symmetry of the porphyrin on the NMR timescale has been lowered from an effective D_{4h} to D_{2h}. This means that there are now two different phenyl and three different β-pyrrolic proton environments. It can also be deduced that the porphyrin rings are reduced at antipodal positions to the tetraazaanthracene bridge as reduction at any other position would break the D_{2h} symmetry.
- Then there are two 'new' signals in the ^{1}H spectrum. The first at 4.2 ppm corresponds to the saturated β-pyrrolic environment; the second at 8.5 ppm corresponds to the two protons on the 1,4,5,8-tetraazaanthracene bridge.
- The NH signal is slightly deshielded and the unsaturated β-pyrrolic protons are slightly shielded compared to the simple porphyrin **45**. This reflects a reduction of the ring currents in going from a porphyrin system to a chlorin system.
- Finally NH-β-pyrrolic proton couplings are now clearly visible. As it is known that the NH protons prefer to reside on opposite sides of the inner cavity[107], this can be used as further evidence for the regiochemistry of the position of reduction of the porphyrins, and that the preferred NH tautomer is in fact that shown in Figure **A1.1**.

^{1}H NMR and its associated techniques such as COSY therefore provide invaluable information about the porphyrin macrocycle. ^{13}C NMR however is less useful. This is because in all but the most symmetrical of systems because the many different carbon environments lead to closely packed signals, making it difficult to interpret without further detailed investigations. Therefore in this thesis ^{13}C NMR has only been used to identify particular environments such as the carbon in a carbonyl group.

A1.2 UV-VIS spectroscopy[191] and electrochemistry

UV-VIS spectroscopy is best used to confirm the structure of a porphyrin rather than to identify the structure of an unknown porphyrin. This is because the spectrum depends on the electronic structure of the porphyrin, and subtle changes in electronic effects can have a noticeable impact on the spectrum. To illustrate these effects, the UV-VIS spectra of three porphyrins with varying degrees of symmetry are shown in Figure **A1.5**.

The spectrum of the copper porphyrin **64** appears simple. Two main bands are observed. The Q band is the lowest energy absorption band, and some vibrational structure is observed. By convention the lower energy peak is assigned to the (υ=0) → (υ=0) transition

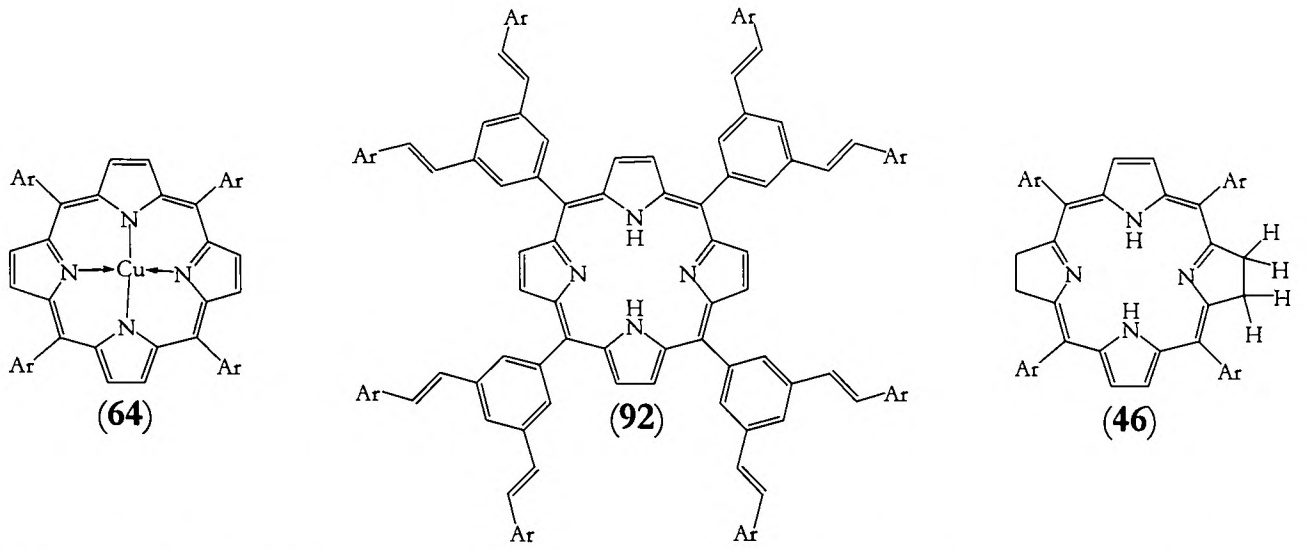

Figure **A1.4**- porphyrin whose UV-VIS spectra are shown in Figure **A1.5**. Ar= 3,5-di-*tert*-butylphenyl.

and is therefore labelled the Q(0,0) band. Similarly the vibrational overtone is labelled the Q(0,1) band. The more intense feature of the spectrum at around 420 nm is called the B band.

The appearance of the two principle bands in the UV-VIS spectrum can be interpreted in terms of a porphyrin's frontier orbitals. A simplistic four orbital model proposed by Gouterman[2] is shown in Figure **A1.6** and its application to a metallated porphyrin is given in

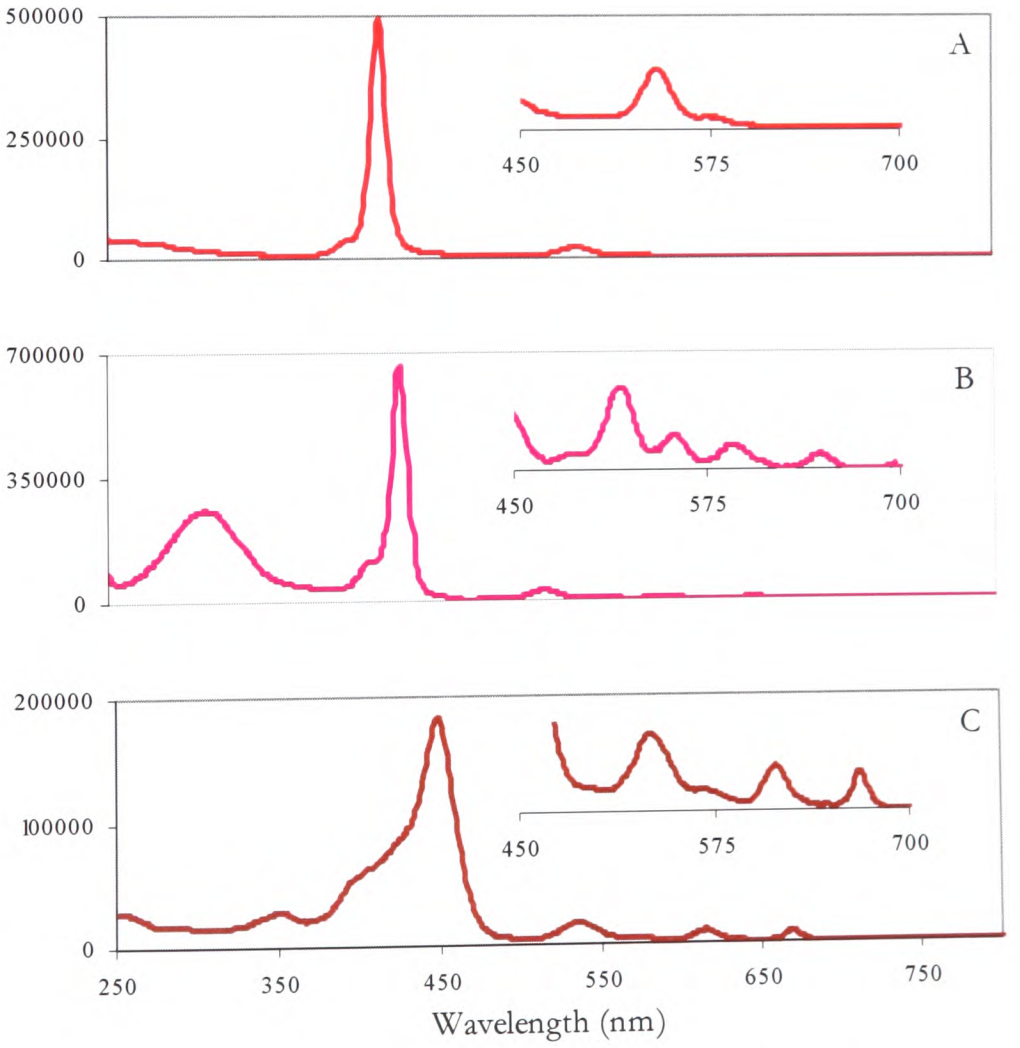

Figure **A1.5**- UV-VIS spectra of the simple copper porphyrin **64** (A), the dendritic free-base porphyrin **92** (B) and the chlorin **46** (C). The vertical axis is the absorbance in units of $dm^3mol^{-1}cm^{-1}$.

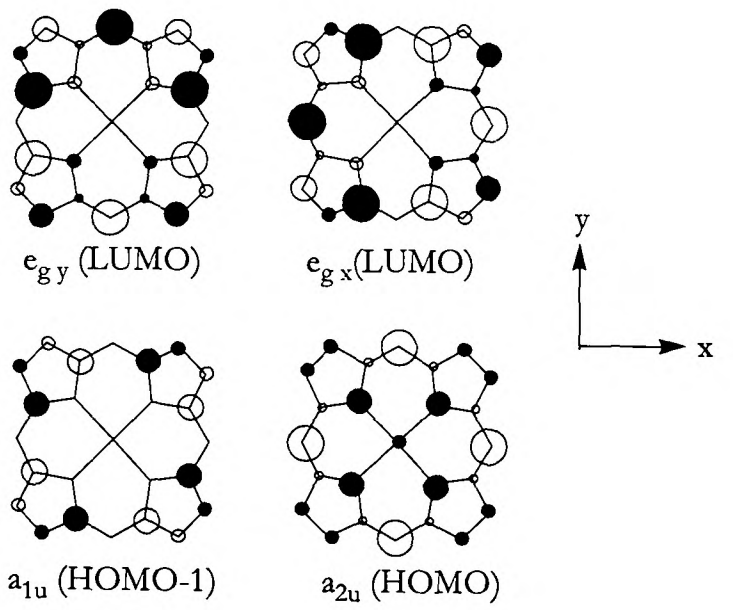

Figure **A1.6**- Gouterman's four orbital model for the frontier orbitals of a porphyrin.

Figure **A1.7**. Gouterman describes the HOMO and (HOMO-1) of such a system as two individual orbitals split slightly in energy, and the LUMO as two degenerate e_g orbitals. The two electronic transitions between the HOMO and LUMO orbitals are of similar energy, so much so that considerable *configurational interaction* leads to the stabilization of the lower energy transition and the destabilization of the higher energy transition. Two bands are therefore apparent in the UV-VIS spectrum, the lower energy 'disallowed' Q band transition and the higher energy 'allowed' B band transition.

On initial inspection, the main difference between the spectrum of the free-base dendritic porphyrin **92** and the copper porphyrin **64** is the characteristic broad absorption of the four dendrons centred around 320 nm. However there is also a more subtle electronic effect at work here. In going from the metallated to the free-base system the symmetry has been lowered from D_{4h} to D_{2h}. This has the consequence of removing the degeneracy of the two

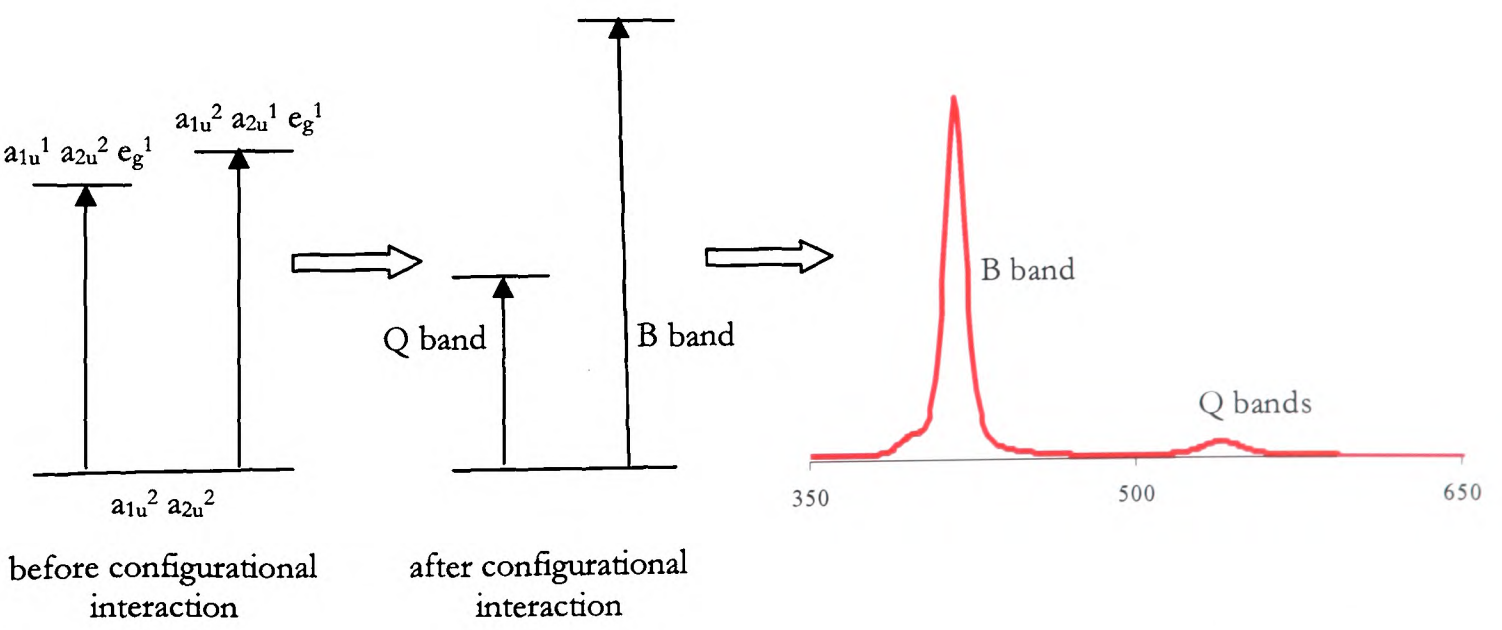

Figure **A1.7**- Gouterman's four orbital model applied to the UV-VIS spectra of a metallated porphyrin.

LUMO orbitals. Thus the transitions from the HOMO and (HOMO-1) are both split into two transitions. Importantly the transition dipole moments associated with these transitions are perpendicular to one another, one orientated in the '*x*' plane of the porphyrin and the other in the '*y*' plane. The two *x*-polarized transitions then undergo configurational interaction, as do the two *y*-polarized transitions. The result of all this is that there are two Q bands of different polarizations, Q_x and Q_y. Gouterman assigned the lower energy Q band to the *x*-polarized transition, where the *x*-axis is orientated along the NH axis. In contrast to the splitting of the Q band, the two 'B' transitions occur at nearly the same energy and only one B transition is apparent in the UV-VIS spectrum.

The UV-VIS spectrum of the chlorin **46** is structurally very similar to that of the free-base dendritic porphyrin **92**. The main difference is the development of a shoulder on the B band absorption. This can be attributed to a further lowering of symmetry in the molecule.

Examining a porphyrin by **electrochemistry** also obtains information about the HOMO and LUMO. However the information gained through electrochemistry rarely matches the information gained through UV-VIS spectroscopy. This is primarily because of the considerable effects of configurational interaction that mean that the lowest energy transition in the UV-VIS spectrum does not itself represent the HOMO-LUMO gap; rather the average energy of the Q and B bands represents the average gap between both the (HOMO-1) and the HOMO and the LUMO[205]. Whereas the electronic states that result from electrochemical oxidation and reduction are not subject to configurational interaction. In addition it must also be considered that electrochemical oxidation and reduction result in the formation of charged species in which there is an incentive of groups attached to the porphyrin, such as phenyl groups in tetraphenyl-porphyrin, to increase their conjugation with the porphyrin[27], and thereby the delocalization of charge, through rotation so that they are more in the plane of the porphyrin ring.

A1.3 Mass spectrometry

Mass spectrometry obtains very useful information for the identification of unknown porphyrin structures. The principle technique is Matrix Assisted Laser Desorption Ionization (MALDI) spectroscopy, although useful information on free-base porphyrins can be also be obtained by electrospray ionization spectroscopy[206]. MALDI is made even more of a useful technique because the best results are often obtained without the use of a matrix[206].

However when certain functional groups are attached to a porphyrin the LDI spectrum becomes complicated. For example the addition of a NO_2 group means that sodium ions are readily picked up by the system even in the presence of a matrix; fragmentation of the nitro group has also been observed. Thus when two nitro-groups are attached to the porphyrin, the parent ion peak in the MALDI spectrum is difficult to identify. Similar complicated spectra are obtained for porphyrin alpha-diones. In addition for alpha-diones and other selected functional groups, a reduction of the porphyrin system can sometimes occur in the ionization process, making the observed parent ion peak two Daltons heavier than it should be[207].

A porphyrin's LDI spectrum is made even more useful as an extra piece of characterization data can be obtained by it, as the comparison of the isotope distribution of the parent ion signal to that of a generated isotope pattern can confirm the elemental composition of the parent ion. An example of this is shown in Figure **A1.8** for the di-nickel(II) dichloro-bis-porphyrin **37**. The spectrum is complicated by the fact that two ions appear to be responsible for the observed isotope pattern, namely the M^+ and $(M+H)^+$ ions. Taking this into consideration the observed isotope pattern seems to be consistent with the proposed molecular structure. Hence when a LDI mass is given it has also been determined that the observed isotope pattern corresponds with the theoretical one.

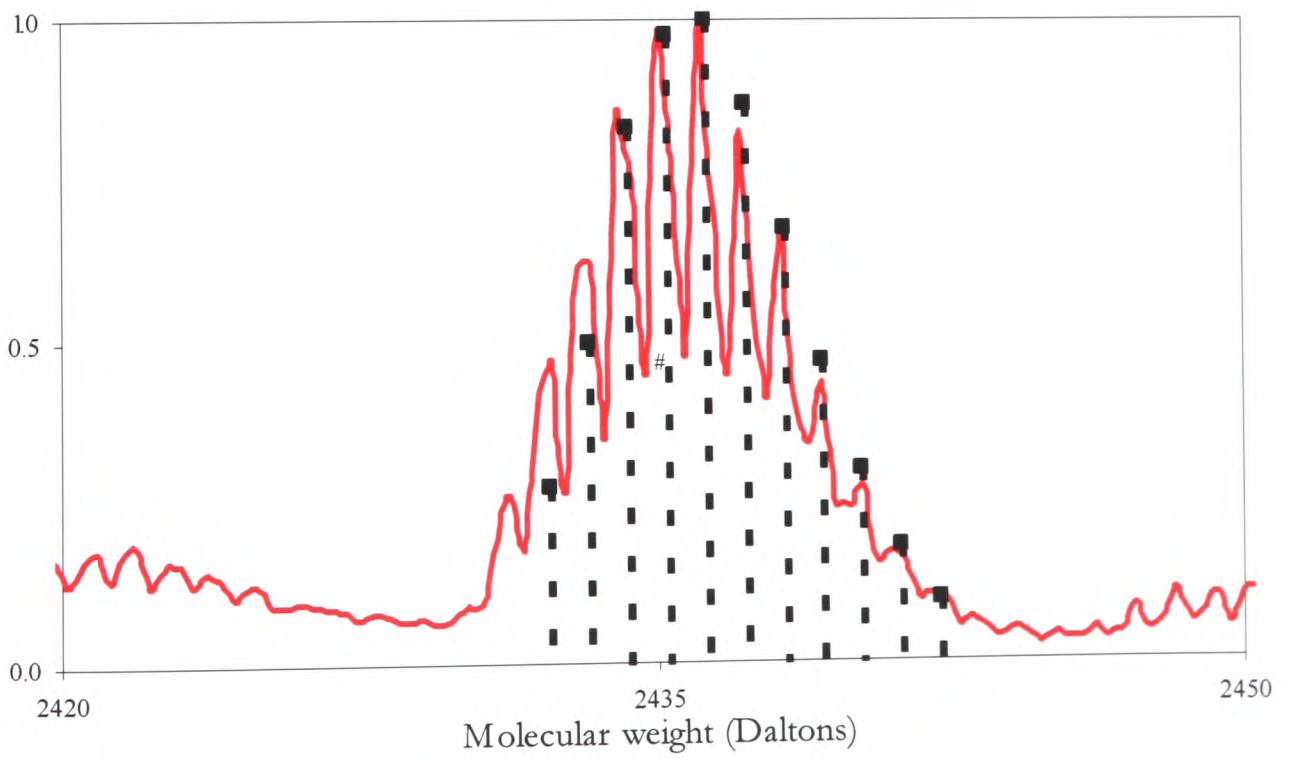

Figure **A1.8**- the LDI spectrum of di-nickel di-chloro bis-porphyrin **37**. The dotted lines show the predicted isotope pattern for the $(M+H)^+$ ion.

A1.4 Other techniques

IR spectroscopy is a useful technique in identifying functional groups attached to a porphyrin. Unfortunately although it is possible to analyze the spectrum in further detail[208], the complexity of the resonances attributed to the porphyrin macrocycle means that this is not practical.

Elemental analysis of porphyrins is a fine art. The porphyrin solid-state structure is particularly good in accommodating solvent molecules in it framework, so much so that zeolite-type structure have been synthesised using a porphyrin motif[209]. It is thought that for this reason samples that have been purified by column chromatography so that they appear as one spot by thin layer chromatography, recrystallised twice from dichloromethane/ methanol and dried for four weeks under high vacuum have still failed their elemental analysis. Therefore in the cases where compounds have passed their elemental analyses this is shown; but a lack of elemental analysis is not necessarily a sign of a poorly purified product.

Appendix Two
Exciton coupling theory

Appendix Two
Exciton coupling theory

When two chromophores are in proximity to one another they can interact either through electronic delocalization mediated by a covalent linkage or through non-covalent dipole-dipole interactions. These dipole-dipole interactions are the focus of exciton coupling theory and they manifest themselves in the chromophores' photophysical properties, in particular in their UV-VIS and fluorescence spectra.

A2.1 Exciton coupling in a dimer[190,210-213]

When a single chromophore is photo-excited from its ground electronic state to an excited state there is necessarily a 'transition dipole moment' associated with the transition. The magnitude of this transition dipole moment corresponds to the observed absorption intensity of the transition. The electronic state of the chromophore that results from this electronic transition consists of a hole residing in the HOMO of the chromophore and an electron residing in the LUMO of the chromophore. The combination of this hole and electron is effectively a hydrogenic state, termed an 'exciton'.

Now, the dipole moment associated with the electronic transition has the ability to interact with its environment, in particular with other dipoles. Hence when a second chromophore is placed in proximity to the first, the transition dipole moment of the first chromophore can interact with and be stabilized or destabilized by the transition dipole moment of the second chromophore, without the requirement of covalent bonding between the two chromophores. In this way the overall electronic transition no longer describes the transition of the single isolated chromophore; rather it becomes a description of the transition of the combination of the two chromophores.

Exciton coupling theory is a description of this combination of electronic states in the electronic transition. If it is assumed that the transition dipole moment of a single chromophore is localized at the centre of the chromophore then the energy of the exciton interaction is given by an expression developed by Kasha:

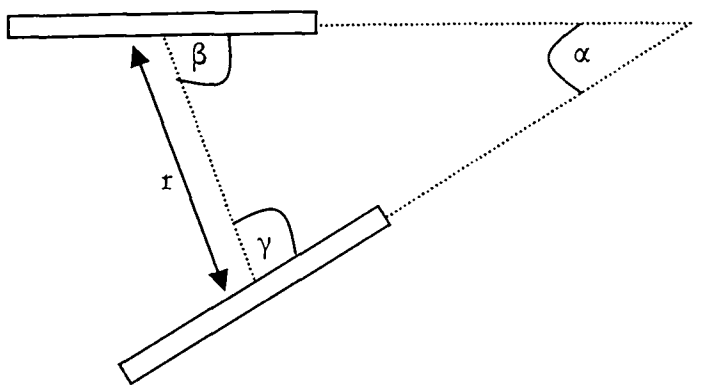

Figure **A2.1**- parameters used for the point-dipole approximation of two interaction chromophores.

$$\Delta E_0 = \frac{2\mu^2(\cos\alpha + 3\cos\beta\cos\gamma)}{r^3} \qquad \text{(equation A2.1)}$$

In this equation ΔE_0 is the energy of interaction of the exciton coupling, μ is the transition dipole moment of the electronic transition, and the other parameters are geometrical parameters given in Figure **A2.1**. When two chromophores are either side-by-side to one another or on top of one another, this equation reduces to:

$$\Delta E_0 = \frac{4\mu^2}{r^3} \qquad \text{(equation A2.2)}$$

To derive these equations it is necessary to separate the electronic and vibrational wavefunctions of the molecules. This requirement corresponds to a 'strong' coupling case (see section **A2.4**).

Whilst the spatial arrangement of the two chromophores is significant in deciding the magnitude of the exciton coupling, the relative orientation of the two transition dipole moments is the crucial factor in determining whether the exciton interaction manifests itself as a stabilization or destabilization in the electronic absorption spectrum. This is because the transition moment of the combined exciton system is given by the sum of the transition moments of the individual components.

To consider the implications of this, two relevant geometries need to be considered. In the first example illustrated in Figure **A2.2** the two transition dipole moments are orientated alongside one another and therefore can adopt a parallel (↑↑) or anti-parallel (↑↓) orientation. Because these arrangements can be considered simply in terms of dipole-dipole interactions, the parallel arrangement is the higher-energy destabilized configuration and the anti-parallel arrangement is the lower-energy stabilized configuration. And because the overall transition moment is given by the sum of the individual components, the parallel arrangement leads to

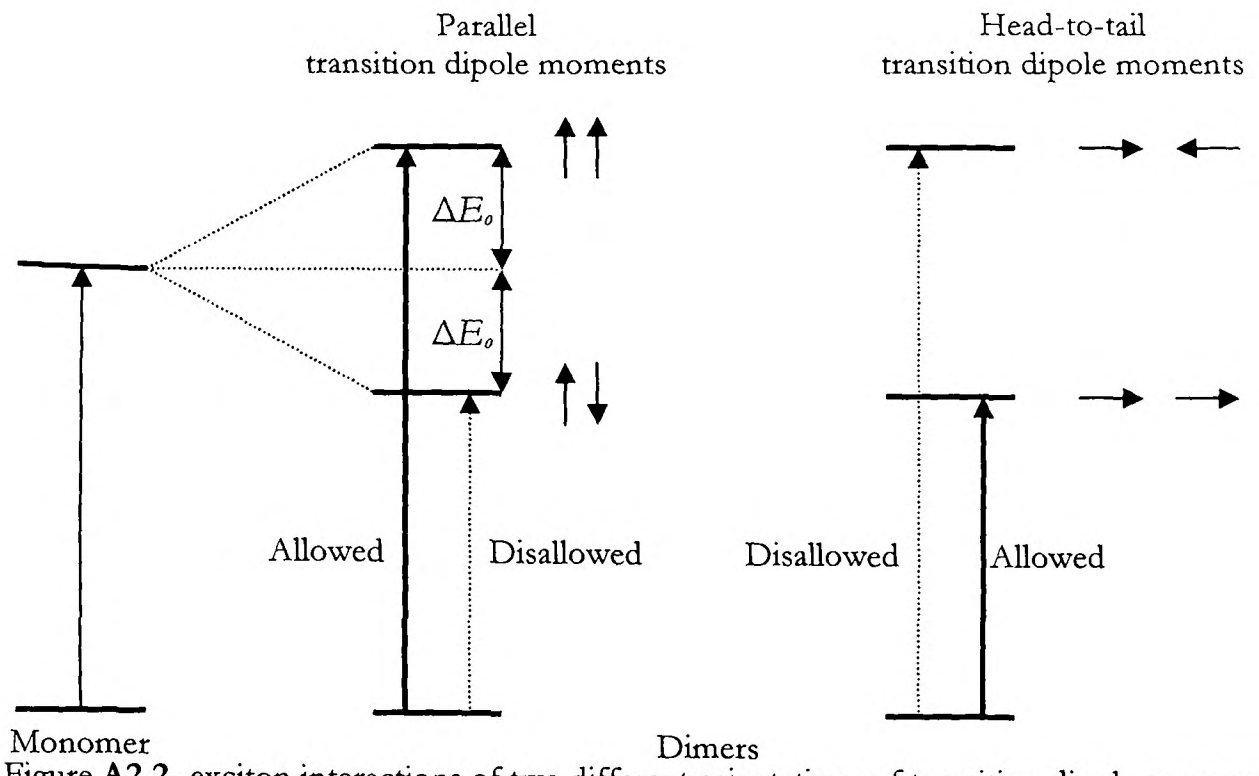

Figure **A2.2**- exciton interactions of two different orientations of transition dipole moments.

an 'allowed' transition whereas the anti-parallel arrangement gives rise to a 'disallowed' transition.

The second example places the two transition dipole moments in a 'head-to-tail' orientation to one another. In this case the allowed transition corresponds to the low-energy configuration (→→) whereas the disallowed transition corresponds to the high-energy configuration (→←).

This simple schematic has direct implications for the interpretation of the electronic spectra of porphyrin aggregates. By geometric necessity if two neighbouring porphyrins in the aggregate are stacked on top of one another (an 'H' aggregate) then their transition dipole moments will adopt a 'parallel' orientation and the electronic spectrum of the aggregate will appear *blue*-shifted compared to the monomer. Whereas if two neighbouring porphyrins are placed side-by-side one another in the same plane (a 'J' aggregate) then a component of their transition dipole moments can adopt a 'head-to-tail' orientation and a proportion of the electronic spectrum appears *red*-shifted compared with the monomer.

A2.2 Exciton coupling in a multi-component system

It might be expected that the electronic spectrum of a multi-component chromophore system would be characterized by a series of electronic transitions ranging from the weakly-

allowed to the strongly-allowed. For example in a trimeric system where the individual components adopt a head-to-tail conformation then it might be expected that the lowest energy transition (→→→) be fully allowed, and the two higher energy transitions (→→← and ←→←) be both weakly allowed. However this is not the case as it is only the fully allowed transition that is observed in the electronic spectrum. This is a consequence of symmetry considerations, defined by the 'Davydov rule' for electric dipole transitions[213] that states: "the number of allowed electric dipole transitions from the ground state to the states of the exciton band will be equal to the number of molecules per unit cell in the molecular aggregate." And in a molecular assembly there is only one molecule per unit cell.

So for a dimer the magnitude of the exciton interaction is given by equation **A2.1**; for a multi-component system the magnitude of the exciton interaction energy of the allowed transition is related to the interaction energy ΔE_0 in the dimer by[193]:

$$\Delta E_N = \Delta E_0 \cos\left(\frac{\pi}{N+1}\right) \qquad \text{Equation } \mathbf{A2.3}$$

where N is the number of chromophores in the molecular system. Hence as the number of components in the system increases, so does the magnitude of the observed exciton interaction. This is applicable in a 'strong coupling' regime (see section **A2.4**); this equation can break down when the magnitude of the exciton coupling becomes less than the spectral bandwidth of the monomer.

A2.3 Exciton coupling in a covalently-bound system[19]

Exciton interactions do not require a covalent interaction between two chromophores. In such a non-covalent situation an exciton can be delocalized over many chromophores, but this delocalization involves the bound exciton state so that the positions of the hole and the electron at any one time correlate closely with one another. This type of tightly-bound exciton is called a '**Frenkel**' exciton.

In multi-chromophore systems that are covalently-linked this type of tightly-bound Frenkel exciton is still very common. However in certain situations, especially where electronic delocalization between two chromophores is significant, the binding of the hydrogenic exciton state becomes less strong. In such a situation this hydrogenic state can itself become delocalized over more than one chromophore, so that the positions of the hole and electron

at any one time no longer strongly correlate with one another. This type of loosely-bound exciton is called a '**Mott-Wannier**' exciton.

In the case of a Mott-Wannier exciton the effect of increasing the number of chromophores in a multi-component array can no longer be described in terms of purely dipole-dipole interactions because of the associated increase in conjugation length and also the possibility of the creation of charge-transfer states. In such situations therefore exciton coupling theory should be applied with caution.

The two different extremes of exciton behaviour are also associated with different kinds of applications:

- **Photonic wires** carry energy from one end of a multi-chromophore array to the other. A Frenkel system is ideal in this situation since it has the ability to carry energy along an array without the dissipation of the energy due to charge separation or other effects.
- **Molecular wires** carry charge from one end of a multi-chromophore array to the other. A Mott-Wannier system is ideal in this situation because it has the ability to easily delocalize the charge and therefore transport it along the length of the array.

A2.4 Deviation from a strong coupling regime[211-213]

In an ideal multi-chromophore system that displays Frenkel-type exciton behaviour, the bound exciton is considered to be delocalized over the whole system. In many molecular systems however the bound exciton is delocalized only over a small number of chromophores. This number of chromophores is described as the 'coherence length' of the system and it is important in determining, for example, the suitability of a multi-chromophore array in exploitation in light-harvesting applications.

This situation describes the intermediacy between a completely 'free' bound exciton and a totally 'localized' bound exciton. This has also been described as the difference between **strong** exciton coupling and **weak** exciton coupling. For exciton coupling to correspond to a 'strong' coupling regime the exciton interaction energy ΔE_0 needs to be much greater than the spectral and vibronic bandwidths of the monomer species. This leads to the Born-Oppenheimer separability of the intramolecular electronic and vibrational wavefunctions. For situations where the coherence length becomes a relevant quantity this condition is not

quite being met, leading to an intermediate regime between the strong and weak exciton coupling regimes. Fortunately it seems that in this intermediate coupling regime equations **A2.1** to **A2.3** can still be applied, so that the magnitude of the exciton coupling is still determined by the properties of the whole molecular system.

It should be noted that this intermediacy between free and localised bound excitons has been previously misinterpreted in terms of the differences between Frenkel and Mott-Wannier excitons[8].

A2.5 Application of exciton coupling theory to photosynthesis[7]

Of the many photosynthetic systems, the best structurally characterized system is that of the purple bacteria. Within its light-harvesting complex there exist two distinct circular systems of porphyrin chromophores. The first is the 'B800' system that consists of 9 chlorophyll pigments set at roughly 18 Ångstroms from one another, whilst the second is the 'B850' system with double the amount of chlorophyll pigments to the B800 system set at half the distance from one another. On photo-excitation, energy transfer occurs within these two systems before it is further transferred to a 'reaction centre' at the centre of the ring systems.

The first conclusion that can be drawn is that excitons formed on photo-excitation will have Frenkel character as the individual chromophores in either system are not directly covalently linked. Within this Frenkel framework it is thought that excitons in the B800 system are essentially localized on one chromophore unit at a time because the large separation of the chromophores reduces the system to the weak exciton coupling regime. However the closer arrangement of the chromophores in the B850 system leads to an intermediate exciton coupling regime so that the bound exciton is delocalized over 4 to 5 chromophore units at a time. In this way the exciton coupling model can lead to greater understanding of the energy-transfer processes occurring in the photosynthetic pathway.

A2.6 Application of exciton coupling theory to Osuka's arrays[193]

Osuka's directly-linked porphyrin arrays excellently illustrate the effects of exciton coupling in synthetic porphyrin systems. In his meso-meso singly-linked arrays two neighbouring chromophores are orientated so that they occupy perpendicular planes to one another and

there therefore exists no ground state electronic delocalization between two neighbouring chromophores. Hence this is a good example of a Frenkel-type exciton system.

The effects of exciton coupling are clearly visible in the UV-VIS spectra of these arrays (Figure **A2.3**). The main effect of moving from the monomer (Z1) to the dimer (Z2) is the splitting of the porphyrin's B band into two components. One component of the dimer remains at the same wavelength as the absorption of the monomer, whilst the second component is red-shifted with respect to the monomer. This can be interpreted in terms of

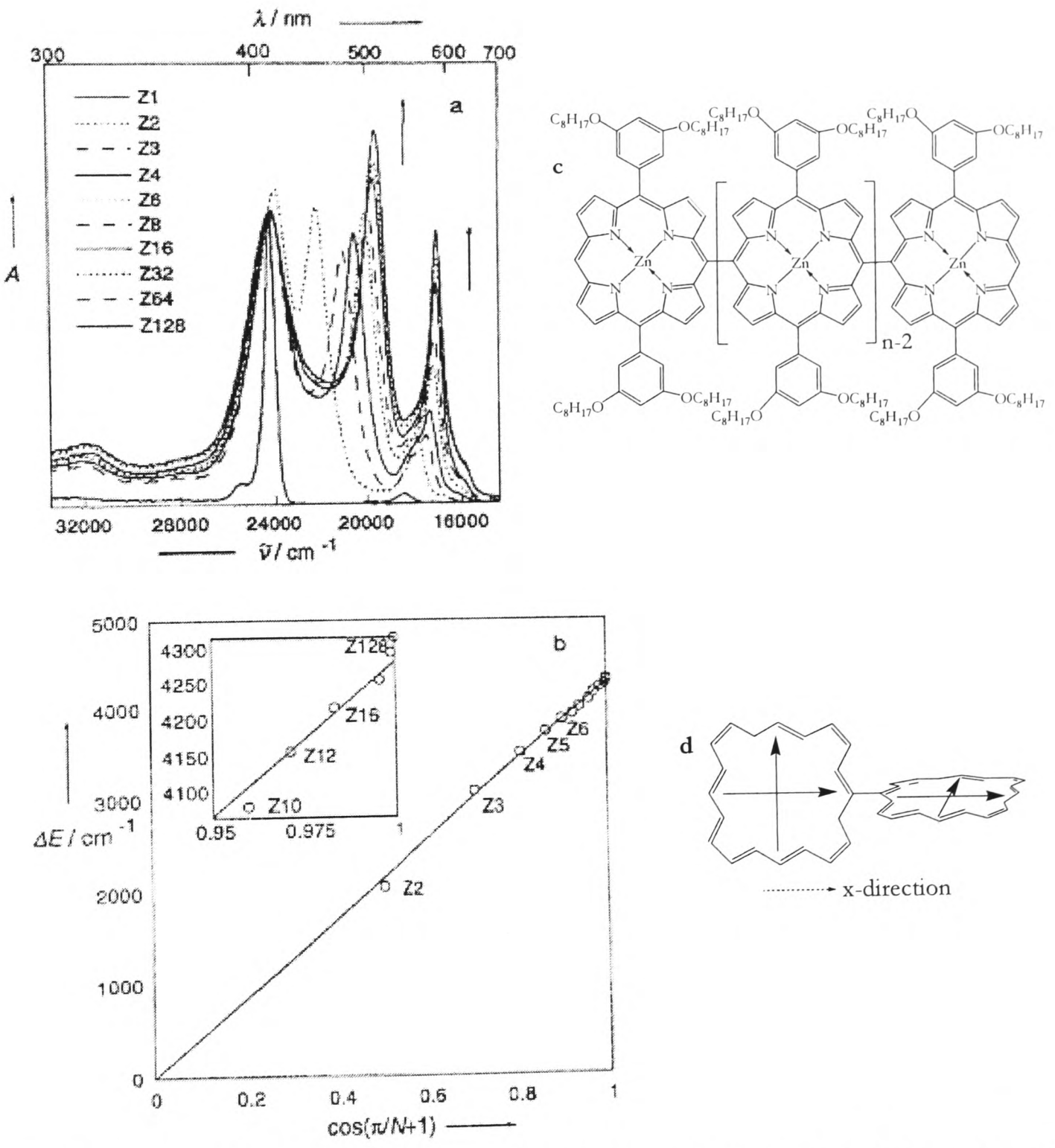

Figure **A2.3**- a) the UV-VIS spectra of Osuka's triply-linked arrays; b) the correlation between the number of units in the array Z(n) and the exciton splitting observed in the B band of the UV-VIS spectrum; c) the chemical structure of Osuka's triply-linked arrays Z(n); and d) the perpendicular orientation of two neighbouring porphyrin units.

the 'head-to-tail' alignment of the *x*-component of the B band leading to the red-shifted component (shown in figure **A2.3d**); whilst the perpendicular orientation of the *y*-components of the B band allows to no excitonic interaction, and therefore the B_y absorption band of the dimer is unshifted with respect to the monomer.

In addition the UV-VIS spectra illustrate the effect of increasing the number of units in the multi-porphyrin array. It is observed that the magnitude of the exciton coupling in the B band correlates well the number of porphyrin units according to equation **A2.3** (Figure **A2.3b**), with a value for ΔE_0 of 4300 cm^{-1} being determined from the gradient of the graph.

A similar interpretation for the red-shift observed in the Q bands leads to a value the exciton coupling of 1150 cm^{-1}. This value is larger than that predicted by a point-dipole model, but this is not wholly surprising due to the close proximity of neighbouring porphyrins. It is also noticed that the relative intensity of the Q band increases with the number of porphyrin units in the array. This can also be explained in terms of the exciton interactions, as intensity transfer between the B and Q band transition dipole moments can be mediated by exciton interactions[192].

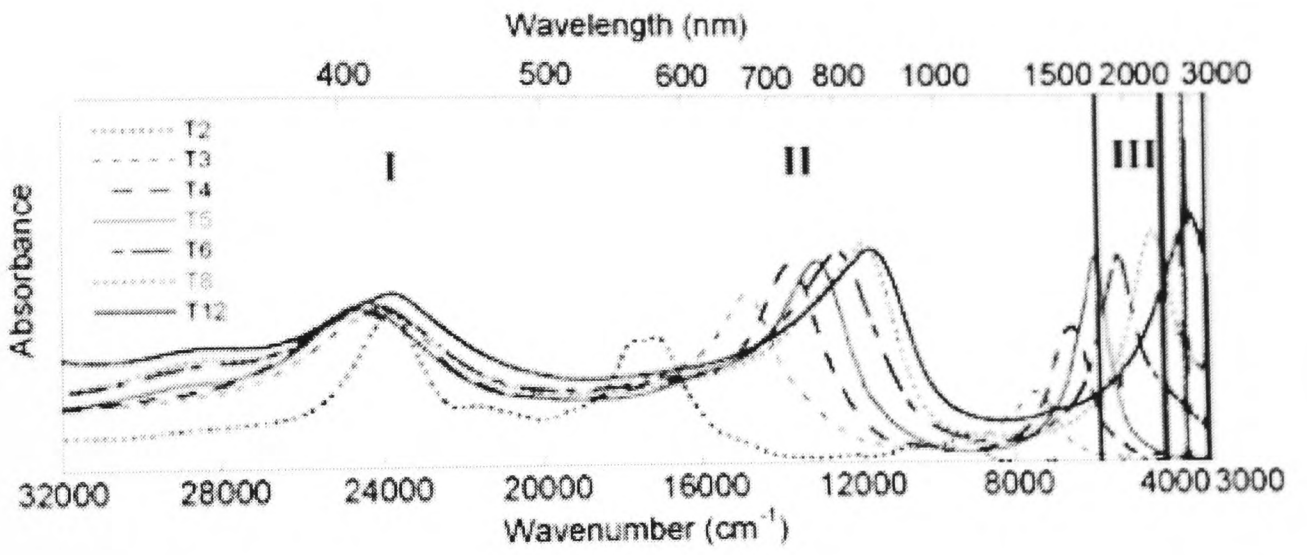

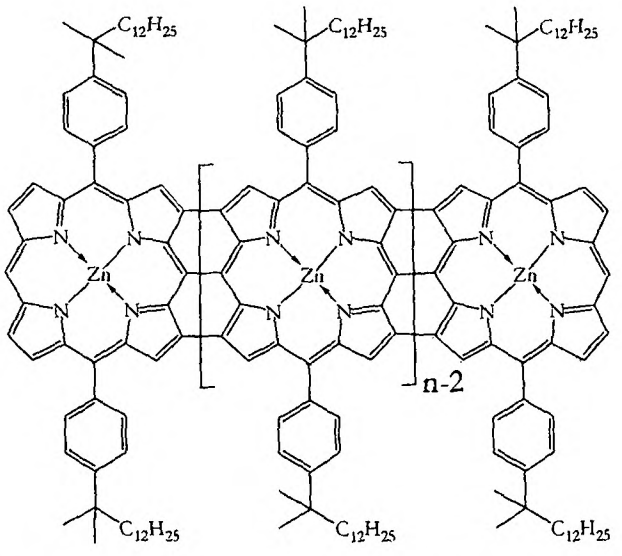

Figure **A2.4**- the UV-VIS spectra of Osuka's meso-meso, *β*-*β*, *β*-*β* triply-linked arrays, T(n), whose structure is shown underneath.

Further investigation into the properties of these arrays suggests that they possess a coherence length of four to five units, very similar to that observed for the B850 photosystem.

Osuka's triply-linked arrays have amazing properties (Figure **A2.4**). It is clear from their UV-VIS spectra that there is extreme conjugation between neighbouring porphyrin units, implying that excitons formed on photo-excitation will possess Mott-Wannier character. Whilst the splitting of the B band, labelled as bands I and II, can be interpreted in terms of an exciton model, the position of the third band cannot. This emphasises that equations **A2.1** to **A2.3** should be applied with care when electronic delocalization exists between neighbouring chromophore units.

References

References

Chapter One- Introduction

General references

1. D. Dolphin, in the *General Preface* to *The Porphyrins*, Ed. D. Dolphin, (Academic Press, New York, 1978), vol.1, pp. xiii.

This used to be the most comprehensive review on porphyrin chemistry, until 'The Porphyrin Handbook' was published in 2000. Sir Walter Raleigh's quote and the reference to red-blooded Englishmen is taken from its preface.

2. H. Fischer, in the citation for: *his Nobel Prize in Chemistry for his researches into the constitution of haemin and chlorophyll and especially for his synthesis of haemin,* (1930).

3. R. B. Woodward, W. A. Ayer, J. M. Beaton, F. Bickelhaupt, R. Bonnett, P. Buchschacher, G. L. Closs, H. Dutler, J. Hannah, F. P. Hauck, S. Ito, A. Langemann, E. LeGoff, W. Leimgruber, W. Lwowski, J. Sauer, Z. Valenta, H. Volz, *J. Am. Chem. Soc.* **82**, 3800-3802 (1960).

The original paper for the synthesis of chlorophyll.

4. J. W. Steed, J. L. Atwood, in *Supramolecular Chemistry* (Wiley, Chichester, UK, 2000) pp. 35-86.

A good general introduction to supramolecular chemistry.

5. D. C. Hodgkin, in the citation for: *her Nobel Prize for chemistry for her determinations by X-ray techniques of the structures of important biochemical substances* (1964).

6. M. G. H. Vicente, K. M. Smith, *Curr. Org. Chem.* **4**, 139-174 (2000).

A surprisingly broad review of porphyrin chemistry, particularly good as an introduction to synthesis and functionalization.

Porphyrin arrays

7. T. Pullerits, V. Sundstrom, *Acc. Chem. Res.* **29**, 381-389 (1996).

One of the many perspectives on the photosynthetic system.

8. P. D. Harvey, in *The Porphyrin Handbook*, Eds. K. M. Kadish, K. M. Smith, R. Guilard, (Elsevier Science, San Diego, 2003), vol. 18, pp. 63-250.

A very broad review of porphyrin arrays from The Porphyrin Handbook.

9. A. K. Burrell, D. L. Officer, P. G. Plieger, D. C. W. Reid, *Chem. Rev.* **101**, 2751-2796 (2001).

A slightly different view on porphyrin arrays. This one is slightly more focused on synthetic aspects

10. Y. Sakakibara, S. Okutsu, T. Enokida, T. Tani, *Thin Solid Films* **363**, 29-32 (2000).

11. C. M. Drain, R. Fischer, E. G. Nolen, J.-M. Lehn, *J. Chem. Soc., Chem. Commun.*, 243-245 (1993).

12. A. Tsuda, S. Sakamoto, K. Yamaguchi, T. Aida, *J. Am. Chem. Soc.* **125**, 15722-15723 (2003).

13. D. Sun, F. S. Tham, C. A. Reed, L. Chaker, P. D. W. Boyd, *J. Am. Chem. Soc.* **124**, 6604-6612 (2002).

14. C. M. Drain, J.-M. Lehn, *J. Chem. Soc., Chem. Commun.*, 2313-2315 (1994).

15. C. M. Drain, F. Nifiatis, A. Vasenko, J. D. Batteas, *Angew. Chem. Int. Ed.* **37**, 2344-2347 (1998).

16. H. Imahori, D. M. Guldi, K. Tamaki, Y. Yoshida, C. Luo, Y. Sakata, S. Fukuzumi, *J. Am. Chem. Soc.* **123**, 6617-6628 (2001).

17. H. Imahori, *Org. Biomol. Chem.* **2**, 1425-1433 (2004).

18. H. Imahori, Y. Sekiguchi, Y. Kashiwagi, T. Sato, Y. araki, O. Ito, H. Yamada, S. Fukuzumi, *Chem. Eur. J.* **10**, 3184-3196 (2004).

19. J. J. Piet, P. N. Taylor, B. R. Wegewijs, H. L. Anderson, A. Osuka, J. M. Warman, *J. Phys. Chem. B* **105**, 97-104 (2001).

20. A. Osuka, N. Tanabe, S. Nakajima, K. Maruyama, *J. Chem. Soc., Perkin Trans. 2*, 199-203 (1996).

21. N. Aratani, A. Osuka, Y. H. Kim, D. H. Jeong, D. Kim, *Angew. Chem. Int. Ed.* **39**, 1458-1462 (2000).

22. N. Aratani, A. Osuka, *The Chemical Record* **3**, 255-234 (2003).

23. A. Osuka, H. Shimidzu, *Angew. Chem. Int. Ed.* **36**, 135-137 (1997).

24. A. Osuka, paper presented at *the International Conference of Porphyrins and Phthalocyanines (ICPP-3)*, New Orleans, 2004.

25. J.-H. Ha, H. S. Cho, J. K. Song, D. Kim, N. Aratani, A. Osuka, *ChemPhysChem* **5**, 57-67 (2003).

26. P. N. Taylor, H. L. Anderson, *J. Am. Chem. Soc.* **121**, 11538-11545 (1999).

27. H. L. Anderson, *Chem. Commun.*, 2323-2330 (1999).

28. K.-i. Sugiura, Y. Fujimoto, Y. Sakata, *Chem. Commun.*, 1105-1106 (2000).

29. A. Kato, K.-i. Sugiura, H. Miyasaka, H. Tanaka, T. Kawai, M. Sugimoto, M. Yamashita, *Chem. Lett.* **33**, 578-579 (2004).

30. M. G. H. Vicente, L. Jaquinod, K. M. Smith, *Chem. Commun.*, 1771-1782 (1999).
A general overview of Kevin Smith's porphyrin arrays.

31. M. G. H. Vicente, M. T. Cancilla, C. B. Lebrilla, K. M. Smith, *Chem. Commun.*, 2355-2356 (1998).

32. R. Paolesse, L. Jaquinod, F. D. Sala, D. J. Nurco, L. Prodi, M. Montalti, C. D. Natale, A. D'Amico, A. D. Carlo, P. Pugli, K. M. Smith, *J. Am. Chem. Soc.* **122**, 11295-11302 (2000).

33. H. Uno, K. Kuroki, H. Yamada, N. Ono, paper presented at *the International Conference of Porphyrins and Phthalocyanines (ICPP-3)*, New Orleans, 2004.

34. S. Ito, K.-i. Nakamoto, H. Uno, T. Murashima, N. Ono, *Chem. Commun.*, 2696-2697 (2001).

35. M. J. Crossley, P. L. Burn, *J. Chem. Soc., Chem. Commun.*, 39-40 (1987).
Synthesis and characterization of the 1,4,5,8-tetraazaanthracene-bridged bis-porphyrin.

36. M. J. Crossley, P. L. Burn, *J. Chem. Soc., Chem. Commun.*, 1569-71 (1991).
Synthesis and characterization of the non-dendritic tetramer.

37. V. Promarak, *Porphyrin Arrays* (DPhil thesis), Oxford University (2002).

38. S. C. Narang, S. Ventura, (General Petrochemical Industries Ltd., Japan), *U.S. patent number:* 4,908,442, (submitted in 1988, published in 1990), 15 pp.
This is a patent, so has not been peer-reviewed as such.

39. S. C. Narang, S. Ventura, T. R. Bhardwaj, (General Petrochemical Industries Ltd., Japan), *U.S. patent number:* 5,091,502, (submitted in 1990, published in 1992), 19 pp., Cont.-in-part of U.S. 4,908,442.
As for the previous reference, this is has not been peer-reviewed as such.

40. A. Tsuda, A. Osuka, *Adv. Mat.* **14**, 75-79 (2002).

41. A. Tsuda, A. Osuka, *Science* **293**, 79-82 (2001).

42. H. S. Cho, D. H. Jeong, S. Cho, D. Kim, Y. Matsuzaki, K. Tanaka, A. Tsuda, A. Osuka, *J. Am. Chem. Soc.* **124**, 14642-14654 (2002).

43. J. Morgado, R. Cacialli, R. H. Friend, R. Iqbal, G. Yahioglu, L. R. Milgrom, S. C. Moratti, A. B. Holmes, *Chem. Phys. Lett.* **325**, 552-558 (2000).

44. H. Segawa, K. Kunimoto, K. Susumu, M. Taniguchi, T. Shimidzu, *J. Am. Chem. Soc.* **116**, 11193-11194 (1994).

45. Y. Kim, M. F. Mayer, S. C. Zimmerman, *Angew. Chem. Int. Ed.* **42**, 1121-1126 (2003).

46. K.-i. Sugiura, H. Tanaka, T. Matsumoto, T. Kawai, Y. Sakata, *Chem. Lett.*, 1193-1194 (1999).
Sugiura's masochistic porphyrin dendrimer.

Field Effect Transistors

47. C. D. Dimitrakopoulos, P. R. L. Malenfant, *Adv. Mat.* **14**, 99-117 (2002).
The first of four good reviews.

48. G. Horowitz, *Adv. Mat.* **10**, 365-377 (1998).
The second of four good reviews.

49. H. E. Katz, Z. Bao, *J. Phys. Chem. B* **104**, 671-678 (2000).
Another good review.

50. H. E. Katz, Z. Boa, S. L. Gilat, *Acc. Chem. Res.* **34**, 359-369 (2001).
The final review- by the same people as the previous one.

51. A. Dodabalapur, L. Torsi, H. E. Katz, *Science* **268**, 270-271 (1995).

52. S. F. Nelson, Y. Y. Lin, D. J. Gundlach, T. N. Jackson, *Appl. Phys. Lett.* **72**, 1854-1856 (1998).

53. P. T. Herwig, K. Mullen, *Adv. Mat.* **11**, 480-483 (1999).

54. See *www.polymervision.com.*

55. A. Assadi, C. Svensson, M. Willander, O. Inganas, *Appl. Phys. Lett.* **53**, 195-197 (1988).

56. J. Paloheimo, H. Stubb, P. Yli-Lahti, P. Kuivalainen, *Synth. Met.* **41-43**, 563-566 (1991).

57. H. Sirringhaus, P. J. Brown, R. H. Friend, M. M. Nielsen, K. Bechgaard, B. M. W. Langeveld-Voss, A. J. H. Spiering, R. A. J. Janssen, E. W. Meijer, P. T. Herwig, D. M. d. Leeuw, *Nature* **401**, 685-688 (1999).

58. H. E. Katz, A. J. Lovinger, J. Johnson, C. Kloc, T. Siergist, W. Li, Y.-Y. Lin, A. Dodabalapur, *Nature* **404**, 478-481 (2000).

59. M. Halik, H. Klauk, U. Zschieschang, G. Shmid, S. Ponomarenko, S. Kirchmeyer, W. Weber, *Adv. Mat.* **15**, 917-922 (2003).

60. A. R. Murphy, J. M. Frechet, P. Chang, J. Lee, V. Subramanian, *J. Am. Chem. Soc.* **126**, 1596-1597 (2004).

61. Z. Bao, A. J. Lovinger, A. Dodabalapur, *Adv. Mat.* **9**, 42-44 (1997).

62. C. Calcavento, G. Conte, S. Salvatori, R. Paolesse, M. Berliocchi, A. D. Carlo, P. Lugli, A. Sassella, *Synth. Met.* **138**, 255-260 (2003).

63. P. Checcoli, G. Conte, S. Salvatori, R. Paolesse, A. Bolognesi, M. Berliocchi, F. Brunetti, A. D'Amico, A. D. Carlo, P. Lugli, *Synth. Met.* **138**, 261-266 (2003).

64. Y.-Y. Noh, J.-J. Kim, K. Yase, S. Nagamatsu, *Appl. Phys. Lett.* **83**, 1243-1245 (2003).

65. S. Aramaki, Y. Sakai, N. Ono, *Appl. Phys. Lett.* **84**, 2085-2087 (2004).

66. N. Ono, Y. Shimizu, H. Uno, paper presented at *the International Conference of Porphyrins and Phthalocyanines (ICPP-3),* New Orleans, 2004.

67. H. Sirringhaus, R. Kawase, R. H. Friend, T. Shimoda, M. Inbasekaran, W. Wu, E. P. Woo, *Nature* **290**, 2123 (2000).

68. M. Halik, H. Klauk, U. Zschieschang, G. Schmid, C. Dehm, M. Schutz, S. Maisch, F. Effenberger, M. Brunnbauer, F. Stellacci, *Nature* **431**, 963-966 (2004).

69. J. Collet, O. Tharaud, A. Chapoton, D. Vuillaume, *Appl. Phys. Lett.* **76**, 1941-1943 (2000).

70. C. Dimitrakopoulos, S. Purushothamn, J. Kymissis, A. Callegari, J. M. Shaw, *Science* **283**, 822-824 (1999).

'Single molecule' devices

71. J. Nygard, D. H. Cobden, P. E. Lindelof, *Nature*, 342-346 (2000).

72. S. J. Tans, A. R. M. Verschueren, C. Dekker, *Nature* **393**, 49-52 (1998).

73. H. Park, J. Park, A.K.L.Lim, E. H. Anderson, A. P. Alivisatos, P. L. McEuen, *Nature* **407**, 57-60 (2000).

74. W. Liang, M. P. Shores, M. Bockrath, J. R. Long, H. Park, *Nature* **417**, 725-729 (2002).

75. J. Park, A. N. Pasupathy, J. I. Goldsmith, C. Chang, Y. Yaish, J. R. Petta, M. Rinkoski, J. P. Sethna, H. D. Abruna, P.L.McEuen, D. C. Ralph, *Nature* **417**, 722-725 (2002).

76. N. B. Zhitenev, H. Meng, Z. Bao, *Phys. Rev. Lett.* **88**, 226801-1 to 4 (2002).

77. S. Kubatkin, A. Danilov, M. Hjort, J. Cornil, J.-L. Bredas, M. Stuhr-Hansen, P. Hedegard, T. Bjornholm, *Nature* **425**, 698-701 (2003).

78. D. H. Yoon, S. B. Lee, K.-H. Yoo, J. Kim, J. K. Lim, N. Aratani, A. Tsuda, A. Osuka, D. Kim, *J. Am. Chem. Soc.* **125**, 11062-11064 (2003).
This is Osuka's demonstration of the electrical conductivity of porphyrin arrays.

Porphyrin array- meso versus □-pyrrolic substitution

79. V. S.-Y. Lin, M. J. Therien, *Chem. Eur. J.* **1**, 645-651 (1995).
It should be noted that in fact Dennis Arnold published the first account of alkyne-linked porphyrin arrays- and as Arnold is willing to point out, many of the ideas that Therien presents in this paper and his Science paper are by no means original. Harry Anderson was also publishing his work on alkyne-linked arrays at a similar time.

80. V. S.-Y. Lin, S. G. DiMango, M. J. Therien, *Science* **264**, 1105-1111 (1994).

1,4,5,8-tetraazaanthracene bridged porphyrin arrays and porphyrin functionalizations

81. P. L. Burn, *Porphyrin Annelations*, PhD thesis, University of Sydney (1989).
Paul's original PhD thesis.

82. M. J. Crossley, L. J. Govenlock, J. K. Prashar, *J. Chem. Soc., Chem. Commun.*, 2379-2380 (1995).
Max Crossley's synthesis of the single porphyrin tetra-one, combined with its two step condensation to make various porphyrin arrays.

83. C. Bruckner, D. Dolphin, *Tet. Lett.* **36**, 9425-9428 (1995).

84. C. Bruckner, D. Dolphin, *Tet. Lett.* **36**, 3295-3298 (1995).

85. H. W. Daniell, S. C. Williams, H. A. Jenkins, C. Bruckner, *Tet. Lett.* **44**, 4045-4049 (2003).
Bruckner started his work under David Dolphin's guidance, and here presents the polished product. Heather Daniell's now working for Harry Anderson.

86. R. D. Knudsen, H. R. Snyder, *J. Org. Chem.* **39**, 3343-3346 (1974).

87. R. Beavington, P. A. Rees, P. L. Burn, *J. Chem. Soc., Perkin Trans. 1*, 2847-2852 (1998).

88. M. J. Crossley, P. L. Burn, S. J. Langford, S. M. Pyke, A. G. Stark, *J. Chem. Soc., Chem. Commun.*, 1567-1568 (1991).

89. V. Promarak, P. L. Burn, *J. Chem. Soc., Perkin Trans. 1*, 14-20 (2001).

90. M. J. Crossley, L. G. King, *J. Chem. Soc., Chem. Commun.*, 920-922 (1984).
'Novel' oxidation products from the oxidation of the porphyrin macrocycle.

91. S. D. Starnes, D. M. Rudkevich, J. Rebek Jr., *J. Am. Chem. Soc.* **123**, 4659-4669 (2001).
Rebek's demonstration of the use of porphyrins as a supramolecular framework- and the synthesis of the single porphyrin tetra-one using osmium tetroxide.

Chapter Two- regiospecific halogenation of a porphyrin

Regiospecific functionalizations

92. L. Jaquinod, in *The Porphyrin Handbook* K. M. Kadish, K. M. Smith, R. Guilard, Eds. (Academic Press, 2000), vol. 1, pp. 202-237.
This is THE review of the functionalization of meso-substituted porphyrins.

93. K. M. Shea, L. Jaquinod, R. G. Khoury, K. M. Smith, *Tet.* **56**, 3139-3144 (2000).

94. J. E. Baldwin, M. J. Crossley, J. DeBernardis, *Tet.* **38**, 685-692 (1982).
Jack Baldwin (working with Max Crossley!) in the probably original synthesis of a porphyrin *alpha*-dione- via the nitration of a capped free-base porphyrin.

Halogenations

95. H. J. Callot, *Tet. Lett.* **50**, 4987-4990 (1973).

96. M. J. Crossley, P. L. Burn, S. S. Chew, F. B. Cuttance, I. A. Newsom, *J. Chem. Soc., Chem. Commun.*, 1564-1566 (1991).

97. L. Jaquinod, R. G. Khoury, K. M. Shea, K. M. Smith, *Tet.* **55**, 13151-13158 (1999).

98. Y. Terazono, D. Dolphin, *J. Org. Chem.* **68**, 1892-1900 (2003).

99. Y. Terazono, B. O. Patrick, D. H. Dolphin, *Inorg. Chem.* **41**, 6703-6710 (2002).

100. P. Ochsenbein, K. Ayougou, D. Mandon, J. Fischer, R. Weiss, R. N. Austin, K. Jayaraj, A. Gold, J. Terner, J. Fajer, *Angew. Chem. Int. Ed.* **33**, 348-350 (1994).

101. M. G. H. Vicente, K. M. Smith, *Tet.* **47**, 6887-6894 (1991).

102. R. Bonnett, I. H. Campion-Smith, A. N. Kozyrev, A. F. Mironov, *J. Chem. Research (M)* **5**, 1012-1043 (1990).

103. W. Su, K. Gossett, P. A. Fleitz, paper presented at *the International Conference of Porphyrins and Phthalocyanines (ICPP-3)*, New Orleans, 2004.

104. T. Wijesekera, A. Matsumoto, D. Dolphin, D. Lexa, *Angew. Chem. Int. Ed.* **29**, 1028-1030 (1990).

105. T. Wijeskera, D. Dupre, M. S. R. Cader, D. Dolphin, *Bull. Soc. Chim. Fr.* **133**, 765-775 (1996).

106. R. W. Boyle, C. K. Johnson, D. Dolphin, *J. Chem. Soc., Chem. Commun.*, 527-528 (1995).

Physical and theoretical investigations of the porphyrin macrocycle

107. M. J. Crossley, M. M. Harding, S. Sternhell, *J. Am. Chem. Soc.* **108**, 3608-3613 (1986).

108. C. Bruckner, J. R. McCarthy, H. W. Daniell, Z. D. Pendon, R. P. Ilagan, T. M. Francis, L. Ren, R. R. Birge, H. A. Frank, *Chem. Phys.* **294**, 285-303 (2003).
The molecular orbital diagrams for the simple chlorin and the porphyrin *alpha*-dione

109. J. R. Reimers, L. E. Hall, M. J. Crossley, N. S. Hush, *J. Phys. Chem. A* **103**, 4385-4397 (1999).
A full molecular orbital treatment for the bis-porphyrin system.

110. M. J. Crossley, P. J. Sintic, R. Walton, J. R. Reimers, *Org. Biomol. Chem.* **1**, 2777-2787 (2003).
A molecular orbital picture of the quinoxaline.

The reaction of polyaromatic hydrocarbons with ICl

111. S. M. Hubig, W. Jung, J. K. Kochi, *J. Org. Chem.* **59**, 6233-6244 (1994).

112. D. E. Turner, R. F. O'Malley, D. J. Sardella, L. S. Barinelli, P. Kaul, *J.Org. Chem.* **59**, 7335-7340 (1994).

Chapter Three- Nucleophilic attack on a halo-porphyrin

Hydroxylations with benzaldehyde oxime

113. M. J. Crossley, L. G. King, S. M. Pyke, *Tet.* **43**, 4569-4577 (1987).

114. R. Beavington, *Porphyrin Arrays,* DPhil thesis, University of Oxford (1997).

115. P. A. Rees, *Porphyrin Functionalization,* Part II thesis, University of Oxford (1996).

$S_{RN}1$ reactions and other porphyrin dehalogenation reactions

116. J. F. Bunnett, *Acc. Chem. Res.* **25**, 2-9 (1992).
Bunnett is the 'daddy' of $S_{RN}1$ reactions, and this is a great review.

117. J. K. Kim, J. F. Bunnett, *J. Am. Chem. Soc.* **92**, 7463-7464 (1970).

118. J. A. Zoltewicz, T. M. Oestreich, A. A. Sale, *J. Am. Chem. Soc.* **97**, 5889-5896 (1975).

119. J. A. Zoltewicz, A. A. Sale, *J. Org. Chem.* **35**, 3462-3467 (1970).

120. M. J. Crossley, J. J. Gosper, M. G. Wilson, *J. Chem. Soc., Chem. Commun.*, 1798-1799 (1985).
Reductive denitration of a β-nitro-porphyrin with 2-thio-aniline.

121. M. J. Crossley, M. M. Harding, C. W. Tansey, *J. Org. Chem.* **59**, 4433-4437 (1994).
Includes the reductive denitration of a β-nitro-porphyrin with *t*-BuMgBr.

122. M. J. Crossley, L. G. King, *J. Chem. Soc., Perkin Trans. 1: Org. Bio. Chem.*, 1251-1260 (1996).

123. Y. Terazono, D. Dolphin, *J. Org. Chem.* **68**, 1892-1900 (2003).

124. O. Siri, K. M. Smith, *Tet. Lett.* **44**, 6103-6105 (2003).

125. F. D'Souza, A. Villard, E. V. Caemelbecke, M. Franzen, T. Boschi, P. Tagliatesta, K. M. Kadish, *Inorg. Chem.* **32**, 4042-4048 (1993).

-SMe products originating from reactions in DMSO

126. J. Clews, A. D. M. Curtis, H. Malkin, *Tet.* **56**, 8735-8746 (2000).

127. R. L. Soulen, J. R. Griffith, *J. Fluorine Chem.* **44**, 195-202 (1989).

128. G. C. Finger, L. D. Starr, D. R. Dickerson, H. S. Guutowsky, J. Hamer, *J. Org. Chem.* **28**, 1666-1668 (1963).

129. J. E. Rowe, K. Lee, D. D. Dolliver, J. E. Johnson, *Aust. J. Chem.* **52**, 807-811 (1999).

130. Y. H. Zhu, P. Lu, H. Lou, X. M. Zheng, *Chinese Chem. Lett.* **14**, 235-238 (2003).

131. F. M'Halla, J. Pinson, J. M. Saveant, *J. Electroanal. Chem.* **89**, 347-361 (1978).

132. F. M'Halla, J. Pinson, J. M. Saveant, *J. Am. Chem. Soc.* **102**, 4120-4127 (1980).

133. S. E. Korostova, A. I. Mikhaleva, S. G. Shevchenko, M. V. Sigalov, V. Y. Vitkovsky, *Sulfur Lett.* **5**, 39-46 (1986)

Nucleophilic displacement versus electron transfer

134. A. Pross, *Acc. Chem. Res.* **18**, 212-219 (1985).

135. L. Eberson, *Electron Transfer Reactions in Organic Chemistry* (Springer, Heidelberg, 1987).

136. G. N. Sastry, D. Danovich, S. Shaik, *Angew. Chem. Int. Ed.* **35**, 1098-1100 (1996).

Oxidation potentials of benzaldehyde oxime anions

137. F. G. Bordwell, Y. Zhao, J.-P. Cheng, *J. Phys. Org. Chem.* **11**, 10-14 (1998).

The role of charge transfer complexes in organic reaction pathways

138. J. K. Kochi, *Acc. Chem. Res.* **25**, 39-47 (1992).
Kochi is the main advocate in favour of charge transfer complexes.

139. L. Eberson, F. Radner, *Acc. Chem. Res.* **20**, 53-59 (1987).

140. E. K. Kim, J. K. Kochi, *J. Am. Chem. Soc.* **113**, 4962-4974 (1991).

141. A. Peluso, G. D. Re, *J. Phys. Chem.* **100**, 5303-5309 (1996).

142. D. Lenoir, *Angew. Chem. Int. Ed.* **42**, 854-857 (2003).

143. S. V. Rosokha, J. K. Kochi, *J. Org. Chem.* **67**, 1727-1737 (2002).

144. P. Sepulcri, R. Goumont, J.-C. Halle, E. Buncel, F. Terrier, *Chem. Commun.*, 789-790 (1997).

145. R. Bacaloglu, A. Blasko, C. A. Bunton, F. Ortega, C. Zucco, *J. Am. Chem. Soc.* **114**, 7708-7718 (1992).

Chapter Four- Introduction to chlorins

Photodynamic therapy

146. R. Ackroyd, C. Kelty, N. Brown, M. Reed, *Photochem. Photobio.* **74**, 656-669 (2001).

147. M. G. H. Vicente, *Curr. Med. Chem.- Anti-Cancer Agents* **1**, 175-194 (2001).
Vicente used to be Kevin Smith's chief PostDoc.

Synthesis of chlorins

148. H. W. Whitlock Jr., R. Hanauer, M. Y. Oester, B. K. Bower, *J. Am. Chem. Soc.* **91**, 7485-7489 (1969).

149. M. S. Somma, F. Denat, L. Jaquinod, K. M. Smith, *Abstr. Gen. Meet. Am. Chem. Soc.* March 21-25, INOR 130 (1999).

150. Y. Harel, J. Manassen, *J. Am. Chem. Soc.* **100**, 6228-6234 (1978).
Note that the photo-reaction of triethylamine with a porphyrin results in the addition of $HCH(CH_3)N(CH_2CH_3)_2$ across one of the β-pyrrolic positions. Purification of this product over silica led to the isolation of a hydroxy-chlorin product.

Chapter Five- The allylic oxidation of chlorins

Identification of biliverdin products

151. J. A. S. Cavaleiro, M. J. E. Hewlins, A. H. Jackson, G. P. M. S. Neves, *J. Chem. Soc., Chem. Commun.*, 142-144 (1986).
The 'correct' identification of biliverdin-type products- c.f. Ref. 165.

The oxidation of chlorins by alumina

152. M. Taniguchi, H.-J. Kim, D. Ra, J. K. Shwartz, C. Kirmaier, E. Hindin, J. R. Diers, S. Prathapan, D. F. Bocian, D. Holten, J. S. Lindsey, *J. Org. Chem.* **67**, 7329-7342 (2002).

153. D. H. Burns, Y. H. Li, D. C. Shi, M. O. Delaney, *Chem. Commun.*, 1677-1678 (1998).

Biliverdin formation as an indicator of a SET mechanism

154. O. Ongayi, F. R. Fronczek, M. G. H. Vicente, *Chem. Commun.*, 2298-2299 (2003).

Possible role of singlet oxygen and/or photoactivation in the oxidation

155. R. Koerner, M. M. Olmstead, A. Ozarowski, A. L. Balch, *Inorg. Chem.* **38**, 3262-3263 (1999).

156. R. Koerner, M. M. Olmstead, A. Ozarowski, S. L. Phillips, P. M. V. Clacar, K. Winkler, A. L. Balch, *J. Am. Chem. Soc.* **120**, 1274-1284 (1998).

157. K. M. Smith, S. B. Brown, R. F. Troxler, J.-J. Lai, *Photochem. Photobiol.* **36**, 147-152 (1982).

158. R. M. Jones, Q. Wang, J. H. Lamb, B. D. Djelah, R. Bonnett, C. K. Lim, *J. Chromatography A* **722**, 257-265 (1996).

159. H. H. Inhoffen, P. Jager, R. Mahlhop, C. D. Mengler, *Justus Liebigs Ann. Chem.* **704**, 188-207 (1967).

160. H. W. Whitlock, M. Y. Oester, *J. Am. Chem. Soc.* **95**, 5738-5741 (1973).
The apparent low pK_a of a chlorin.

161. R. Dabestani, J. Higgin, D. Stephenson, I. N. Ivanov, M. E. Sigman, *J. Phys. Chem. B* **104**, 10235-10241 (2000).

162. P. P. Levin, S. M. B. Costa, L. F. V. Ferreira, J. M. Lopes, F. R. Ribeiro, *J. Phys. Chem. B* **101**, 1355-1363 (1997).

Mechanism of heme oxygenase in biliverdin-formation

163. P. K. Sharma, R. Kevorkiants, S. P. deVisser, D. Kumar, S. Shaik, *Angew. Chem. Int. Ed.* **43**, 1129-1132 (2004).

164. P. R. O. deMontellano, *Curr. Op. Chem. Bio.* **4**, 221-227 (2000).

Single electron transfer in the formation of biliverdins

165. J. A. S. Cavaleiro, K. M. Smith, *J. Chem. Soc. Perkin Trans. 1*, 2149-2155 (1973).

Miscellaneous oxidations

166. P. H. Hynninen, K. Hyvarinene, *J. Org. Chem.* **67**, 4055-4061 (2002).
The allomerization of chlorophyll

167. R. K. Ralph, *The Chemistry of Silica- Solubility, Polymerization, Colloid and Surface Properties, and Biochemistry* (Wiley Interscience, New York, 1979).

168. C. Aronovitch, Y. Mazur, *J. Org. Chem.* **50**, 149-150 (1985).

169. D. T. Sawyer, *Oxygen Chemistry*, International Series of Monographs on Chemistry, vol. 26, (Oxford University Press, Oxford, 1991).

170. J.-H. Fuhrhop, S. Besecke, J. Subramanian, *J. Chem. Soc., Chem. Commun.*, 1-2 (1973).

171. B. D. Flockhart, I. R. Leith, R. C. Pink, *J. Catalysis* **9**, 45-50 (1967).

172. G. M. Strunz, C.-M. Yu, A. Salonius, *Phytochemistry* **28**, 2861-2863 (1989).

173. J. S. Calderon, R. H. Thomson, *J. Chem. Soc. Perkin Trans. 1*, 583-586 (1988).

174. P. J. Schofield, B. J. Ralph, J. H. Green, *J. Phys. Chem.* **68**, 472-476 (1964).

175. L. W. Marasas, J. S. Harington, *Nature* **188**, 1173-1174 (1960).

176. W. K. Hall, *J. Catalysis* **1**, 53-61 (1962).

177. R. Dabestani, K. J. Reszka, M. E. Sigman, *J. Photochem. Photobio. A: Chemistry* **117**, 223-233 (1998).

178. T. A. Konovalova, L. D. Kispert, *J. Chem. Soc., Faraday Trans.* **94**, 1465-1468 (1998).

179. M. Deflin, I. M. Eltantawy, M. Baverez, *J. Catalysis* **54**, 345-347 (1978).

180. T. Melvin, S. W. Botchway, A. W. Parker, P. O'Neill, *J. Am. Chem. Soc.* **118**, 10031-10036 (1996).

181. J. Cadet, T. Douki, D. Gasparutto, J. -L. Ravanat, *Mutation Res.* **531**, 5-23 (2001).
Note that oxidative guanine products can also result from the attack of a hydroxy radical as well as the attack of water on a carbocation intermediate.

182. H. Seto, S. Fujioka, S. Takatsuto, H. Koshino, T. Shimizu, S. Yoshida, *Steroids* **65**, 443-449 (2000).

183. O. Sterner, W. Steglich, *Liebigs Ann. Chem.*, 823-824 (1988).

Chapter Six- Synthesis and characterization of porphyrin arrays

Solubilizing groups on porphyrin arrays

184. T. E. O. Screen, J. R. G. Thorne, R. G. Denning, D. G. Bucknall, H. L. Anderson, *J. Mater. Chem.* **13**, 2796-2808 (2003).

Possible role of single electron transfer in the nitration of a porphyrin

185. M. M. Catalano, M. J. Crossley, M. M. Harding, L. G. King, *J. Chem. Soc., Chem. Commun.*, 1535-1536 (1984).

186. O. Siri, L. Jaquinod, K. M. Smith, *Tet. Lett.* **41**, 3583-3587 (2000).

187. G. H. Barnett, K. M. Smith, *J. Chem. Soc., Chem. Commun.*, 772-773 (1974).

188. E. C. Johnson, D. Dolphin, *Tet. Lett.* **26**, 2197-2200 (1976).

Electronic properties of tetraazaanthracene-bridged arrays

189. K. Sendt, L. A. Johnston, W. A. Hough, M. J. Crossley, N. S. Hush, J. R. Reimers, *J. Am. Chem. Soc.*, **124**, 9299-9309 (2002).

Chapter Seven- Photophysical properties of porphyrin arrays

190. H. L. Anderson, *Inorg. Chem.* **33**, 972-981 (1994).
Harry's original butadiyne-linked porphyrins.

191. M. Gouterman, *J. Mol. Spec.* **6**, 138-163 (1961).
The bible for analyzing UV-VIS spectra of porphyrins- well worth a read.

192. J. Zimmermann, U. Siggel, J.-H. Fuhrhop, B. Roder, *J. Phys. Chem. B* **107**, 6019-6021 (2003).
Exciton coupling within an aggregate- including intensity transfer between B band Q bands.

193. D. Kim, A. Osuka, *Acc. Chem. Res.* **37**, 735-745 (2004).
The most recent of Osuka' publications in this area, and perhaps the best for a general overview.

194. R. E. Martin, U. Gubler, J. Cornil, M. Balakina, C. Boudon, C. Bosshard, J.-P. Gisselbrecht, F. Diederich, P. Gunter, M. Gross, J.-L. Bredas, *Chem. Eur. J.* **6**, 3622-3635 (2000).

195. R. E. Martin, T. Mader, F. Diederich, *Angew. Chem. Int. Ed.* **38**, 817-821 (1999).

196. A. Tsuda, H. Furuta, A. Osuka, *J. Am. Chem. Soc.* **123**, 10304-10321.
The electrochemical properties of Osuka's various arrays. Note that the magnitude of the splitting of the 1st and 2nd oxidation potentials is dependent on the central metal.

Theoretical investigations in tetraazaanthracene-bridged porphyrin arrays

197. T. X. Lu, J. R. Reimers, M. J. Crossley, N. S. Hush, *J. Phys. Chem.* **98**, 11878-11884 (1994).

198. J. R. Reimers, T. X. Lu, M. J. Crossley, N. S. Hush, *Nanotechnology* **7**, 424-429 (1996).

199. J. R. Reimers, T. X. Lu, M. J. Crossley, N. S. Hush, *Chem. Phys. Lett.* **256**, 353-259 (1996).

Chapter Eight – New Porphyrin architectures

200. K. Naemura, H. Miyabe, Y. Shingai, Y. Tobe, *J. Chem. Soc. Perkin Trans. 1*, 1073-1077 (1993).

201. C. Bruckner, E. Sternberg, J. K. MacAlpine, S. J. Rettig, D. Dolphin, *J. Am. Chem. Soc.* **121**, 2609-2610 (1999).

Chapter Nine – Experimental details

202. J. N. G. Pillow, M. Halim, J. M. Lupton, P. L. Burn, I. D. W. Samuel, *Macromol.* **32**, 5985-5993 (1999).

203. J. Geuze, C. Ruinard, J. Soeterbroek, P. E. Verkade, B. M. Wepster, *Rec. Trav. Chim. Pays-Bas et Belgique* **75**, 301-310 (1956).

204. M. S. Newman, L. F. Lee, *J. Org. Chem.* **37**, 4468 (1972).

Appendix One- Methods of porphyrin characterization

205. R. A. Binstead, M. J. Crossley, N. S. Hush, *Inorg. Chem.* **30**, 1259-1264 (1991).

206. N. Srinivasan, C. A. Haney, J. S. Lindsey, W. Zhang, B. T. Chait, *J. Porphyrins Phthalocyanines* **3**, 283-291 (1999).

207. J.-H. Fuhrhop, *J. Chem. Soc., Sec. D, Chem. Commun.*, 781-782 (1970).

208. J. Hu, I. Pavel, D. Moigno, M. Wumaier, W. Kiefer, Z. Chen, Y. Ye, Q. Wu, Q. Huang, S. Chen, F. Niu, Y. Gu, *Spectrochim. Acta A* **59**, 1929-1935 (2003).

209. Y. Diskin-Posner, S. Dahal, I. Goldberg, *Angew. Chem. Int. Ed.* **39**, 1288-1292 (2000).

Appendix Two- Exciton coupling theory

210. C. A. Hunter, J. K. M. Sanders, A. J. Stone, *Chem. Phys.* **133**, 395-404 (1989).

211. M. Kasha, *Radiation Research* **20**, 55-71 (1963).

212. M. Kasha, H. R. Rawls, M. A. El-Bayoumi, *Pure Appl. Chem.* **11**, 371-392 (1965).

213. M. Kasha, in *NATO Advanced Study Institute Series, Series B: Physics. Spectroscopy of the Excited State.* (1976 (volume date 1975)) pp. 337-363.

214. J. M. Ribo, J. M. Bofill, J. Crusats, R. Rubires, *Chem. Eur. J.* **7**, 2733-2737 (2001).
Note that this is an unreliable reference.